

AD-A087 793

DEFENSE COMMUNICATIONS ENGINEERING CENTER RESTON VA F/G 17/2.1
PROCEEDINGS OF SEMINAR ON FREQUENCY SELECTIVE FADING AND ITS EF--ETC(U)
JAN 80 D R SMITH
DCEC-TN-2-80

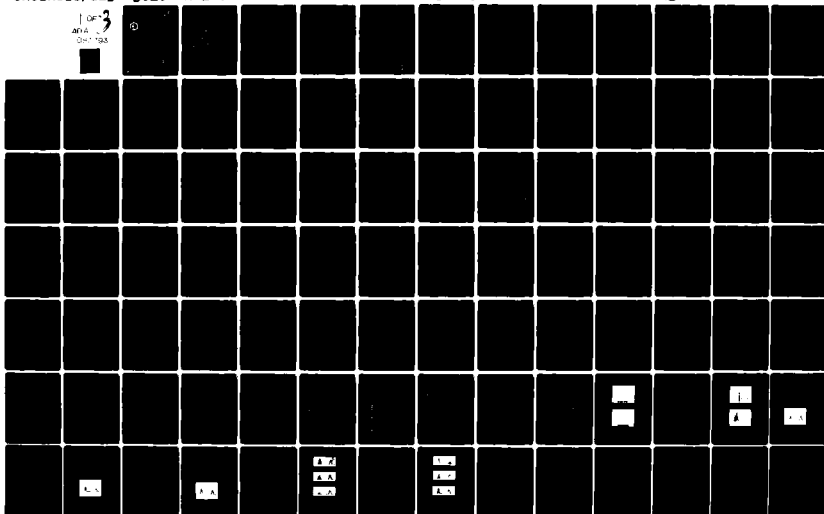
SBIE-AD-E100 375

NL

UNCLASSIFIED

1 OF 3
AD-A
DCEC-TN-2-80

1



LEVEL II

AD-E100375

2

TN 2-80



DEFENSE COMMUNICATIONS ENGINEERING CENTER

ADA 087793

TECHNICAL NOTE NO. 2 - 80

PROCEEDINGS OF SEMINAR ON FREQUENCY SELECTIVE
FADING AND ITS EFFECT ON DIGITAL LOS RADIO
(REPORT NO. 2)

THIS DOCUMENT IS BEST QUALITY PRACTICALLY
THE COPY FURNISHED TO DDC CONTAINED A
SIGNIFICANT NUMBER OF PAGES WHICH DO NOT
REPRODUCE LEGIBLY.

JANUARY 1980

DTIC
ELECTE
AUG 12 1980
S D

APPROVED FOR PUBLIC RELEASE; DISTRIBUTION UNLIMITED

80 8 4 191

DDC FILE COPY

DISCLAIMER NOTICE

**THIS DOCUMENT IS BEST QUALITY
PRACTICABLE. THE COPY FURNISHED
TO DTIC CONTAINED A SIGNIFICANT
NUMBER OF PAGES WHICH DO NOT
REPRODUCE LEGIBLY.**

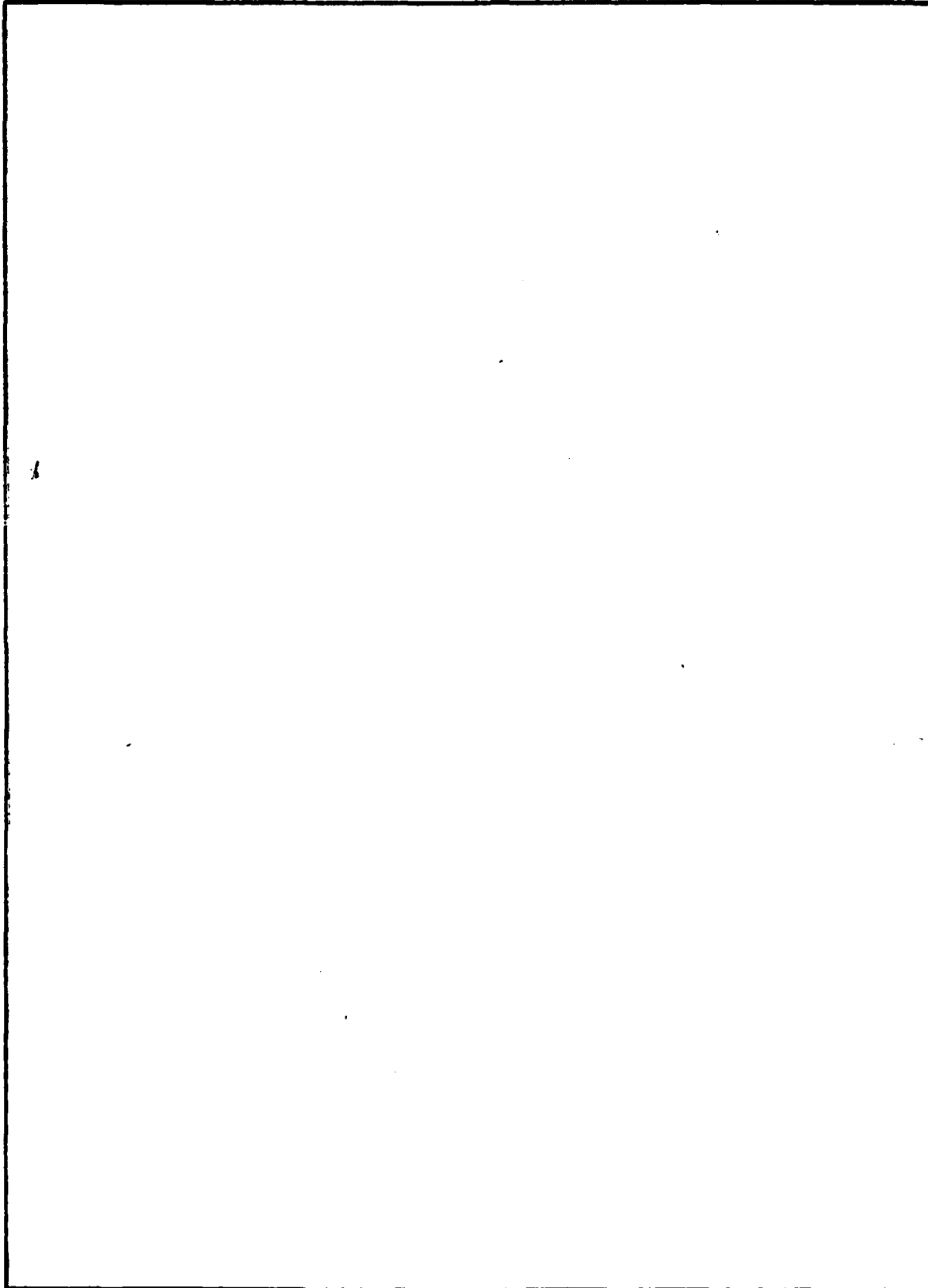
UNCLASSIFIED 1 JAN 1980

ADE 100-375

SECURITY CLASSIFICATION OF THIS PAGE (When Data Entered)

REPORT DOCUMENTATION PAGE		READ INSTRUCTIONS BEFORE COMPLETING FORM
1. REPORT NUMBER DCEC-TN-2-80	2. GOVT ACCESSION NO. AD-A087793	3. RECIPIENT'S CATALOG NUMBER
4. TITLE (and Subtitle) Proceedings of Seminar on Frequency Selective Fading and Its Effect on Digital LOS Radio		5. TYPE OF REPORT & PERIOD COVERED Technical Note
7. AUTHOR(s) Dr. David R. Smith		6. PERFORMING ORG. REPORT NUMBER
9. PERFORMING ORGANIZATION NAME AND ADDRESS Defense Communications Engineering Center Transmission Engineering Division 1860 Wiehle Ave., Reston, VA 22090		8. CONTRACT OR GRANT NUMBER(s)
11. CONTROLLING OFFICE NAME AND ADDRESS SAME AS #9.		10. PROGRAM ELEMENT, PROJECT, TASK AREA & WORK UNIT NUMBERS N/A
14. MONITORING AGENCY NAME & ADDRESS (if different from Controlling Office) N/A		12. REPORT DATE January 1980
		13. NUMBER OF PAGES 245
		15. SECURITY CLASS. (of this report) Unclassified
		15a. DECLASSIFICATION/DOWNGRADING SCHEDULE N/A
16. DISTRIBUTION STATEMENT (of this Report) Approved for publication; distribution unlimited.		
17. DISTRIBUTION STATEMENT (of the abstract entered in Block 20, if different from Report) N/A		
18. SUPPLEMENTARY NOTES Review relevance 5 years from submission date.		
19. KEY WORDS (Continue on reverse side if necessary and identify by block number) Frequency Selective Fading Diversity Digital LOS Radio Availability Adaptive Equalization Multipath		
20. ABSTRACT (Continue on reverse side if necessary and identify by block number) Recent analysis and testing of digital LOS radio links reported in the literature indicate that frequency selective fading may be responsible for performance degradation in the form of inband amplitude and phase distortion. To facilitate an exchange of information among interested groups from government and industry, a seminar was organized by and held at DCEC on the subject of frequency selective fading and its effect on digital LOS radio. This TN presents the proceedings of that seminar.		

SECURITY CLASSIFICATION OF THIS PAGE(When Data Entered)



SECURITY CLASSIFICATION OF THIS PAGE(When Data Entered)

TECHNICAL NOTE NO. 2-80


PROCEEDINGS OF SEMINAR ON FREQUENCY
SELECTIVE FADING AND ITS EFFECT ON DIGITAL LOS RADIO
(REPORT NO. 2)

January 1980

Edited by:

- David R. Smith

Approved for Publication:


HOWARD L. MCKINLEY, JR.
Colonel, USAF
Chief, Transmission
Engineering Division

Accession For	
NTIS GRA&I	<input checked="checked" type="checkbox"/>
DDC TAB	<input type="checkbox"/>
Unannounced	<input type="checkbox"/>
Justification	
By _____	
Distribution/	
Availability Codes	
Dist.	Avail and/or special
A	23

FOREWORD

The Defense Communications Engineering Center (DCEC) Technical Notes (TN's) are published to inform interested members of the defense community regarding technical activities of the Center, completed and in progress. They are intended to stimulate thinking and encourage information exchange; but they do not represent an approved position or policy of DCEC, and should not be used as authoritative guidance for related planning and/or further action.

Comments or technical inquiries concerning this document are welcome, and should be directed to:

Director
Defense Communications Engineering Center
1860 Wiehle Avenue
Reston, Virginia 22090

DTIC
ELECT
S
AUG 12 1980
D

PREFACE

This publication¹ presents results of a seminar organized by and held at DCEC on 26 November 1979 for the purpose of exchanging information among industry and government representatives on the subject of frequency selective fading and its effects on digital LOS radio performance. The seminar was prompted by DCEC interest in frequency selective fading effects on LOS radio and by similar interest shown by other organizations as indicated in the available literature. It is hoped that results of this seminar will lead to further exchange of analytical and test results in the future.

Each seminar speaker provided a copy of the materials used in his presentation, and these copies are presented herein.² In some cases, these are only the visuals that were used with extemporaneous speeches. In other cases, copies of supplemented materials prepared by authors than the speakers are included because these materials were a key element in the presentation.

Further questions regarding the proceedings of the seminar may be directed to Dr. David R. Smith, (COM) 703-437-2316, (VON) 364-2316.

¹ This publication is the second in a series of DCEC reports on frequency selective fading and its effects on DCS transmission system performance.

² For those presentations which used previously published articles, permission of the author(s) has been obtained and copyright information has been provided in accordance with requirements of the IEEE and Bell Telephone Laboratories.

TABLE OF CONTENTS

	<u>Page</u>
PREFACE	111
 PRESENTATIONS	
(1) Assessment of Selective Fading Effects on Digital LOS Links by David R. Smith	1-1
(2) Multipath Degradation of Digital Microwave Link Availability by John K. Webb	2-1
(3) Amplitude Distortion Measurements on LOS Links by Larry Hause	3-1
(4) Overview of Multipath Measurements Using a PN Probe by Bob Hubbard	4-1
(5) Path Testing of Long, Over Water Digital Radio Paths by Jim Weblemoe	5-1
(6) Multipath Fading Channel Model by Tom Giuffrida	6-1
(7) Effects of Frequency Selective Fading on Digital Radio by A. Vigants	7-1
(8) The Effects of Selective Fading on Digital Radio by Steve Barber	8-1
(9) Atmospheric Structure and Multipath Effects by Owen Cote'	9-1
(10) Adaptive Equalization for Correction of Multipath Distortion in a 8 PSK Digital Radio by Paul Hartmann	10-1
(11) Adaptive Equalization by Robert Wallace	11-1
 APPENDIX	
A. List of Seminar Attendees	A-1

1. ASSESSMENT OF SELECTIVE FADING EFFECTS ON DIGITAL LOS LINKS

David R. Smith
Defense Communications Engineering Center
Reston, VA

NOTE: The materials provided in this section are copies of the visuals used with the extemporaneous remarks given by Dr. Smith.

ASSESSMENT OF FREQUENCY SELECTIVE FADING ON DIGITAL MICROWAVE LOS LINKS

- OBJECTIVE: TO ASSESS THE IMPACT OF FREQUENCY SELECTIVE FADING ON THE
ALLOCATION OF SYSTEM PERFORMANCE AND LOS LINK DESIGN FOR DIGITAL
RADIO APPLICATIONS

- BACKGROUND:

- I. DCA SYSTEMS ENGINEERING
- II. CHARACTERIZATION OF DIGITAL RADIO LINKS

- APPROACH:

- I. PHENOMENOLOGICAL DESCRIPTION
- II. OVERVIEW OF STUDIES/MEASUREMENTS
- III. EVALUATION VIA HYBRID SIMULATION
- IV. TEST AND EVALUATION EFFORTS

BACKGROUND

I. DCA SYSTEMS ENGINEERING

A. HIGH PERFORMANCE OBJECTIVES FOR LOS LINKS

- E.G., .99999 AVAILABILITY FOR BER = 5×10^{-9}

DCS DESIGN CRITERIA ASSUMES FLAT FADING CHANNEL FOR LOS

- CLOSE APPROXIMATION FOR RELATIVELY LOW RATE, SMALL

BANDWIDTH LINKS

- QUESTIONABLE ASSUMPTION FOR HIGHER RATE LINKS

BACKGROUND (CONTINUED)

II. DCS LOS LINK CHARACTERIZATION

A. DCS OWNED & OPERATED LOS LINKS

- DISTANCE
 - MEDIAN OF 20 MILES
 - 90% LESS THAN 50 MILES
- 4 & 8 GHZ BANDS
- DUAL DIVERSITY, USUALLY SPACE
- MAXIMUM OCCUPIED BANDWIDTH OF 14 MHZ
- ALL TYPES OF TERRAIN AND CLIMATE

B. 1ST GENERATION DIGITAL LOS LINK

- DCS STANDARD MICROWAVE RADIO
- PARTIAL RESPONSE INTERFACE (1 BPS/HZ)
- MAXIMUM 13 MBPS

C. 2ND GENERATION DIGITAL LOS LINK

- DRAMA RADIO
- QPSK/QPR MODULATION (2 BPS/HZ)
- MAXIMUM OF 28 MBPS

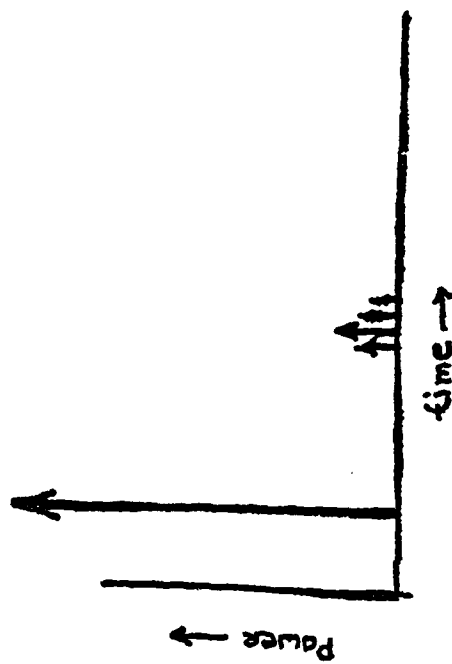
BACKGROUND (CONTINUED)

D. LEASED LOS LINKS

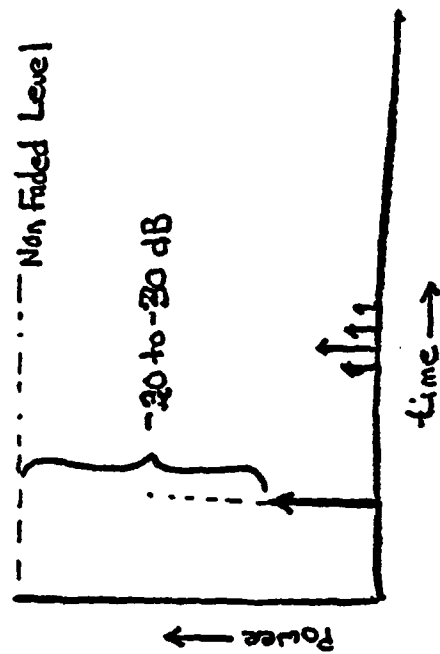
- COMMERCIAL RADIO EQUIPMENT (E.G., COLLINS)
- 6, 11 GHZ BANDS
- WIDEBAND WITH MAXIMUM OF 90 MBPS
- PERFORMANCE SPECIFIED BY BER AND AVAILABILITY

I. PHENOMENOLOGICAL DESCRIPTION

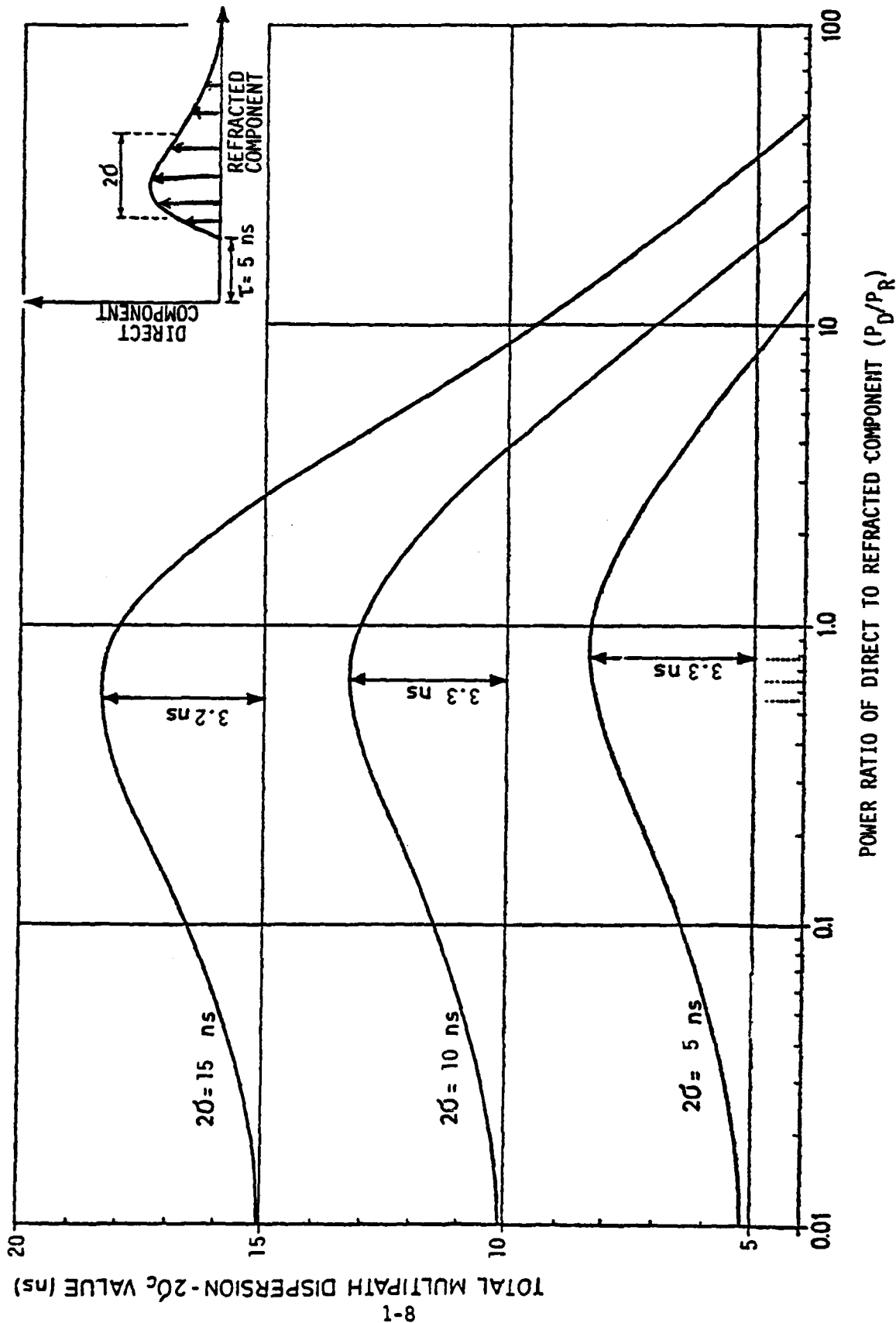
- LOS CHANNEL COMPOSED OF A DIRECT COMPONENT PLUS A DELAYED
RESIDUAL REFRACTED COMPONENT.
 - Δ DIRECT COMPONENT MAY BE COMPOSED OF TWO COMPONENTS WITH
SMALL PROPAGATION DELAY DIFFERENCE
 - Δ REFRACTED COMPONENT CAUSED BY REFRACTION (OR SCATTERING) FROM
ELEVATED TROPOSPHERIC ANISOTROPIES.
- DELAY DISTORTION PROPORTIONAL TO THE RELATIVE POWERS OF DIRECT
AND REFRACTED COMPONENTS
 - Δ LARGE DELAY SPREADS GENERALLY ACCOMPANIED BY DIRECT PATH FADE
 - Δ DELAY DISTORTION LINK LENGTH AND BEAMWIDTH DEPENDENT

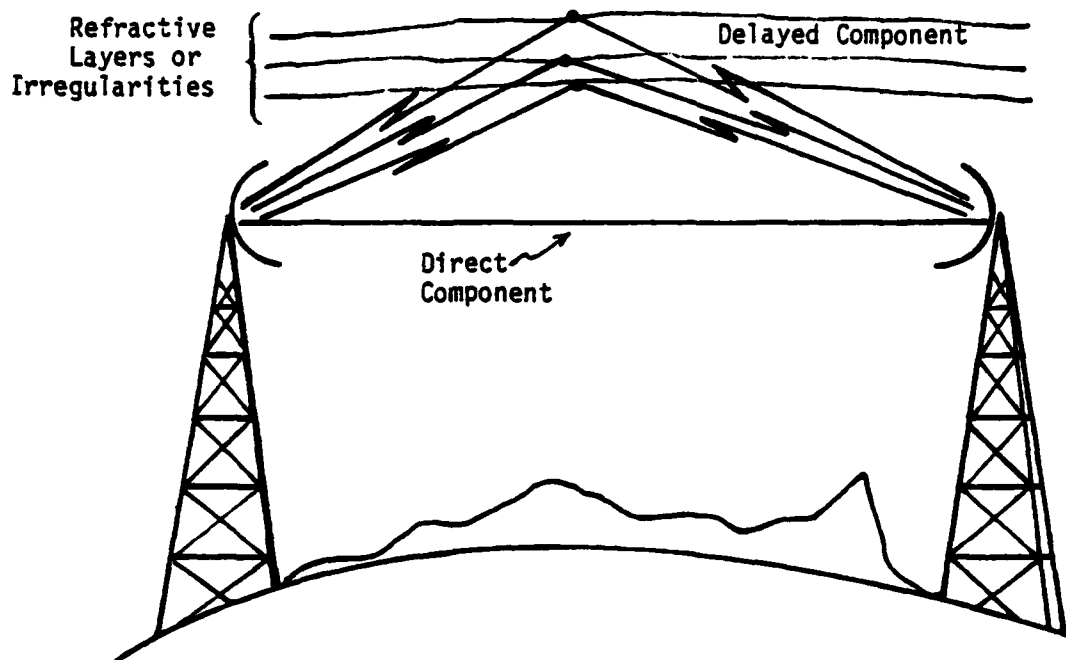


(g) UNFADED STATE



(h) FADED STATE





II. OVERVIEW OF STUDIES/MEASUREMENTS

- PROPAGATION STUDIES/MEASUREMENTS
 - Δ BELL MEASUREMENTS OF DELAY DISTORTION
 - Δ DOD STUDIES OF SELECTIVE FADING ON LOS
- BTL DIGITAL COMMUNICATIONS STUDIES (76 MB/S 8 PSK)
 - Δ BER MEASURED DURING FADING POORLY CORRELATED WITH TOTAL POWER RECEIVED
 - Δ LOSS OF FADE MARGIN (10-20 DB)
 - Δ DIVERSITY COMBINER CONCERNS (PERFORMANCE MONITOR ACCURACY AND RESPONSE)
- BNR DIGITAL COMMUNICATIONS STUDIES (90 MB/S QPR)
 - Δ HIGH (10^{-4}) BER MEASURED DURING SHALLOW FADES
 - Δ ADAPTIVE EQUALIZER DESIRABLE AT HIGH RATES

III. EVALUATION VIA HYBRID SIMULATION

A. DCS DIGITAL LOS RADIO

1. QPSK & QPR MODULATION
2. DIVERSITY CONFIGURATION
3. FILTERING OPTIONS
4. BER VS SNR PERFORMANCE

B. FREQUENCY SELECTIVE FADING LOS CHANNEL

1. TAPPED DELAY LINE
 - 1 - 12 TAPS
 - SELECTABLE TAP GAINS
 - SELECTABLE INTERTAP SPACING
2. SETTABLE CORRELATION BETWEEN DIVERSITY CHANNELS
3. SETTABLE FADING RATE

III. EVALUATION VIA HYBRID SIMULATION (CONTINUED)

C. ADAPTIVE EQUALIZATION

1. IF & BASEBAND
2. APPLICABLE TO QPSK, QPR AND DUAL DIVERSITY
3. COMPARATIVE EVALUATION BY
 - BER
 - EASE OF IMPLEMENTATION
 - STABILITY

D. DIVERSITY COMBINER

1. SELECTION COMBINER
2. PERFORMANCE MONITORS
 - OFFSET THRESHOLD
 - AUTOMATIC GAIN CONTROL

IV. TEST AND EVALUATION EFFORTS

A. DIGITAL EUROPEAN BACKBONE

1. THREE OPERATIONAL DIGITAL LINKS IN ITALY

- 8 GHZ
- 56 - 82 MILES IN LENGTH

2. FM RADIOS

- 3 LEVEL PARTIAL RESPONSE
- 12.6 MBPS IN 14 MHZ BANDWIDTH
- DUAL DIVERSITY

3. MEASURE SPECTRUM AMPLITUDE DISTORTION AND CORRELATE WITH

- FADE DEPTH
- ANOMALOUS PROPAGATION CONDITIONS
- BIT ERROR RATE

IV. TEST AND EVALUATION EFFORTS (CONTINUED)

B. EXPERIMENTAL ASSESSMENT

1. STANDBY LOS LINK IN WASHINGTON, DC AREA
 - 6 GHZ
 - 39 MILES
 - REFRACTIVE CONDITIONS SIMILAR TO EUROPE
2. DIGITAL RADIO
 - COLLINS 8 PSK
 - 90 MBPS IN 30 MHZ OF BANDWIDTH
 - SPACE DIVERSITY
 - NO ADAPTIVE EQUALIZATION

IV. TEST AND EVALUATION EFFORTS (CONTINUED)

3. DATA COLLECTION

- AMPLITUDE AND GROUP DELAY CHARACTERISTICS
- SEQUESTRIAL PULSE RESPONSE
- FADING STATISTICS (RATE OF, DURATION, AND DEPTH)
- BER MEASUREMENT

4. DATA ANALYSIS

- DISTRIBUTION OF
 - FADE DEPTHS
 - BIT ERROR RATE
 - MULTIPATH DISPERSION
 - RECEIVED POWER
- CORRELATION OF
 - DIVERSITY CHANNEL POWER
 - DIVERSITY CHANNEL GROUP DELAY
 - BER AND GROUP DELAY
 - BER AND RECEIVED POWER
 - BER AND EACH DIVERSITY CHANNEL

FOR EACH OF

TWO DIVERSITY

CHANNELS

2. MULTIPATH DEGRADATION OF DIGITAL MICROWAVE LINK AVAILABILITY

John K. Webb
The MITRE Corporation
Bedford, MA

NOTE: The material provided in this section is a text of the
remarks given by Mr. Webb.

The MITRE Corporation provides technical support to the Air Force AFTEL Program Office which has Program Management responsibility for the DEB system. DEB will introduce all-digital transmission to the European DCS. Stage I now largely completed, uses 3-level partial response 12.⁶ Mb/s with FM radios. Stages 2 thru 4 will install 117 links of up to 26.8 MB/s with the Army DRAMA radios using QPRS at 4 and 8 GHz for 2 bits per Hz bandwidth efficiency. The DRAMA radio has an alternate 1.0 bit/Hz QPSK capability.

In July 78, I was asked to examine the performance that should be expected on the longer DEB links with higher rate QPRS modulation. Concern was suggested by several BTL and BNR papers presented at ICC-78. They showed that outages due to multipath degradation of signal quality could exceed outages due to signal power fading below the receiver threshold. Barnett's work measured considerable outage due to multipath degradation alone on a 26 mile link with a margin so high that fading below threshold would not happen. Papers by Prabhu, Greenstein, Rumler and Emshwiller showed that the outages observed by Barnett were consistent with the intersymbol interference to be expected with the time dispersive multipath delays observed during the test period.

(2) Jakes' paper offered a statistical model for cumulative outage prediction that was based in several sources. It embodies:

- . Ruthroff's atmospheric delay model which assumes atmospheric conditions that allow delay to increase as the third power of distance.
- . Coefficients for mean values of delay from Prabhu and Greenstein.
- . and coefficients that fit the model expression to samples of outage data measured on several test links and measured multipath tolerance for several modulation methods.

The Jakes model fits outage measurements from earlier tests, none of which were accompanied by reported or measured collateral atmospheric data. Nevertheless, it is the only model we have that can be directly applied to the lower data rates and the longer distances of the DEB system.

The work reported by Barber, Anderson and Patel of BNR provided a basis for including some form of diversity improvement and another check on the Jakes model at a 33 mile distance. Also it provides an estimate of the relative multipath tolerance of QPRS and 4 or 8 PSK. BNR found QPRS to be nearly the same as 8 PSK; later private communication with Jakes suggests BNR's conclusion to be based on linear amplitude and slope effects and that QPRS should perform more like QPSK with multipath as it exists in nature.

(3) This graph shows the Jakes model calculation of non-diversity cumulative outage for 26.8 Mb/s DEB links at 4 and 8 GHz as a function of distance. The curve shows outage time growing exponentially with distance. The lower curve shows the effect of diversity improvement in the amount measured by BNR in their tests. However, the DRAMA radios use hitless baseband switched diversity, not coherent IF combining and adaptive equalization as in the BNR radios. Application of BNR's diversity improvement to a system using a different diversity technique is of course not supportable; rather we need to refine our understanding of how a switching diversity system would work in terms of correlation of multipath degradation in the diversity pair. The inadequacy of the cumulative prediction is further highlighted by the DCS-allocated LOS performance requirement; it is expressed in terms of probabilities of outage of several durations, not as cumulative outage. The results did show that multipath degradation may significantly add to the outages expected from signal power fading alone. The concern was sufficient to develop an extended model, that led to a proposal for tests to refine uncertainties that were inherent in the model. More about the tests later, but first the extended model.

The model was extended, largely by layered hypotheses, to provide a numerical basis for accommodating diversity features. The Jakes model is used initially to calculate cumulative non-diversity multipath outages; (4) the cumulative outage is allocated to each fade depth according to this population reported by Barnett. It is a histogram showing the percentage of the total multipath outage associated with each fade depth. Here we assume that fades of say 30 dB will contribute nine percent of the cumulative outage for either BIL or DOD. Now each fade depth has an average duration and a distribution. (5) Here we used relationships suggested by Vigants for signal fading with the implicit assumption that in fades where multipath outages occur, the duration of the outage will correspond with duration of the fade. Thus we can sum the outage time contribution of each fade depth above threshold for a specified fade duration (t). For simultaneous fades of both channels below threshold, we used conventional expressions from Vigants--there we don't care about multipath degradation because both channels have inadequate signal level. For conditions where the protected channel fades below threshold, we put in a provision to add the outage contribution due to multipath degradation of the protection channel. Lack of data so far prevents us from exercising this feature of the model. Outage reductions due to switching diversity protection are included by multiplying the outage contribution of each fade depth by the correlation coefficient of multipath outage on a diversity pair for each fade depth--that data of course is not available from measurements reported in the literature.

(6) The non-diversity outages summed by this extended model are shown in this table for a 50 mile link with a fade margin of 32 dB. Here we see that outages of all durations are predominantly due to multipath. The 38,500 figure is from Jakes's model but allocated for fade depths less than 32 dB according to Barnetts

histogram. To the right we see outage time decreasing with outage duration as Vigants average duration and statistics are applied to each fade depth. Below, a line of small numbers shows that outages due to the signal fading below threshold tend toward insignificance beside multipath caused outages. Also, we see that outage time decreases slowly as outage duration increases. This is because fade durations are long at the shallower fade depths at which much of the multipath degradation occurs.

(7) The next figure is a graph of the same numbers computed over a range of distances. The same 32 dB margin applies in all cases. Again we see the same alarming growth of outages with distance for all outage durations, primarily because the Jakes and Ruzhroff models allow outages to grow as the third power of distance. Observations of multipath delay on longer links do not support that such growth really happens; therefore we should expect these curves to truncate in some fashion with a trend in evidence somewhere between 30 and 40 miles. But if we erect an ordinate at say 40 miles we see over 10^4 seconds of .2 second outages that have to be dealt with by the diversity switch.

So far, we have seen how the model works without outage reductions or improvements available with the hitless diversity switch. For a diversity evaluation, fading correlation coefficients were taken from a sample of data for 30-foot vertical antenna separation, the coefficients approached unity in the shallower fade region we are concerned about. As expected, that run showed negligible outage reduction. We could see in the data why switching diversity works in analog systems---they fall below threshold in deep fades and deep fades become quite uncorrelated in time. Thus a low probability of simultaneous fading below threshold and small durations of outage. Now we can conclude that conditions which de-correlate multipath degradation in shallow fades on a diversity pair are essential to achieving diversity improvement in the

digital radio that does not otherwise ameliorate multipath by adapting the receiver to the corrupted waveform.

This modeling activity then suggests several features for a link test to refine our ability to predict the performance of longer digital radio links. Two of the more important features are distance dependence and correlation of diversity degradation as a function of antenna installation criteria. (8) On distance dependence, there are several reasons to suggest that the curves of outage versus distance increase more slowly with distance than the model shows. The 10 ns of delay predicted by Ruthoff's model and used in the Jakes model is in agreement with measurements on the 26 mile Georgia path; however, that value has to increase as the cube of distance to support use of the model at greater distances. The atmospheric delay observed by channel probes is not known to have ever exceeded 30 ns on any path of up to 65 miles. When the BNR system parameters are plugged into the Jakes model, the outage calculated at 32 miles is 3 times greater than was measured in BNR's non-diversity test. These facts suggest that realistic delay values for distances longer than 30 miles will increase more slowly than Ruthoff's model. This seems reasonable because longer paths involve higher terminal elevations; accordingly a smaller fraction of a long path involves the lower elevation atmosphere where many anomalous refractive conditions are known to occur. If the multipath degradation is due to lower atmosphere anomalies than performance should not degrade as severely with path length. Tests on long paths are required to resolve this uncertainty.

The diversity question is one of how the correlation of multipath degradation on a diversity pair is related to antenna installation. If correlation of fade intervals is closely tied to intervals of multipath

degradation, then 30 feet or less of spacing appears inadequate; however, ITS observations at Ft. Huachuca of a 100 foot spaced antenna pair showed very uncorrelated multipath outages. Certainly, measurements of multipath degradation need to be made with antenna spacing as a variable. The tests should establish antenna installation criteria that enable realization of diversity improvement with the switching technique.

(9) This figure shows on a data-rate/distance coordinate system where the test data is in relation to DEB. DEB is shown as a variable distance with numbers beside the ordinate to show the population of links in each decade of distance. There is not much near DEB. The BTL and BNR points are in the lower right corner. The BTL point might move in the future toward higher data rates but surely not to longer distances. The Haw-tel data at 90 miles is an exception--but it didn't work. Haw-tel observed whole days of outage which correlated with an elevated inversion layer. The Army tested a link similar to DEB, 12.9 Mb/s, over 33 miles at Ft. Huachuca. Fading was not observed which is typical of microwave tests in the high dry climate. Therefore, none of the other existing work provides data on a system like DEB in the European location. We have recommended testing the DEB equipment on a long path in a climate approximating central Europe. Two paths have been recommended in the Massachusetts/New Hampshire region, one 45 miles, the other 68 miles. A test thru a summer fading season on either of these paths should greatly refine our ability to predict DEB digital radio performance in Europe.

(10) As part of our recommendations to do live link testing considerable thought has been given to location dependence in terms of atmospheric phenomenology. The first question we addressed is "Why not do the testing at Ft. Huachuca where the Army has an established test facility? First the available atmospheric gradient statistics for Germany and a high dry climatic area were compared--Haw-tel data is in black, El Paso, Texas is red and El Paso is climatically

similar to Ft. Huachuca. Summer is solid lines and winter is dashed lines. The red lines (El Paso) show little winter to summer difference and are not very different from the black dashed line--winter in Germany. The refractive index extremes, both sub and super refraction shown by the solid black line which is the summer fading season in Germany, is not in evidence in the El Paso or Ft. Huachuca climate. It is no surprise that microwave links work extremely well at Ft. Huachuca and if the deployment area was Algeria or Afghanistan, Ft. Huachuca would be a representative test area. It is for these reasons that we have recommended New England as a test location; it is more representative of the central Europe climate and terrain than are Arizona, Washington, D.C., or Eglin AFB Florida.

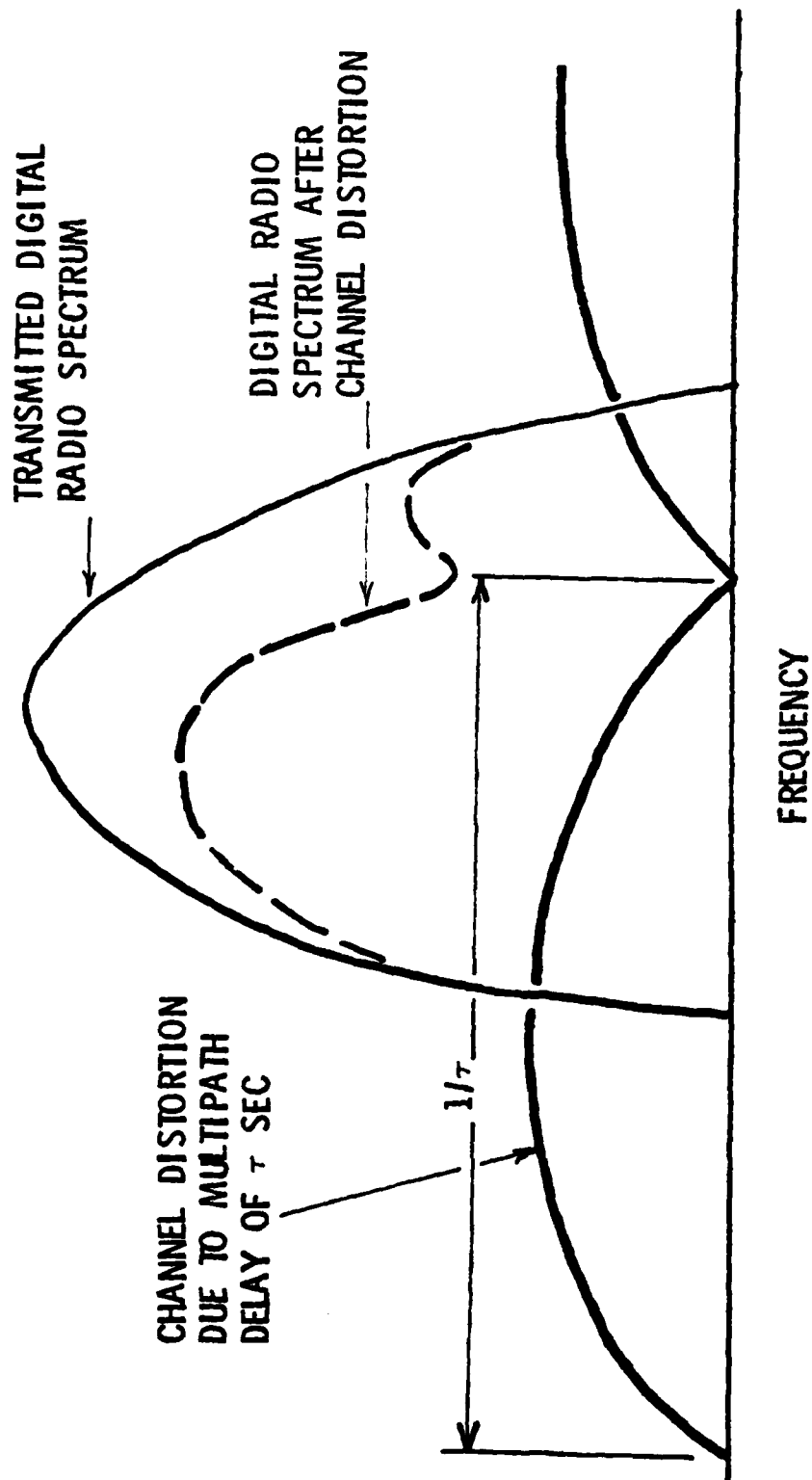
(11) The proposed test would operate a space diversity digital radio link in parallel with a channel probe such as the ITS apparatus. The radio link would be instrumented to measure digital error rate and signal level in each tenth second interval. Pre-processing would discard data for uninteresting intervals while the interesting data would be saved on tape for later analysis. The channel probe would measure delays on the path for correlation with errored intervals. A proposed site is a 45 mile path from Waltham, MA to Pack Monadnock, N.H. A NOAA weather radar looks down on the path from Worcester, MA; this aids in identifying outages caused by precipitation. The tests should be accompanied by radio sonde flights during periods of observed multipath degradation. Such a test would add a great deal to the body of knowledge as to the interrelationship of the atmosphere, delays in the medium and digital radio performance.

These recommendations for tests were made in December 1978. The results should be important to both the Army who is procuring the DRAMA radios and who should speak for their limitations as well as agencies who apply the radio in systems. The tests have not happened for at least two reasons: the radios being procured are allocated to tests at Ft. Huachuca and to the production

installation schedule. Existing program direction would have to be changed to allocate radios to the proposed tests and provide funding to a designated testing agency.

(12) Since the publication of this work there has been a report of a newer test by Mr. Giuffrida of BTL at ICC 79. The test methods were similar to those reported earlier by Barnett, the equipment and location were the same and probably much of the instrumentation. The tests used three periods during a fading season, each greater than a month, to measure cumulative outage with combinations of switching, coherent IF combining and adaptive equalization. This graph plots together Giuffrida's separately plotted test results. The system that provided the lowest outage was the lowest black dashed line, it is functionally the same as the system that BNR selected for production after their 1977 tests. The highest red line is functionally like the DRAMA radio; space diversity with baseband switching. There are many questions that can be asked by those who would choose to discount the significance of this data; nevertheless it is a comparison of six diversity techniques that suggests the technique embodied in the DRAMA radio to provide among the poorest diversity improvement of those techniques tested. One can say the test might have been done wrong, or that adaptive equalization is a requirement for either switching diversity or IF combining, or the data can support that tests and work are needed to determine how to obtain significant diversity improvement by such means as antenna installation criteria where radios are constrained to dependence on switching diversity.

DIGITAL RADIO MULTIPATH DEGRADATION MECHANISM



P, THE NUMBER OF SECONDS OF OUTAGE (BER > 10^{-4}) PER WORST-FADING MONTH:

$$P = \frac{1.6 m k^{(.85)}}{U V} \left(1 + \frac{U}{V}\right)$$

WHERE:

m = $6.575 C f D^3$

C = terrain factor, $1/4 < C < 4$

f = frequency in GHz

D = distance in statute miles

k = 0.2 (8-PSK) or 0.7 (QPSK)

U = $\beta \tau_s k^{(.85)}$

$\beta = 1/\tau_0$

τ_0 = mean delay = $\mu \tau_m = 3.7 \left(\frac{D}{20}\right)^3 \mu$

$\mu = 0 < \mu < 1$; 0.07 was chosen

τ_s = symbol length in nanoseconds

V = $\alpha + U$; 10.0 was chosen for α

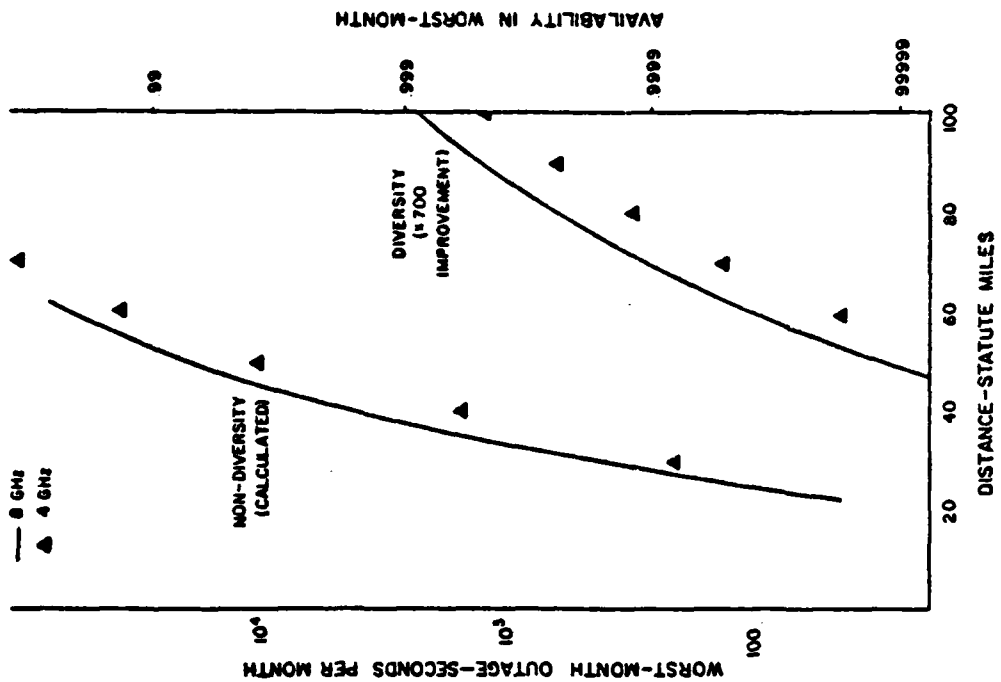
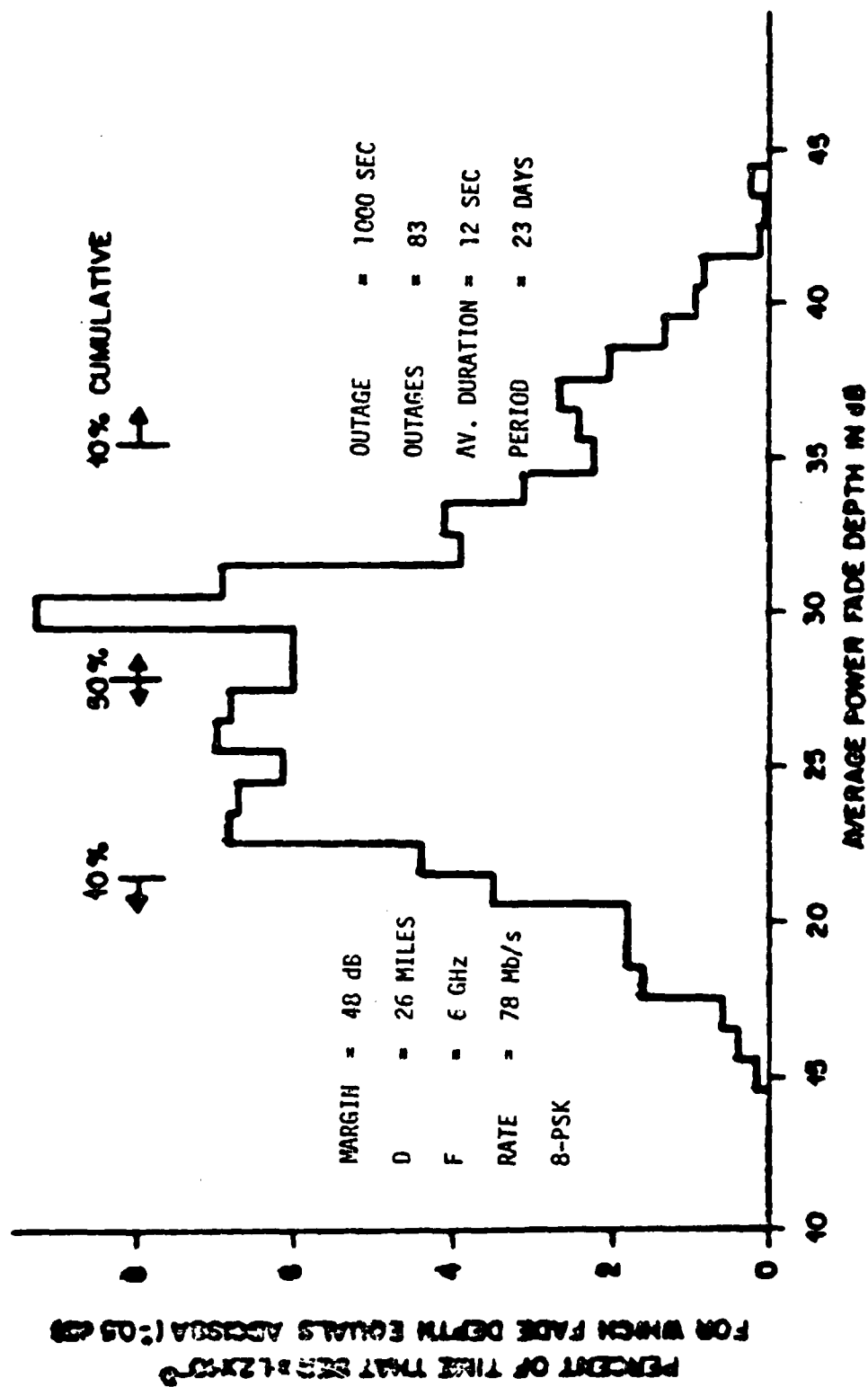


Figure 7 PERFORMANCE OF 26.8 Mb/s QPRS (k=0.2)
AT 8 AND 4 GHz



CORRELATION OF BER 2.12×10^{-3} WITH RECEIVED POWER, NON DIVERSITY-HORN REFLECTOR, 6/17-7/5 AND 7/19-7/26, 1977

AVERAGE FADE DURATION: $t_o = 450L$

WHERE $L = 10^{-(F/20)}$

$F =$ FADE DEPTH IN dB

AVERAGE DURATION OF SIMULTANEOUS FADES BELOW THRESHOLD

$t_o = 225L$

$P(t) = e^{-1.15 (t/t_o)^{2/3}}$

OUTAGE VERSUS OUTAGE DURATION FOR ALL FADE DEPTHS

FROM 0 TO 32 dB

(50 MILES)

OUTAGE IN SECONDS PER MONTH DUE
TO FADES EXCEEDING t SECONDS

ALLOCATED
CUMULATIVE
OUTAGE

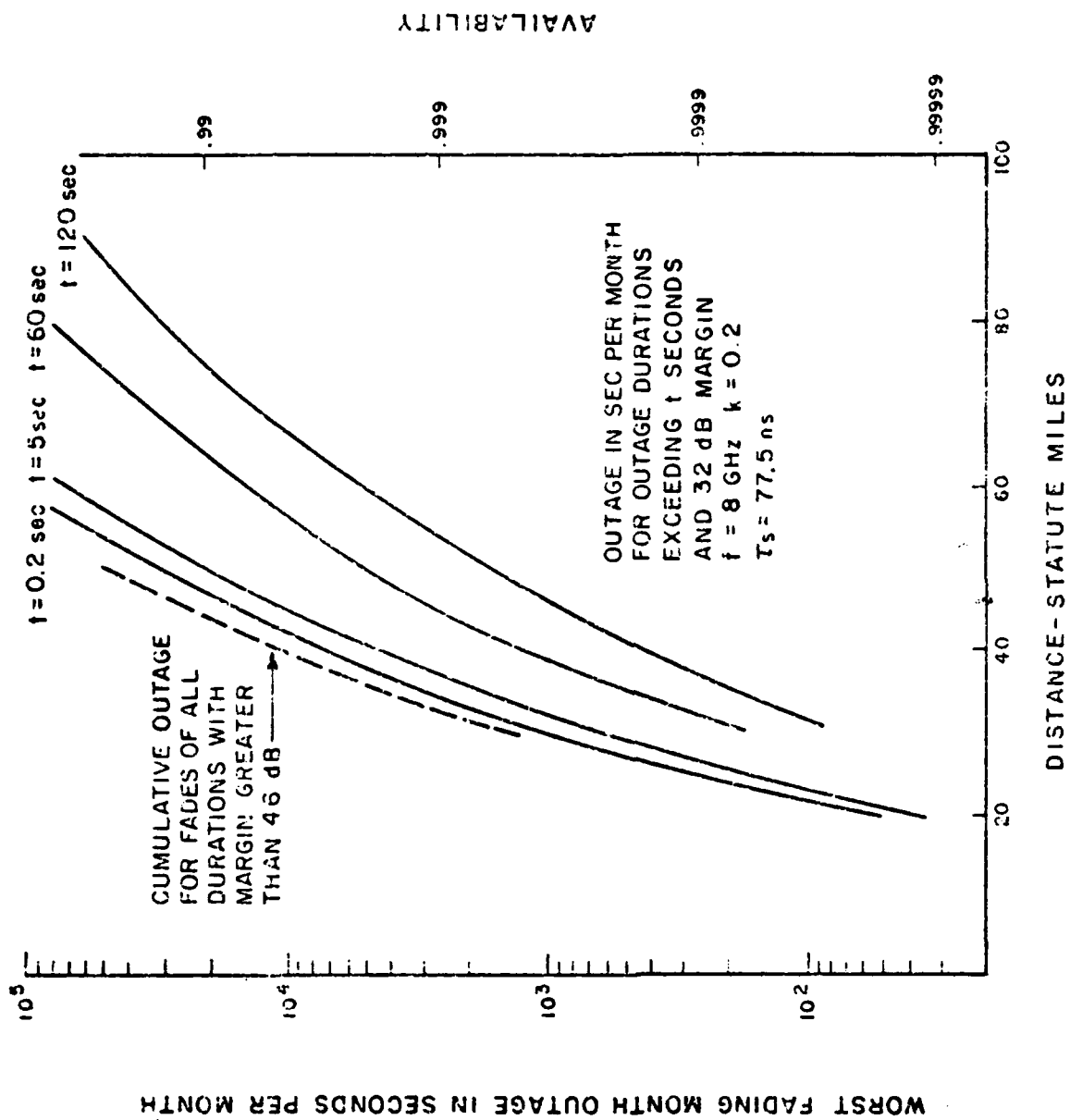
t = 0,2 t = 5,0 t = 60 t = 120

FADES FROM
0 TO 32 dB

36,500 25,300 4,641 1,541

SIMULTANEOUS
FADES BELOW
32 dB

283 111 0 0

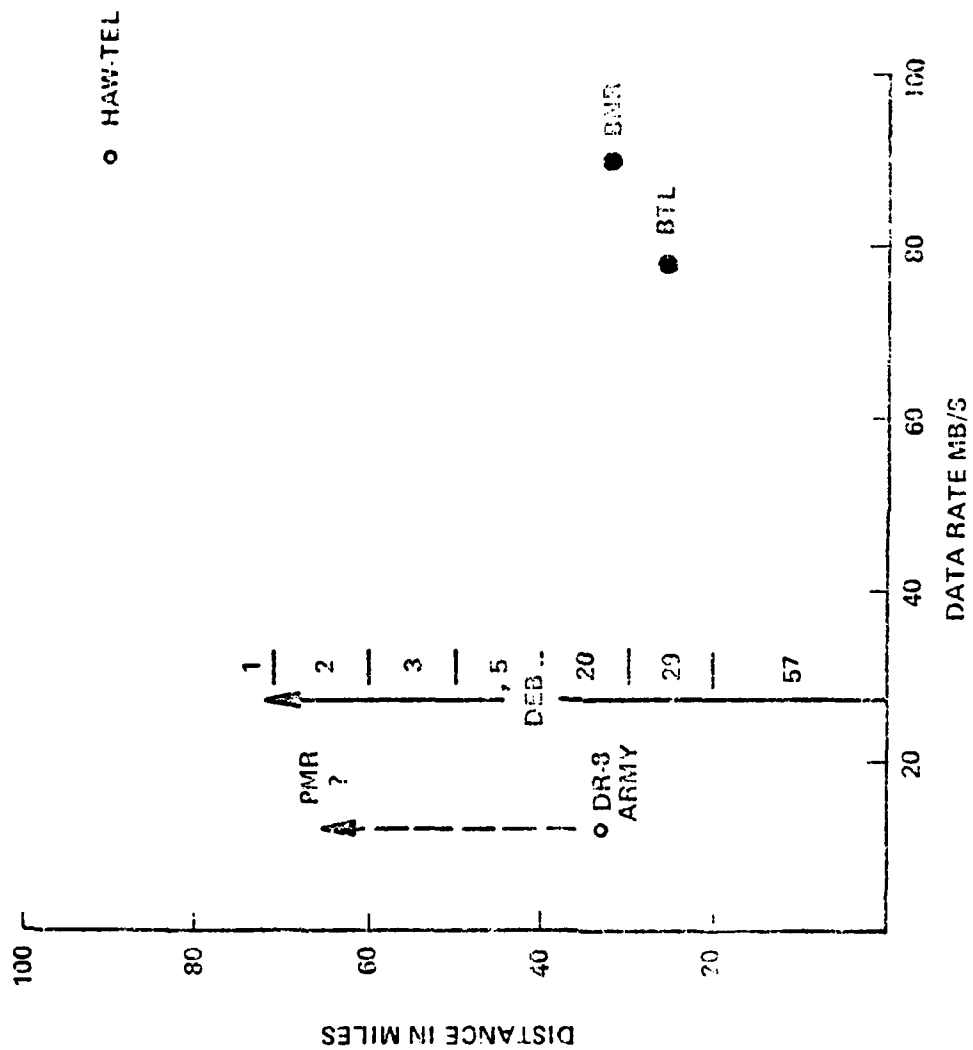


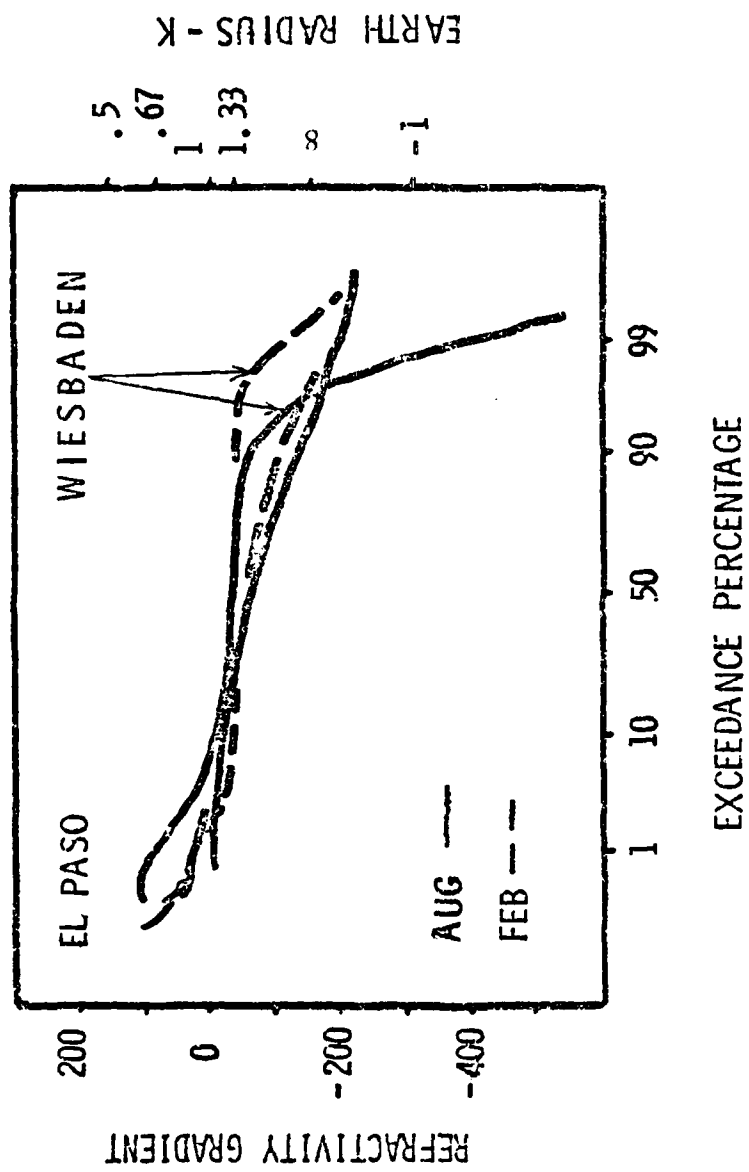


DEB

MEASUREMENT PROGRAM

1. VALIDATE NON-DIVERSITY PREDICTION MODEL FOR DEB
DISTANCES AND DATA RATES.
2. MEASURE CORRELATION OF MULTIPATH DEGRADATION IN
A DIVERSITY PAIR.





TEST RESOURCES

ATMOSPHERIC INSTRUMENTATION

- WEATHER RADAR
- RADIOSONDE

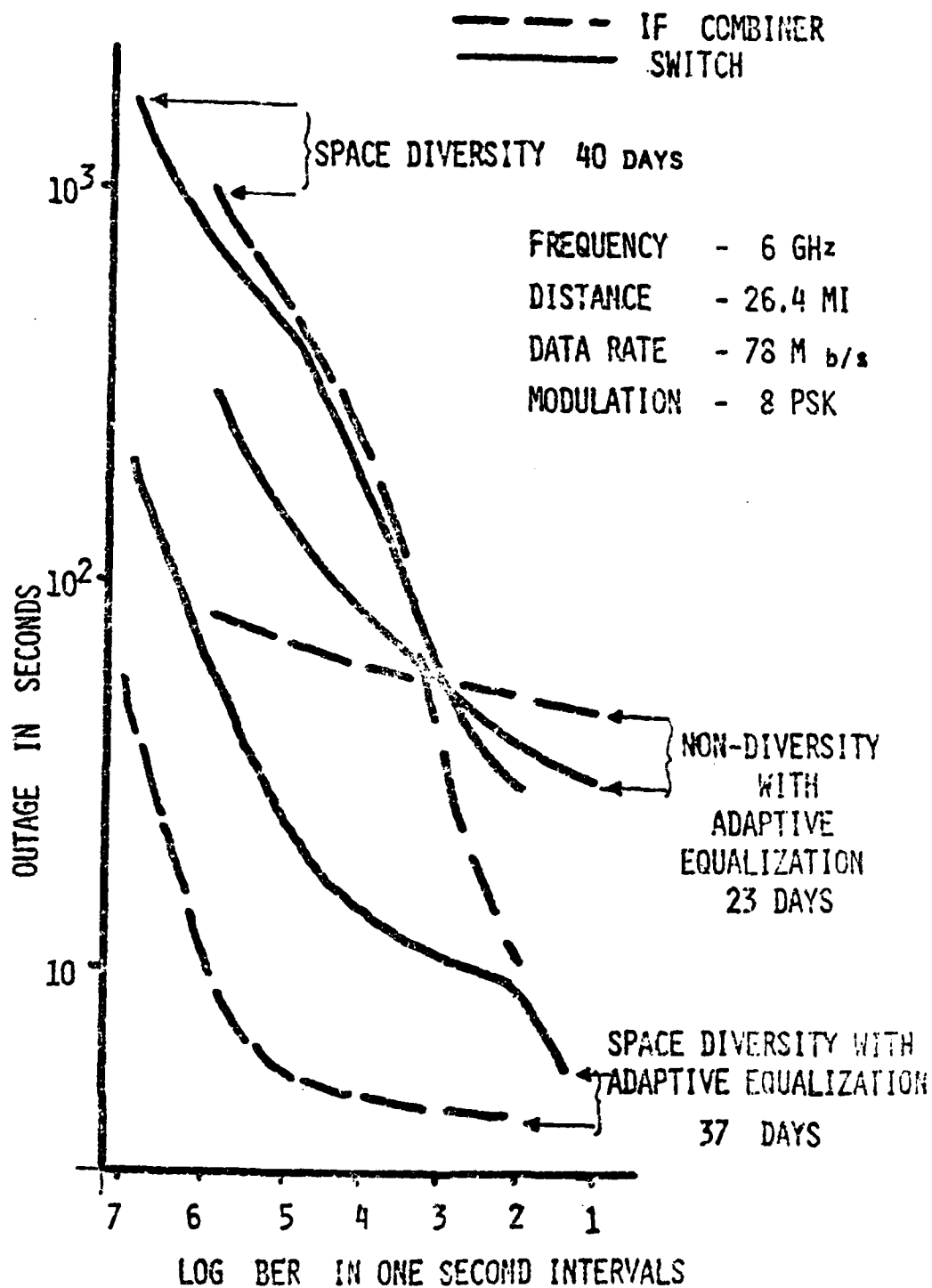
CHANNEL PROBE - ITS

- MEASURE DIFFERENTIAL MULTIPATH DELAY
- MEASURE BIPHASE ERROR RATE

DIGITAL RADIO

INSTRUMENTATION

- ERROR RATE MEASUREMENT SETS
- CLOCK
- BIT COUNT INTEGRITY COMPARATOR
- DIGITAL FORMATTER
- DIGITAL RECORDER



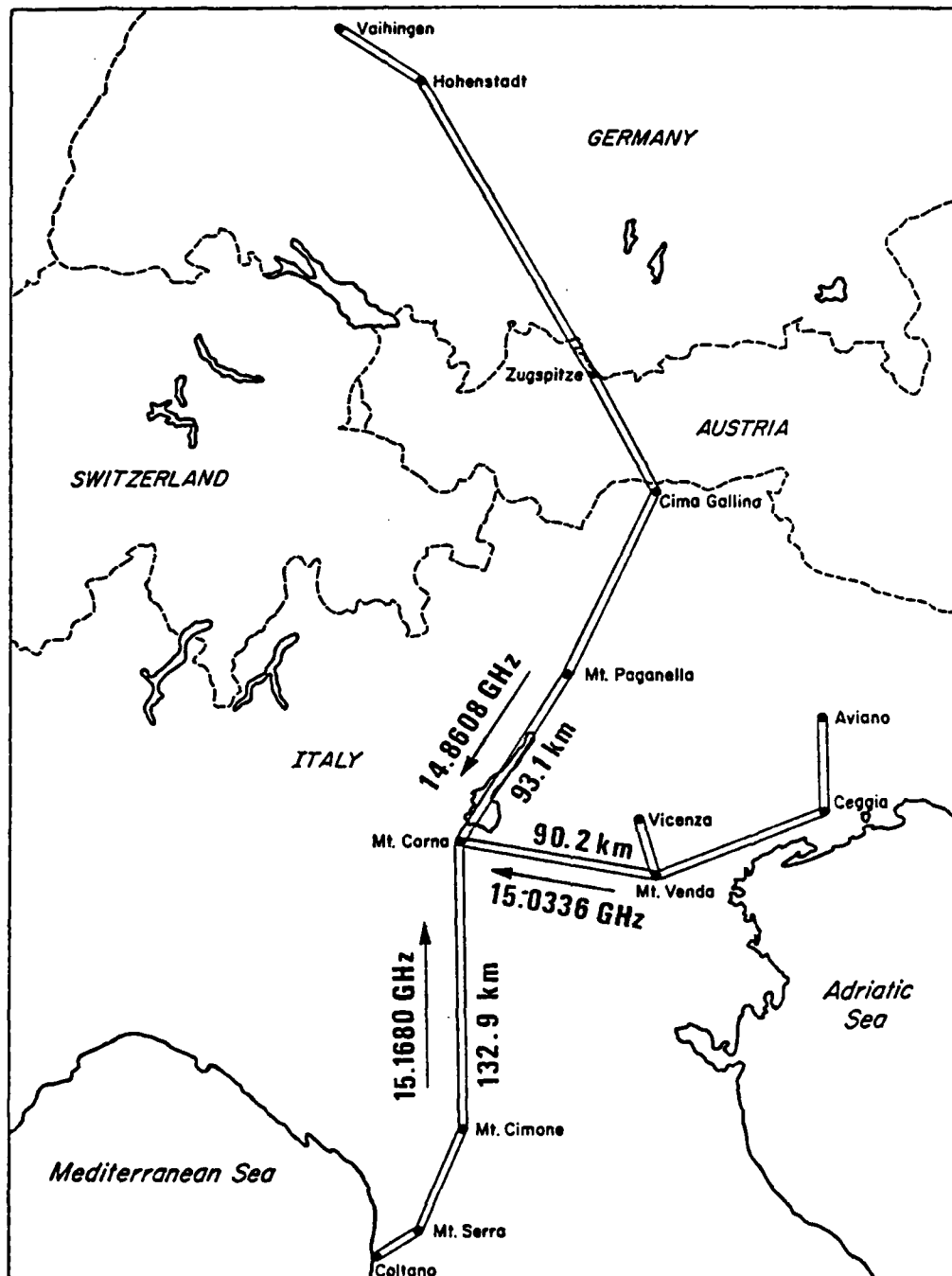
3. AMPLITUDE DISTORTION MEASUREMENTS ON LOS LINKS

Larry Hause
Institute of Telecommunications Sciences
National Telecommunications and Information
Administration
Boulder, CO

NOTE: The materials provided in this section are copies of the
visuals used with the extemporaneous remarks given by
Mr. Hause.

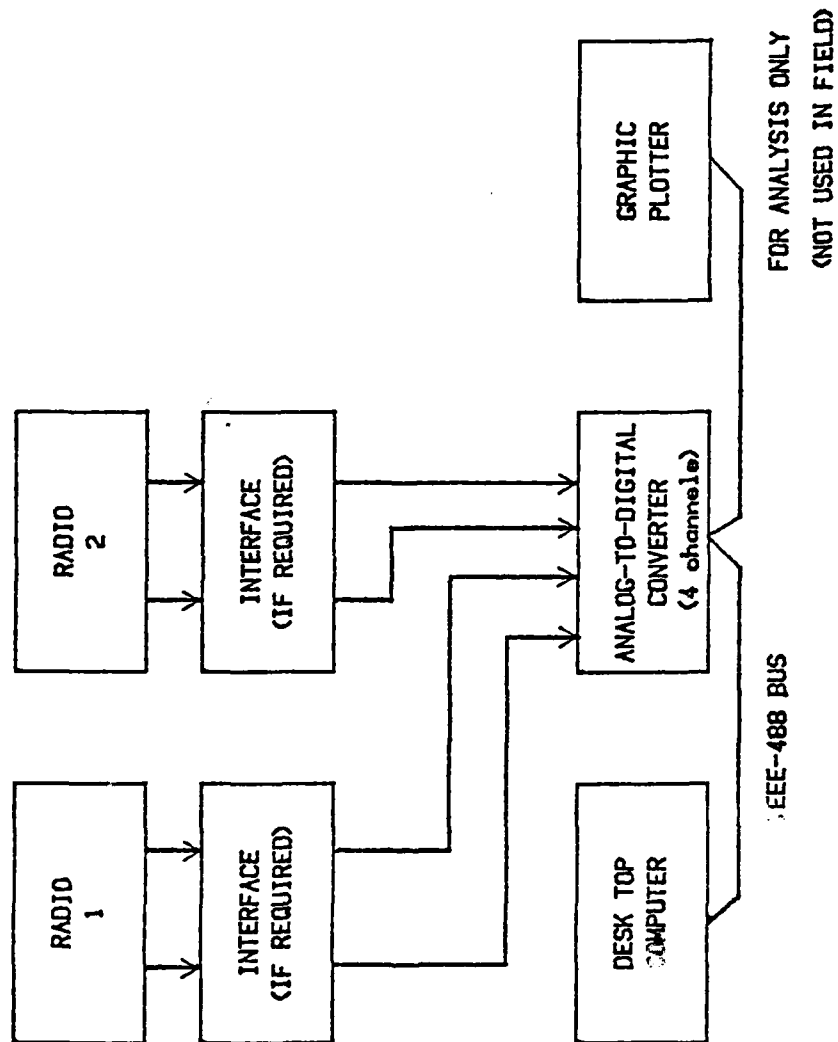
AMPLITUDE DISTORTION MEASUREMENTS
ON LOS LINKS

1. REVIEW PREVIOUS ITS WORK AT MT. CORNA, ITALY.
2. ENUMERATE THE PURPOSES OF THE PROPOSED
AMPLITUDE DISTORTION MEASUREMENTS.
3. DESCRIBE WHAT MEASUREMENTS WILL BE MADE.
4. DESCRIBE PROPOSED DATA ANALYSIS.

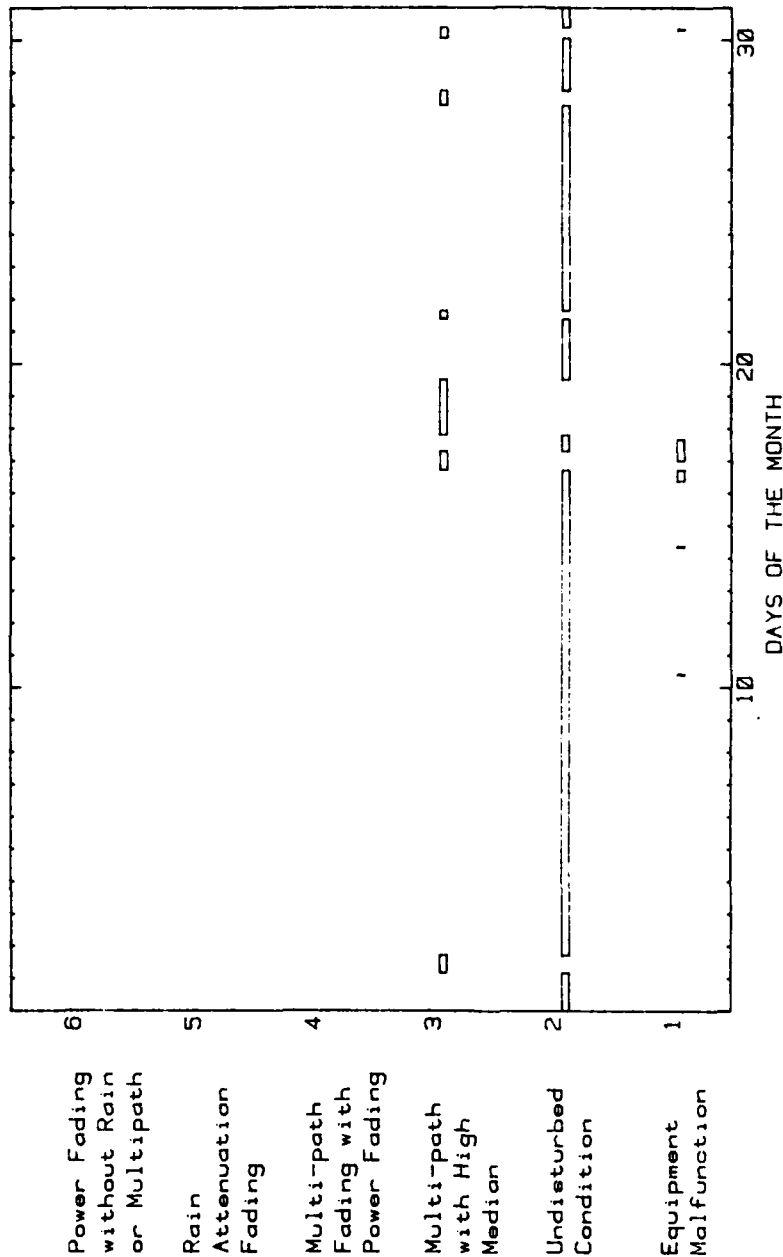


MEASUREMENTS THAT ITS HAS BEEN MAKING ON
THE CONVERGING PATHS AT MT. CORNA

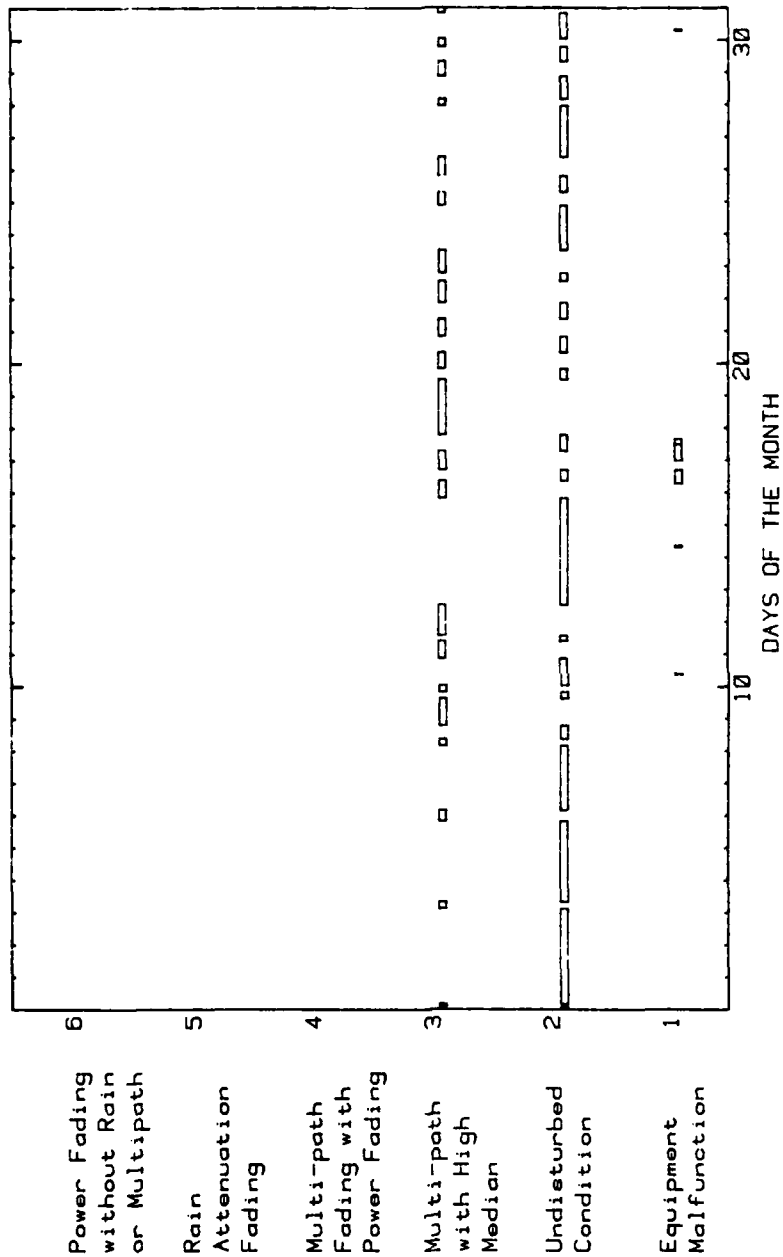
1. 1 YEAR OF RECEIVED SIGNAL LEVEL DATA.
2. DIVIDE THE DATA INTO 5 CATEGORIES.
3. ONE 15 GHz CHANNEL ON EACH PATH.
4. TWO 8 GHz CHANNELS ON EACH PATH EXCEPT
PAGANELLA - CORNA.
5. OBTAIN FADING DEPTH DISTRIBUTIONS FOR EACH
CATEGORY.
6. SHOW THE PERIODS THAT EACH FADING MODE
CATEGORY IS ACTIVE.



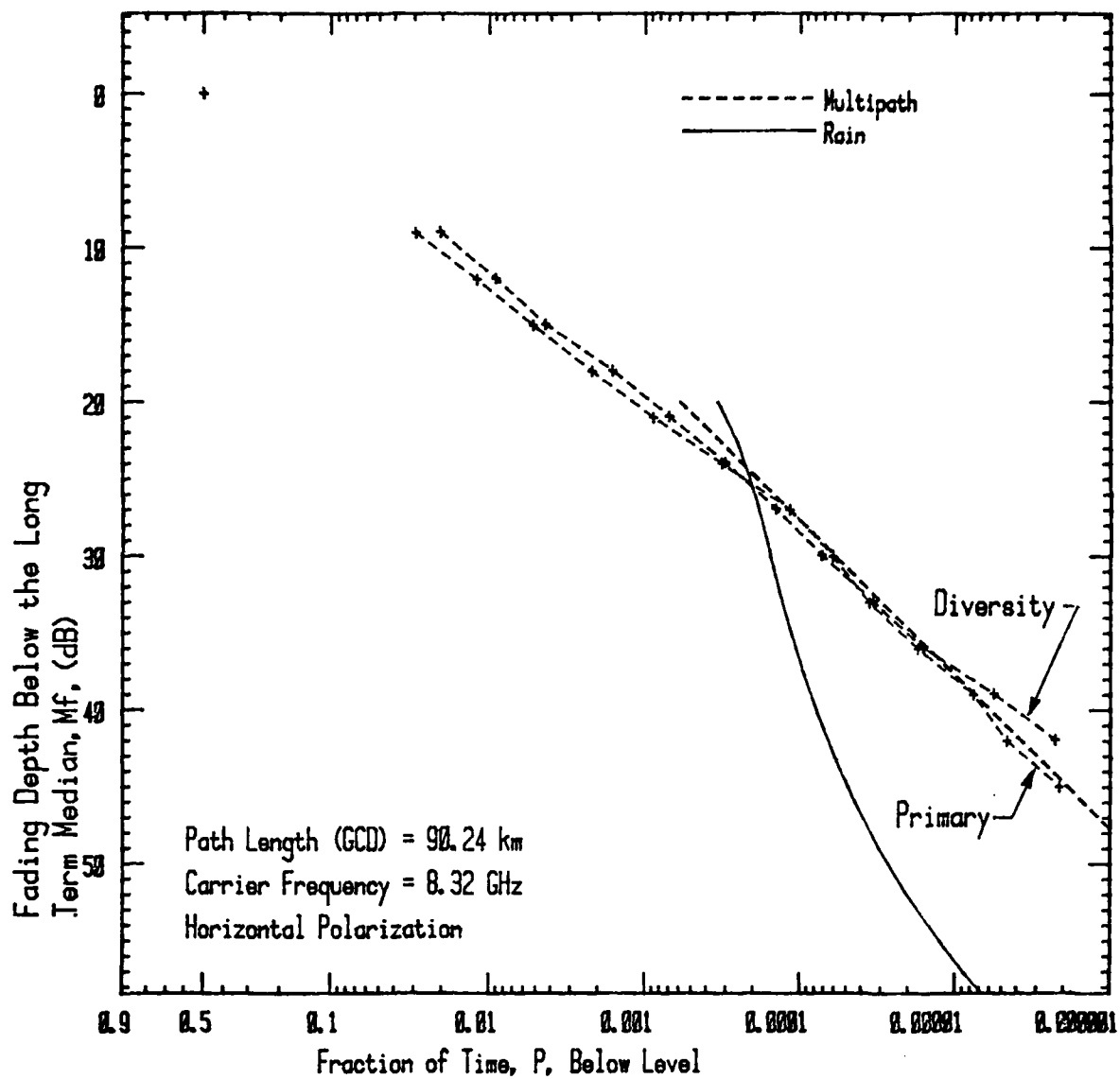
Block Diagram of RSL-3



Chronological occurrence of each data category for the path from Mt. Paganella to Mt. Corna 8 GHz primary receiver during May 1979.



Chronological occurrence of each data category for the path from Mt. Venda to Mt. Corna 8 GHz primary receiver during May 1979.



Terrain Type - average
 Avg. Annual Temp. = 27 °C

Wet Radome Loss per Ant. = 1.7 dB
 Mean Annual Rainfall = 800 mm
 No. of Rainy Days/yr. = 111
 Thunderstorm Ratio B = 0.15

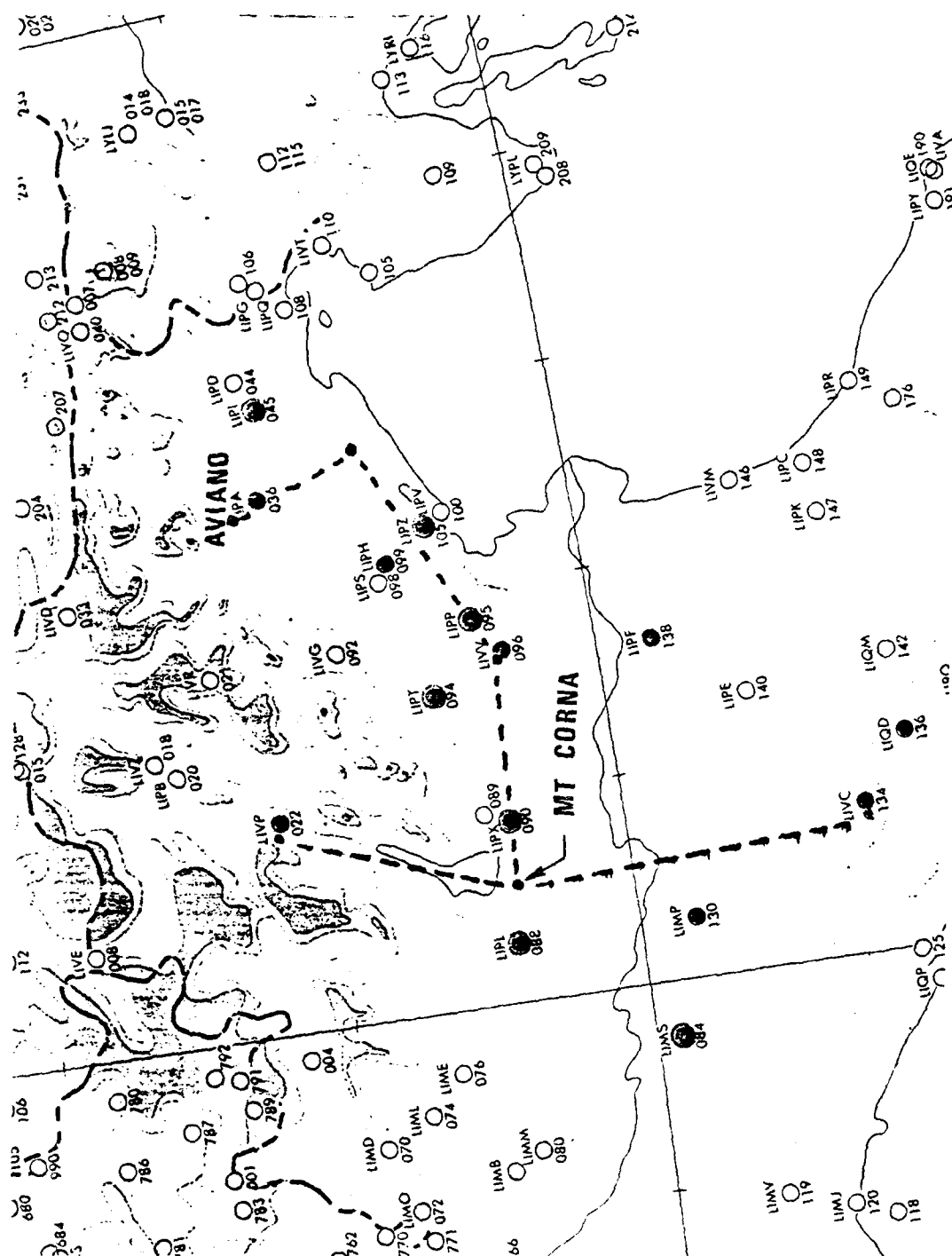
Multipath and rain loss variability for the path from Mt. Venda tower to Mt. Corna tower.

ITS MEASUREMENTS AT CEGGIA

1. PATHS CONVERGING AT CEGGIA ARE MONITORED.
2. THESE PATHS ARE MONITORED ONLY ON 8 GHz.
3. THE CEGGIA PATHS DO NOT MEET THE DESIRED CLEARANCE CRITERIA FOR LOS PATHS.

WEATHER STATISTICS GATHERED FOR ITS
BY AFCS

1. DATA FROM SEVEN WEATHER STATIONS.
2. DATA FROM MORE STATIONS ARE AVAILABLE BUT NOT APPLICABLE.
3. THE DATA IS PRIMARILY TEMPERATURE AND RAIN STATISTICS.



Location of meteorological data monitoring stations near the 8 and 15 GHz links.

PURPOSES OF THE AMPLITUDE
DISTORTION MEASUREMENTS

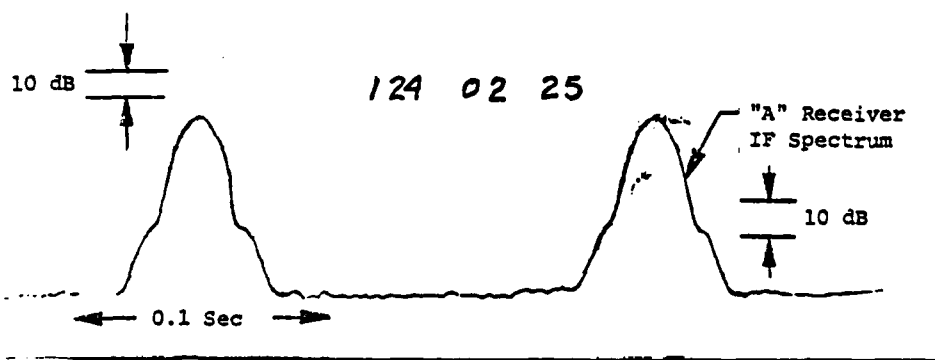
1. CAN WE DETECT THE DISTORTION?
2. HOW OFTEN DOES IT OCCUR?
3. WHAT IS THE RANGE OF SEVERITY?
4. WHAT EFFECT DOES THE DISTORTION HAVE
ON THE SYSTEM?

THE SYSTEM AND TYPES OF PATHS

1. ITS WILL MONITOR THE DEB SYSTEM IN NORTH CENTRAL ITALY.
2. IT IS A 12 MB/s SYSTEM WITH A 14 MHz BANDWIDTH AND 8 GHz CARRIERS.
3. IT USES THREE LEVEL PARTIAL RESPONSE MODULATION.
4. THERE ARE THREE LINE-OF-SIGHT PATHS WHICH TERMINATE AT THE RECEIVING AND RECORDING SITE.
5. TWO OF THE PATHS ARE ABOUT 90 KM AND ONE IS ABOUT 130 KM LONG.

DATA GATHERING

1. THE SPECTRUM FROM BOTH THE PRIMARY AND DIVERSITY RADIOS WILL BE MONITORED.
2. THE SIGNALS WILL BE MONITORED PRIMARILY DURING PERIODS OF MULTIPATH FADING.
3. THE SIGNALS WILL BE MONITORED OVER A PERIOD OF TWO MONTHS ON VARIOUS OF THE THREE PATHS.
4. THE IF SPECTRUM WILL BE MONITORED AT A TEST POINT AFTER AGC ACTION.

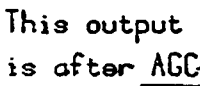


RECORDER CHANNELS

1. TIME CODE.
2. SPECTRUM ANALYZER SAW TOOTH.
3. SPECTRUM WITH FREQUENCY MARKER.
4. RECEIVED SIGNAL LEVEL.
5. IDENTITY OF RECEIVER ON LINE.
6. FRAME VIOLATION EVENTS.
7. FORMAT VIOLATION EVENTS.

DATA ANALYSIS

1. ITS WILL OBTAIN SPECTRAL DENSITY GAIN DIFFERENCE VALUES IN DB FOR CORRESPONDING FREQUENCIES.
2. A STANDARD SPECTRUM OBTAINED DURING A QUIET RSL PERIOD WILL BE USED FOR COMPARISON.
3. ALL SIGNAL DIGITIZING THAT IS REQUIRED WILL BE DONE AT ITS LABS IN BOULDER, CO.
4. DATA SEARCHES WILL BE MADE ON BOTH THE BASIS OF FRAME/FORMAT EVENTS AND MAGNITUDE OF SPECTRAL DENSITY DIFFERENCES.



DATA CLASSIFICATION SPECIFICATIONS

The purpose of these specifications is to categorize the RSL data within each hour in terms of the various types of mechanisms that are operating on the radio path or possible adverse equipment situations that prevailed within the hour. These specifications are used to prepare a data analysis log so that data contaminated by equipment malfunction can be removed and so that data having the characteristics typical of certain fading mechanisms are properly classified and can be checked against meteorological data and site operations log entries. The log is needed in order that signal level time distributions can be prepared for the various propagation mechanisms of interest.

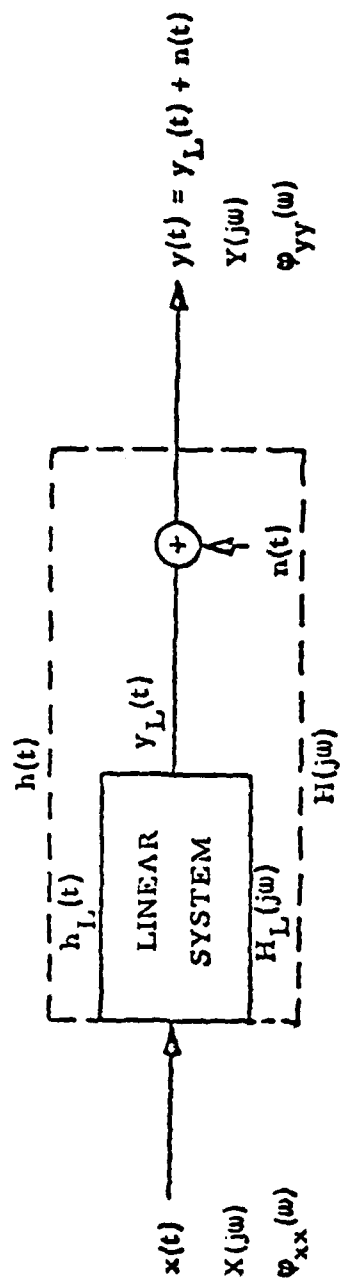
Six types of received signal level recording, hourly period classifications will be used:

1. (Equipment Malfunction, EM)
Communications or test equipment malfunction such that data taken on that particular channel should not be used.
2. (Undisturbed Condition, UC)
Essentially undisturbed signal level period during which the signal does not fade even momentarily more than 10 dB below the long term median.
3. (Multipath with High Median, MHM)
A period during which multipath fading occurs (greater than 10 dB below the median) but the hourly median signal level does not fade more than 6 dB below the long term median signal level.
4. (Multi-path Fading with Power Fading, M&P)
A period during which multipath fading occurs (greater than 10 dB below the hourly median) but the hourly median is also depressed by more than 6 dB below the long term median.
5. (Rain Attenuation Fading, RA)
A period of rain attenuation fading (greater than 10 dB below the long term median at some time during the hour). Rain attenuation fading leaves a distinctive trace on the chart recorder and also produces highly correlated recordings between the primary and space diversity channels.
6. (Power Fading without Rain or Multipath, PF)
A period of depressed median signal level (greater than 6 dB) but without multipath or rain attenuation characteristics.

4. OVERVIEW OF MULTIPATH MEASUREMENTS USING A PN PROBE

Bob Hubbard
Institute of Telecommunications Sciences
Boulder, CO

NOTE: The materials provided in this section are copies
of the visuals used with the extemporaneous remarks
given by Dr. Hubbard



$$y(t) = h(t) \otimes x(t) \quad (1)$$

$$y(t) = \int H(j\omega) X(j\omega) e^{j\omega t} d(\omega/2\pi) \quad (2)$$

$$Y(j\omega) = \int \{h(t) \otimes x(t)\} e^{-j\omega t} dt \quad (3)$$

$$Y(j\omega) = H(j\omega) \cdot X(j\omega) \quad (4)$$

MODEL OF A LINEAR SYSTEM

THE WIENER RELATIONSHIP

1. FREQUENCY TRANSFER FUNCTION

$$\Phi_{yy}(\omega) = |H(j\omega)|^2 \Phi_{xx}(\omega) \quad (1)$$

$$\Phi_{xy}(\omega) = H(j\omega) \Phi_{xx}(\omega) \quad (2)$$

2. IMPULSE RESPONSE FUNCTION

$$R_{xy}(\tau) = h(\tau) \otimes R_{xx}(\tau) \quad (3)$$

Since $h(t) = F \left\{ H(j\omega) \right\}$

$$R_{xx}(\tau) = F \left\{ \Phi_{xx}(\omega) \right\}$$

$$R_{xy}(\tau) = F \left\{ \Phi_{xy}(\omega) \right\}$$

Where $F \left\{ \right\}$ denotes a Fourier transform.

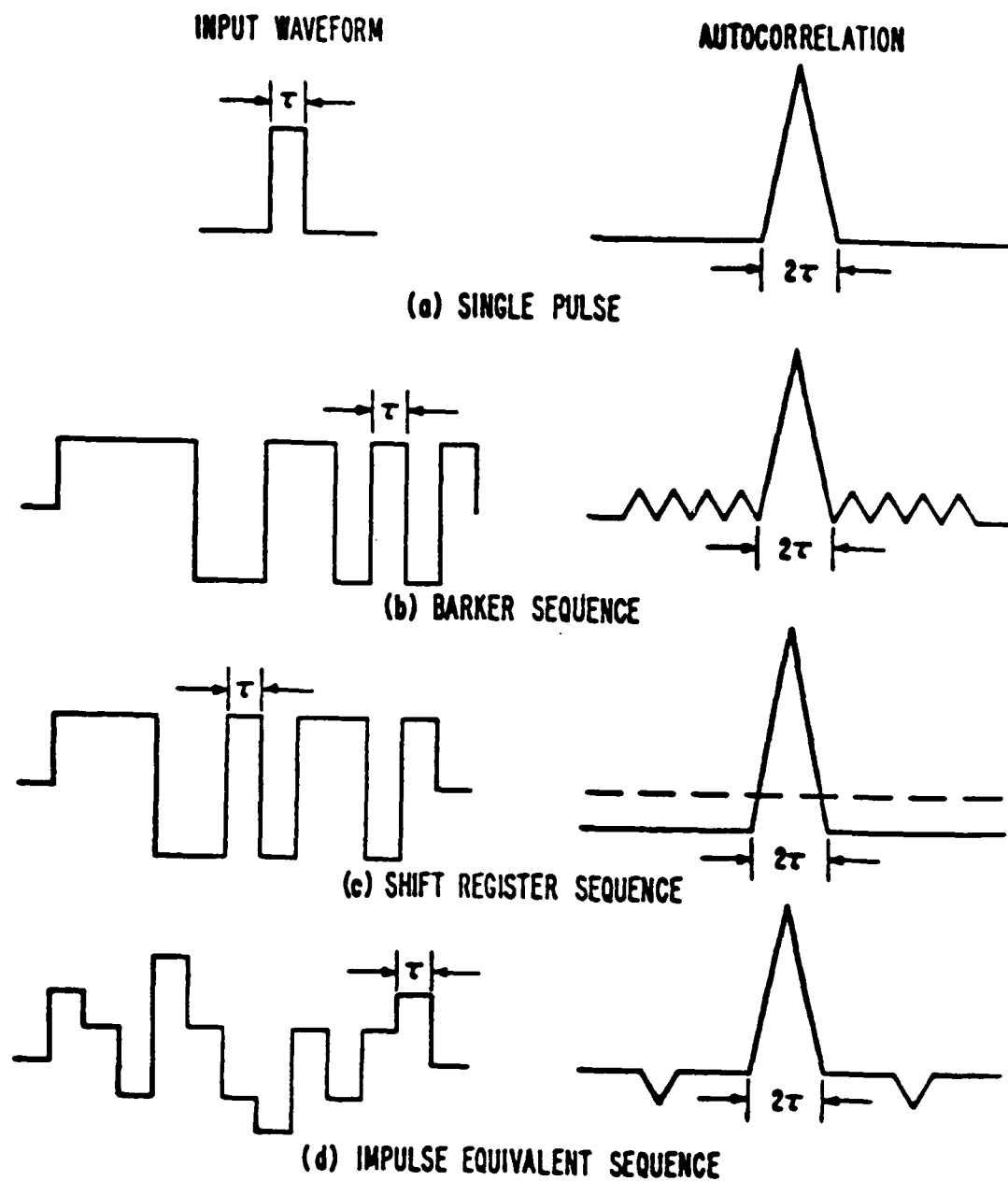
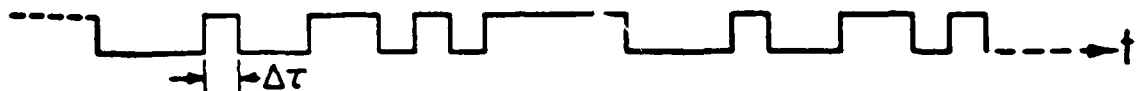


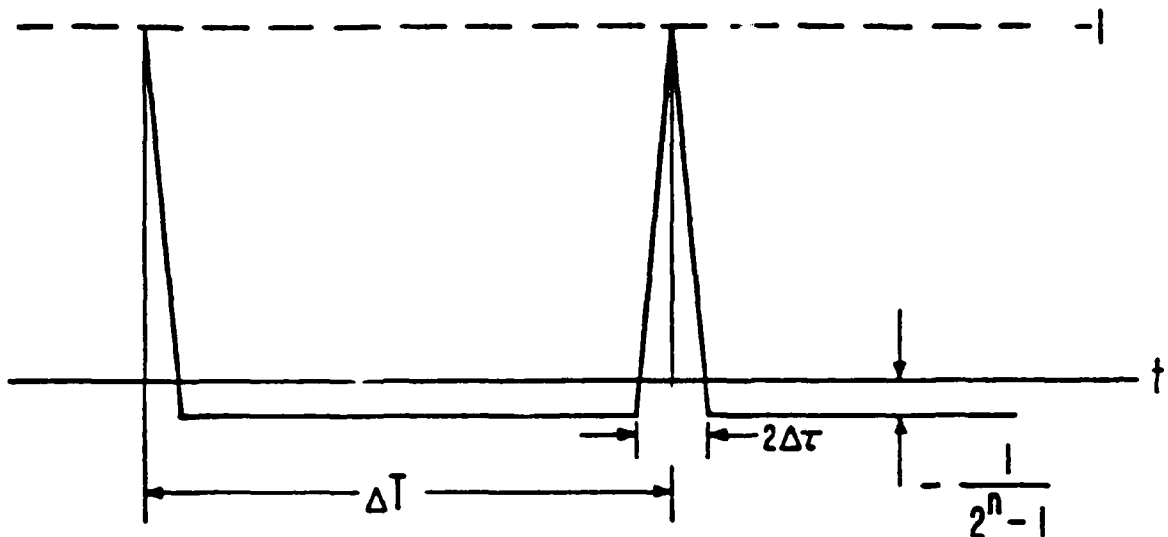
Figure 5. Example of signalling waveforms and their autocorrelation functions.

0 0 0 1 0 0 1 1 0 1 0 1 1 1 0 0 0 1 0 0 1 1 0 1

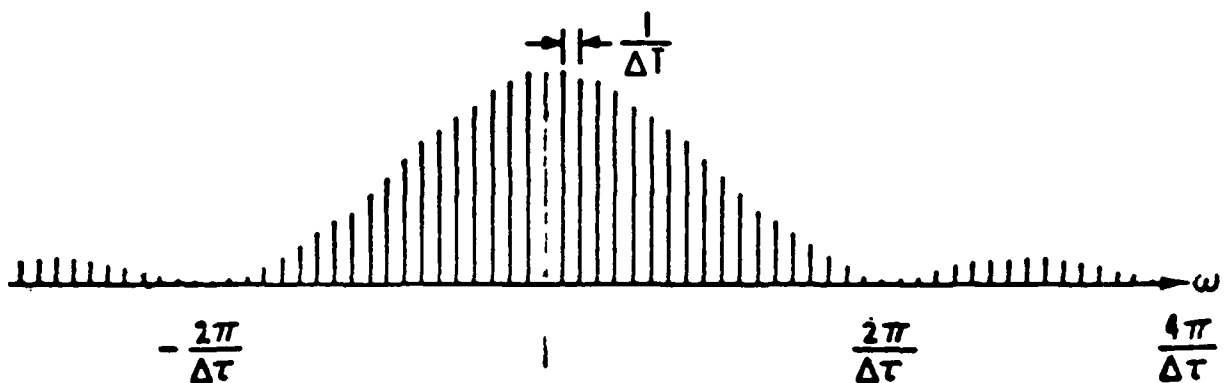
(a) BINARY SEQUENCE



(b) RECTANGULAR WAVEFORM

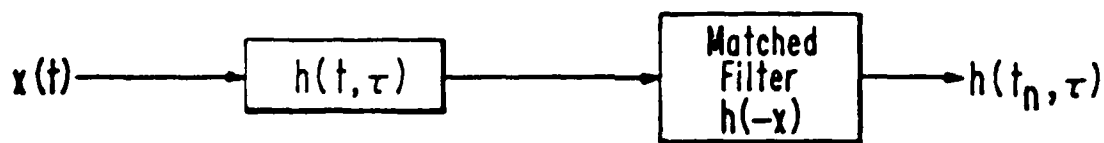


(c) NORMALIZED AUTOCORRELATION FUNCTION

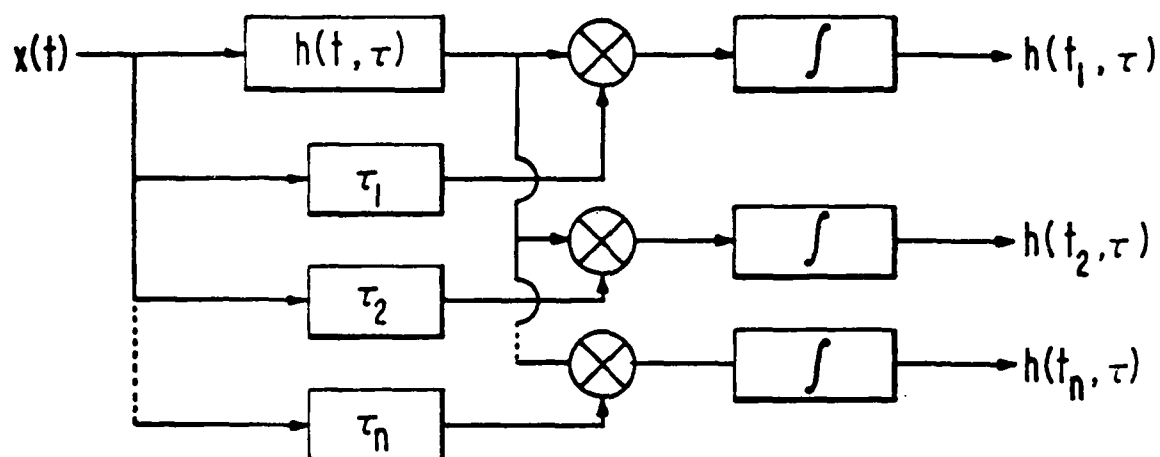


(d) POWER SPECTRUM

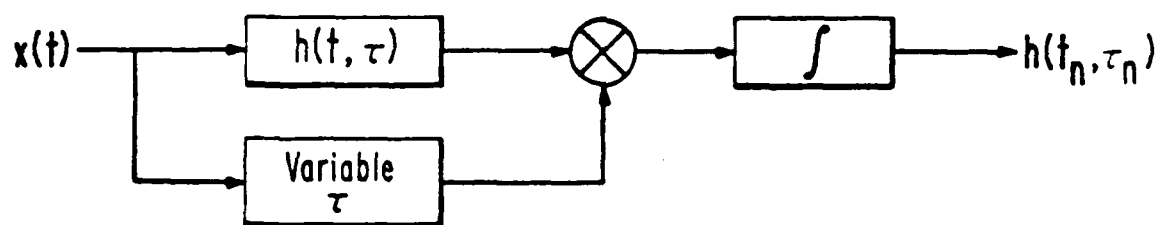
Figure 13. Maximum length shift register sequence characteristics.



(a) MATCHED FILTER TECHNIQUE



(b) MULTIPLE CORRELATORS



(c) TIME MULTIPLEXED CORRELATOR

Figure 2. Simplified block diagram of measurement schemes.

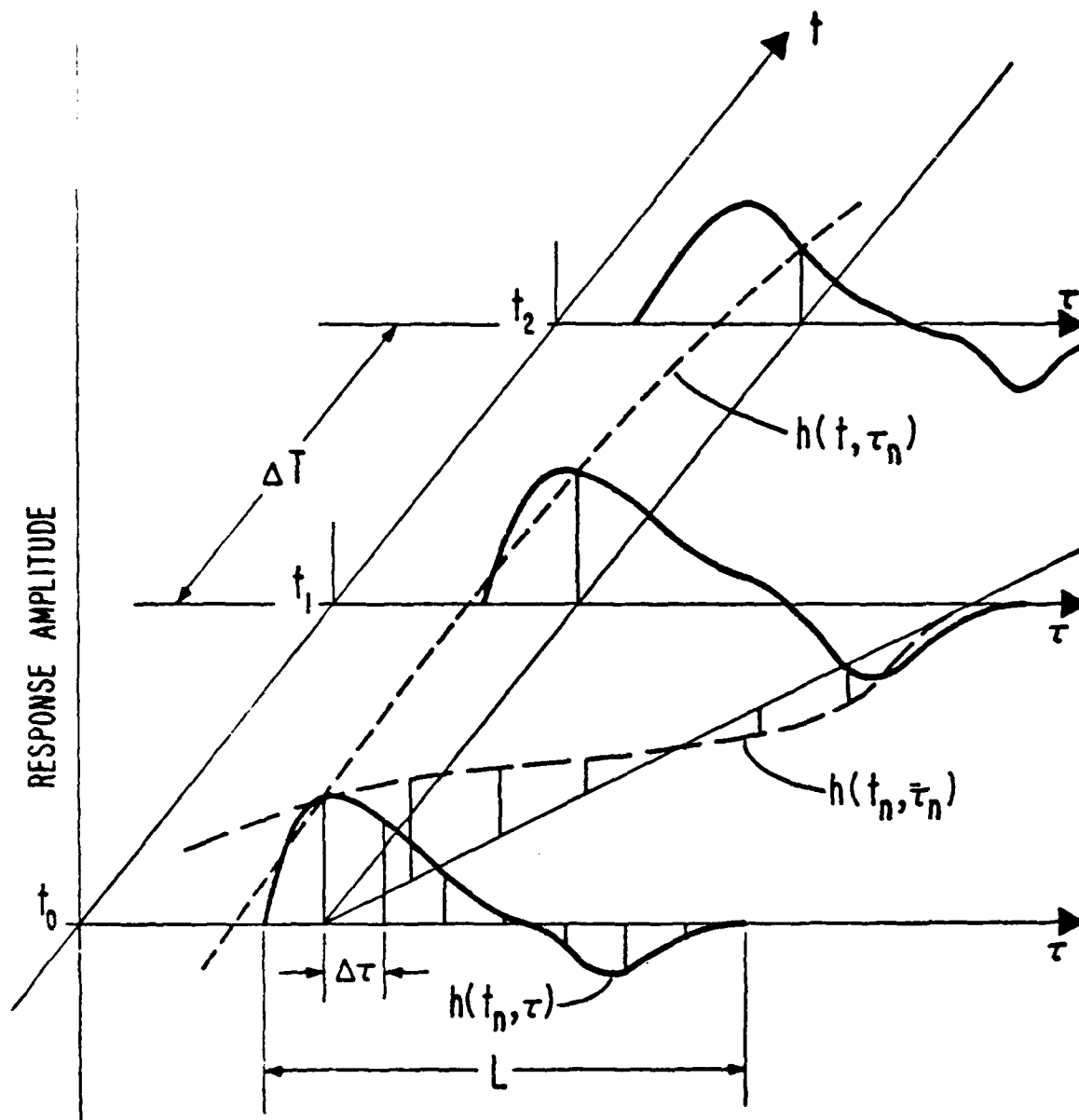


Figure 1. Time variant filters response representations.

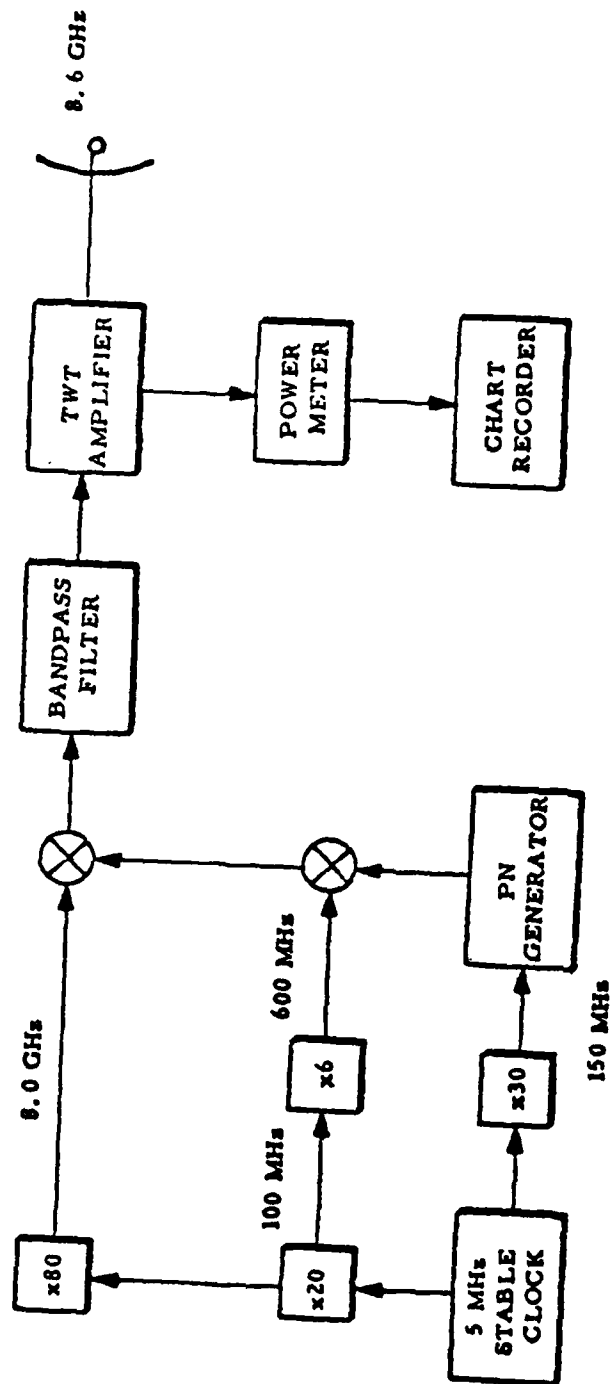
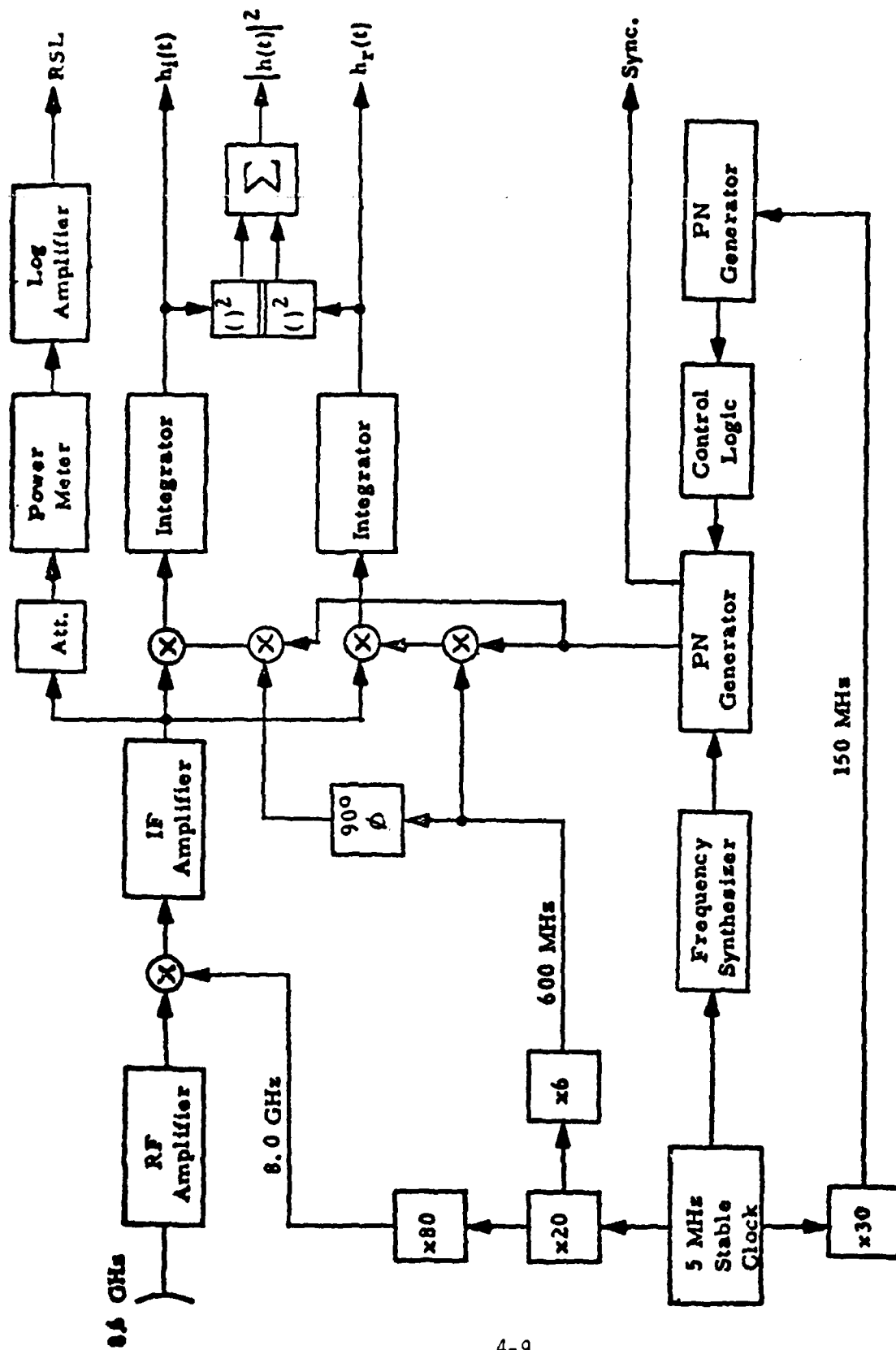


Figure 1. Block diagram of the ITS Channel Probe transmitter.



RECEIVER FOR 8.6 GHz CHANNEL PROBE

Figure 4.

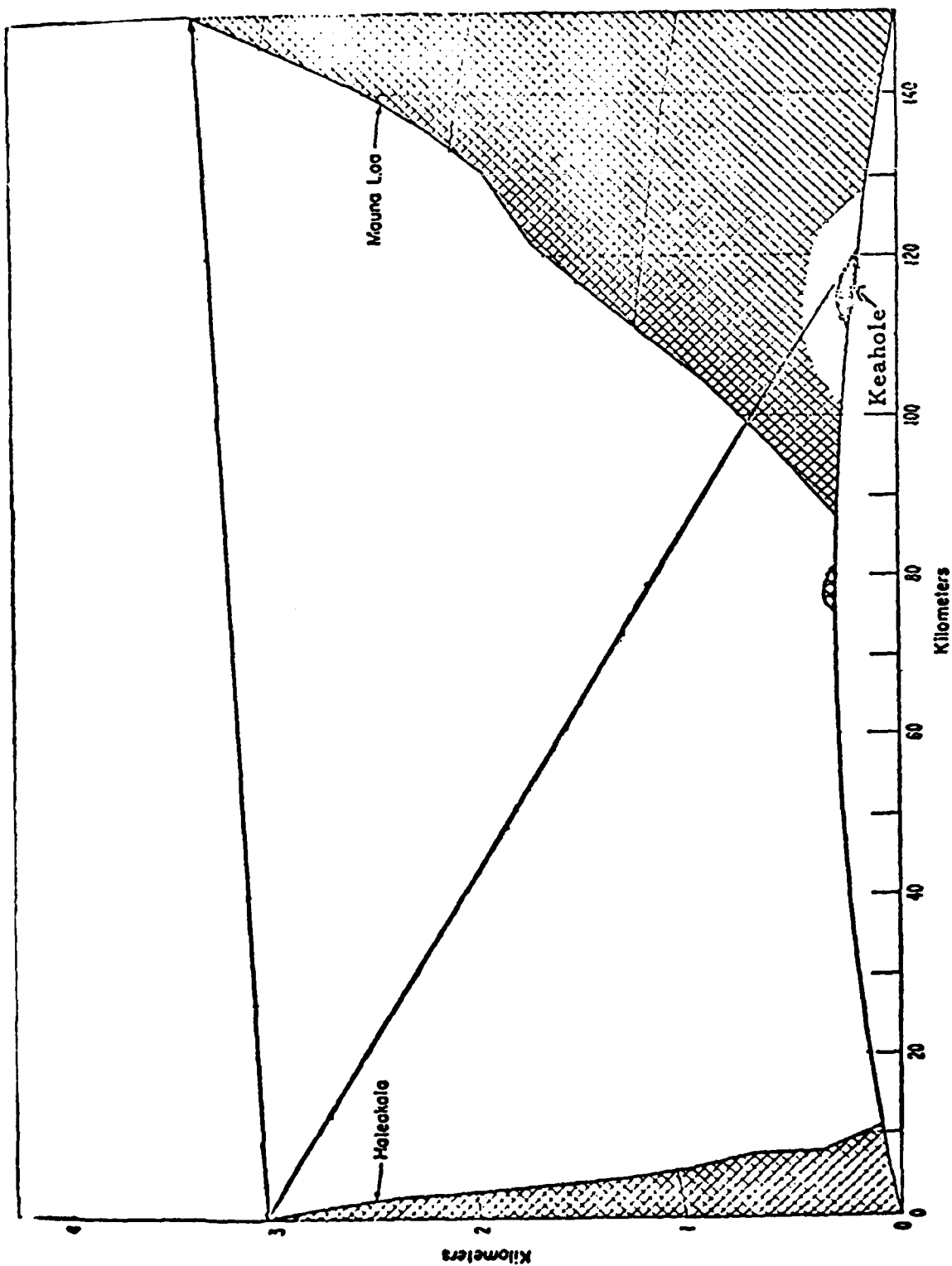


Figure 4. Profiles of proposed paths simulating air-to-ground and air-to-air geometries.

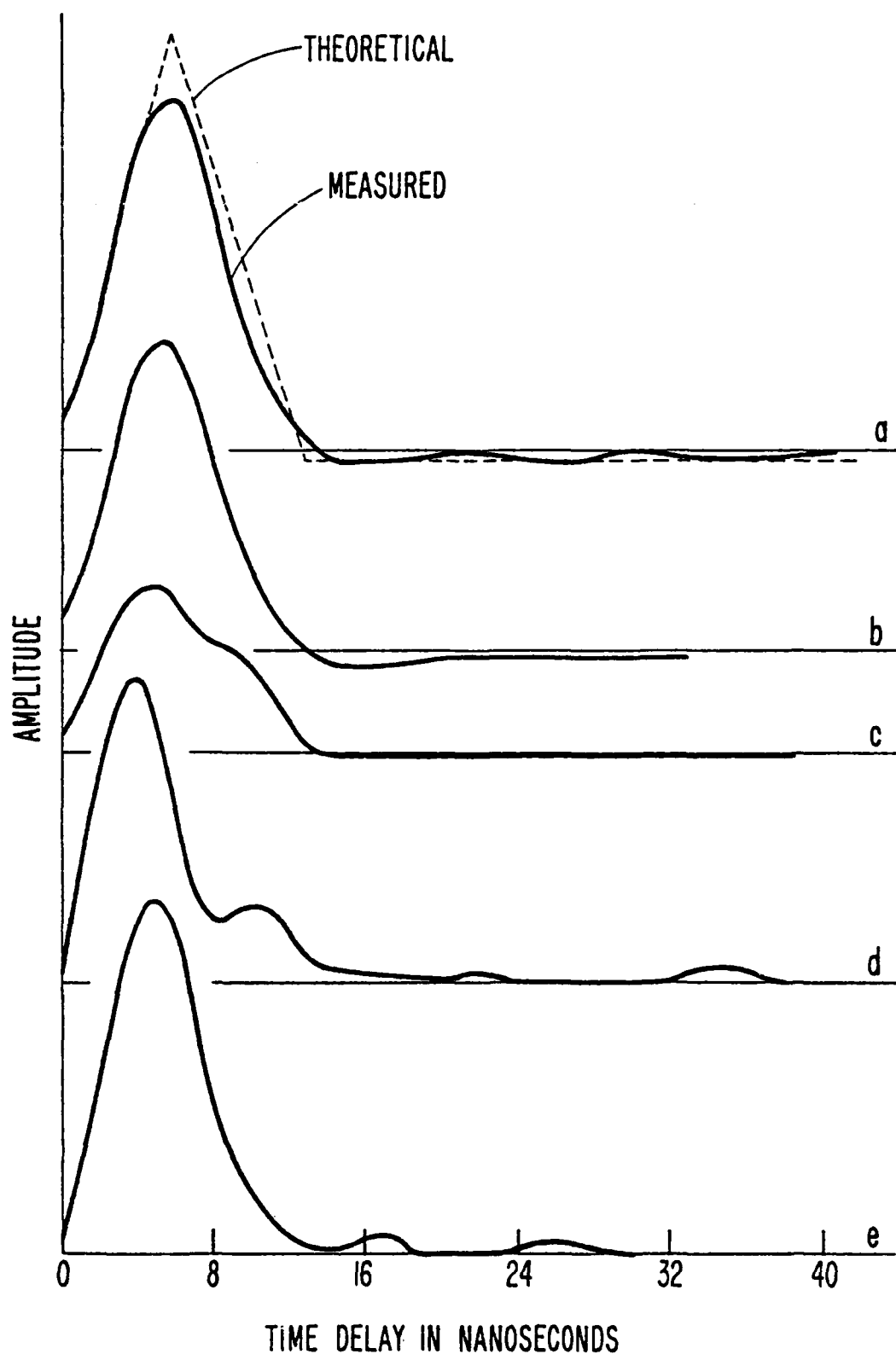


Figure 17. Impulse response between Haleakala and Kona, Hawaii, March 18, 1974 at 2 second intervals.

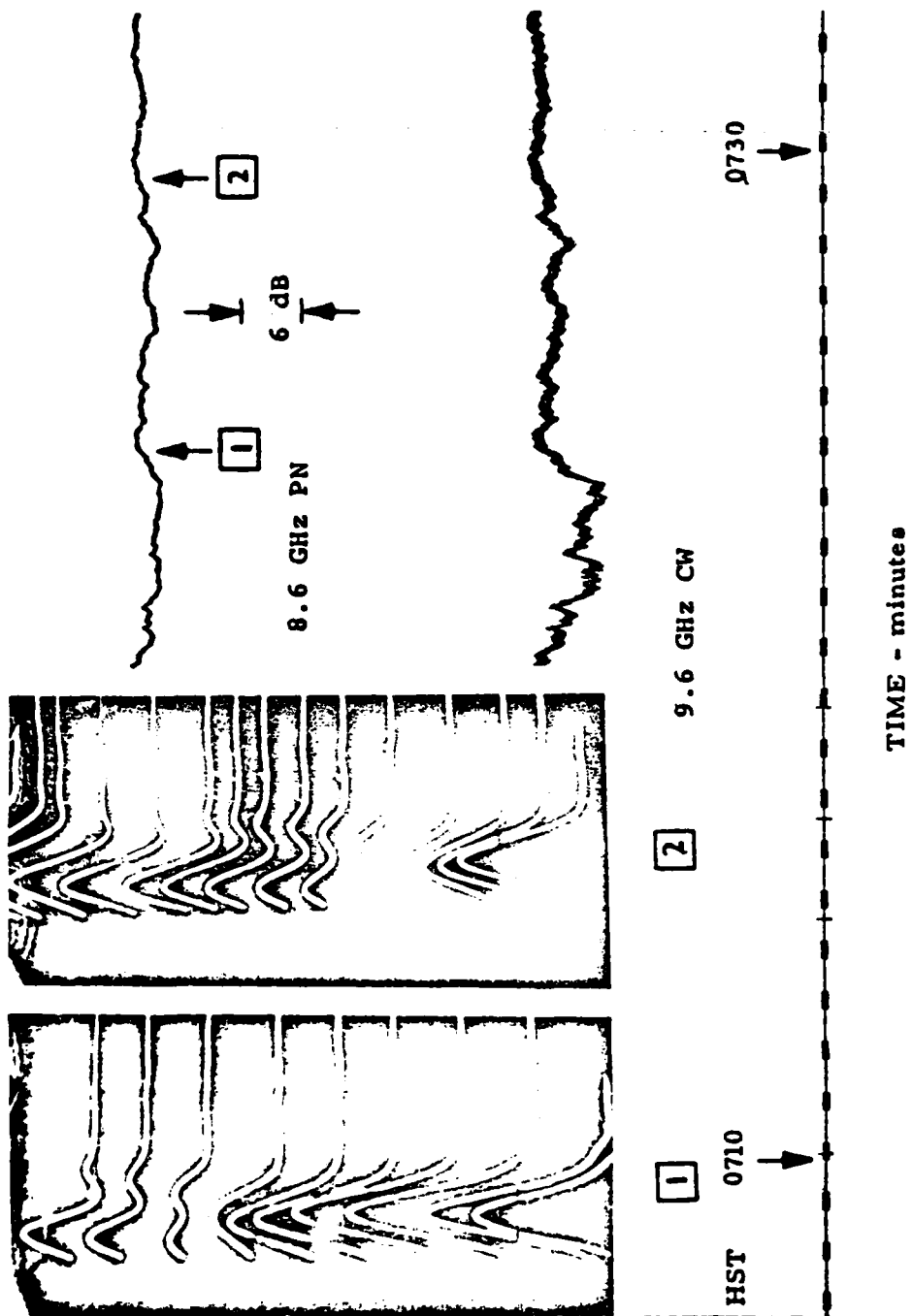


Figure 5. Sample of the fading records over the Keahole-Haleakala path on 20 March 1974.

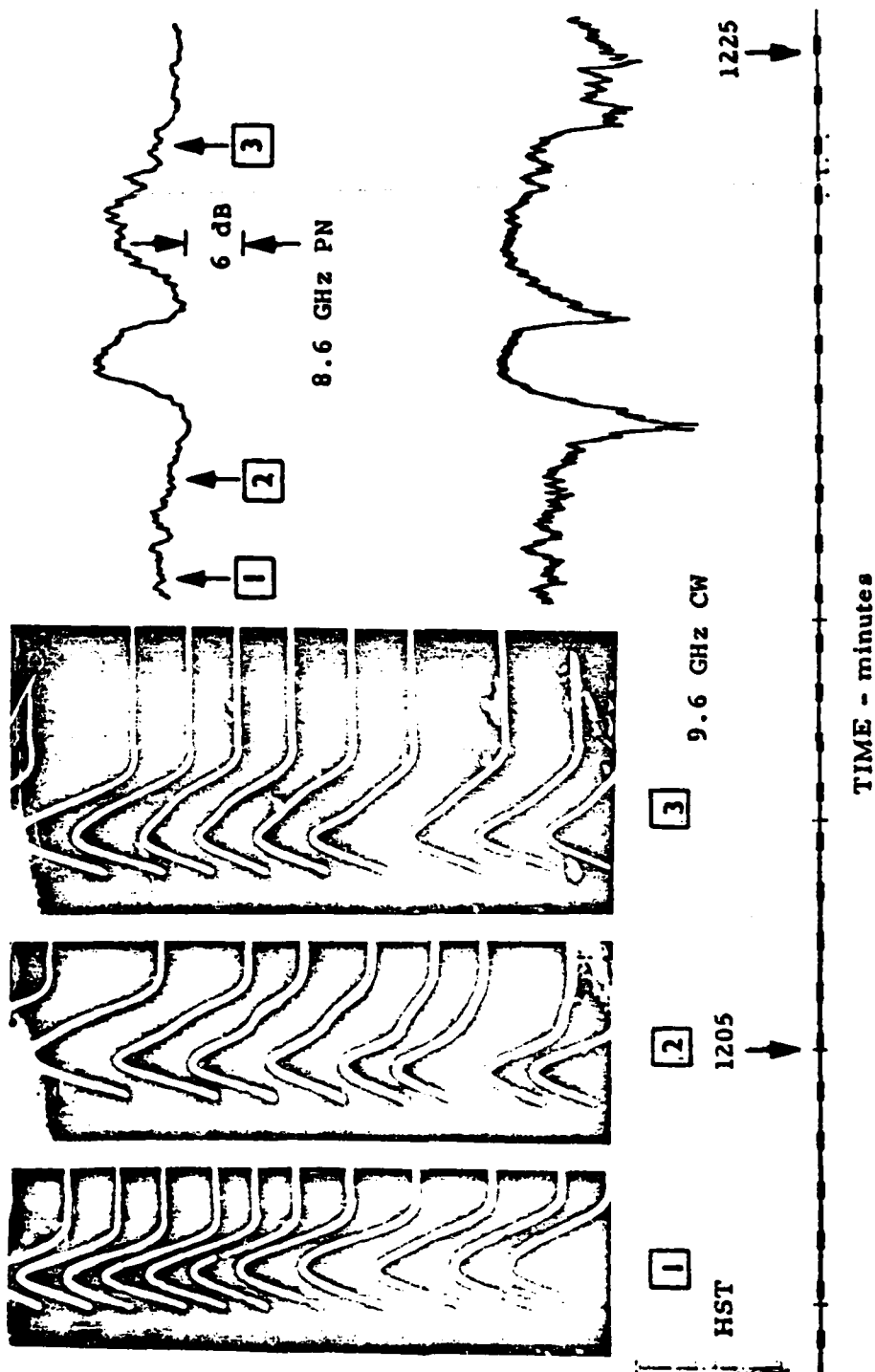


Figure 6. Sample of the fading records over the Keahole-Haleakala path on 24 March 1974.

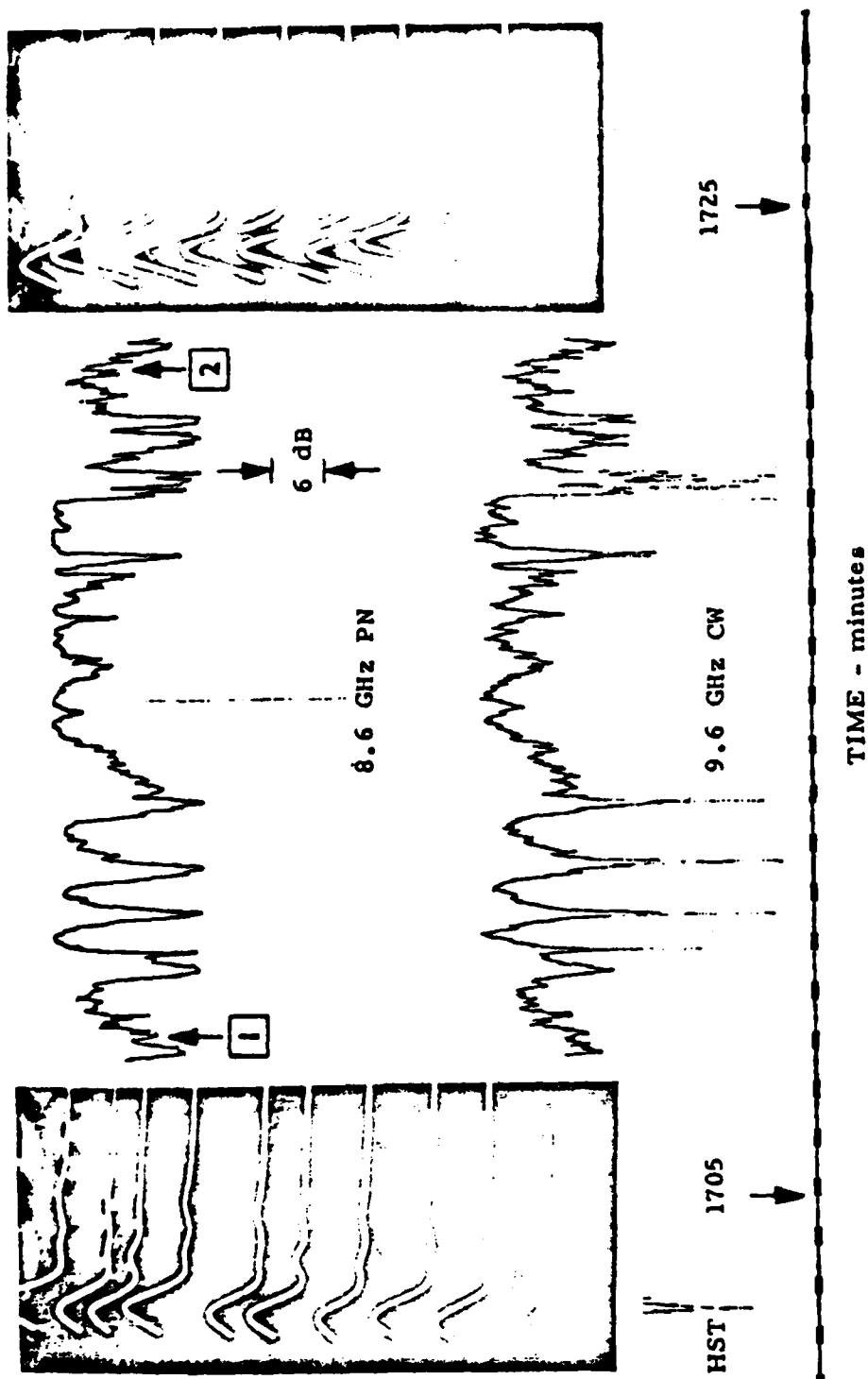
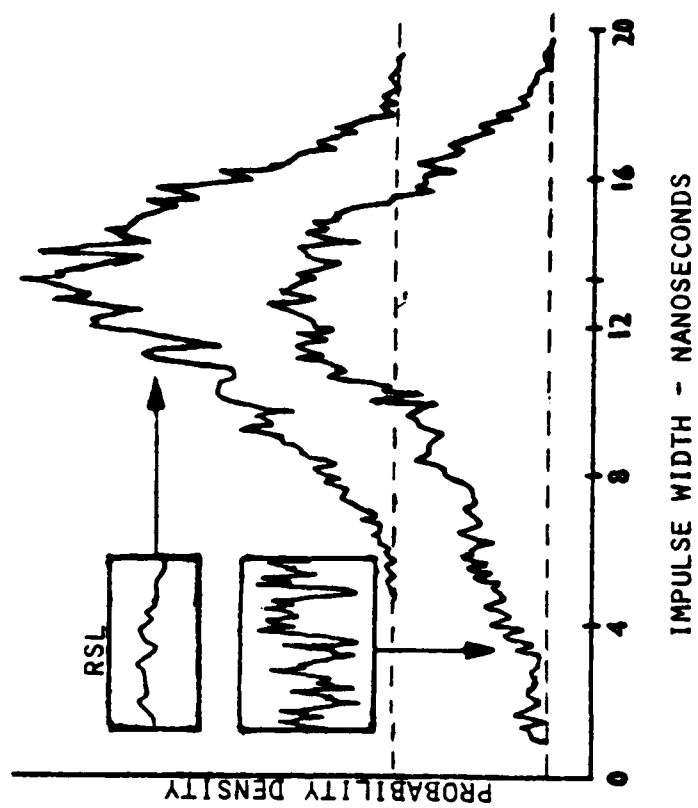
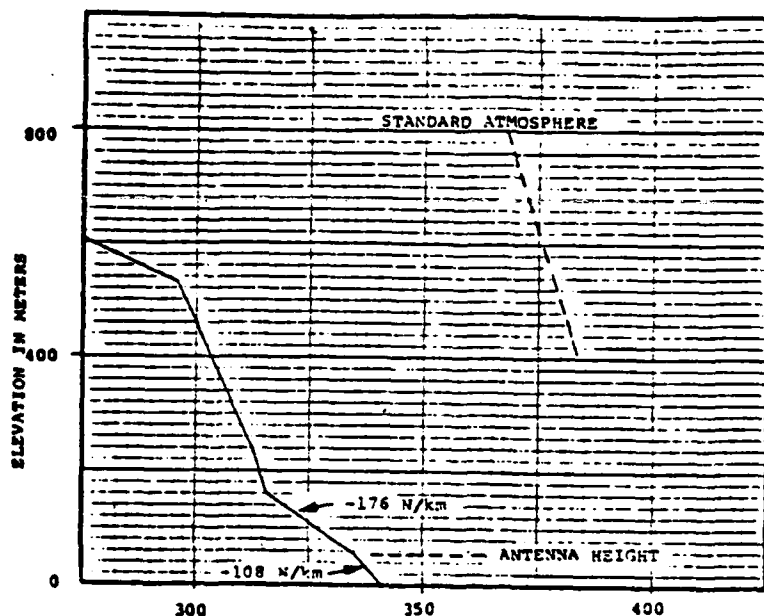


Figure 7. Sample of the fading records over the Keahole-Haleakala path on 2 August 1974.





(a) Refractivity profile measured at 1700 CST on 18 November, 1976.

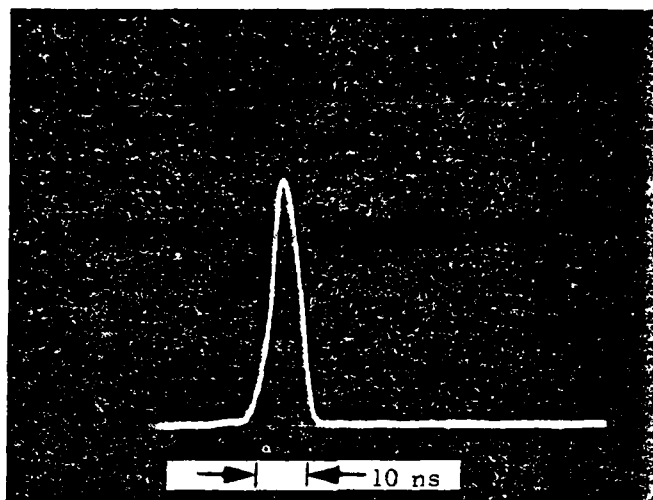


(b) Impulse response during ducting (+7 dB).

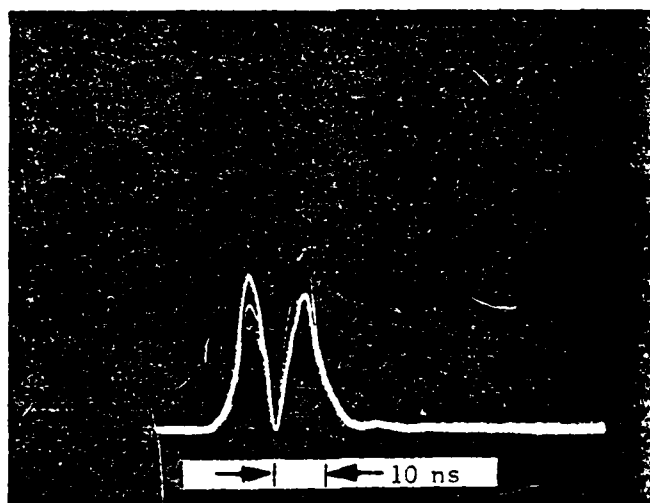


(c) Impulse response during a 15 dB fade.

Figure 12. Refractivity profile and power impulse responses recorded during a ducting propagation condition along the Gulf Coast of Florida.



(a) Clear channel response; impulse width is 13.3 ns.



(b) Response with a multipath component delayed 10 ns.

Figure 3. Examples of the power impulse response measured over the SNI-LP link with a PN clock rate of 150 MHz.

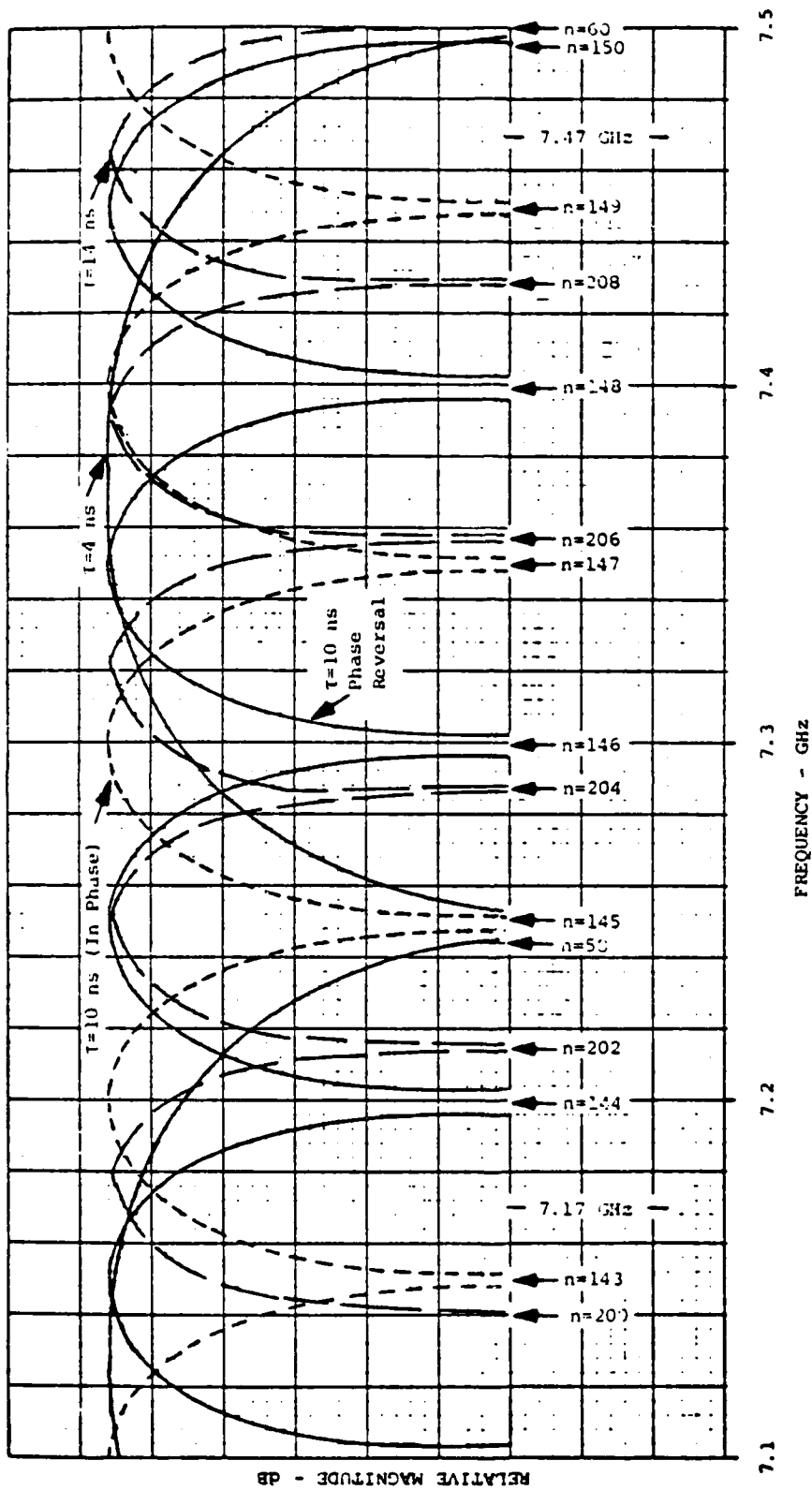
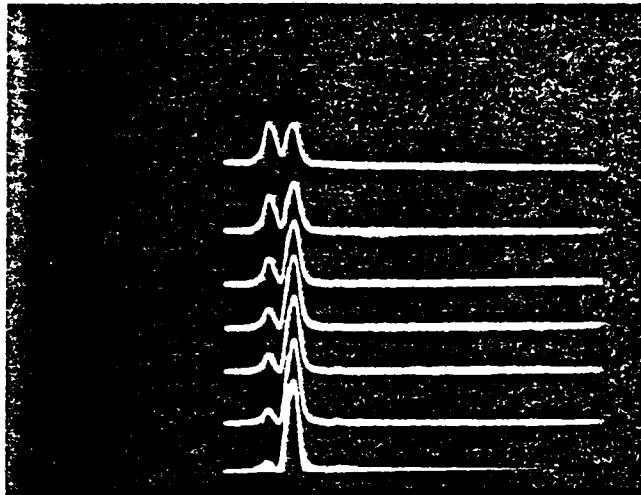
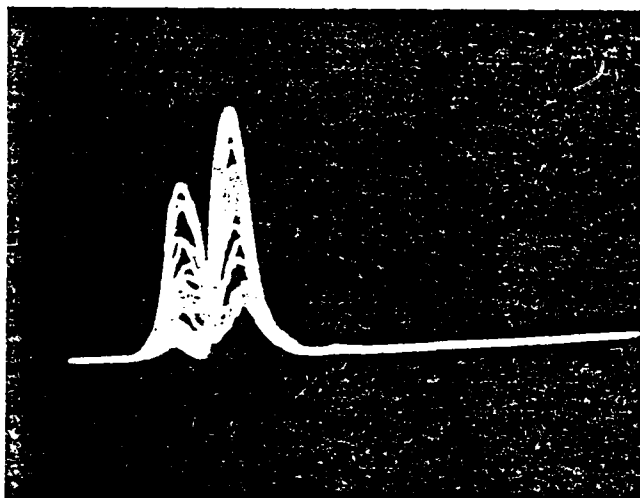


Figure 4. The theoretical frequency transfer function for a channel with a multipath component equal in magnitude to the direct component, at the delay times indicated.

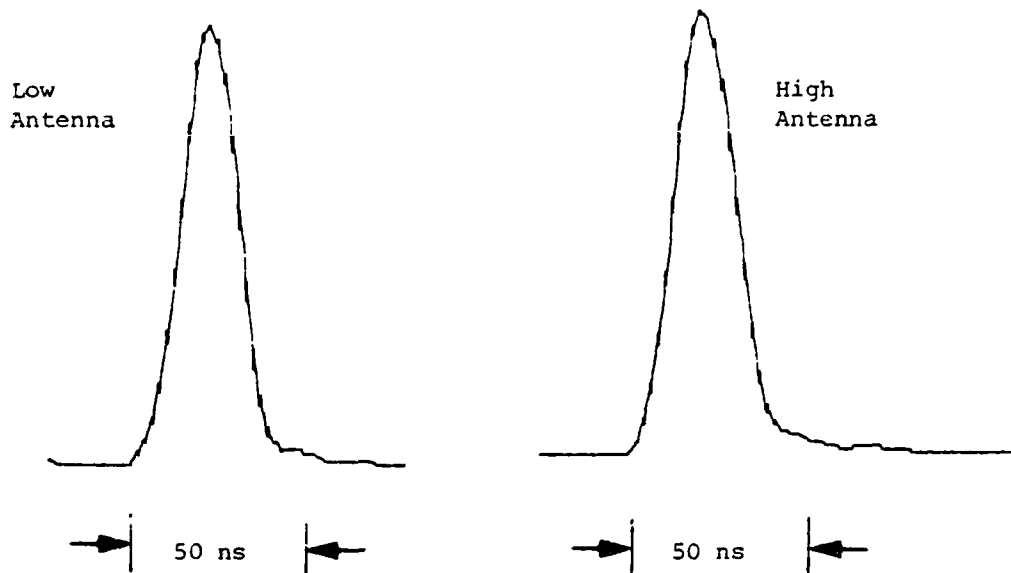


(a) Sequential responses, 500 ms apart from top to bottom.

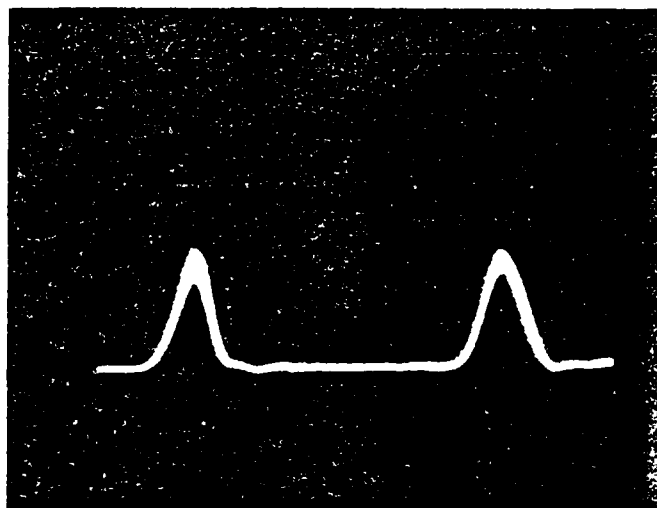


(b) Time-lapse photograph of the sequence in (a) on an expanded scale.

Figure 7. An example of the dynamic magnitude change between multipath components.

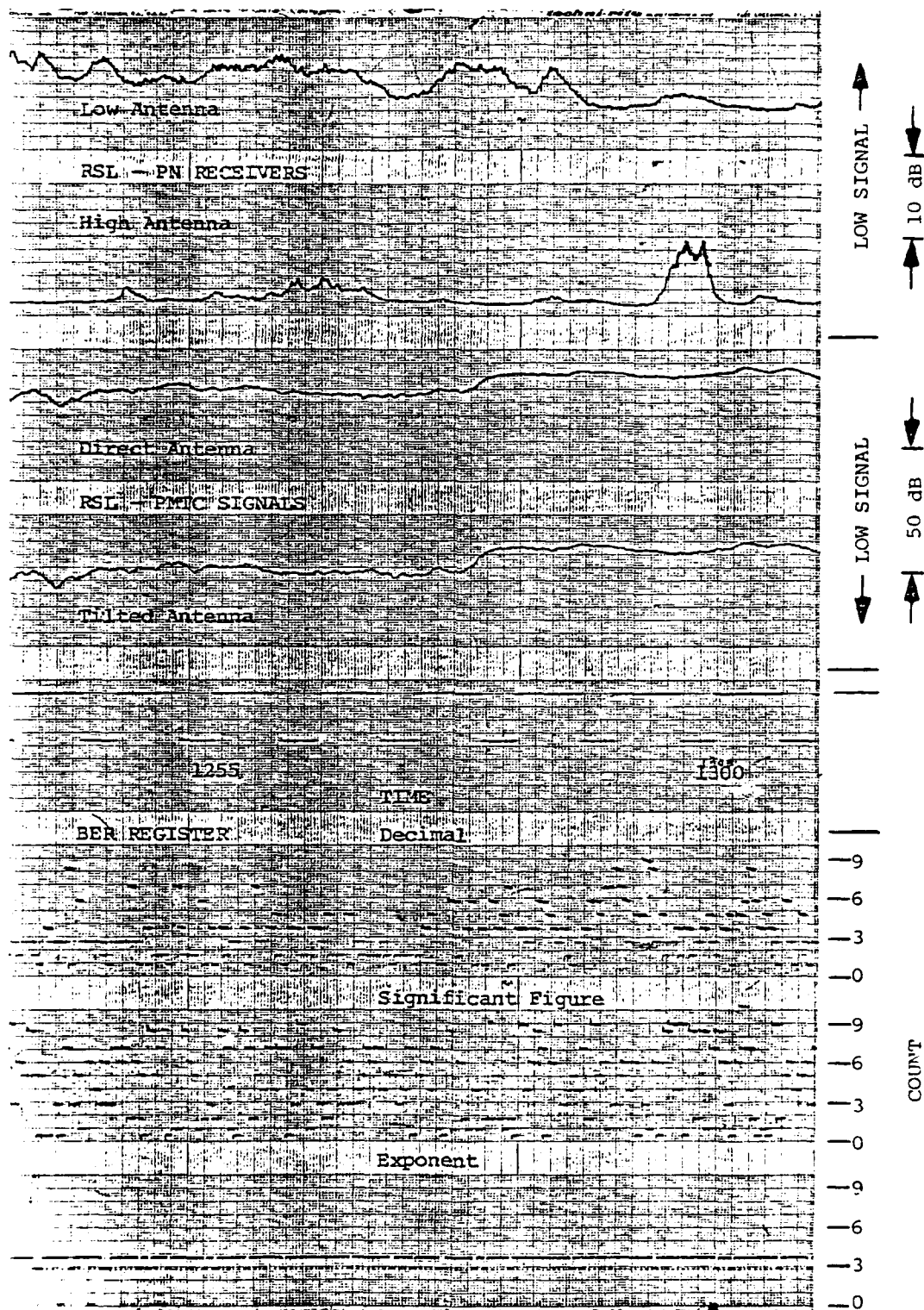


(a) Five-minute time averages.

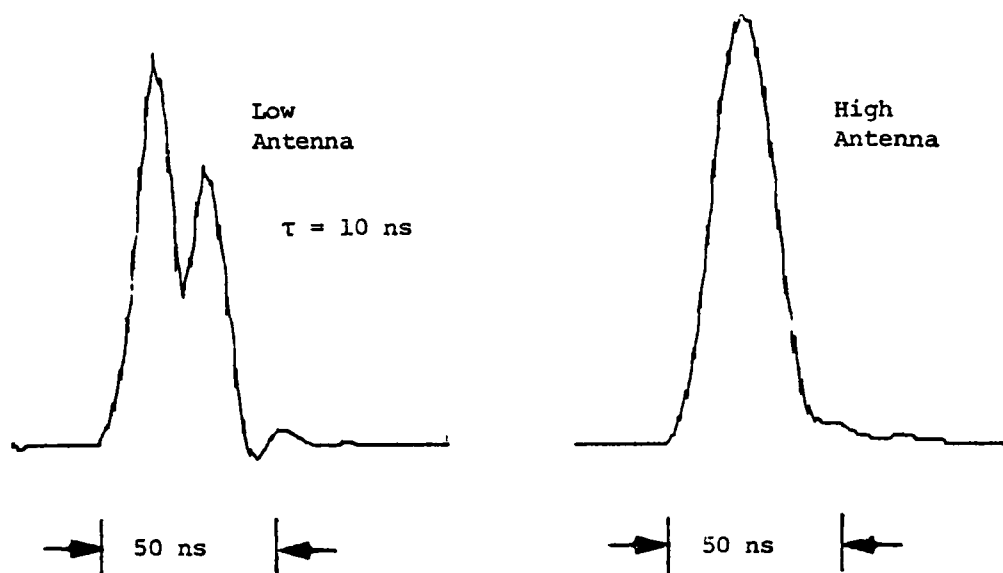


(b) Time-lapse photograph of 20 s period at 1256 PST.

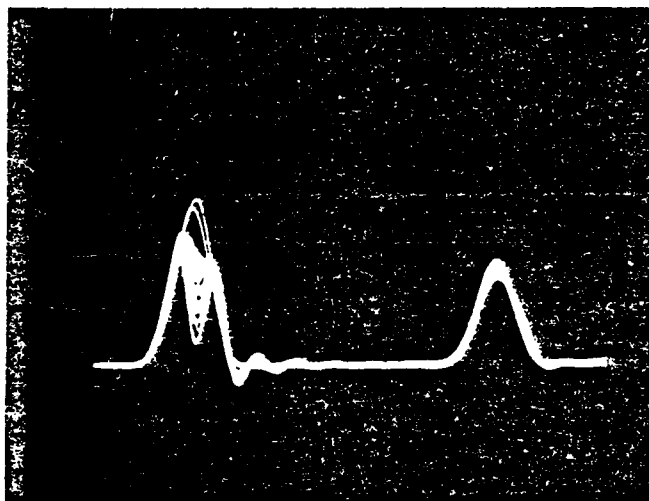
Figure 10(a). The average power impulse response measured between 1255 and 1300 PST, 31 August 1978, at a PN clock rate of 50 MHz.



(b). Strip chart record for 1255 - 1300 PST, 31 August 1978.



(a) Five-minute time averages.



(b) Time-lapse photograph of 20 s period at 1304 PST.

Figure 11(a). The average power impulse response measured between 1300 and 1305 PST, 31 August 1978, at a PN clock rate of 50 MHz.

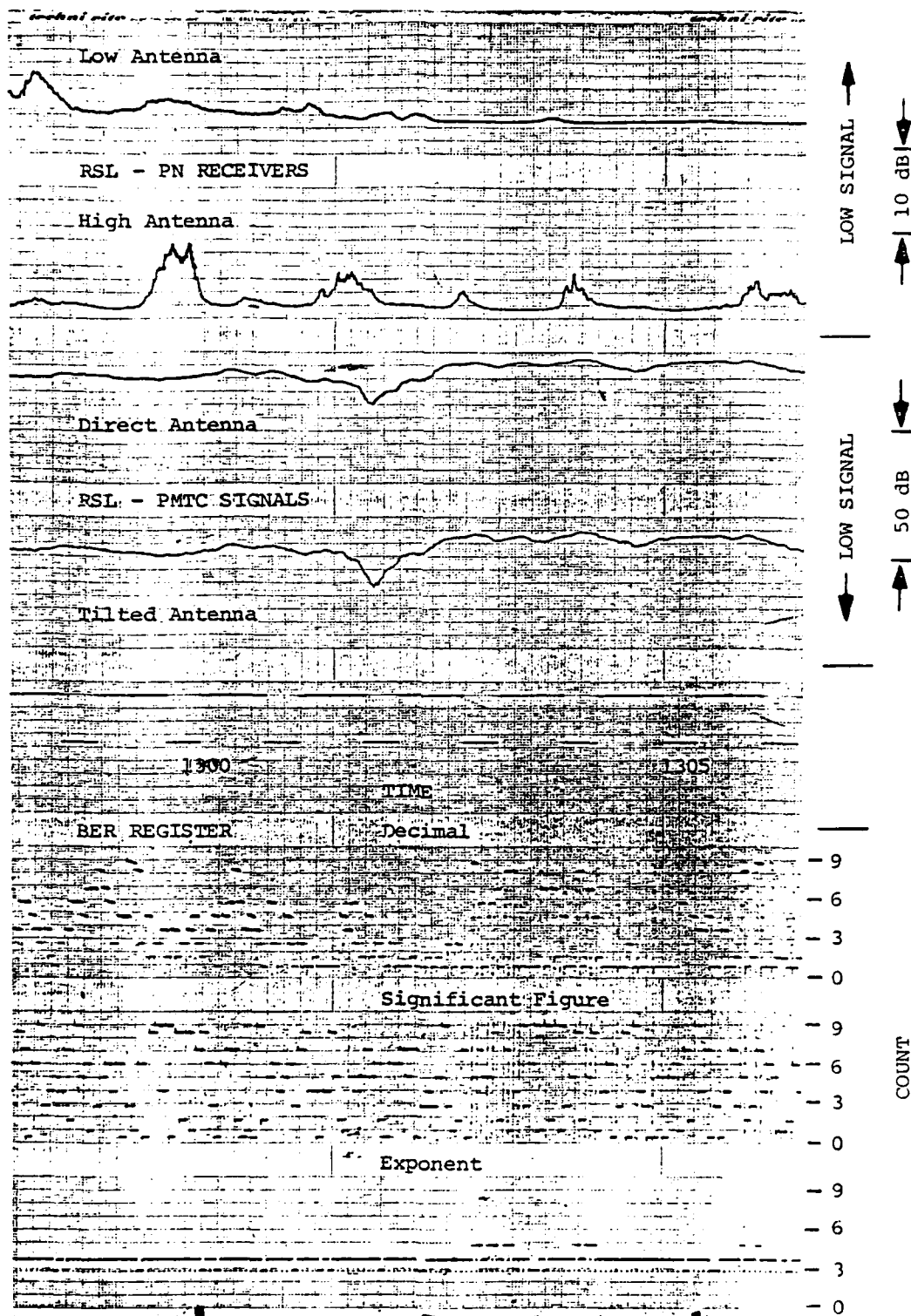
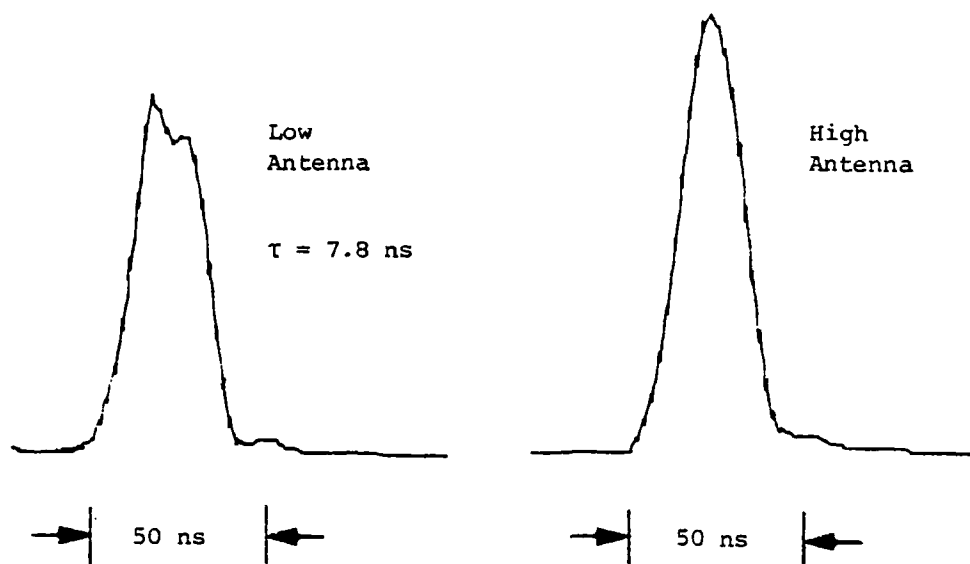
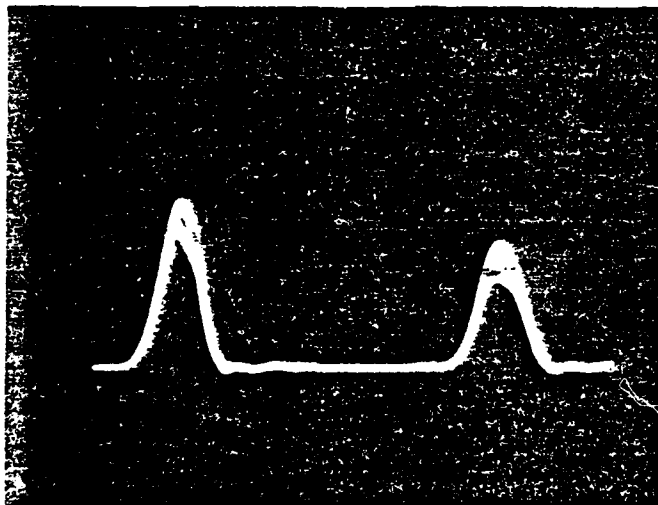


Figure 11(b). Strip chart record for 1300 - 1305 PST, 31 August 1978.



(a) Five-minute time averages.



(b) Time-lapse photograph of 20 s period at 1311 PST.

Figure 13(a). The average power impulse response measured between 1310 and 1315 PST, 31 August 1978, at a PN clock rate of 50 MHz.

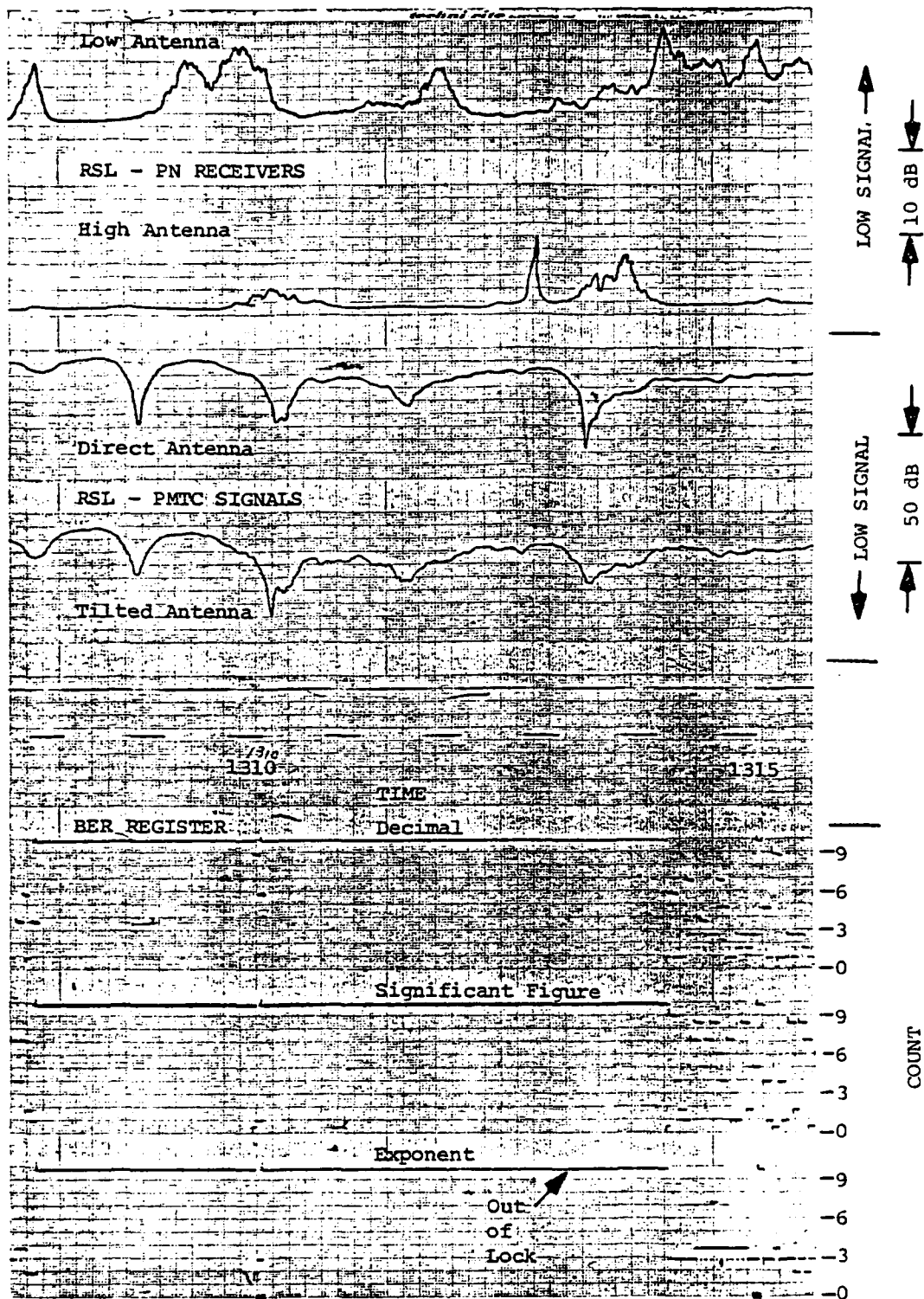
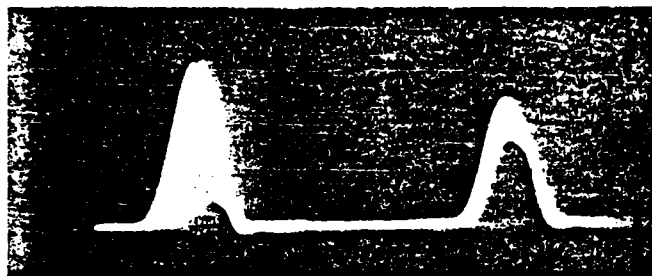
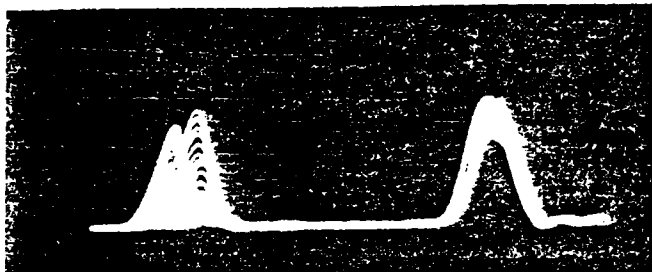


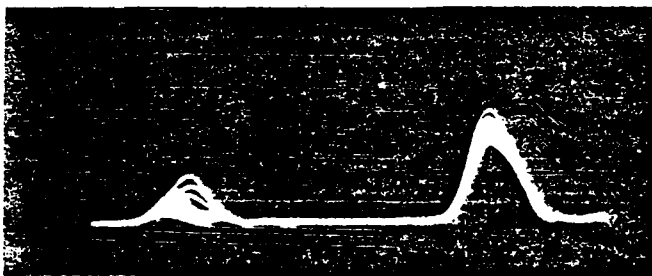
Figure 13(b). Strip chart record for 1310 - 1315 PST, 31 August 1978.



(a) Time-lapse response measured at 1308 PST, corresponding to the fade in Ch. 1 and the loss of synchronization in the data stream shown in Figure 12(b).



(b) Time-lapse response measured at 1314 PST, where the data stream resynchronized.



(c) Time-lapse response measured at 1310 PST, where the data stream resynchronized for a few seconds.

Figure 14. Time-lapse photographs of the power impulse response measured during the fading period in Ch. 1 beginning at 1308 PST, 31 August 1978.

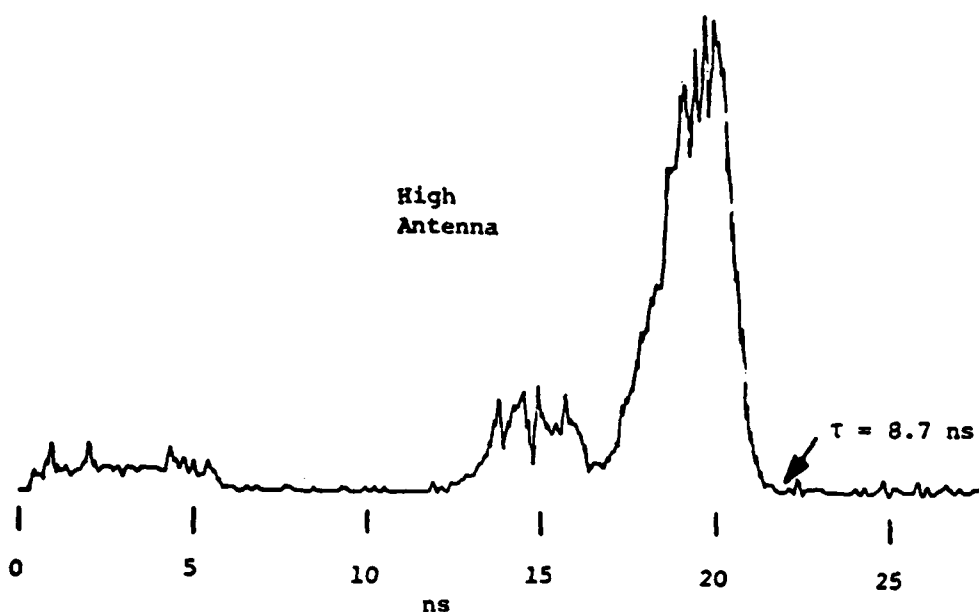
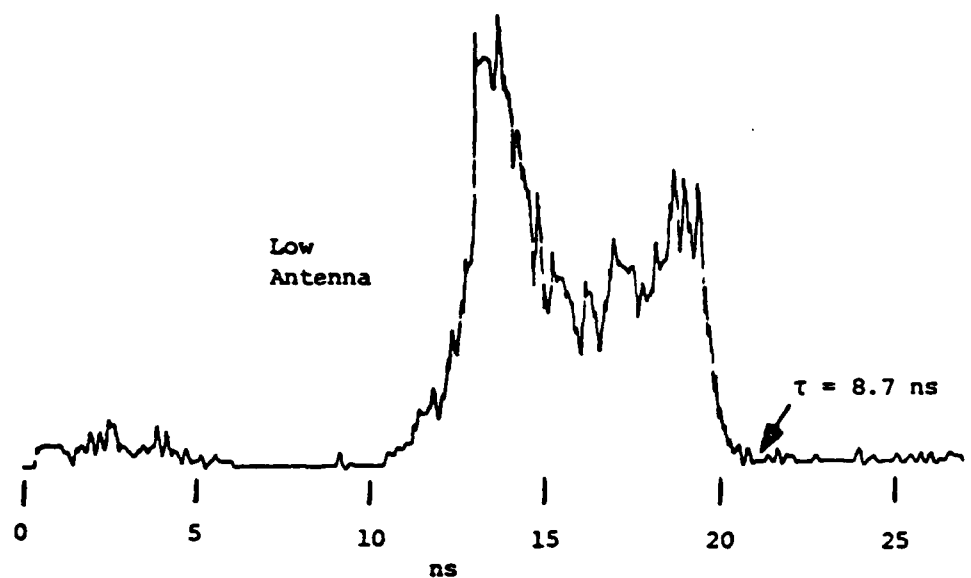
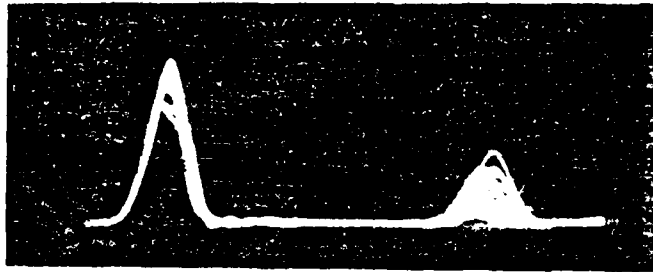
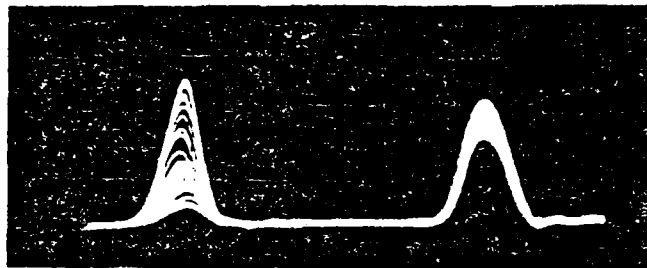


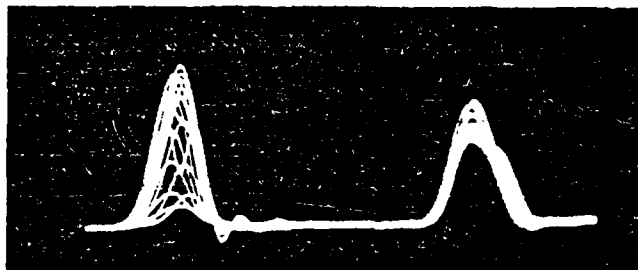
Figure A-5. The power impulse width distribution functions for the data of 31 August 1978. These data were measured between 1112 and 1200 PST at a PN clock rate of 150 MHz, just prior to the period discussed in Section 4.



(a) Dynamic multipath measured in Ch. 2 (high antenna) at 1317 PST.



(b) A flat-fade response observed in Ch. 1 (low antenna) at 1331 PST.



(c) Another example showing a power shift between components in Ch. 1, with only minor change in the Ch. 2 response at 1346 PST.

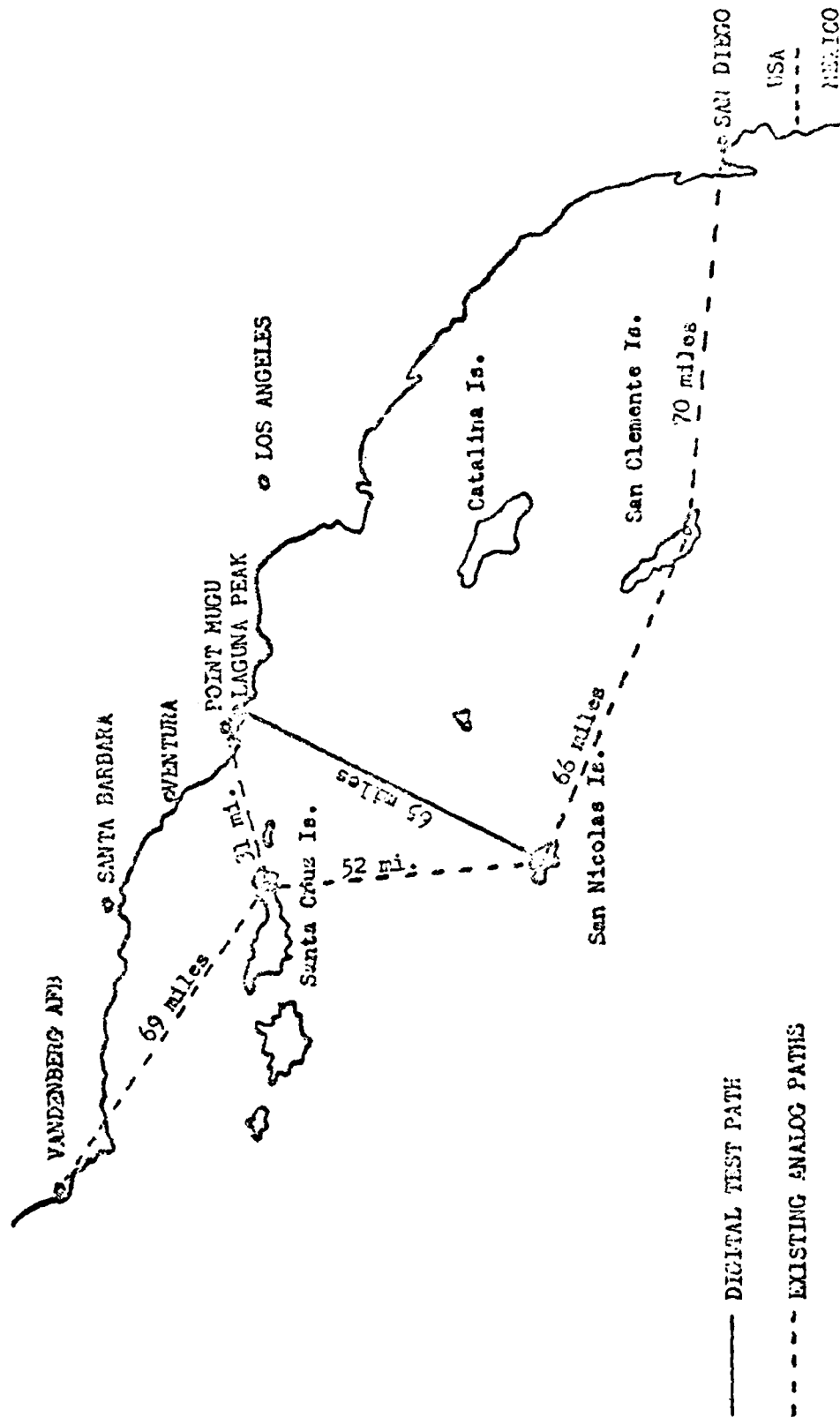
Figure 17. Time-lapse photographs of the power impulse response measured between 1317 and 1346 PST, 31 August 1978.

5. PATH TESTING OF LONG, OVER WATER DIGITAL RADIO PATHS

Jim Weblemoe
Pacific Missile Test Center
Pt. Mugu, CA

NOTE: The materials provided in this section are copies
of the visuals used with the extemporaneous remarks
given by Mr. Weblemoe.

SOUTHERN CALIFORNIA
OFFSHORE MICROWAVE PATHS



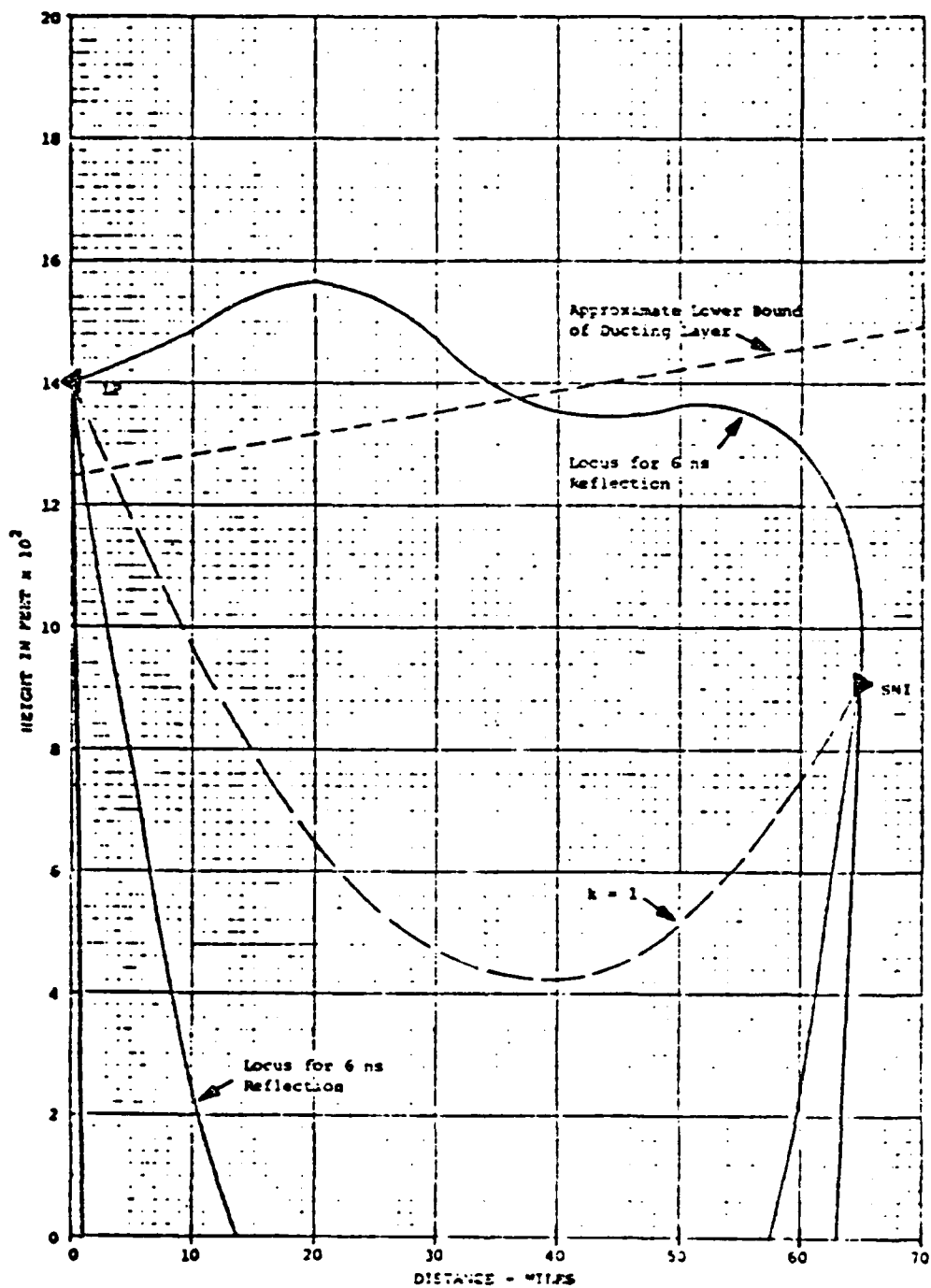


Figure A-19. Illustration of possible reflection type multipath from a strong ducting layer on 1 September 1978.

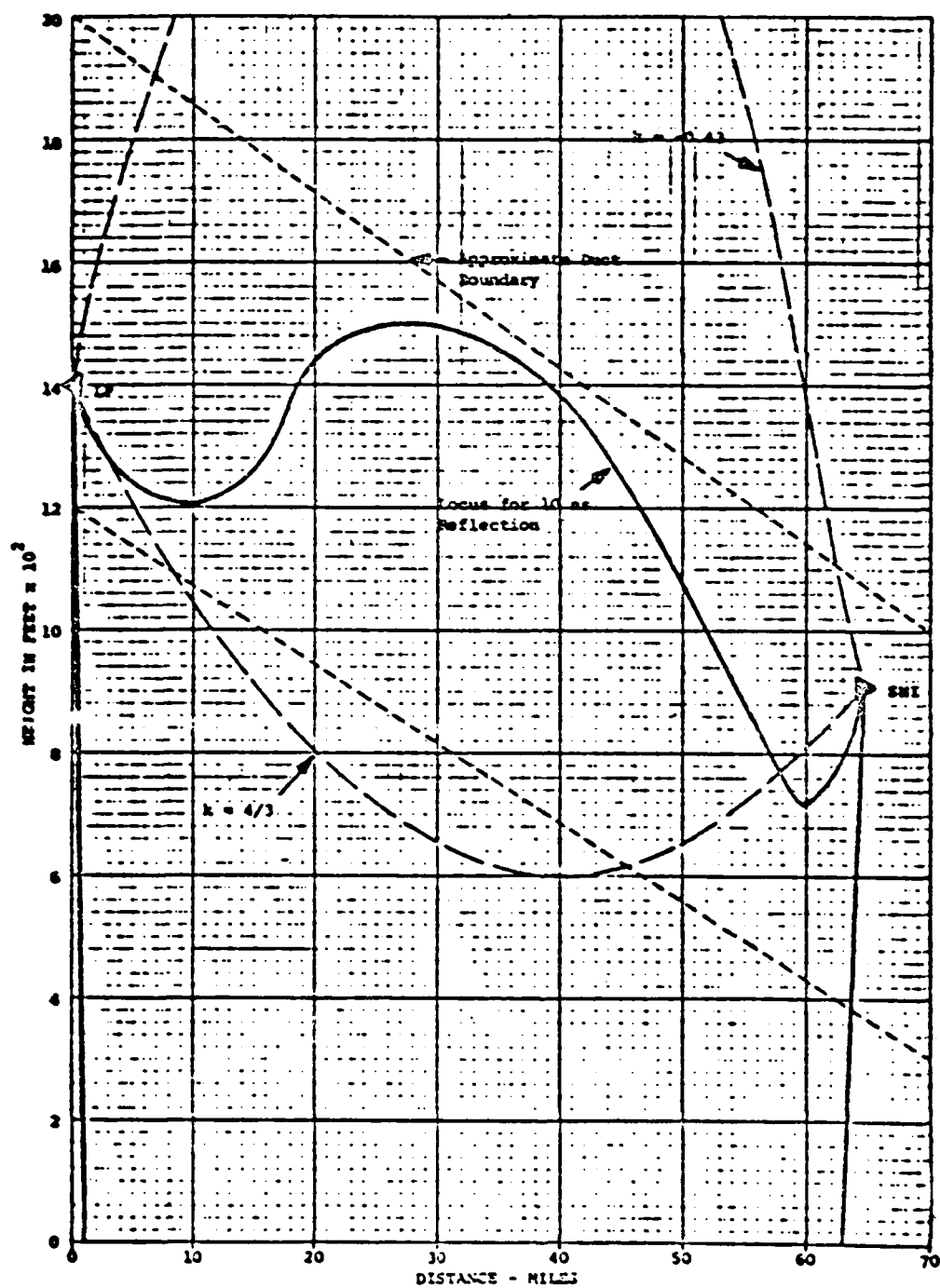


Figure A-18. Illustration of possible reflection type multipath from a strong ducting layer on 1 September 1978.

PHTC PATH TEST PROGRAM
PROPOSED DIGITAL MICROWAVE RADIO SYSTEMS

0 NAME	DEB	DRAMA PROTOTYPE	C
0 MODEL NO.	AM/FRC-162	AVANTEK DR-8A	C
0 MODULATION	3 LEVEL PARTIAL RESPONSE	QPR	8 100
0 MESSAGE BIT STREAM	12.6 MB/S	12.6 MB/S	13.7 100
0 MAX. NO. VOICE CH.	102	192	002
0 OCCUPIED BANDWIDTH	14 MHz	7 MHz	20 100
0 BITS/Hz	0.9	1.8	2.2

DIGITAL MICROPHONE PAIR TEST
LAWRENCE H. HARRIS

RADIO PARAMETERS

- 0 RSL
- 0 BER
- 0 ERROR CLUSTERS
- 0 ADAPTIVE EQUALIZER CONTROL VOLTAGES
- 0 DIVERSITY SWITCH STATUS
- 0 IF TUNER DISTRIBUTION
- 0 EFFICIENCY

PROPAGATION PARAMETERS

- 0 IFS "P" VALUE / MIN. ELEMENTS
- 0 METEOROLOGICAL DATA

AD-A087 793

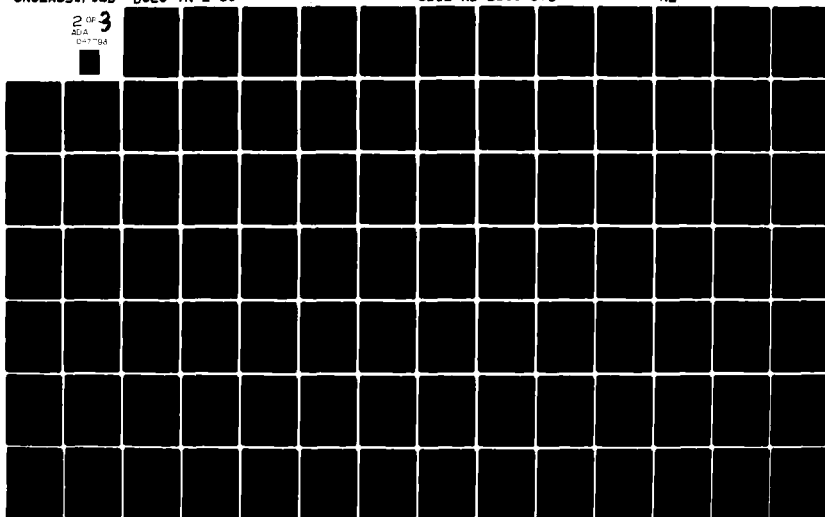
DEFENSE COMMUNICATIONS ENGINEERING CENTER RESTON VA F/G 17/2.1
PROCEEDINGS OF SEMINAR ON FREQUENCY SELECTIVE FADING AND ITS EF--ETC(U)
JAN 80 O R SMITH
DCEC-TN-2-80

SBIE-AD-E100 375

NL

UNCLASSIFIED

2 OF 3
ADA
C-1-794



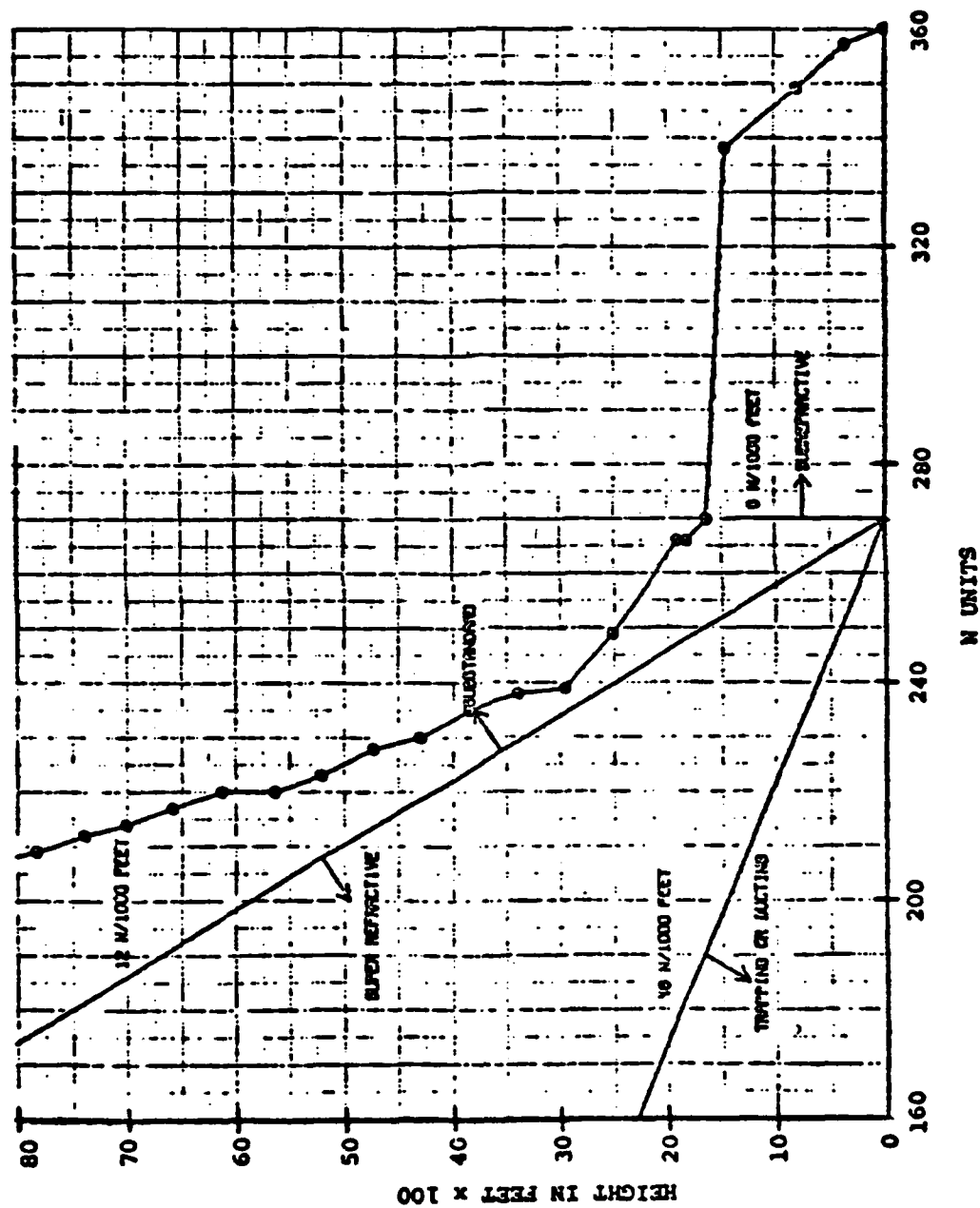


Figure 5(a). Refractive index profile for Pt. Mugu at 1058 PST, 31 August 1978.

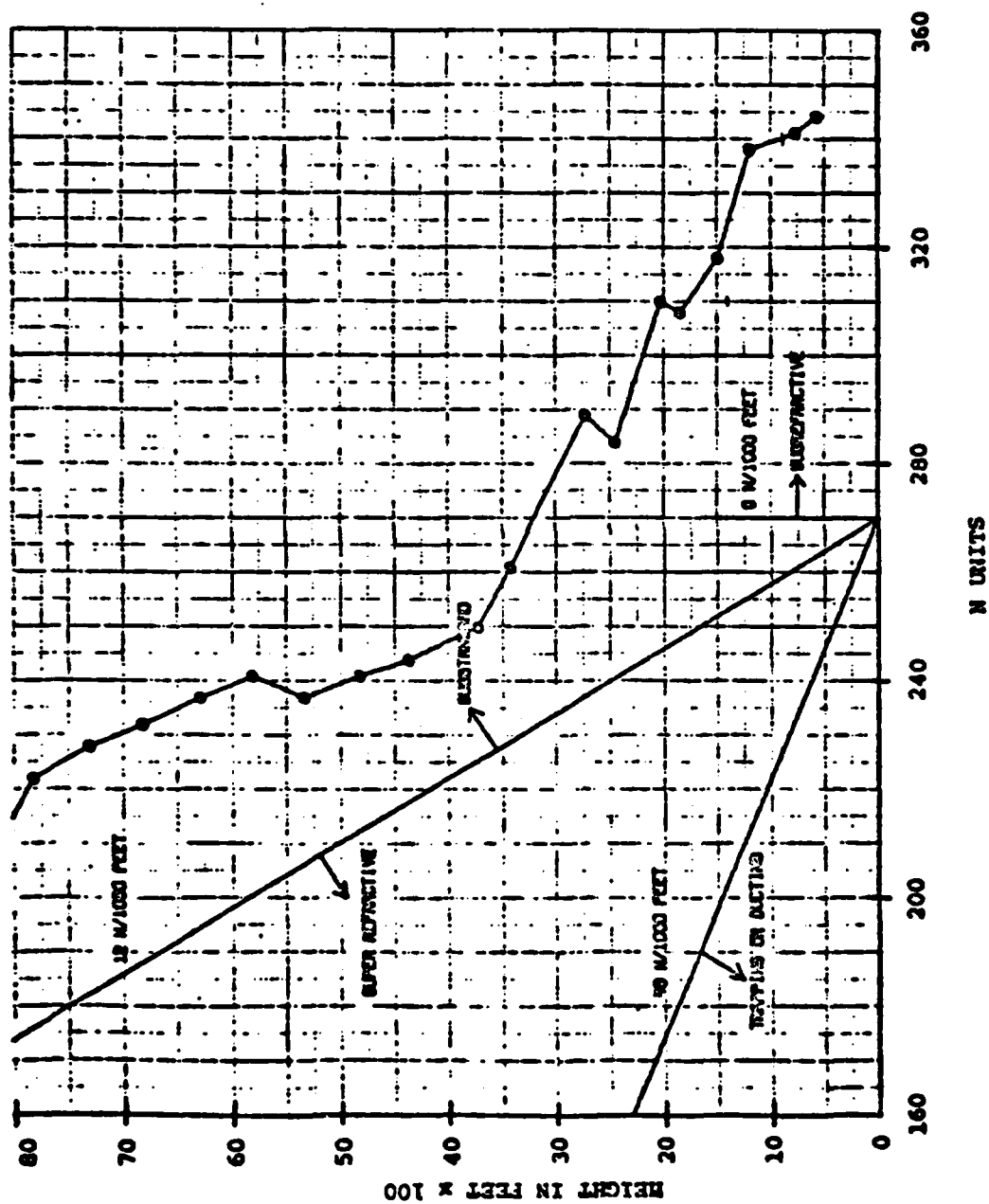


Figure 5(b). Refractive index profile for SN1 at 0904 PST, 31 August 1978.

6. MULTIPATH FADING CHANNEL MODEL

Tom Giuffrida
Bell Telephone Laboratories
Holmdel, NJ

NOTE: The materials provided in this section are copies of two Bell System Technical Journal articles used as the basis for the extemporaneous remarks given by Dr. Giuffrida.

A New Selective Fading Model: Application to Propagation Data

By W. D. RUMMLER

(Manuscript received September 21, 1978)

Channel transmission models for use in estimating the performance of radio systems on line-of-sight paths at 6 GHz are explored. The basis for this study is the simple three-ray multipath fade, which provides a channel transfer function of the form $H(\omega) = a[1 - b \exp - j(\omega - \omega_0)\tau]$, where a is the scale parameter, b is a shape parameter, τ is the delay difference in the channel, and ω_0 is the (radian) frequency of the fade minimum. This model is indistinguishable from an ideal channel model, within the accuracy of existing measurements. The propagation data that confirm the model were obtained in summer 1977 from a 26.4-mile hop near Atlanta, Georgia. The received power at 24 sample frequencies spaced at 1.1 MHz and centered on 6034.2 MHz was continuously monitored and recorded during periods of anomalous behavior. The model is applied to estimating the statistics of the channel delay difference, τ . The average delay difference giving rise to significant selectivity in the channel is between 5 and 9 ns. The distribution of delay difference is obtained for delay differences greater than 10 ns. The channel is found to have more than 3 dB of selectivity (difference between maximum and minimum attenuation in band) due to delay differences greater than 20 ns for more than 70 seconds in a heavy fading month. (This is comparable to the time the channel attenuation of a single frequency exceeds 40 dB.) The three-path model requires further simplification for narrowband channel application. For a channel with 30 MHz bandwidth, a model with fixed delay of 6.3 ns provides a sufficiently accurate representation of all observed channel conditions. The resulting nonphysical model is used to statistically characterize the condition of the fading channel. The statistics of the parameters of the fixed delay model are almost independent and of relatively simple form. The distribution of the shape parameter b is of the form $(1 - b)^{2.5}$. The distribution of a is lognormal. For $b > 0.5$, the mean and standard deviation of $-20 (\log a)$ are 25 and 5 dB, respectively; the

mean decreases to 15 dB for smaller values of b . The probability density function of ω_0 is uniform at two levels; measuring ω_0 from the center of the band, the magnitude of $\omega_0\tau$ is five times as likely to be less than $\pi/2$ than to be greater. A companion paper describes the use of this model for determining the bit error rate statistics of a digital radio system on the modeled path.

1. INTRODUCTION

Performance prediction of a digital radio system on a line-of-sight microwave channel requires an accurate statistical model of the channel. Because different digital radio systems may have different sensitivities to the various channel impairments, the model must be complete to the extent that it must be capable of duplicating the amplitude and phase (at least approximately) of all observed channel conditions. To facilitate laboratory measurements and computer simulations for calculating outage, the model should be realizable as a practical test circuit and should have as few parameters as possible. Most important, the parameters should be statistically well behaved.

Two types of models have been generally considered for line-of-sight microwave radio channels: power series type models¹⁻³ and multipath models.⁴⁻⁶ A power series model will require a few terms only if the channel is a multipath medium with a small spread of delays relative to the reciprocal bandwidth of the channel.³ This implies that one must understand the channel as a multipath medium to understand the behavior of a power series model. Hence, we have limited our characterization efforts to multipath models.

The basis for this study is the simple three-ray multipath fade.⁷ If the fading in a channel can be characterized by a simple three-path model, the channel will (as shown in Section II) have a voltage transfer function of the form

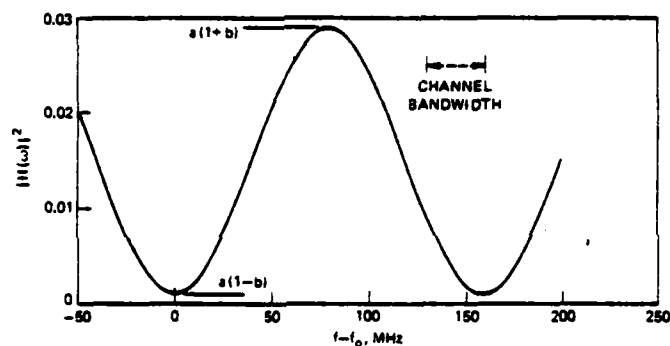
$$H(\omega) = a[1 - be^{j(\omega - \omega_0)\tau}]. \quad (1)$$

where the real positive parameters a and b control the scale and shape of the fade, respectively, τ is the delay difference in the channel, and ω_0 is the radian frequency of the fade minimum. The plus and minus signs in the exponent correspond, respectively, to the channel being in a nonminimum phase or minimum phase state. Note that, with appropriate choices of parameters, this model can be reduced to a two-path model or a scaled two-path model, etc.

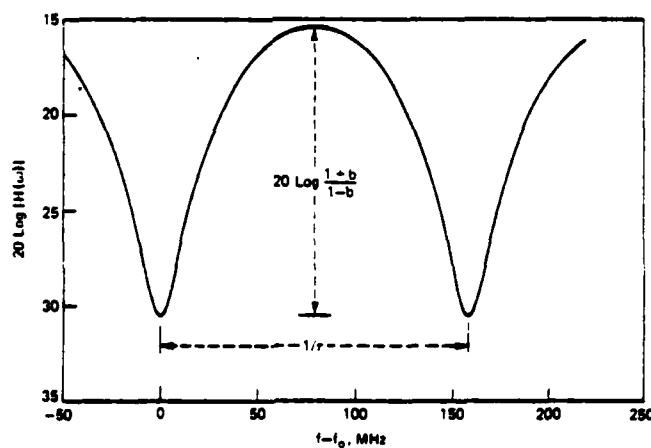
It has been shown previously,⁷ and is illustrated in Section II, that the simple three-path fade overspecifies the channel transfer function if the delay is less than $1/4 B$, where B is the observation bandwidth. The critical value of τ for a 30-MHz channel is about 5.5 ns, which is comparable to the mean delay in the channel. As a consequence, unless

the channel response can be determined to an accuracy on the order of 0.001 dB, a unique set of parameters a , b , τ , and f_0 cannot be determined for more than half the faded channel conditions encountered. To avoid this problem, one must suppress or fix one of the model parameters. Section II shows that the delay, τ , is the only parameter which, when fixed, produces a reasonable model.

While a model with a fixed delay may appear to be a strange choice, it has all the required characteristics for modeling the channel transfer function. Figure 1 shows the amplitude of the channel transfer function of eq. (1) on a power scale and on a decibel scale for $\tau = 6.31$ ns. With τ fixed, the response minimum is shifted with respect to frequency by varying f_0 . Varying a changes the overall level and b changes the



(a) MODEL POWER RATIO



(b) MODEL ATTENUATION IN DECIBELS

Fig. 1—Channel model function. $H(\omega) = a[1 - b \exp(-j 2 \pi (f - f_0) \tau)]$, for $\tau = 6.3$ ns, $a = 0.1$, $b = 0.7$.

"shapeliness." If the minimum is within the 30-MHz bandwidth of a channel, the fixed delay model can generate notches with a wide range of levels and notch widths. With the minimum out of band, it can generate a wide range of combinations of levels, slopes, and curvatures within the channel bandwidth. Section VI shows that the model versatility, with τ chosen to be 6.31 ns, is sufficient to characterize a 30-MHz channel in the 6-GHz common carrier band.

Section II provides a brief discussion of the simple three-path fade. A comparative discussion of the relative merits of the different possible simplifications of this model leads to the choice of the fixed delay model.

The data used for detailed evaluation of models were obtained from a 6-GHz experiment in Palmetto, Georgia, in June 1977. The radio channel was equipped with a general trade 78-Mbit/s, 8-PSK digital radio system, and the received spectrum was monitored with a set of 24 filters with bandwidths of 200 kHz spaced at a 1.1-MHz separation across this channel. During fading activity, the received power of each of these frequencies was measured five times each second, or once every 2 seconds, depending on how rapidly the channel was changing; sampled power, quantized in 1-dB steps, was recorded by the MIDAS system.* The data base used for this study consists of approximately 25,000 scans representing 8400 seconds of fading activity; about 8700 scans were recorded during periods when the equipment was indicating errors. These data represent about 60 percent of the fading activity of a heavy fading month; therefore, the derived statistics must be viewed as provisional and subject to some modification as additional data are processed. At the very least, the data base is sufficiently large to indicate what can happen on the channel and to form a basis for choosing and validating a model.

As described in Section III, the model parameters were estimated for each scan by fitting the magnitude squared of the transfer characteristic [eq. (1)] to the observed channel shape as characterized by the power received at the sampling frequencies. Phase is subsequently derived by assuming the channel is minimum phase. Problems are encountered in realizing a minimum-phase solution because of quantization noise and the presence of certain channel shapes caused by large delays. The procedure for handling these difficulties is described.

The statistics of the parameters of the fixed delay model are discussed in Section IV. Equations providing an idealized description of the statistics of the parameters of the model are also given here.

In Section V, the determination of the delay difference present in the channel is considered. In the first subsection, it is demonstrated

* Multiple Input Data Acquisition System, constructed by G. A. Zimmerman; see Ref. 1.

that, during the observed period of fading activity, the average delay is 9 ns. A lower bound on the distribution of delay difference for large delays is developed in the second subsection. A third subsection provides an example of a channel scan that can best be approximated by a three-path fade with a delay difference of 26 ns. Fades with at least this delay and with a more moderate amount of shape (2 dB or more) were encountered for about 60 seconds of the data base studied. Thus, one might expect 26-ns delays to be present during about 100 seconds of a heavy fading month.

The presence of such large apparent delays raises questions as to the accuracy with which the fixed delay model represents the channel. These questions are addressed in Section VI where the statistics of the errors in modeling scan fits are described. The errors are small and do not compromise the usefulness of the model.

Results and conclusions are briefly summarized in Section VII.

II. CHOICE OF MODEL

In this section, we provide a brief description of the simple three-path model and show why it cannot be used to estimate delays when the delay bandwidth product is less than $\frac{1}{2}$. In a comparative discussion, we show why the fixed delay model is the only simplification of the model that is manageable.

2.1 Simple three-path model

Consider a channel characterized by three paths or rays. The amplitude of the signal on each of these three paths, as seen by the receiver, is 1, α_1 , and α_2 . The second and third paths are delayed with respect to the first by τ_1 and τ_2 seconds, respectively, where $\tau_2 > \tau_1$. We define the simple three-path model by requiring the delay between the first two paths to be sufficiently small, i.e.,

$$(\omega_2 - \omega_1)\tau_1 \ll 1, \quad (2)$$

where ω_2 and ω_1 are the highest and lowest (radian) frequencies in the band. The complex voltage transfer function of the channel at a frequency ω may be illustrated with a phasor diagram. Figure 2a shows the phasor diagrams for ω_1 and ω_2 superimposed. By designating the amplitude of the (vector) sum of the first two paths by a ; the angle of the sum by $\phi = \omega_0\tau - \pi$, where τ is equal to τ_2 , the delay difference in the channel; and the amplitude of the third ray by ab , we obtain the simplified diagram in Fig 2b.*

* Note that, if the third amplitude is greater than the sum of the first two, we interchange the assignments of amplitudes a and ab and obtain a nonminimum phase fade.

The simple three-path fade cannot be used for a channel model because the path parameters lack uniqueness. The basic difficulty is illustrated by the two superimposed fades in Fig. 3. Note that the amplitudes of the transfer functions of these two fades match, at

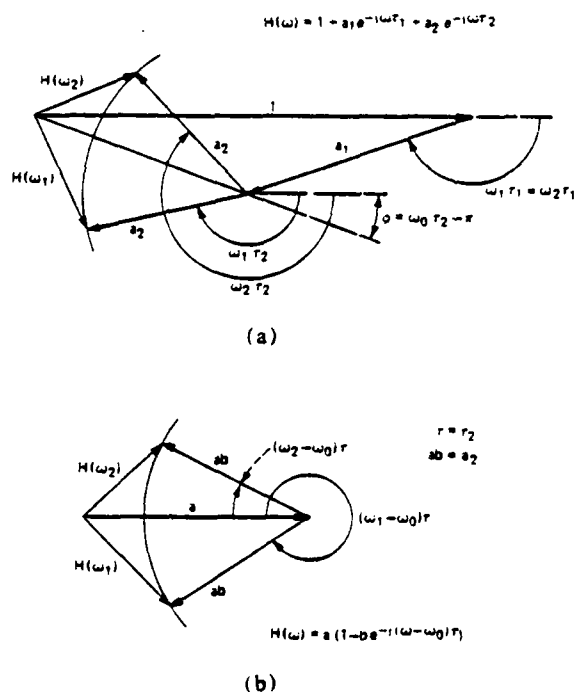


Fig. 2—Simple three-path fade. (a) Three rays shown. (b) Simplified.

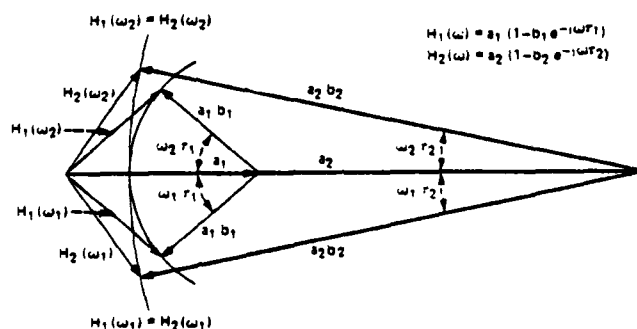


Fig. 3—Two degenerate simple three-path fades with $\omega_0 r = 0$.

midband and at both edges. It has been shown elsewhere⁷ that fades matched in this way will be identical in band to within a few tenths of a decibel at most, and will have almost identical envelope delay distortion. Given noisy quantized measurements of $|H(\omega)|$ over the band, it is impossible to distinguish between such fades unless we fix one of the four parameters. Let us consider each of the four possibilities.

2.2 Pseudo two-path fade

If one fixes the amplitude, a , at unity, the simple three-path fade reduces to a two-path fade with independent control of the frequency of the minimum of the response. The difficulty with this model, as may be seen by referring to Fig. 2b, is that it can provide in-band minima only for $|H(\omega)| < 1$ and maxima in-band only for $|H(\omega)| > 1$. In other words, the model cannot match an in-band maximum at an arbitrary fade level. In addition, it was found that during approximately half the periods when the radio equipment was indicating errors, the channel could not be well modeled with a pseudo two-path model.

2.3 Scaled two-path fade

If one fixes the phase, $\phi = \omega_0\tau - \pi$, in the simple three-path model at 0, the fade reduces to a scaled two-path fade. (For a two-path fade, we require the additional condition $a = 1$.) This is the most physically desirable of the reduced three-path models because it may be derived without recourse to the three-path formalism. Unfortunately, it is mathematically intractable, particularly when dealing with amplitude data only. In fitting the model to a given channel shape (in the manner described in Section III for the fixed delay model), one obtains a function of a , b , and τ that must be minimized to obtain the best fit. Because of the $\omega\tau$ term in the exponent of the model, this function has a local minimum in every interval of τ of length 0.17 ns, the reciprocal of 6 GHz. Since the possible range of τ extends to about 30 ns, one may have to perform hundreds of minimizations to find the best fit to a single channel scan. Even then this "best fit" may have no minimum phase realization, and there is no known procedure that leads to one.

2.4 Fixed b model

If one fixes the amplitude b in the simple three-path model, the resulting reduced model has all the mathematical difficulties of the scaled two-path model and no satisfactory physical interpretation.

2.5 Fixed delay model

It is demonstrated in the remainder of this paper that the fixed delay model described in Section I is useful and effective in characterizing the channel.

III. ESTIMATION PROCEDURES

This section describes how the model parameters are estimated from the channel scans and how realizability difficulties are surmounted.

3.1 Parameter estimation

The channel data consist of a set of 25,000 scans of the channel power spectrum. Each scan consists of a power measurement at each of 24 frequencies at 1.1-MHz spacing across the channel. (Actually, only 23 frequencies are used since the 19th was inoperative during this test period). The power measurements are recorded in decibels, and each must be referenced to the average power level of that frequency at mid-day. With proper conversion and calibration, the basic data characterizing a scan are a set of power ratios. We designate the power ratio at n th frequency by Y_n , where

$$Y_n = Y(\omega_n) \quad n = 1, 2, \dots, 24. \quad (3)$$

We wish to model the channel with a voltage transfer function of the form given in eq. (1), which we repeat here for convenience

$$H(\omega) = a[1 - be^{z/(\omega - \omega_0)\tau}], \quad (1)$$

Thus our estimate of Y_n will be

$$Y_n = |H(\omega_n)|^2 = \alpha - \beta \cos(\omega_n - \omega_0)\tau, \quad (4)$$

where

$$\begin{aligned} \alpha &= a^2(1 + b^2) \\ \beta &= 2a^2b. \end{aligned} \quad (5)$$

For convenience, we measure frequency in the units of the frequency separation of the power measurements. Thus,

$$\omega_n = 2\pi f_n = 2\pi n(1.1 \times 10^6) \quad n = 1, 2, 3, \dots, 24. \quad (6)$$

If we choose

$$\tau = \frac{1}{N(1.1 \times 10^6)}, \quad (7)$$

then

$$\omega_n \tau = 2\pi \frac{n}{N}. \quad (8)$$

For the fixed delay model, we choose $N = 144$ which gives a model τ of 6.31 ns. Thus, the in-band frequencies correspond to n values between 1 and 24, and the channel transfer function given by the model is periodic for n modulo 144, corresponding to a frequency shift of $144 \times 1.1 \times 10^6 = 158.4$ MHz.

The weighted mean-square error between the estimated and observed power is given by

$$E = \frac{\sum_{n=1}^{24} C_n (Y_n - \hat{Y}_n)^2}{\sum_{n=1}^{24} C_n}, \quad (9)$$

where the summation skips $n = 19$ as described above, and where C_n is a weighting applied to the measurement at frequency ω_n . Since the original data, from which the Y_n 's were derived, were uniformly quantized on a logarithmic scale, it is appropriate to use a weighting that is approximately logarithmic. Hence, we use the weighting function

$$C_n = \frac{1}{Y_n^2}. \quad (10)$$

A number of different weighting functions were tested, but the one given by (10) is, generally, the most satisfactory.

Estimates of α , b , and f_0 may be obtained by minimizing the weighted mean-square error, E . It is shown in the appendix that one may obtain closed form estimators for α , β , and f_0 by substituting eq. (4) into (9) and minimizing E , first with respect to α , then with respect to β (or vice versa), and last with respect to f_0 . In the resulting scheme, the estimator of f_0 , the frequency of the model minimum, is a function of data only. The estimators of α and β are functions of the estimated f_0 and the data.*

After estimates of α and β have been calculated, the parameters a and b of the model are obtained by inverting the relationships given by eq. (5).

$$b = \frac{\alpha}{\beta} - \left[\left(\frac{\alpha}{\beta} \right)^2 - 1 \right]^{1/2} \quad (11)$$

$$a = \left[\frac{\beta}{2b} \right]^{1/2}. \quad (12)$$

It is clear from (11) and (12) that we can realize the channel shape with the model only if $\alpha \geq \beta$. This is to be expected. Since $|H(\omega)|^2$ is a power transfer function, it must be positive for all frequencies, which is possible only if $\alpha \geq \beta$ [see eq. (4)]. Thus, the condition $\alpha \geq \beta$ allows us to obtain a minimum (or nonminimum) phase transfer function whose magnitude squared is the minimum weighted mean-square error fit to the observed power transfer response of the channel.

* For mathematical simplicity, we actually use an estimator for β conditioned on f_0 , α , and the data.

3.2 Application of estimators

If the procedure described above is strictly applied to the set of 25,000 scans in the data base, one finds that about 35 percent of the scans cannot be modeled with real values of a and b . A study of these problem scans revealed that the estimator for f_0 , the frequency of the fade minimum, was biased for two types of scans. One type is a scan with little shape, dominated by quantization noise; the other is a selective channel shape having a steep slope across the band. Both types of scan are illustrated in Fig. 4. The scan in Fig. 4, which is almost flat, was fabricated to illustrate the severity of the quantization problem. The other scan is typical of the more shapely troublesome scans.

To obtain a good realizable fit to such channel shapes requires degrading the quality of the fit; that is, moving the parameters away from the values that minimize the fit error, eq. (9). Given the form of the estimation scheme, this is easily accomplished by moving the frequency of the fade minimum, f_0 , away from its original "optimum" value and reoptimizing the remaining parameters to obtain values of a and b that are optimum for the new value of f_0 . Figures 5 and 6 illustrate the results of such a quasi-optimization regarding f_0 as a free parameter. They show the fit error E and the values of a and b as f_0 is varied from its original optimum value. Figure 5 corresponds to the flat fade in Fig. 4 and Fig. 6 to the sloped fade.

The shapes of the curves in Figs. 5 and 6 are typical of those obtained when the channel has no minimum in band. The weighted error in the fit, E , is not very sensitive to the estimate of f_0 , the

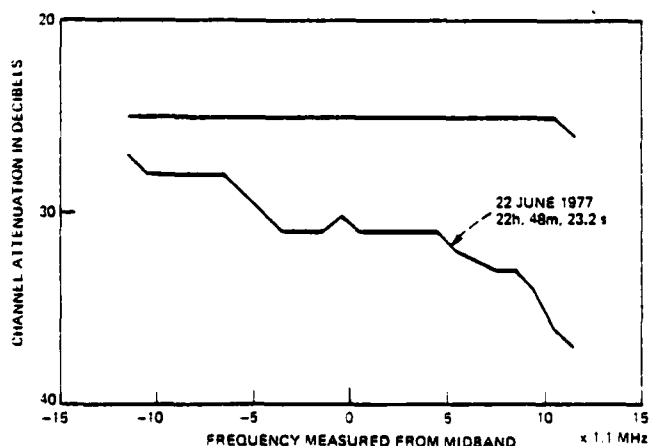


Fig. 4—Two channel scans that produce realization difficulties.

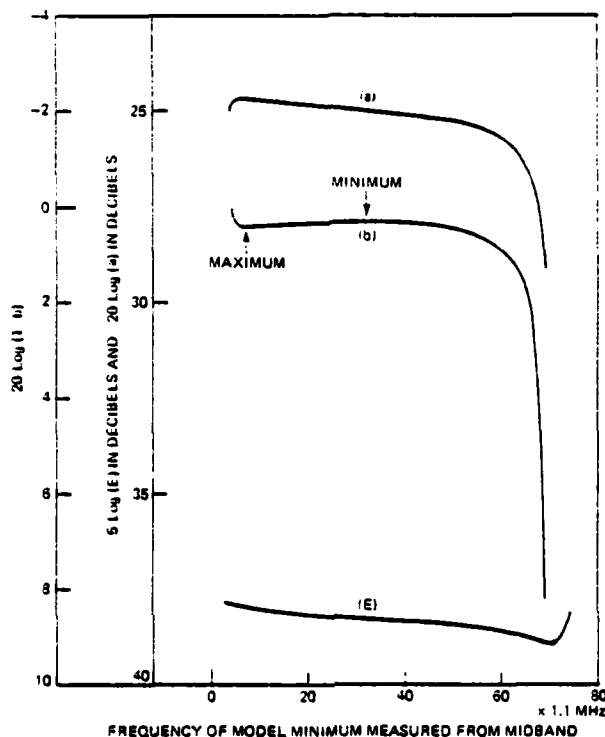


Fig. 5—Locus of weighted fit error and model parameters with f_0 as a free variable for flat fade in Fig. 4.

frequency of the modeled fade minimum. The minimum of E is broad and flat, due to quantization and instrumentation noise in the channel. The variation of the parameter a with f_0 is also typically very gradual. The salient features of the variation of b with respect to f_0 are clearly seen in Fig. 6, and are also present and labeled in Fig. 5. As f_0 is varied from its original optimum value, b varies from a value of 1 to a value of 0 in a sideways s-curve with two stationary points, a maximum and a minimum. Extensive simulations with known channel characteristics indicate that a good choice of parameters is the set corresponding to the point where b is locally minimized. To illustrate this point, assume that the channel shape is that given by the model, with 6.3-ns delay, f_0 at 18.5×1.1 MHz, $a = 0.04$, and $b = 0.7$. One can construct a plot similar to Figs. 5 and 6 for this simulated fade, with the result shown in Fig. 7. The curves in this figure illustrate the results cited above, in that the true value of f_0 occurs near a minimum value of b . A better

NEW SELECTIVE FADING MODEL

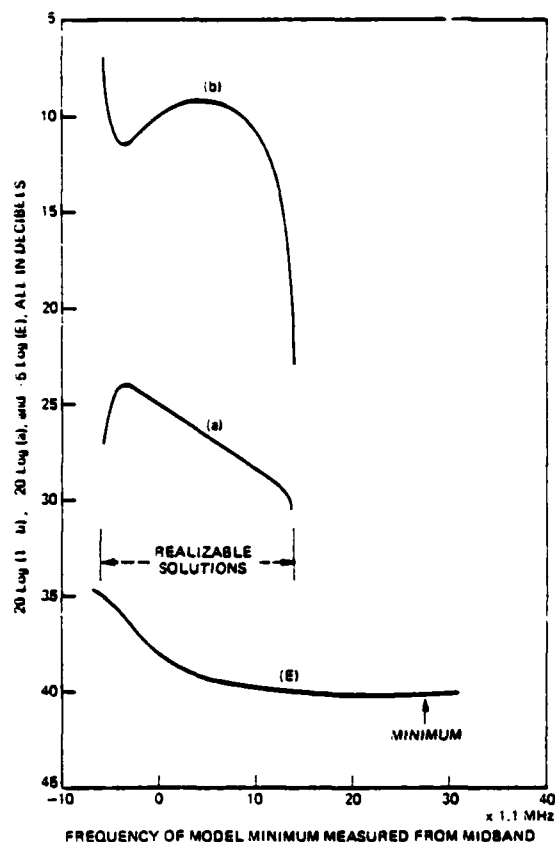


Fig. 6—Locus of weighted fit error and model parameters with f_0 as a free variable for typical scan in Fig. 4.

choice for the case shown and for others that have been simulated would be "on the shoulder" between the minimum and $b = 1$; however, such a criterion is difficult to quantify.

To summarize, if the standard routine does not provide a realizable fit to a scan, one merely varies f_0 , the position of the minimum, until one obtains a realizable solution with a value of b that is stationary* with respect to variations in f_0 . We recognize that this procedure introduces additional sources of error into the estimates of the model parameters. The errors in a and b are small because b is near a stationary value and a is slowly varying. The error in f_0 is also small,

* Since b is a monotone function of a/β , it is only necessary to invert solutions with stationary values of the ratio, a/β .

usually less than 3 MHz, but is always in the direction corresponding to moving the minimum nearest to the band closer. We consider the effects of these errors in Section VI.

IV. MODEL STATISTICS

Applying the procedures described in Section III to the scans in the data base results in 25,000 sets of values of a , b , and f_0 . The relative joint frequency of occurrence of these three parameters may be described by the set of distribution functions shown in Figs. 8 to 12. The distribution of the parameter b is described in Fig. 8 in terms of the distribution of $-20 \log(1 - b)$, which is approximately exponentially distributed with a mean of 3.8 dB. This distribution gives the time that b exceeds the value given by the abscissa as a fraction of the time in a heavy fading month that the rms level in the channel is depressed by more than 15 dB. For instance, we see that 40 percent of the time

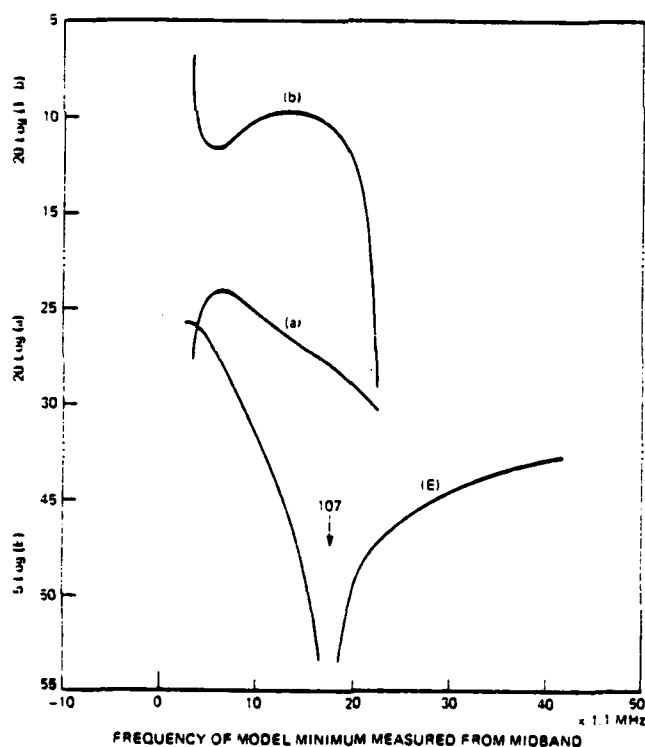


Fig. 7.—Locus of weighted fit error and model parameters with f_0 as a free variable. For channel given by model with $\tau = 6.31$ ns, $a = 0.04$, $b = 0.7$, $f_0 = 18.5 \times 1.1$ MHz.

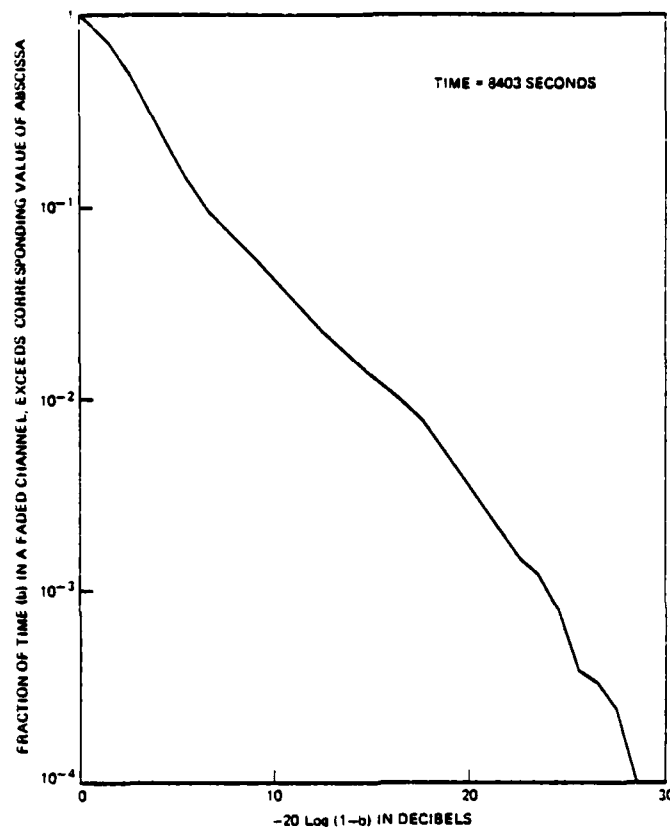


Fig. 8—Distribution of b .

when the channel is depressed the value of b exceeds 0.3. It exceeds 0.7 for 4 percent of that time, and 0.99 about 0.3 percent of that time. The distribution of b can be modeled in the form

$$P(1 - b < X) = X^{\frac{20}{-1.8 \log 10}} = X^{2.3}. \quad (13)$$

The distribution of a is conditioned on b and is approximately lognormal as shown in Figs. 9 and 10. The mean and standard deviation of the distributions in Figs. 9 and 10 are plotted in Fig. 11. From Figs. 9 to 11 it is apparent that a and b are almost independent; however, less shapely fades tend to occur at less depressed values. We note that shape occurs when the average depression is 20 to 25 dB,* that the

* The value of a corresponds to average power level over a large frequency span and not strictly to the average power in a narrowband channel.

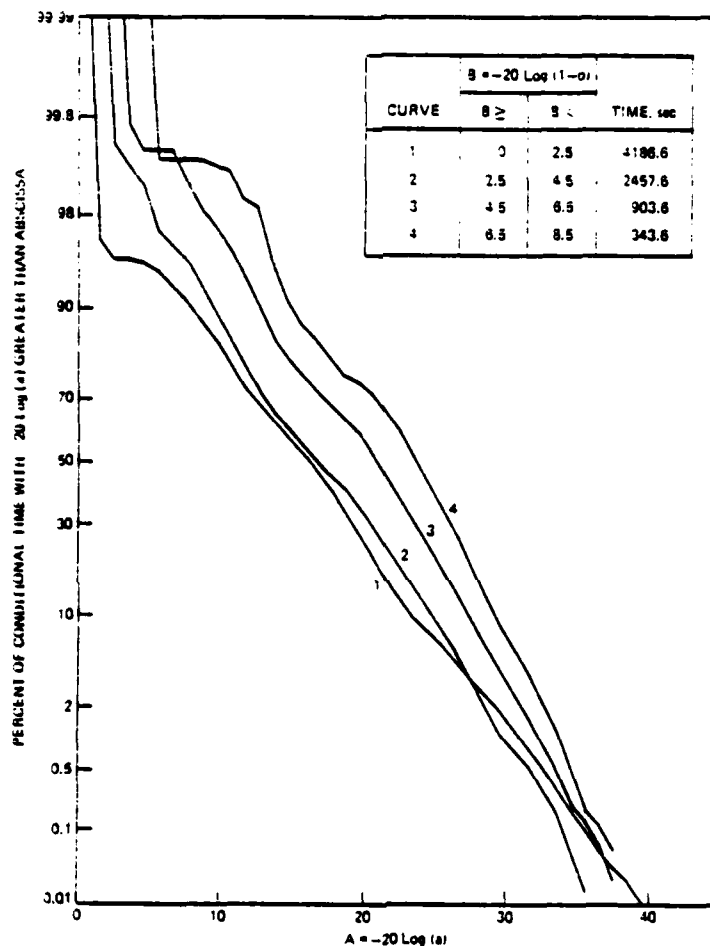


Fig. 9—Distribution of a conditioned on the value of b for $-20 \log (1 - b)$ less than 8.5 dB.

average depression is near 25 dB for b greater than 0.7, and that it falls off gradually to 15 dB for small b . The distribution of $A = -20 \log a$ is conditioned on b and may be modeled as

$$P(A > Y) = 1 - P \left[\frac{Y - A_0(b)}{5} \right], \quad (14)$$

where P is the cumulative distribution function of a zero mean, unit variance, and Gaussian random variable, and $A_0(b)$ is the mean of A for a given value of b as given in Fig. 11. We see from Fig. 11 that the

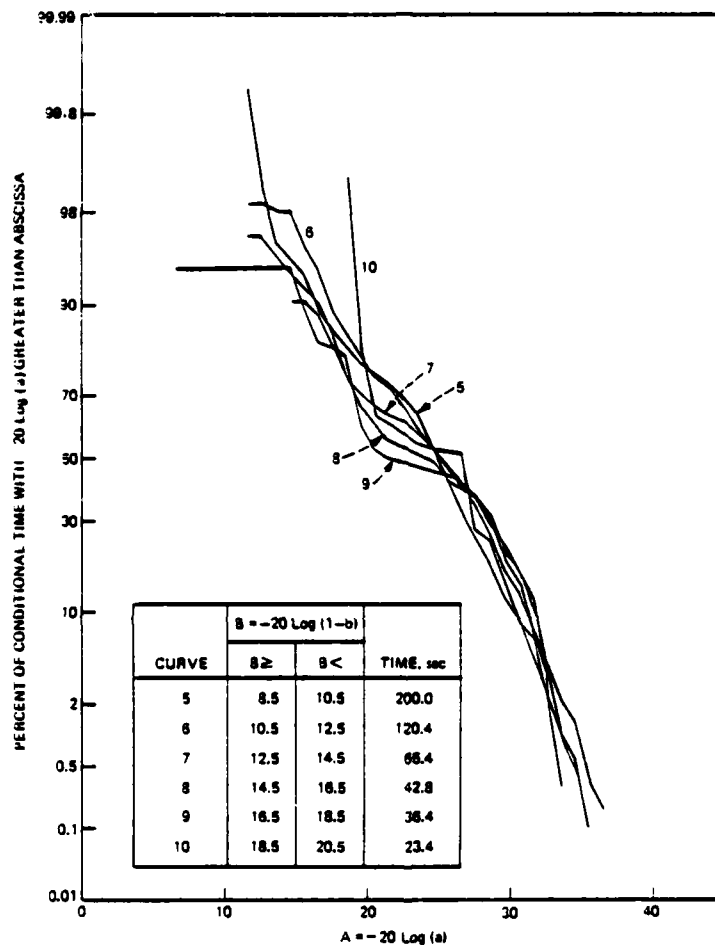


Fig. 10—Distribution of a conditioned on the value of b for $-20 \log(1-b)$ greater than 8.5 dB.

standard deviation of A may be taken as 5 dB regardless of the value of b ; the variations near $-20 \log(1-b) = 20$ are due to small sample problems.

Figure 12 shows the time during which scans had f_o in 4×1.1 -MHz frequency intervals. It is, in effect, an estimate of the density function of the distribution of f_o and is, consequently, quite noisy. The maxima near $\pm 30 \times 1.1$ MHz from the center of the band are due in part to the movement of estimates of f_o to achieve realizability. While, on physical grounds, one would expect f_o to have a uniform distribution, the fixed

delay model is decidedly not a physical model. Consider a simulated set of simple three-path fades having a uniform distribution of f_0 , fixed values for a and b , and a delay τ , fixed at a value other than 6.31 ns. This set of fades will engender a nonflat probability density function for the f_0 's obtained in fitting to the 6.31-ns model. The probability density function is flat within the band regardless of the fixed delay of the set of simulated fades; however, it will more nearly resemble that shown in Fig. 12 if the delay of the set is greater than 6.31 ns than if it is less than 6.31 ns. In short, Fig. 12 is characteristic of a channel with a considerable fraction of delay differences greater than 6 ns.

Based on Fig 12, we approximate the probability density function of f_0 by a two-level function. Note that f_0 is defined on an interval of length $1/\tau$, where τ is 6.3 ns the delay of the model. Thus, with f_0 measured from the center of the band, the probability density function for f_0 may be approximated by

$$p_{f_0}(f_0) = \begin{cases} \frac{5\tau}{3} & |f_0| \leq \frac{1}{4\tau} \\ \frac{\tau}{3} & \frac{1}{4\tau} < |f_0| < \frac{1}{2\tau} \end{cases} \quad (15)$$

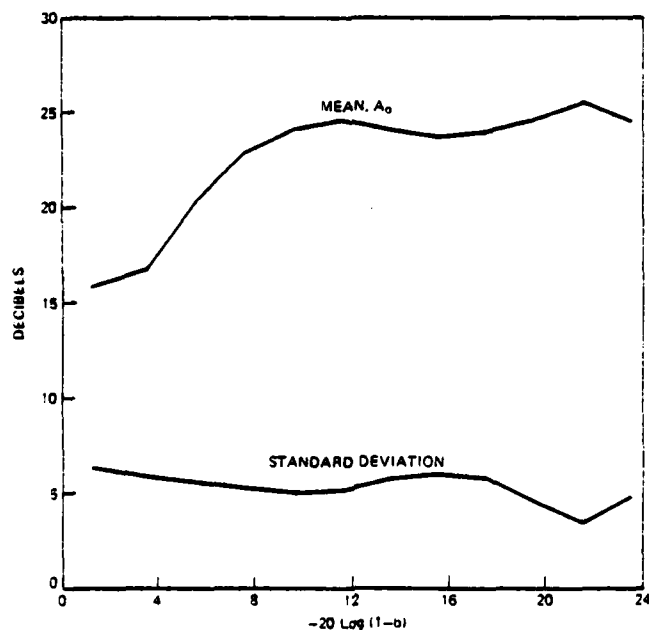


Fig. 11—Mean and standard deviation of the distribution of $-20 \log a$ as a function of $-20 \log (1 - b)$.

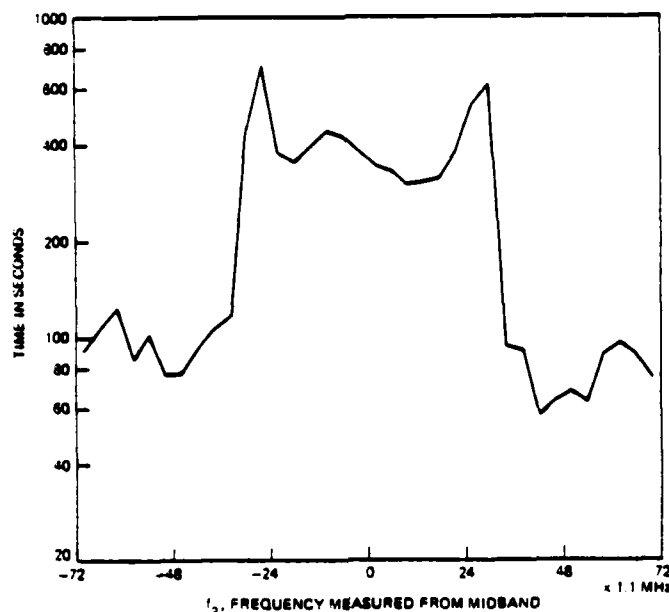


Fig. 12—Time that model parameter, f_m , was in intervals of width 4×1.1 MHz.

An extensive examination of various conditional distributions has established that there are no other obvious and pervasive dependencies among the statistics of the parameters.

V. CHANNEL DELAY DIFFERENCE

This section presents some results obtained in estimating the channel delay difference. Some techniques described here are used in the error analysis in Section VI. Three topics are considered in this section. First a simple method is presented of estimating the average delay spread in the channel. A second subsection shows that the distribution of large delays (larger than 10 ns) can be obtained for a simple three-path fade model. The delay distribution is shown to be consistent with the estimate of average delay. A third subsection illustrates the problem with an observed channel shape that can be matched most successfully using a simple three-path model with a delay of approximately 26 ns.

5.1 Mean delay difference in the channel

The mean delay difference of a channel that can be characterized by a simple three-path model is easily estimated. Consider a fade with a delay, τ . If f_m , the frequency of the minimum, is uniformly distributed,

the probability that such a fade produces a minimum in a band B Hz wide is equal to the ratio of the bandwidth to the spacing of the minima, or

$$\frac{B}{1/\tau} = B\tau. \quad (16)$$

If $p(\tau_k)\Delta\tau$ is the fractional number of fades having delays between $(k-1)\Delta\tau$ and $k\Delta\tau$, then the fractional number of fades having a minimum in band will be P_{\min} , where

$$P_{\min} = \sum_k B\tau_k p(\tau_k)\Delta\tau = B\bar{\tau} \quad (17)$$

and

$$\bar{\tau} = \sum \tau_k p(\tau_k)\Delta\tau = \int \tau p(\tau) d\tau. \quad (18)$$

It follows from eq. (17) that one may estimate the mean delay, $\bar{\tau}$, from a knowledge of P_{\min} , the fractional number of scans having a minimum in a band of width B . Since any method of determining P_{\min} is acceptable, consider estimates of P_{\min} from the parameters estimated using the fixed delay model. The method of estimating the frequency parameter in the model involved moving null positions of some fades that had out-of-band minima. These fades can be excluded by using only the central two-thirds of the band in estimating $\bar{\tau}$. Of the 24,920 scans in the data base, 3974 had minima between the 4th and 20th frequencies. Hence,

$$\bar{\tau} = \left[\frac{3974}{24920} \right] \frac{1}{16 \times 1.1 \times 10^3} = 9.1 \text{ ns.} \quad (19)$$

One might argue that the mean delay should be estimated for a more carefully screened set of scans. Table I shows the mean delay estimates obtained from scan populations qualified by having the estimate of the model parameter α in a given 5-dB interval. Table II

Table I—Mean delay for scans selected by value of parameter, α

-20 Log α , dB	Number of Scans	Scans with Min. in Band	Delay, $\bar{\tau}$, ns
0-5	101	31	17.4
5-10	725	235	18.4
10-15	4299	875	11.6
15-20	6591	1161	9.6
20-25	7644	906	6.7
25-30	4184	606	8.2
30-35	1019	159	8.9
All	24920	3974	9.1

Table II—Mean delay for scans selected by value of parameter, b

$-20 \log 1-b$, dB	Number of Scans	Scans With Min. in Band	Delay, $\bar{\tau}$, ns
0-2	10,442	1186	6.5
2-4	7040	1712	13.8
4-6	3721	538	8.2
6-8	1474	191	7.4
8-10	892	118	7.5
10-12	527	68	7.3
12-14	282	28	5.6
14-16	190	21	6.3
16-18	146	46	17.9
18-20	99	32	18.4
All	24920	3974	9.1

shows mean delay estimates qualified by the model parameter b , which specifies the shapeliness of the fade.

With several exceptions, the estimated delay spreads given in Tables I and II are reasonably constant. One exception is seen for large values of b ($-20 \log 1 - b$ greater than 16). This is consistent with a channel for which large differential attenuation across the channel is more likely to occur when long delays are present. The existence of such a correlation should not be surprising. The other exception is the large delays estimated for small values of b and for values of α between 0 and 10 dB. We provide strong evidence of the existence of such a class of fades in the next subsection. The existence of this subclass of fades suggests that they have a different physical source than the other fades in the population.

5.2 Distribution of delay difference

To further enhance our knowledge of the distribution of delay in the channel, the data base was processed to extract a delay estimate. Recall that, for the fixed delay model, parameter estimates are chosen to minimize the weighted fit error [E in eq. (9)] for a given fixed τ . The present calculation was performed for a set of different values of τ and the value which produced the smallest weighted fit error and corresponded to a realizable fade was designated as the delay for that scan if it met certain qualifications.

Because of the degeneracy in the simple three-path model, changing the delay in the fixed delay model will not appreciably improve the fit for any scan that can be well approximated by a fixed delay of 6 ns or less. In performing the optimum delay calculation, the weighted fit error was minimized for a predetermined set of delays; the differences between adjacent delay values were chosen to be approximately 15 percent. A given scan was assigned a delay different from 6.3 ns only if the third best value of the weighted fit error was at least 0.1 dB worse than the best value. (We use the third best value because we

must examine three values to detect a minimum.) This criterion sets a threshold on the acceptable sharpness of the minimum in the fit error with respect to changes in delay.

The selection criterion was chosen, after several iterations, to insure regularity in the estimates derived from successive scans. With the chosen criterion, the scans that were assigned a new delay occurred in groups of consecutive scans and may be said to constitute fading events. During any of these events, the delay was consistent in that indicated delays were within ± 15 percent. If we assume that the physical channel does not change between scans, we can associate a time with each scan and plot the distribution of the time periods during which the characterizing delay was greater than a specified delay.

A series of such plots, conditioned on the concurrently estimated value of b , is given in Fig. 13. The uppermost curve contains the data derived from all scans which met the selection criterion; its shape is

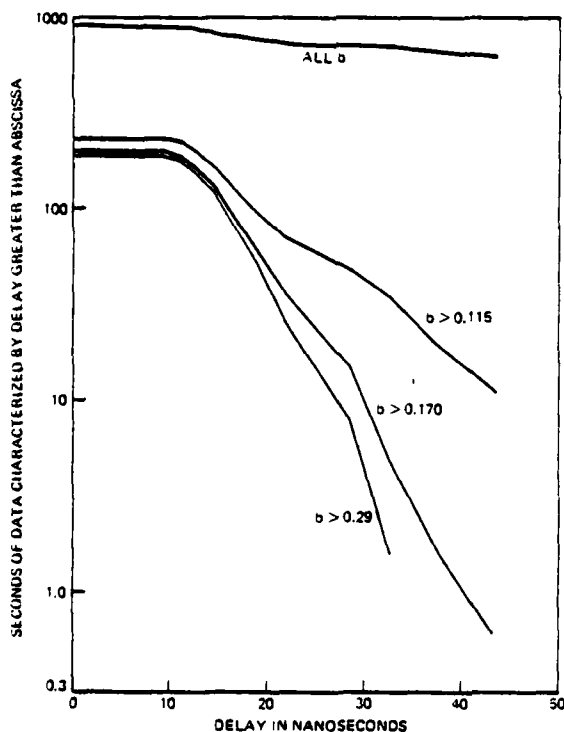


Fig. 13—Distribution of optimum delay for simple three-path model, as qualified by realizability, the sharpness of minimum, and by several values of the model parameter b .

dominated by the 627 seconds during which the channel was best modeled by a delay of 43 ns (the largest delay in the test set) or more, but had little shape ($b < 0.115$). These characteristics contribute to the large (18 ns) mean delays noted in the previous subsection for small values of b . They may be due to quantization but are apparently not artifacts of the estimation scheme. Although the origin of this type of channel defect is currently not understood, it should not trouble any existing radio system.

It is apparent from the distributions in Fig. 13 that very few scans qualified for a new delay with delays less than 10 ns. Consequently, the distribution should not be trusted for delays less than 12 or 15 ns; beyond 15 ns, it may be interpreted as a lower bound to the true distribution. The three curves qualified by the parameter b correspond to fades with peak-to-peak variability of 2, 3, and 6 dB. (Peak-to-peak variability is $20 \log(1 + b/1 - b)$, as may be seen in Fig. 1.) If the delay were exponentially distributed, the distribution of delay would be a straight line on Fig. 13 and would have the form

$$P(\tau > x) = e^{-x/\bar{\tau}}. \quad (20)$$

Fitting a straight line to the three distributions in Fig. 13 for which $b > 0.115$ shows that the average delay decreases with increasing b . The corresponding values are 5, 5.5, and 11 ns. Note that this implies that b and τ in a simple three-path model are not independent.

5.3 An example of a long delay scan

To confirm the existence of long delay scans, consider an event that covered approximately 10 seconds on 22 June 1977, from 23 h, 28 m, 54 s. A representative scan from the middle of this period is shown with the fit obtained with the fixed delay (6.3 ns) model in Fig. 14a. To emphasize the consistency of this channel condition, an average of the channel condition for the central 4.2 seconds (21 scans) of this event is compared to the selected scan in Fig. 14b.

It is apparent from Fig. 14a that the 6.3 ns delay does not have enough curvature (delay is too short) to precisely model the channel shape. Figure 15 shows the same scan modeled by three-path fades having delays of 22.7, 26, and 30.3 ns. The 26-ns fit is the best; it has a weighted fit error 0.4 dB better than the 22.7-ns fit and 0.8 dB better than the 30.3 ns fit. However, the closeness of all three fits illustrates the difficulties in estimating channel delay differences. Visually, one would choose the 26-ns model on the basis that the 30.3-ns fit has too much curvature and the 22.7-ns fit too little.

VI. ERROR ANALYSIS

To verify that the model adequately represents the transmission characteristics of the channel, we examine the errors between the

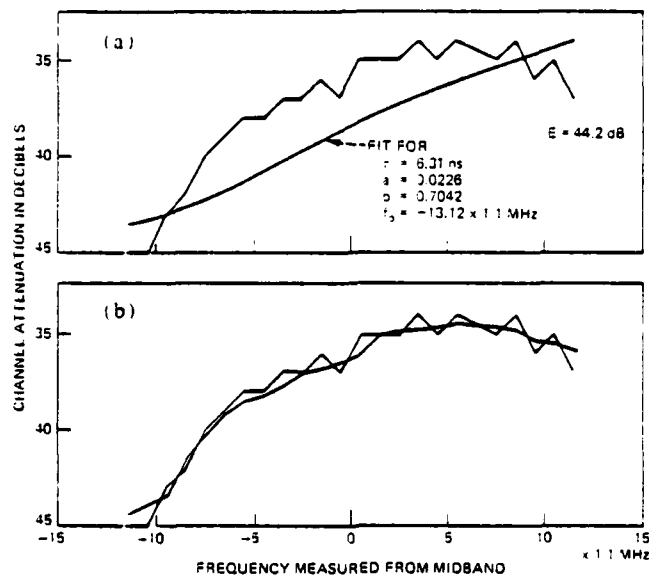


Fig. 14—Scan from 22 June 1977, 23 h, 28 m, 48.6 s. (a) Comparison with fixed delay model. (b) Comparison with average of scans from 23 h, 28 m, 46.4 s to 23 h, 28 m, 50.4 s.

channel as observed and as modeled. In this section we consider the statistics of the rms errors and the maximum errors.

6.1 RMS errors

A useful measure of the quality of the fit of the model to a given channel scan is the root-mean-square value of the decibel error at each of the sampled frequencies. Denoting this error as E_{rms} , we have

$$E_{rms} = \left[\frac{1}{23} \sum_{n=1}^{24} (\text{dB error at } f_n)^2 \right]^{1/2}. \quad (21)$$

The model parameters were estimated, as described in Section III, to minimize the error, E , which is a weighted sum of the squares of the power differences at each frequency [see eq. (9)]. The weighting was chosen [eq. (10)] so that the error E would approximate the error E_{rms} as given by eq. (21).^{*} Indeed, one may show directly that the two expressions are equivalent as long as

$$\left| 1 - \frac{Y_n}{Y_n} \right| \ll 1 \text{ for all } n. \quad (22)$$

^{*} Note that the parameter estimation problem cannot be solved in closed form by minimizing E_{rms} .

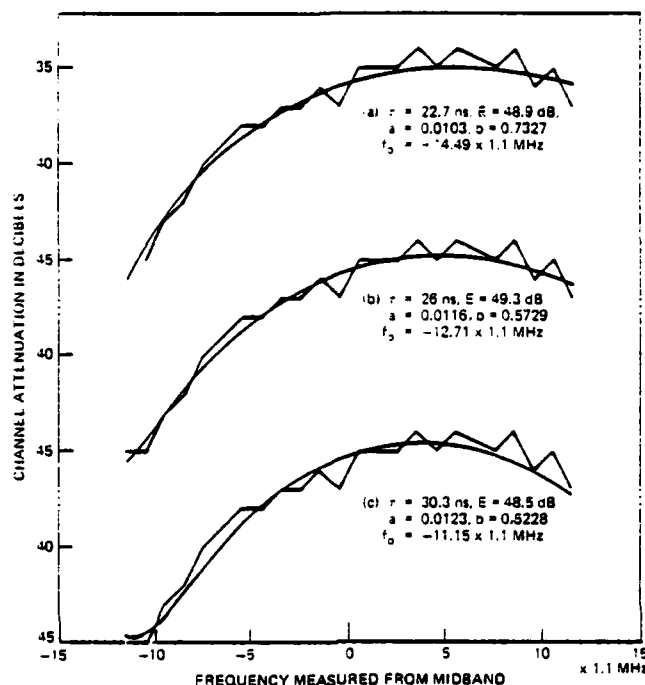


Fig. 15—Model fits to long delay scan for three different model delays.

As we have seen in Fig. 14, this inequality is not always satisfied. Consequently, in using E_{rms} as a standard of comparison, we are evaluating not only how well the model fits the observed channel, but also how well we have chosen the parameters to make the match.

The error E_{rms} is a desirable quantity to work with because we can estimate its distribution under the assumption of perfect matching. We observe that if the decibel error were Gaussian with unit variance and zero mean, $23 E_{rms}^2$ would be a χ^2 variable with 20 degrees of freedom (to account for the three parameters estimated per scan). Observations of a simulated channel with the transmitter and receiver back-to-back indicate that the instrumentation errors are approximately Gaussian with a standard deviation, σ_i , of about 0.65 dB. Observations of the channel at mid-day with the channel nominally flat and unfaded indicate that the standard deviation of the errors is between 0.68 and 0.73, varying frequency to frequency and day to day by a few hundredths of a decibel. Hence, if we enter a table of the χ^2 distribution, $Q(\chi^2 | 20)$, with

$$\chi^2 = \frac{23 E_{rms}^2}{\sigma_i^2}, \quad (23)$$

we can determine the distribution of E_{rms} under the assumption of perfect matching.* This distribution is shown as a reference on Figs. 16 and 17. It is indicated by a solid curve labeled "ideal" for $\sigma_i = 0.70$ and by o's for $\sigma_i = 0.75$.

Figure 16 presents the distribution of the rms error for two scan subpopulations using the fixed delay (6.3 ns) model. The subpopulation of the distribution labeled "standard" consists of all scans that could be modeled directly; the distribution labeled "modified" shows the rms error distribution for all scans which required an adjustment of the frequency of the modeled fade to achieve realizability. Figure 17 shows the distribution of the rms error for the composite of all samples using the fixed delay (6.3 ns) model. The distribution labeled simple three-path model indicates the error distribution that was obtained when the scan fitting allowed unqualified variation in model delay to achieve the best fit. That is, the calculation described in Section 5.2 was performed and the results were qualified only on the basis of realizability.†

In each case described above, the mean value of the rms error is close to the median value. For the two subpopulations shown in Fig. 16, the calculated mean fit errors correspond to σ_i values of 0.76 and 0.85 dB, or the errors are about 0.09 dB larger when a realizable fit is obtained by varying the frequency of the model minimum. Comparing the composite distributions in Fig. 17, we find that the mean error in the fixed delay (6.3 ns) model corresponds to $\sigma_i = 0.78$ dB or about 0.08 dB higher than that observed when the channel is quiescent. The simple three-path model has a distribution of rms error that very nearly matches the ideal distribution (with 19 degrees of freedom) for $\sigma_i = 0.75$. This is consistent with the instrumentation error imputed to the standard distribution in Fig. 16 and is indicative of the instrumentation error in the presence of multipath fading. It is exceptionally good considering that the data are obtained from time sequential measurements on a dynamically changing channel. One concludes that the modeling error is negligible for the simple three-path model. For the fixed delay model under the assumption that the instrumentation and modeling errors add in quadrature, the modeling error has a tolerable value on the order of 0.2 dB. That is,

$$[(0.75)^2 + (0.2)^2]^{1/2} = 0.776.$$

The tails of the distributions in Figs. 16 and 17 for large errors are of considerable interest. The tails near small values are of little

* From the central limit theorem, we know that E_{rms}^2 will be approximately Gaussian, as is χ^2 , regardless of whether or not the measurement errors are precisely Gaussian.

† Note that although one cannot always reliably localize the values of the parameters in fitting with the simple three-path model (see discussions in Section 2.1 and Ref. 7), the error in the fit is always well defined.

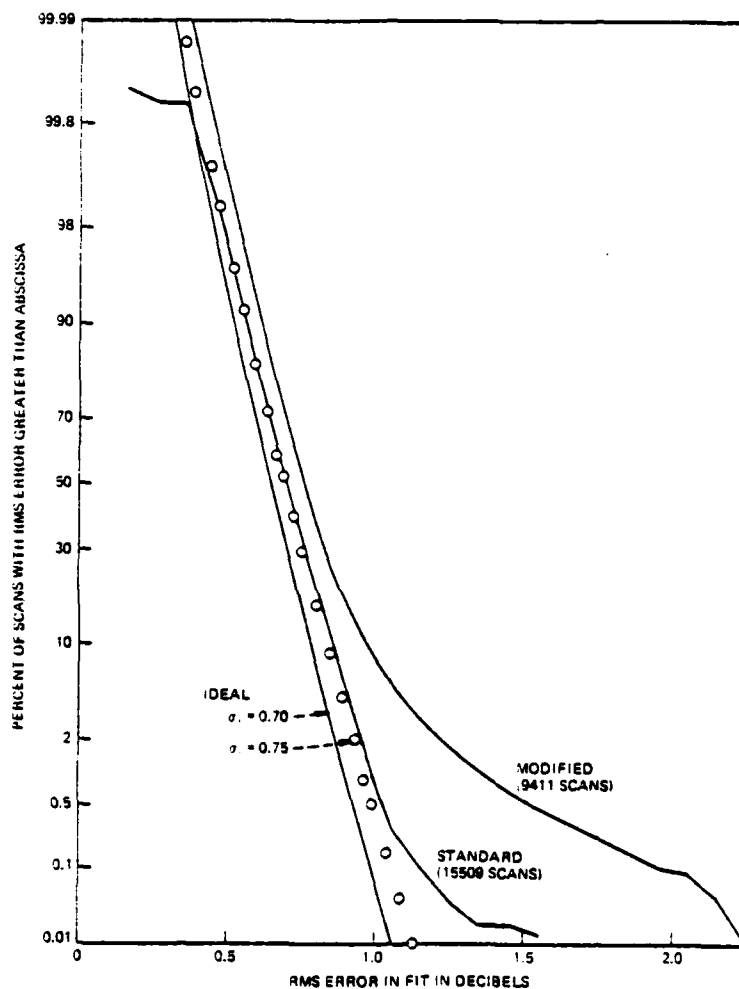


Fig. 16—Distribution of rms fit error for two scan subpopulations with fixed delay (6.3 ns) model.

consequence; they are distorted by quantization because one cannot associate any error with the 12 flat fades included in the data base. The deviation of the distributions from the ideal distribution at large errors is significant.

The large deviation of the modified fits in Fig. 16 reflects the failure of the fixed delay (6.3 ns) model to accurately fit the long delay fades. The tail deviation from ideal is modest down to about the 0.5 percent level, corresponding to a few tens of seconds per month. For compar-

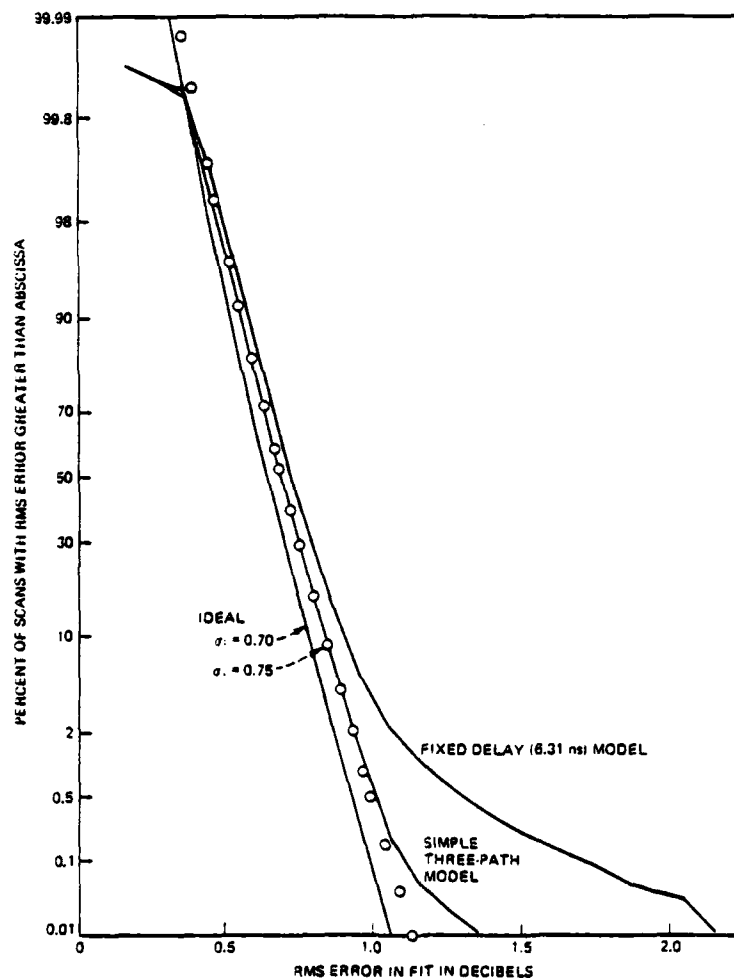


Fig. 17—Distribution of rms fit error for composite population with fixed delay and simple three-path models.

ison, we note that the rms error of the fit shown in Fig. 14a is 2.3 dB; this was the worst fit encountered for the fixed delay (6.3 ns) model. However, even in this case the model failure is hardly describable as severe. The model of the channel is depressed by 40 dB and has 9.5 dB of gain slope; the actual channel is depressed by 39 dB and has 11 dB of gain slope. Also, we note that the 6.3-ns delay model has the response minimum at about the same frequency as the best representation, the 26-ns delay model shown in Fig. 15.

NEW SELECTIVE FADING MODEL

The deviation of the tail of the error distribution for the three-path fade (Fig. 17) reflects the fact that there are fades that even this model has difficulty in fitting. An example of such a fade is shown in Fig. 18 along with the fit provided by the fixed delay (6.3 ns) model. The same rms error (1.6 dB) is obtained for all values of model delay between 0.05 and 9 ns; the fit degrades for larger delays. Either more than three rays are needed to describe the channel shape in Fig. 18, or the channel is so depressed that the amplitudes in the notch are distorted due to closeness to the noise level in the measuring equipment. The scan shown in Fig. 18 is one of three similar scans and has little statistical significance.

6.2 Maximum errors

Another type of error that can be used to judge the quality of the fit of the model to the channel is the worst-case error. That is, after fitting to each scan, one records the magnitude of the largest difference (in decibels) between the observed channel shape and the shape calculated from the model. The following paragraphs consider the distribution of these worst-case errors.

As in the preceding subsection, we can calculate an ideal distribution; however, the ideal distribution is not as realistic in this case since it is strongly dependent on the tails of the distributions of the individual measurement errors. We assume that each power measurement had

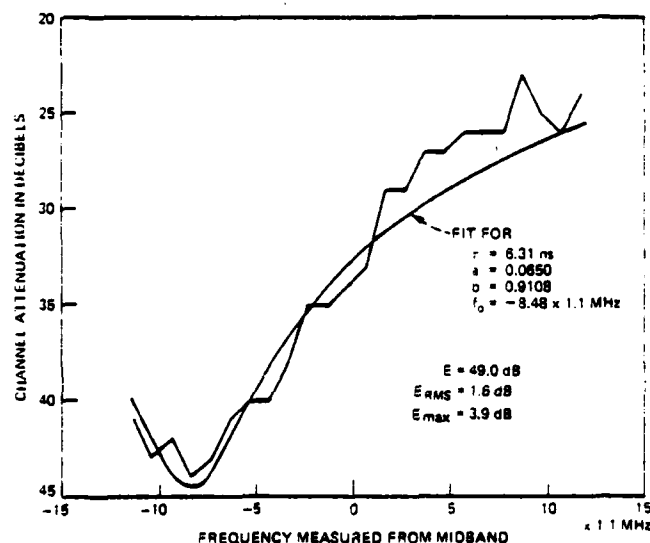


Fig. 18—Severe fade observed on 22 June 1977 at 22 h. 29 m. 8.6 s.

an error in decibels that was Gaussian, with zero mean, a standard deviation of $\sqrt{20/23} \sigma_i$ to account for the three parameters estimated from the 23 observations per scan,* and that the errors are independent frequency to frequency. If the probability of any one measurement having an error less than x is denoted by $P_1(x)$, the probability that all 23 have values less than x is

$$P_{23}(x) = [P_1(x)]^{23}. \quad (24)$$

This is the probability that the maximum error is less than x , whereas we want the probability that it is greater than x which we denote $Q_{23}(x)$. It follows immediately from eq. (24) that

$$\begin{aligned} Q_{23}(x) &= 1 - [P_1(x)]^{23} \\ &= 1 - [1 - Q_1(x)]^{23}. \end{aligned} \quad (25)$$

The distribution given by (25) is used as a reference in Figs. 19 and 20, which show the distribution of the maximum error for the same cases as in Figs. 16 and 17. Since the tails of these distributions are well behaved for larger errors, the distribution of the maximum errors is apparently dominated by the instrumentation noise. That is, if we use for the standard deviation of the measurement noise the value obtained from the mean of E_{rms} for one of these cases (as given in Section 6.1), the resulting worst-case error distribution calculated with eq. (25) will closely match the observed maximum error distribution.

VII. CONCLUSIONS

By analyzing the errors in fitting the observed channel characteristics in Section VI, we demonstrated that the simple three-path fade model is indistinguishable from a perfect model of a line-of-sight microwave radio channel.

The simple three-path model was used in Section V to characterize the channel delay difference. By two different methods, it was shown that, when there is 3 dB or more shape present in the channel, the average delay difference is between 5 and 8 ns. We developed a lower bound on the tails of the distribution of delay difference. From these results, which are shown in Fig. 13, we observe that a differential channel attenuation in-band of 3 dB or more may be due to delay differences as great as 43 ns. In another dimension, one would expect to see differential attenuation of 3 dB or more in-band due to delays greater than 20 ns for at least 70 seconds in a heavy fading month. This is comparable to the time the channel attenuation at a single frequency exceeds 40 dB.

* For comparisons with the three-path model, it is appropriate to use $\sqrt{19/23} \sigma_i$.

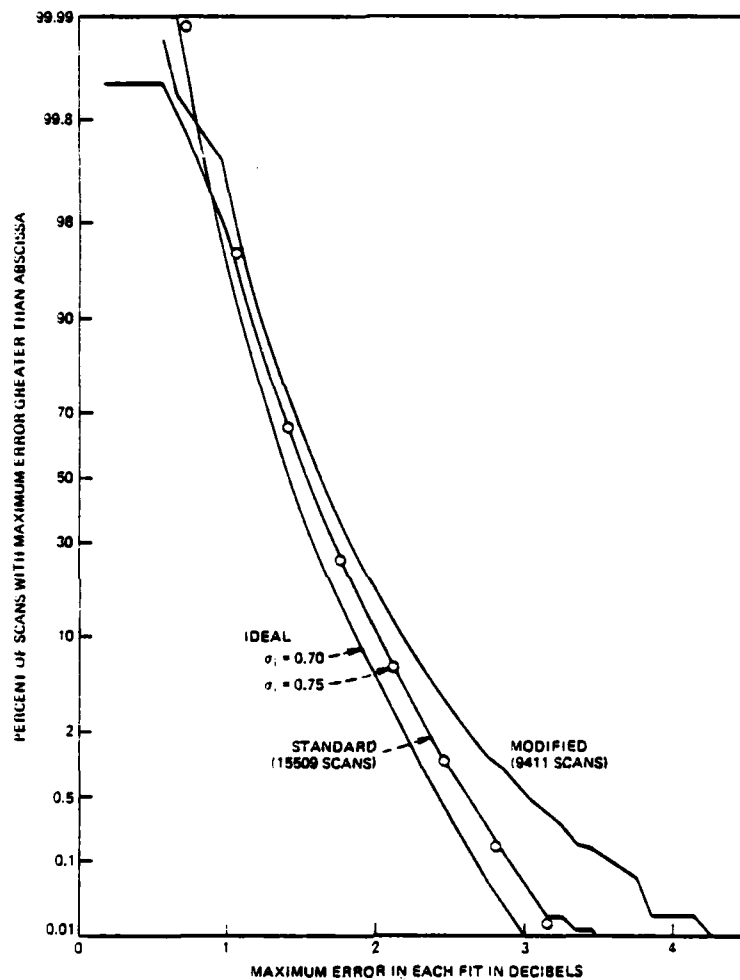


Fig. 19—Distribution of maximum (dB) fit error for two scan subpopulations with fixed delay (6.3 ns) model.

From the error analysis in Section VI, we also conclude that the fixed delay (6.3 ns) model is a very good approximation to the channel for all observed conditions. This conclusion is further substantiated by Figs. 14 and 18, which show the scans for which the fits with the fixed delay model exhibited the largest rms fit error (2.3 dB) and the largest maximum error (3.9 dB), respectively. The fixed delay model is preferable to the three-path model for channel modeling because it requires

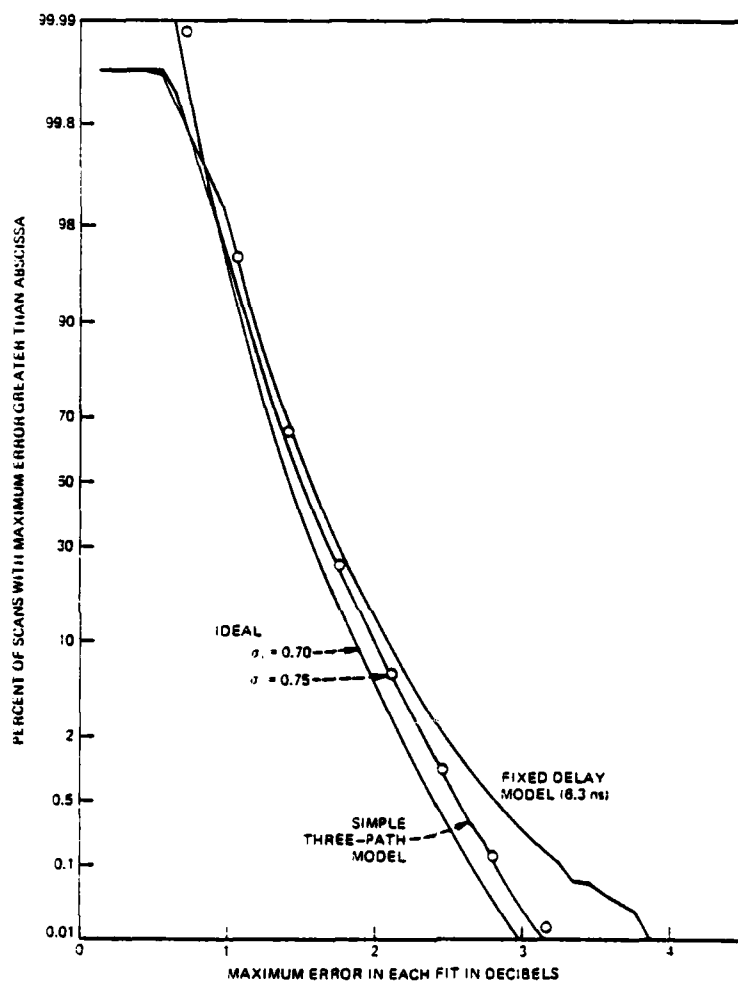


Fig. 20—Distribution of maximum (dB) fit error for composite population with fixed delay and simple three-path models.

only three parameters, and these can always be uniquely determined from a channel amplitude scan.

The statistics of the parameters of the fixed delay model as described in Section IV and shown in Figs. 8 to 12 provide the means of statistically generating all the channel conditions that one expects to see on a nominal hop channel operated at 6 GHz. If one determines, by laboratory test, the parameter values that will cause a particular

error rate in a digital radio system, one can easily calculate the time during a heavy fading month that the error rate will equal or exceed this critical value. A companion paper describes the laboratory test and the required calculations.⁸

Future work will be directed toward verifying the model and model statistics with additional fading data obtained both at 6 GHz and at 4 GHz. Using coherent data obtained in 1973, it will be possible to determine the extent to which the channel is actually a minimum phase channel.

VIII. ACKNOWLEDGMENTS

This study would not have been possible without the contributions of many individuals. In particular, the radio equipment was installed, aligned, and maintained by R. A. Hohmann, C. W. Lundgren, and L. J. Morris with instrumentation designed by G. A. Zimmerman. The data processing expertise in setting up and calibrating the data base was provided by M. V. Pursley.

APPENDIX

Estimation of Parameters

The problem of estimating the parameters α , β , and f_0 in Section III is equivalent to the problem of determining the first three terms in a subharmonic Fourier series expansion of a function in the frequency domain. Since such expansions are not standard, we provide a complete description of the methodology here.

From eqs. (4) and (9), we may express the weighted mean-square error between estimated and observed power as*

$$E = \frac{\sum C_n (Y_n - \alpha + \beta \cos(\omega_n - \omega_0)\tau)^2}{\sum C_n} \quad (26)$$

For simplicity, we use a normalized weighting function, d_n , defined by

$$d_n = \frac{C_n}{\sum C_n} \quad (27)$$

so that

$$\sum d_n = 1. \quad (28)$$

In terms of the normalized weighting we may write (26) as

$$E = \sum d_n (Y_n - \alpha + \beta \cos(\omega_n - \omega_0)\tau)^2 \quad (29)$$

* Throughout this appendix, all summations are taken over all values of n corresponding to all frequencies observed in a scan.

or in expanded form as

$$E = \sum d_n Y_n^2 + \alpha^2 + \beta^2 \sum d_n \cos^2(\omega_n - \omega_0) \tau + 2\beta \sum d_n Y_n \cos(\omega_n - \omega_0) \tau - 2\alpha\beta \sum d_n \cos(\omega_n - \omega_0) \tau - 2\alpha \sum d_n Y_n. \quad (30)$$

The error E is a minimum when α , β , and ω_0 are chosen so that the partial derivatives of E with respect to α , β , and ω_0 are all equal to zero. Setting the partial derivative of eq. (30) with respect to β equal to zero and solving for β gives

$$\beta = \frac{\alpha \sum d_n \cos(\omega_n - \omega_0) \tau - \sum d_n Y_n \cos(\omega_n - \omega_0) \tau}{\sum d_n \cos^2(\omega_n - \omega_0) \tau}. \quad (31)$$

Substituting (31) into eq. (30), we find E_β , the error minimized with respect to β , as

$$E_\beta = \sum d_n^2 Y_n^2 + \frac{1}{\sum d_n \cos^2(\omega_n - \omega_0) \tau} \cdot \{ \alpha^2 [\sum d_n \cos^2(\omega_n - \omega_0) \tau - (\sum d_n \cos(\omega_n - \omega_0) \tau)^2] - 2\alpha [(\sum d_n Y_n) (\sum d_n \cos^2(\omega_n - \omega_0) \tau) - (\sum d_n \cos(\omega_n - \omega_0) \tau) (\sum d_n Y_n \cos(\omega_n - \omega_0) \tau)] - (\sum d_n Y_n \cos(\omega_n - \omega_0) \tau)^2 \}. \quad (32)$$

Minimizing this with respect to α requires that we set the partial derivative of E_β with respect to α equal to zero. This gives

$$\alpha = \frac{(\sum d_n Y_n) (\sum d_n \cos^2(\omega_n - \omega_0) \tau) - (\sum d_n \cos(\omega_n - \omega_0) \tau) (\sum d_n Y_n \cos(\omega_n - \omega_0) \tau)}{\sum d_n \cos^2(\omega_n - \omega_0) \tau - (\sum d_n \cos(\omega_n - \omega_0) \tau)^2}. \quad (33)$$

Substituting (33) into (32) gives $E_{\alpha\beta}$, the error minimized with respect to both α and β , as

$$E_{\alpha\beta} = \sum d_n Y_n^2 - \bar{Y}^2 - \frac{(\sum d_n (Y_n - \bar{Y}) \cos(\omega_n - \omega_0) \tau)^2}{\sum d_n \cos^2(\omega_n - \omega_0) \tau - (\sum d_n \cos(\omega_n - \omega_0) \tau)^2}, \quad (34)$$

where

$$\bar{Y} = \sum d_n Y_n. \quad (35)$$

We note that we could have obtained this same expression by first minimizing with respect to α and then with respect to β ; however, one obtains different but equivalent expressions for α and β , depending on

the order of differentiation. We develop the alternative expressions for α and β in the following paragraphs.

Let us define some new quantities to simplify these expressions. Let the difference between the observed power and the weighted mean power in the band be designated by X_n ; then

$$X_n = Y_n - \sum d_n Y_n = Y_n - \bar{Y}. \quad (36)$$

If we also define the quantities

$$X_c = \sum d_n X_n \cos \omega_n \tau, \quad (37)$$

$$X_s = \sum d_n X_n \sin \omega_n \tau, \quad (38)$$

$$D_c = \sum d_n \cos^2(\omega_n - \omega_0) \tau, \quad (39)$$

$$D_s = \sum d_n \cos(\omega_n - \omega_0) \tau, \quad (40)$$

we may rewrite α and β from eqs. (31) and (33) as

$$\alpha = \bar{Y} - \frac{[X_c \cos \omega_0 \tau + X_s \sin \omega_0 \tau] D_s}{D_c - D_s^2} \quad (41)$$

and

$$\beta = \frac{1}{D_s} \{(\alpha - \bar{Y}) D_s - (X_c \cos \omega_0 \tau + X_s \sin \omega_0 \tau)\}. \quad (42)$$

Using (41) to eliminate α from (42), we obtain

$$\beta = - \frac{X_c \cos \omega_0 \tau + X_s \sin \omega_0 \tau}{D_c - D_s^2}. \quad (43)$$

We may use (43) in (41) to obtain

$$\alpha = \bar{Y} + \beta D_s. \quad (44)$$

Equations (43) and (44) are the estimators that would have been obtained if the order of taking partial derivatives in the preceding development had been reversed. It is apparent that, after one has estimated ω_0 , one may estimate α and β by using either eqs. (41) and (42), (43) and (44), or eqs. (41) and (43).

The estimate of ω_0 that minimizes the weighted error is obtained by minimizing $E_{\beta\beta}$ with respect to ω_0 . Using eqs. (35) to (40) in eq. (34), we write

$$E_{\beta\beta} = \sum d_n X_n^2 - \frac{[X_c \cos \omega_0 \tau + X_s \sin \omega_0 \tau]^2}{D_c - D_s^2}. \quad (45)$$

To see the explicit dependence of $E_{\beta\beta}$ on ω_0 , we define the following quantities

$$d_c = \sum d_n \cos^2 \omega_n \tau - (\sum d_n \cos \omega_n \tau)^2. \quad (46)$$

$$d_s = \sum d_n \sin^2 \omega_n \tau - (\sum d_n \sin \omega_n \tau)^2, \quad (47)$$

$$d_{cs} = \sum d_n \cos \omega_n \tau \sin \omega_n \tau - (\sum d_n \cos \omega_n \tau)(\sum d_n \sin \omega_n \tau). \quad (48)$$

Substituting these into (45) gives

$$E_{\beta s} = \sum d_n X_n^2 - \frac{[X_c \cos \omega_0 \tau + X_s \sin \omega_0 \tau]^2}{d_c \cos^2 \omega_0 \tau + 2d_{cs} \cos \omega_0 \tau \sin \omega_0 \tau + d_s \sin^2 \omega_0 \tau}. \quad (49)$$

Setting the partial derivative of $E_{\beta s}$, as given by (49), equal to zero gives the estimator for ω_0 as

$$\omega_0 \tau = \tan^{-1} \left[\frac{d_c X_s - d_{cs} X_c}{d_s X_c - d_{cs} X_s} \right]. \quad (50)$$

Obviously, two values of $\omega_0 \tau$ in the interval $(-\pi, \pi]$ will satisfy eq. (50). One of these, the principal value, lies in the interval $(-\pi/2, \pi/2]$, the other differs from the first by $\pm\pi$. We shall show that the two solutions are equivalent, but that our chosen solution is unique.

If we replace $\omega_0 \tau$ by $\omega_0 \tau \pm \pi$ in eqs. (39), (40), (43), (44), and (45), we see that D_s and β change sign and α and $E_{\beta s}$ are unchanged. Since we want the solution with β greater than zero, we take the principal value solution to (50) if the resulting estimate of β is positive. Otherwise we add or subtract π to obtain a positive value for β and a value of $\omega_0 \tau$ in the appropriate interval.

While we could substitute the result of eq. (50) into (49) to obtain the minimum error, $E_{\beta s \omega_0}$, it is more generally useful to evaluate $E_{\beta s}$ for the optimum ω_0 . This is especially true when we do not use the optimum ω_0 , as given by eq. (50). The simplest form for $E_{\beta s}$ is obtained by substituting (43) into (45) to give

$$E_{\beta s} = \sum d_n X_n^2 - (D_s - D_s^2) \beta^2. \quad (51)$$

These equations were implemented, with the modifications described in Section 3.2, to obtain all the fits described in this paper.

REFERENCES

1. G. M. Babler, "A Study of Frequency Selective Fading for a Microwave Line-of-Sight Narrowband Radio Channel," B.S.T.J., 51, No. 3 (March 1972), pp. 731-757.
2. G. M. Babler, "Selectively Faded Nondiversity and Space Diversity Narrowband Microwave Radio Channels," B.S.T.J., 52, No. 2 (February 1973), pp. 239-261.
3. L. J. Greenstein, "A Multipath Fading Channel Model for Terrestrial Digital Radio," IEEE Trans. Commun. Tech., COM-26, No. 8 (August 1978), pp. 1247-1250.
4. R. L. Kaytor, "A Statistical Study of Selective Fading of Super-High Frequency Radio Signals," B.S.T.J., 32, No. 5 (September 1953), pp. 1187-1202.
5. G. M. Babler, unpublished work.
6. W. C. Jakes, Jr., "An Approximate Method to Estimate An Upper Bound on the Effect of Multipath Delay Distortion on Digital Transmission," ICC '78 Conference Record, June 1978, 3, pp. 47.1.1-5.
7. W. D. Rummler, "A Multipath Channel Model for Line-of-Sight Digital Radio Systems," ICC '78 Conference Record, June 1978, 3, pp. 47.5.1-4.
8. C. W. Lundgren and W. D. Rummler, "Digital Radio Outage Due to Selective Fading—Observation vs Prediction from Laboratory Simulation," B.S.T.J., this issue, pp. 1073-1100.

Digital Radio Outage Due to Selective Fading—Observation vs Prediction From Laboratory Simulation

By C. W. LUNDGREN and W. D. RUMMLER

(Manuscript received July 7, 1978)

A statistical model (introduced in a companion paper) of fading on a radio path is used with laboratory measurements on a digital radio system to estimate the outage due to multipath fading, where outage is the time that the bit error rate (BER) exceeds a threshold. Over the range of BER of interest (10^{-6} to 10^{-3}), the calculated outage agrees favorably with the outage observed during the period for which the fading model was developed. It is further shown that the calculated outage, when scaled to a heavy fading month on the basis of single-frequency, time-faded statistics, agrees equally well with the outage observed on the same path during a heavy fading month. The agreement between measured and predicted outage substantiates the selective fading model. The prescribed laboratory measurements characterize the sensitivity of the radio system to selective fading. Thus, the methodology provides a useful basis for comparing the outage of alternative realizations of digital radio systems.

I. INTRODUCTION

Present interest in using high-speed common carrier digital radio¹⁻⁵ has precipitated a need for estimating the performance of such systems during periods of selective (multipath) fading. This paper describes a method of characterizing a digital radio system in the laboratory which allows the outage to be accurately estimated. For a digital radio system, outage requirements are stated in terms of the number of seconds in a time period (usually a heavy fading month) during which the bit error rate (BER) may exceed a specified level; typically, 10^{-3} or 10^{-4} is appropriate to voice circuit application.

The method is based upon a statistical channel model⁶ developed from measurements on an unprotected 26.4-mile hop in the 6-GHz band in Palmetto, Georgia in 1977 using a general trade 8-PSK digital

radio system as a channel measuring probe. The modeled fading occurrences were scaled to the basis of a heavy fading month using the occurrence of time faded below a level at a single frequency as the means of calibration. The bit error rate performance of the digital radio system was measured during the time period used for channel modeling and for an extended period corresponding to a heavy fading month. This same radio system was later subjected to a measurement program in the laboratory using a multipath simulator which provides a circuit realization of the fading model. The measured results are used with the channel model to determine the occurrence of channel conditions which will cause the BER to exceed a given threshold. Comparisons on the basis of the modeling period and a heavy fading month show good agreement between calculated and observed outages for BERs between 10^{-6} and 10^{-3} .

The properties of the fixed-delay channel model are reviewed briefly in Section II as a basis for describing the measurements and for the subsequent outage calculations. This three-parameter channel model is realized in the laboratory by an IF fade simulator. The simulator and its use in obtaining the necessary laboratory data are described in Section III. The procedures to be followed in calculating outage times for a given BER are described in Section IV. Calculated and observed outage times are compared in Section V. Conclusions are provided in Section VI.

II. MODEL DESCRIPTION—METHODOLOGY

It has been demonstrated⁶ that the complex voltage transfer function of a line-of-sight microwave radio channel is well modeled by the function

$$H(\omega) = a [1 - be^{-(\omega - \omega_0)\tau}] \quad (1)$$

with τ fixed. A 6-GHz channel (30-MHz bandwidth) has been characterized statistically by the model with $\tau = 6.3$ ns. Such a channel has a power transfer function given by

$$|H(\omega)|^2 = a^2 [1 + b^2 - 2b \cos(\omega - \omega_0)\tau] \quad (2)$$

and an envelope delay distortion function, i.e., the derivative of the phase of $H(\omega)$ with respect to ω , given by

$$D(\omega) = \frac{b\tau(\cos(\omega - \omega_0)\tau - b)}{1 + b^2 - 2b \cos(\omega - \omega_0)\tau} \quad (3)$$

In the following paragraphs, we summarize the properties of the model, the statistics of the model parameters, and the measurement objectives.

2.1 Fixed delay model

A plot of the attenuation produced by the fixed delay model of eq. (1) is shown in Fig. 1. Since the delay is fixed at 6.3 ns, the spacing between nulls of the response, 158.4 MHz, is much larger than the channel bandwidth. The parameters a and b control the depth and shape of the simulated fade, respectively. The parameter $f_0 (= \omega_0/2\pi)$ determines the position of the fade minimum or notch. Both the notch frequency, f_0 , and the response frequency, f , are measured from the center of the 30-MHz channel for convenience.

The model function of eq. (1) may be interpreted as the response of a channel which provides a direct transmission path with amplitude a and a second path providing a relative amplitude b at a delay of 6.3 ns and with a phase of $\omega_0\tau + \pi$ (independently controllable) at the center frequency of the channel. This interpretation is represented in Fig. 2 by a phasor diagram at $\omega = 0$, the center frequency of the channel. Varying the frequency, ω , over the channel bandwidth (30 MHz) moves the angle of the interfering ray through an arc of about 60 degrees ($2\pi \times 30 \text{ MHz} \times 6.3 \text{ ns} \approx \pi/3$), centered at the position shown. This diagram is useful for understanding the fade simulation; it also provides an alternate means of describing the position of the notch. The notch position may be specified by its frequency, f_0 , or by ϕ , the angle of the interfering path at the center of the channel.

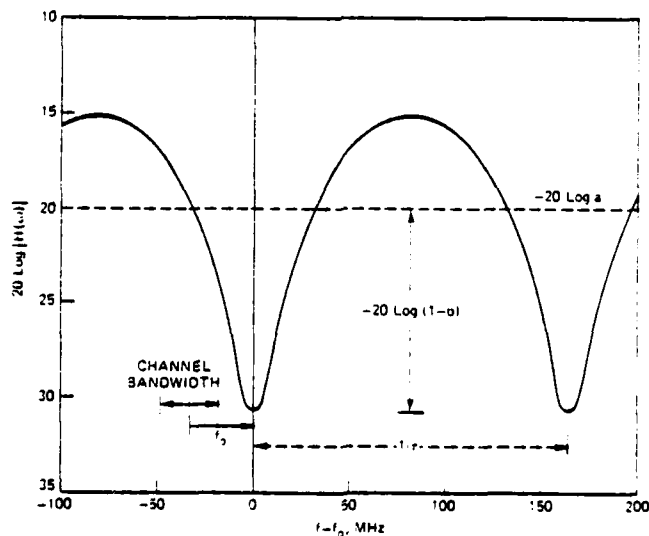


Fig. 1—Attenuation of channel model function, $H(\omega) = a[1 - b \exp(-j(\omega - \omega_0)\tau)]$, for $\tau = 6.3 \text{ ns}$, $a = 0.1$, $b = 0.7$.

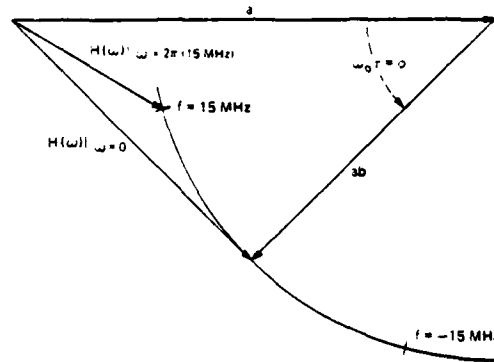


Fig. 2—Phasor diagram of a modeled fade, $\phi = 45^\circ$, $b = 0.7$.

From Figs. 1 and 2, or eq. (1), it may be seen that varying a changes the overall level and varying b changes the shapeliness of the modeled fade. Furthermore, if the minimum is within the 30-MHz channel bandwidth ($|\phi| < 30^\circ$), the fixed delay model can generate notches with a wide range of levels and notch widths. With the minimum out of band, it can generate a wide range of combinations of levels, slopes, and curvatures within the channel bandwidth.

2.2 Model statistics

The statistics of the model parameters were obtained from a selected data base during which heavy fading activity was observed.⁶ The distribution of b is best described in terms of $B = -20 \log(1 - b)$. Figure 3 shows the distribution of B and the least-squares straight line fit to the distribution over the region where it best represents selective fading—between B values of 3 and 23 dB. The channel is described by B greater than 23 dB for less than 0.15 percent of the observed time which makes the distribution less certain beyond this point. At the other extreme, during the periods of time when there is little or no selective fading, the channel is characterized by values of B less than 3 dB. Thus, the fitted line represents a lower bound on the distribution for B less than 3 dB. Since the fitted line has an intercept of 5400 seconds, we may model the fraction of 5400 seconds during which B exceeded a value X by the probability distribution

$$P(B > X) = e^{-X/3.8}. \quad (4)$$

Thus the probability of finding a value of B between X and $X + dX$ is

$$p_B(X) dX = \frac{dX}{3.8} e^{-X/3.8}. \quad (5)$$

The distribution of a is lognormal with a standard deviation of 5 dB and a mean that is dependent on B (or b). Hence, the probability that

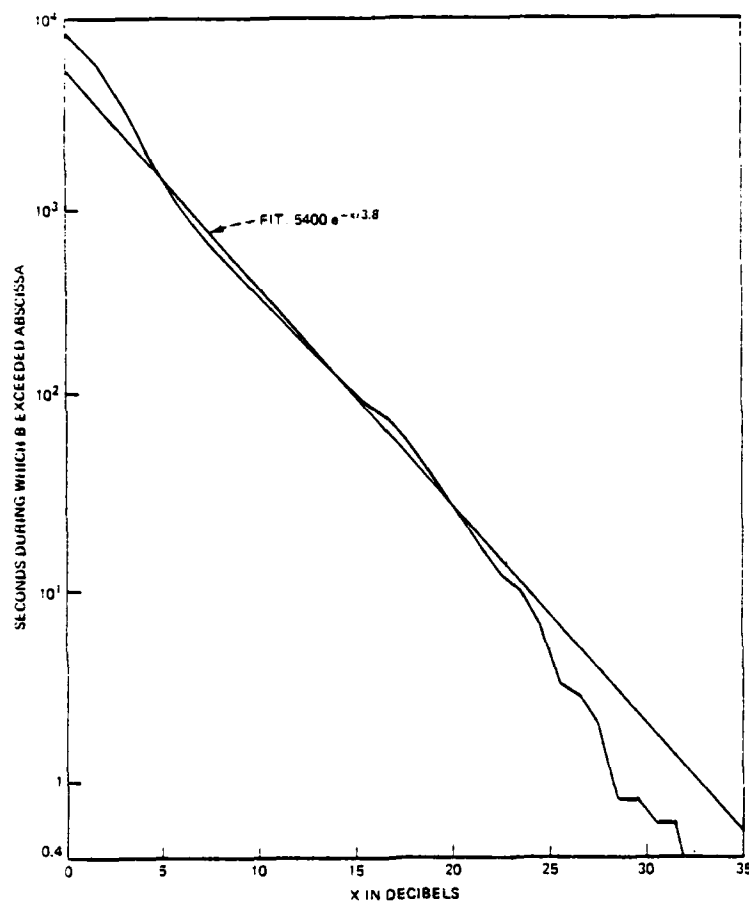


Fig. 3—Distribution of B for model data base period.

$A = -20 \log \alpha$ has a value between Y and $Y + dY$ is given by

$$p_A(Y) dY = \frac{dY}{5\sqrt{2\pi}} e^{-\{Y - A_0(B)\}^2/50}. \quad (6)$$

The relationship between A_0 , the mean of the distribution, and B is given in Fig. 4.

The distribution of f_o is found to be independent of A and B . It is usually simpler to work with ϕ rather than f_o . The two variables are simply related in that ϕ is defined on the interval $(-\pi, \pi)$ and a 2.5-degree change in ϕ corresponds to a 1.1-MHz change in f_o . For the fixed delay model, the variable ϕ has been found to have a probability density function that can be described as uniform at two levels, with

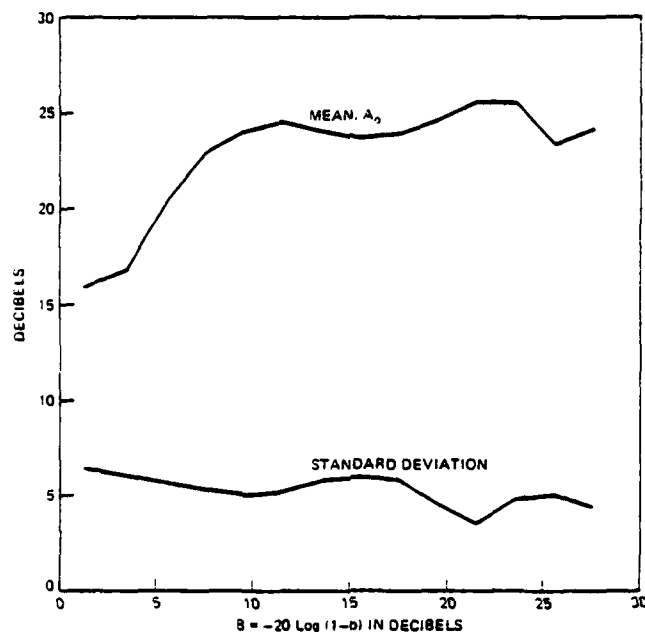


Fig. 4—Mean and standard deviation of the distribution of $A = -20 \log \alpha$ as a function of B .

values less than $\pi/2$ being five times more likely than values greater than $\pi/2$. Thus, we have the probability density function per degree as:

$$p_\phi(\phi) = \begin{cases} \frac{1}{216} & |\phi| < 90^\circ \\ \frac{1}{1080} & 90^\circ \leq |\phi| \leq 180. \end{cases} \quad (7)$$

The functions in eqs. (5) to (7) can be used to determine the probability of finding α , b , and f_0 in some region of α - b - f_0 space. This probability can be converted to number of seconds in the observation period by multiplying by 5400 seconds. To convert this probability to the number of seconds in a month requires scaling the data base. The scaling may be obtained from Fig. 5 which shows, for several frequencies in the band, the time during the model data base period that the channel was faded below a given level. Distributions are shown for average power in the band and for power at selected frequencies at the center and near the edges of the radio channel. (Frequencies indicated are at 1F where the center frequency is at 70 MHz.) For the path used,

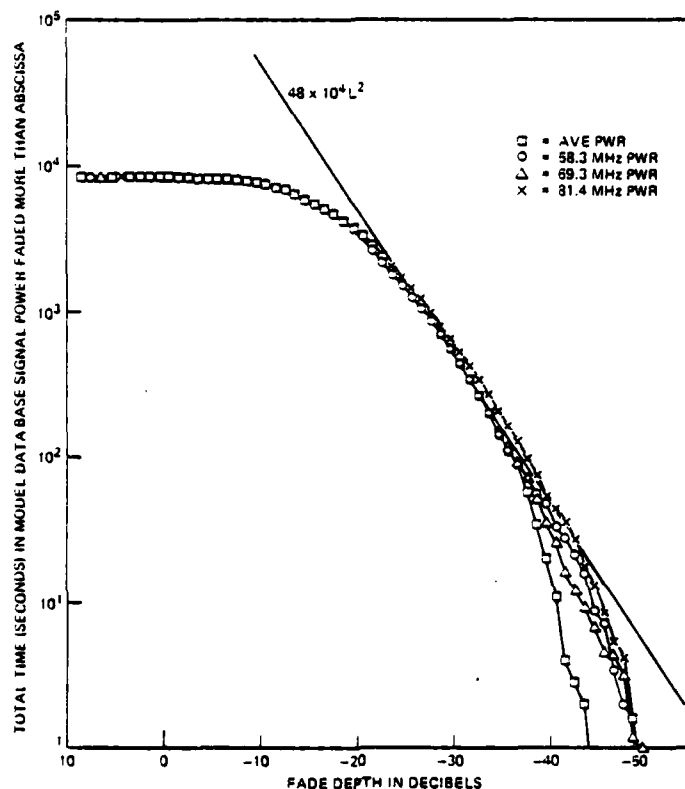


Fig. 5—Amplitude distributions for model data base period.

one expects the received voltage (single frequency) relative to midday average to be less than L for $72.5 \times 10^4 L^2$ seconds in a month.⁷ For the data base used, the fading is best described by $48 \times 10^4 L^2$ hence, the data represent $\frac{2}{3}$ of a fading month. To obtain outage on a seconds-per-heavy-fading-month basis, the probabilities calculated with eqs. (5) to (7) must be multiplied by 5400×1.5 or 8100 seconds.

2.3 Outage estimation

The fixed delay model described above can be simulated with an equivalent circuit laboratory measurement to determine the equipment response to multipath fading. Conceptually, one determines critical values of A and B for which a specified error rate is achieved for each fade notch position. In practice, it is difficult to maintain a constant BER; it is more expedient to fix b and vary the carrier-to-noise ratio (a) while plotting the BER. From the resulting curves, one may

DIGITAL RADIO OUTAGE DUE TO FADING

compute critical contours of A and B for each prescribed notch location and BER. Using eqs. (5) and (6), the probability that A and B lie on the high error rate side of a given critical contour may be calculated.

By repeating this calculation for a uniform set of notch positions and using (7) to determine the probability weighting given to each and summing, one may estimate the probability of all selective fades that produce a BER exceeding the prescribed one. Multiplying this probability by 5400 gives the outage time expected over the data base period; multiplying by 8100 gives the expected outage time per heavy fading month.

The following section describes the laboratory measurement; Section IV describes the reduction of the measured curves and parameters to outage times.

III. LABORATORY MEASUREMENTS

Figure 6 illustrates stressing of a digital radio system by means of an IF fade simulator. The simulator, which is inserted after linear IF preamplification but before any high-gain amplification, shapes both the desired signal and the effective received noise. It is necessary to operate the simulator at a sufficiently large input carrier-to-noise ratio that the concomitantly shaped noise at its output remains a negligible contributor to degraded system performance throughout the operating range of interest.

Within its restricted frequency range of operation, the IF simulator is adjusted to achieve those specific shapes implied by Fig. 2. Although the measurements could have been made using an RF fade simulator, the choice of an IF simulator was based primarily upon considerations of signal and noise levels, and the repeatability of adjustments. The following section describes an IF shape-stressing measurement in the minimum detail necessary to qualify the data collected.

3.1 Representative IF two-path fade stressing measurement

The block diagram of Fig. 7 illustrates an arrangement employing an IF fade simulator and an IF flat noise source. A pseudo-random test

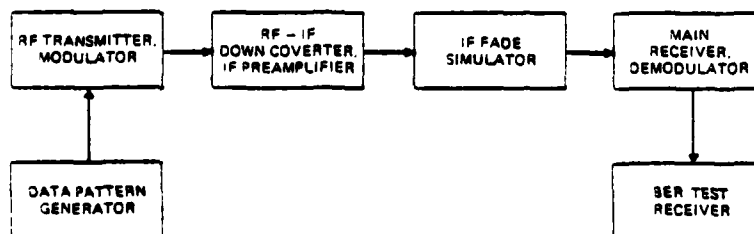


Fig. 6—IF fade stressing.

pattern modulates the 6-GHz radio transmitter whose output is nominally 5 watts (Ⓐ, in Fig. 7). The output spectrum is usually shaped by a bandpass filter following the microwave power amplifier to comply with FCC regulations.

To enable back-to-back operation of the transmitter and receiver of a single repeater which normally operate on different radio channels, a radio test translator was employed. The translator output power was approximately -30 dBm (adjustable, at Ⓑ) to simulate the unfaded received signal level (RSL) observed typically in the field.

Assuming a linear RF-IF conversion gain of 20 dB, the signal power at the input (Ⓒ) to the IF fade simulator is -10 dBm. The simulator incorporates low-noise linear amplification. A reference insertion loss for the main unfaded ray is 10 dB, including the output power summer. Hence the maximum desired signal power at the input to the main IF amplifier (Ⓓ) is -20 dBm.

Assuming a 30-MHz receiver noise bandwidth and a current-art receiving system noise figure of 5 dB, the total system noise power is approximately -95 dBm, referred to the receiver's input port. This results in a flat receiver noise contribution of -85 dBm at input Ⓒ to the main IF amplifier. Consequently, the maximum attainable carrier-to-simulator-shaped RF noise ratio is $10 \log (C_0/N_{rf}) = -20 - (-85) = 65$ dB. The noise contributed by the fade simulator amplifiers must not exceed -100 dBm, to be negligible.

Flat IF noise much larger than the unwanted and shaped system noise is added artificially at Ⓒ and is adjusted in magnitude by a calibrated attenuator Ⓔ to superpose thermal noise degradations upon the simulated selective fading degradations of the desired signal. One would ideally measure the added IF noise power in the final predetection bandwidth of the digital radio system, or twice the Nyquist bandwidth. It is more convenient in the laboratory to reference carrier-to-noise ratios to the output of the main IF amplifier by using the precalibrated AGC voltage (assuming that wideband AGC detection is employed), to measure both the unshaped signal and noise powers. The carrier-to-noise ratio at the detector would be higher—by the ratio of the system noise bandwidths that would be measured at the respective points.

The noise source output in Fig. 7 may be adjusted so that an attenuator setting of 0 dB Ⓔ results in a noise power equivalent to that of the unfaded signal power (the attenuator is then calibrated directly in uncorrected C_0/N_{if} , in dB). As the IF fade simulator is readjusted to achieve different prescribed fade shapes, its mean insertion loss may also change. The change in insertion loss is determined by monitoring the change in signal power at Ⓒ; the same loss increment (dB) must be added to the noise attenuator Ⓔ to reestablish the 0 dB reference.

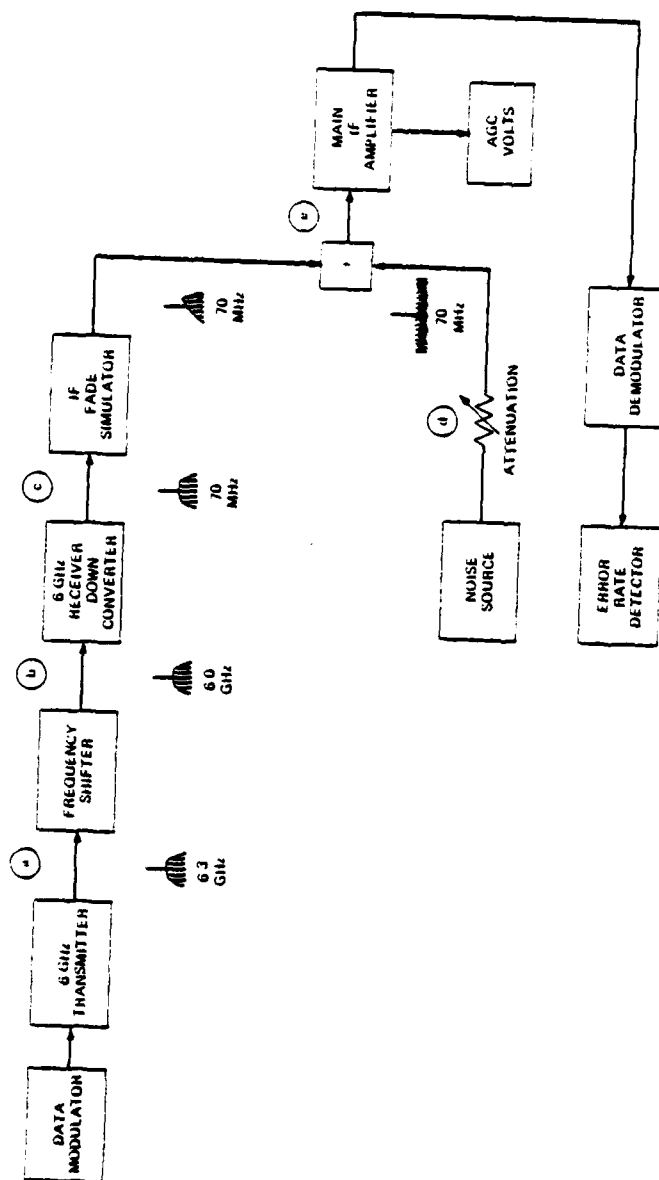


Fig. 7—Laboratory test arrangement.

3.2 IF two-path fade simulator

Figure 8 illustrates splitting the desired IF signal into an arbitrarily phased, adjustable "main" component and a "delayed" component fixed in delay (τ ns) but adjustable in magnitude. The main component is further resolved into orthogonal components (inset to Fig. 8) using wideband networks exhibiting flat gain and well-behaved delay. A particular sum vector is constructed by adjusting the orthogonal components to establish a simulated fade notch frequency; in practice, the phase sense of 0- and 90-degree components are independently reversible, as indicated by the switches in the figure, for complete flexibility in notch frequency selection.

The 6.3-ns fixed delay added to the delayed path imparts a phase shift of 159 degrees at the 70-MHz IF center frequency. This is shown built out to 225 degrees, relative to the 0-degree transmission path, using a 66-degree wideband network of the same type. The delayed vector is fixed in direction opposite the midrange position of the adjustable main vector, corresponding to a channel-centered fade ($\phi = 0$ degrees).

Since $1/\tau = 158.4$ MHz, a change of 1 degree in direction of the main vector corresponds to a frequency displacement of the fade notch location of 0.44 MHz. For $\phi = -45$ degrees, the notch location is displaced 19.8 MHz below the channel center ($f_0 = -19.8$ MHz). The magnitude of the delayed component is then adjusted to achieve the desired notch depth.

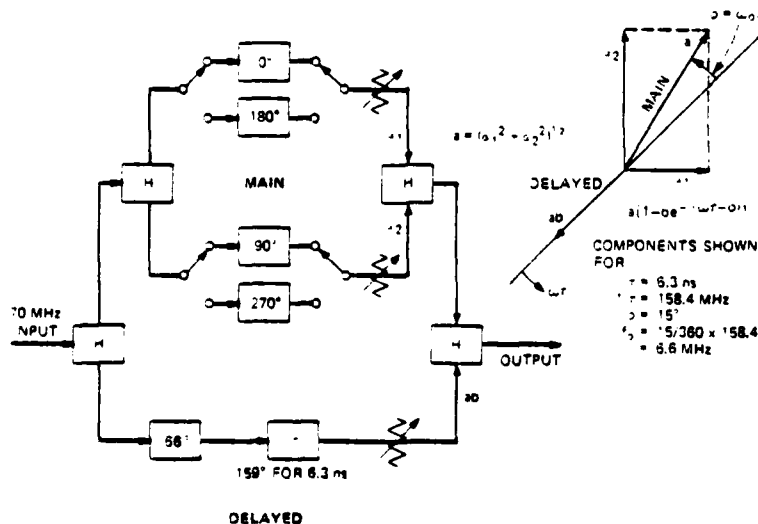


Fig. 8—IF fade simulator—conceptual block diagram.

DIGITAL RADIO OUTAGE DUE TO FADING

3.3 Digital radio performance stressed by in-band selectivity and thermal noise

The radio equipment was measured at uniformly spaced notch frequencies separated by 4.4 MHz ($\Delta\phi = 10$ degrees). To fully characterize a period of variation in ϕ , or f_o , one would need to make 36 sets of measurements. *Ideally*, half may be omitted because of symmetry. For given values of A and B , the same error rate should obtain for a notch at a given frequency displacement above or below the channel band center. Variations in B ought not to have a significant effect for $|\phi|$ greater than 90 degrees. It was determined that detailed measurements were required for nine different values of f_o to characterize the digital radio tested.

Using a wideband RF fade simulator in the field, the digital radio performance for out-of-channel notch locations was relatively independent of whether minimum or nonminimum-phase fade simulations were employed. The nonminimum phase fade is modeled by eq. (1) with the sign of the phase term reversed. This leaves the amplitude [eq. (2)] unchanged, but reverses the sign of the envelope delay distortion [eq. (3)]. We conclude that the minimum phase channel model is sufficiently general for use in simulating the channel and in estimating performance.

The IF fade simulator was adjusted for each notch frequency, and the depth of notch was varied by adjusting the magnitude of the delayed component. Then various amounts of IF thermal noise were added. Figure 9 typifies the performance data collected. BERs are plotted *versus* the uncorrected IF carrier-to-noise ratio (C/N_{if}), for a constant fade notch offset from midchannel ($f_o = -19.8$ MHz, $\tau = 6.3$ ns). Each curve corresponds to a different notch depth ($B = -20 \log(1-b)$ dB), and hence a different amplitude and delay shape in the radio channel. Each curve is also identified with an in-band selectivity, defined as the difference between the maximum and minimum attenuation present in the (25.3-MHz) channel bandwidth. The lower-left "baseline" curve presents the unshaped signal, flat fading performance obtained by adding only IF thermal noise. This curve was verified (without the added IF noise) by attenuating the received RF input signal in the back-to-back configuration.

Consideration was given to matching the order of measurements to characteristics of the particular digital radio tested. For example, considerable scattering of data at low error rates can result from synchronizations involving different reference carrier phases. The authors elected to perform several synchronizations while observing the BER for each phase, and then chose that phase giving the worst performance.* Synchronization was accomplished at the low error rate

* Because the phase information in the measured system was Gray coded and digital access was on a per-rail basis, one rail had twice the BER of the other two. All measurements in the field and in the laboratory were made on this worst-case rail.

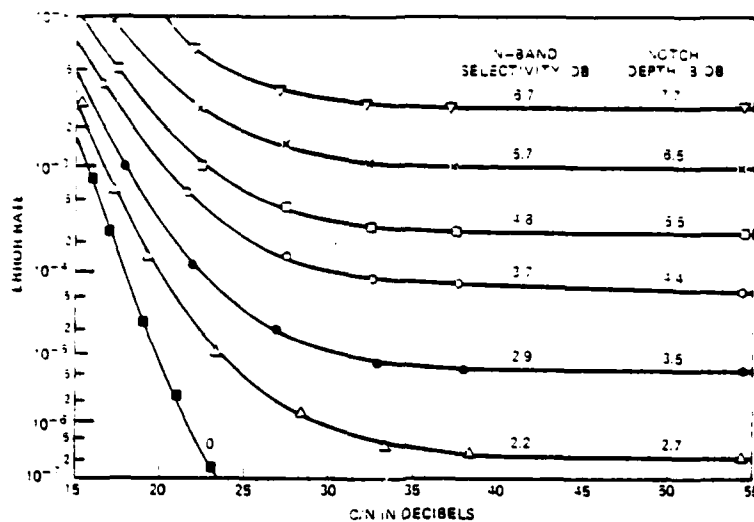


Fig. 9—High-speed digital radio IF dispersive fade simulations. $\tau = 6.3$ ns, $f_0 = -19.8$ MHz.

(bottom) of each curve, and this phase relationship was maintained for all data points obtained for each curve.

From the baseline curve of Fig. 9, a $\text{BER} = 1 \times 10^{-6}$ obtains for $10 \log(C/N_f) \approx 21.5$ dB. For the digital radio system installed on the instrumented hop and reported in the figure, the measured flat fade margin for a threshold $\text{BER} = 1 \times 10^{-6}$ was 40.5 dB. This leads to an unfaded IF carrier-to-noise ratio $10 \log(C_0/N_{if}) \approx 21.5 + 40.5 = 62$ dB.

From the baseline curve for a $\text{BER} = 1 \times 10^{-7}$, note that insertion of a fade whose notch depth is 6.5 dB results in four orders of magnitude degradation in BER performance; equivalently, an in-band selectivity of only 5.7 dB in 25.3 MHz results in a $\text{BER} > 1 \times 10^{-3}$.

The asymptotic regions in Fig. 9, corresponding to high values of C/N_f , are not normally presented in characterizations of this type; however, system outage depends primarily upon the performance in these asymptotic regions. Thus, under typical fading conditions, the transmitted carrier power might be increased at will without improving the BER significantly. The effects of decreasing the carrier power are discussed in Section 4.4.

A family of curves like those shown in Fig. 9 was obtained (but are not given here) for each of nine uniformly spaced frequency offsets below midchannel to characterize the digital radio system sufficiently for the prediction of outage. A number of spot checks were also made using both RF and IF fade simulators at symmetrical positive and negative offset frequencies, to establish that acceptable symmetry existed.

IV. CALCULATION OF OUTAGE

This section describes four methods of calculating outage. The derivation of the critical curves of A and B , which provide the basis for making and understanding these calculations, is given in Section 4.1. In Section 4.2 the detailed calculation of outage from the critical A - B curves is described. It is shown in Section 4.3 that for the present system this method may be greatly simplified by calculating only selectivity-caused outage (i.e., neglecting thermal noise). Section 4.4 presents an approximate method of accounting for the effects of thermal noise. Section 4.5 provides a basis for estimating the selectivity-caused outage from a single measurement.

4.1 Derivation of critical characteristics

To calculate the outage for a fixed bit error rate, one must first obtain the critical curves of A and B at each simulated value of f_o , the notch position. Thus, from Fig. 9 which corresponds to $f_o = -19.8$ MHz (or $\phi = -45^\circ$), we obtain six points on the critical curve of A and B for a BER of 10^{-3} , one point from each of the six curves which cross the critical BER. The value of B is obtained from the value of b since

$$B = -20 \log(1 - b). \quad (8)$$

For the curve in Fig. 9 corresponding to $B = 4.4$ dB, we obtain the corresponding critical value of A for a BER of 10^{-3} from the value of carrier-to-noise ratio, which is 20.2 dB where this curve crosses the 10^{-3} BER line. Since the carrier-to-noise ratio is 62 dB when the channel is unfaded, the 20.2 dB value corresponds to a relative average power loss of 41.8 dB,

$$L_s = 62 - 20.2 = 41.8 \text{ dB}. \quad (9)$$

Without loss of generality, we assume that the PSK signal has a rectangular spectrum of width f_b ; consequently, the relative power transmitted by the model is obtained from eq. (2) as*

$$\begin{aligned} P_{\text{av}} &= \frac{1}{2\pi f_b} \int_{-\pi f_b}^{\pi f_b} |H(\omega)|^2 d\omega \\ &= a^2 \left\{ 1 + b^2 - 2b \cos 2\pi f_o \tau \left(\frac{\sin \pi f_b \tau}{\pi f_b \tau} \right) \right\}. \end{aligned} \quad (10)$$

* The calculated result is not critically dependent on the flatness of the signal spectrum or the spectral width chosen. We have used for f_b a value of 25.3 MHz as representing the effective width of the signal.

Defining a correction term by

$$C = -10 \log \left\{ 1 + b^2 - 2b \cos 2\pi f_o \tau \left(\frac{\sin \pi f_b \tau}{\pi f_b \tau} \right) \right\}, \quad (11)$$

we may express the signal loss as

$$L_s = -10 \log P_{av} = A + C. \quad (12)$$

Thus, we obtain the critical value of A as

$$A = L_s - C. \quad (13)$$

For $B = 4.4$ dB ($b = 0.4$) and $f_o = -19.8$ MHz, we find $C = 2.06$ dB and the critical value of A is $41.8 - 2.1 = 39.7$ dB.

Carrying out these calculations for the six curves in Fig. 9, one can generate the critical curve of A and B for $f_o = -19.8$ MHz and a BER of 10^{-3} . The curve is shown in Fig. 10 along with the critical curves for several other values of the BER. A complete set of curves must be generated for all values of f_o .

The curves in Fig. 10 are typical of the critical curves obtained for $|f_o| \leq 33$ MHz. The intercept with the A -axis represents the flat fade margin for the given BER; this margin is independent of notch position. The intercept of a critical contour with the B -axis represents the shape, or relative fade depth, margin for the given notch position. For values of B to the right of this intercept, the critical value of BER cannot be obtained at any carrier-to-noise ratio for the given notch position.

4.2 Outage calculation—detailed method

The probability, P_o , of finding A and B outside all critical contours may be written with eqs. (5), (6), and (7) as

$$P_o = \int_{-\pi}^{\pi} p_o(\phi) P_c(\phi) d\phi, \quad (14)$$

where

$$P_c(\phi) = \int_0^{\infty} \int_{A_c(X)}^{\infty} p_A(Y) p_B(X) dY dX, \quad (15)$$

and $A_c(X)$ is the functional relation of the critical values of A to B (or X), for B less than B_c , the B -axis intercept, and for a given BER and ϕ value.* Since measurements were made for a uniformly spaced set of notch positions with spacing $\Delta\phi = 10^\circ$, we may approximate (14) by

* The dependence of the function $A_c(X)$ and the asymptote B_c on BER and ϕ is not explicitly denoted to keep notation simple.

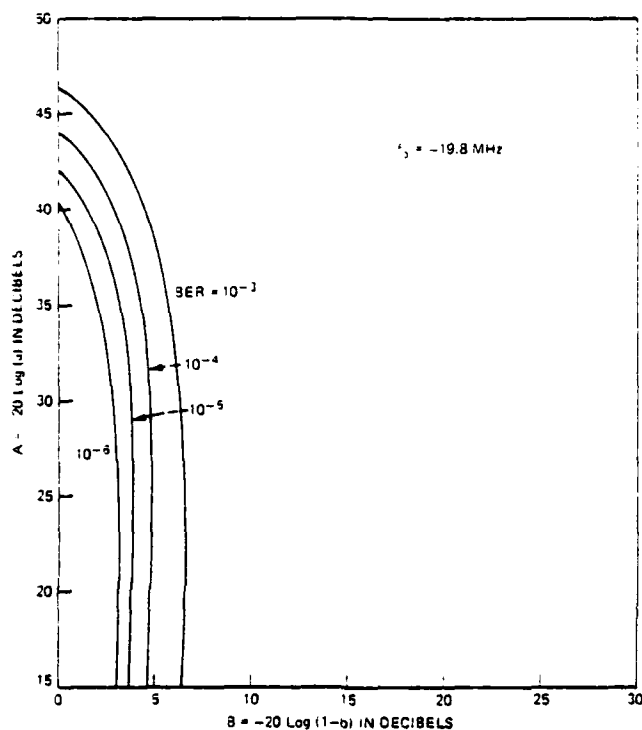


Fig. 10—Critical curves of A and B for $f_o = -19.8$ MHz.

$$P_o = \Delta\phi \sum_{\text{All } \phi_i} p_A(\phi_i) P_c(\phi_i). \quad (16)$$

To illustrate the calculation of outage probability with eqs. (15) and (16), we shall calculate the term in the summation of eq. (16) corresponding to a BER of 10^{-3} and $\phi_i = -45^\circ$ (or $f_o = -19.8$ MHz). From Fig. 11, which is taken from Fig. 10, we note that the double integral in eq. (15) may be broken into integrations over two regions. Thus

$$P_c(\phi_i) = \int_{B_c}^{\infty} \int_{-\infty}^{\infty} p_A(Y) p_B(X) dY dX \quad (17)$$

$$+ \int_0^{B_c} \int_{A_c(X)}^{\infty} p_A(Y) p_B(X) dY dX,$$

where the two double integrals correspond to integrations over Regions 1 and 2, respectively, in Fig. 11. Outage due to the occurrence of A and B in Region 1 may be described as outage due only to shape or

selectivity. In Region 2, outage is due to the combined effects of signal loss and selectivity.

Using eqs. (5) and (6), the integral over Region 1 is obtained as $e^{-B_c/3.8}$. The contribution due to thermal noise and shape (Region 2) is slightly more complicated. Dividing the interval 0 to B_c in Fig. 11 into N subintervals, as shown in Fig. 12, the probability of being in Region 2 is the sum of the probabilities for each subinterval. Thus eq. (17) becomes

$$P_c(\phi_i) = e^{-B_c/3.8} + \sum_{k=1}^N [e^{-B_{k-1}/3.8} - e^{-B_k/3.8}] P_s \left(\frac{A_k - A_0(B_k)}{5} \right), \quad (18)$$

where

$$P_s(X) = \frac{1}{\sqrt{2\pi}} \int_X^\infty e^{-x'^2/2} dx. \quad (19)$$

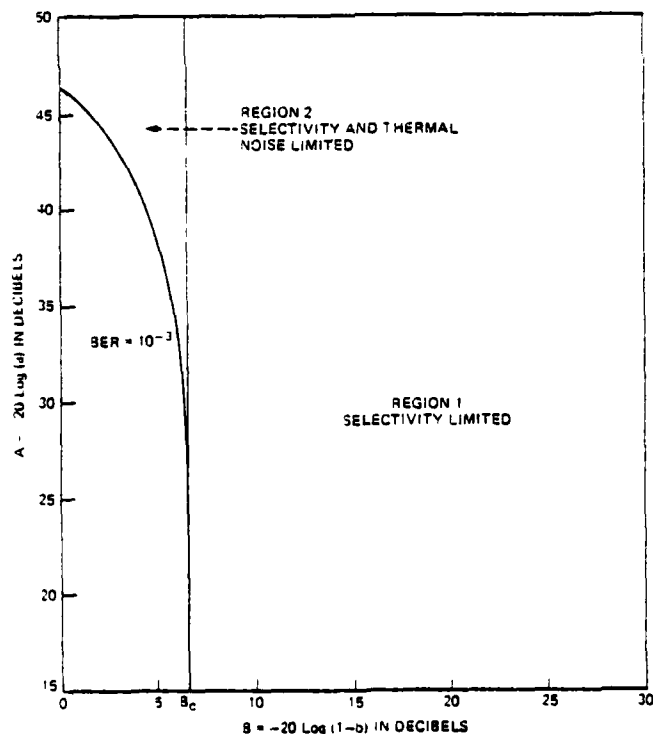


Fig. 11—Classification of outage with respect to critical curve for $\text{BER} = 10^{-3}$, $f_0 = 19.8 \text{ MHz}$.

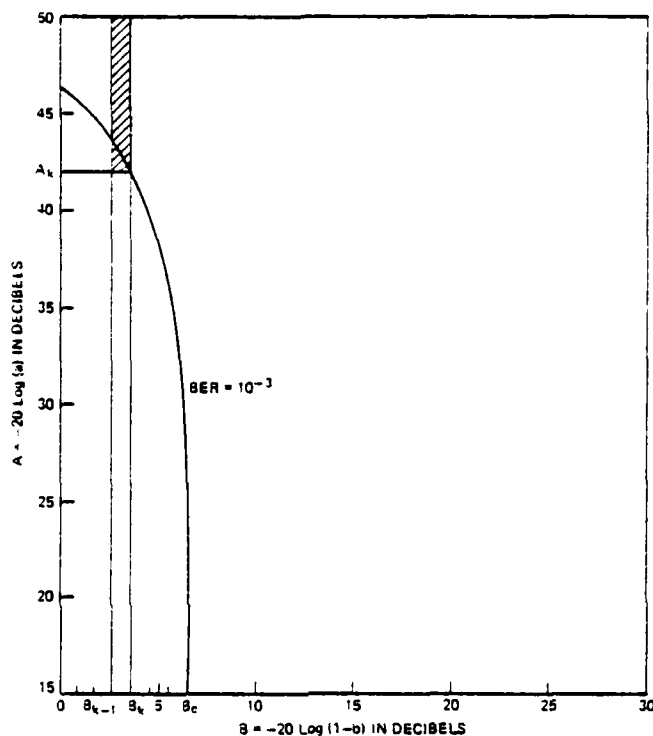


Fig. 12—Outage calculation for an incremental interval.

Evaluating the two components of eq. (18) from Fig. 11, we find

$$P_c(-45^\circ) = 0.181 + 0.003 = 0.184. \quad (20)$$

This calculation was performed for 10 values of ϕ_i from -5 to -85 degrees in 10-degree steps. Using these results in eq. (16) and multiplying by two to account for positive values of ϕ_i which are assumed to contribute equally, we find the probability, P_o for a BER of 10^{-3} as

$$P_o = 0.0996.$$

The expected outage for the data base period is, then,

$$T_o = 5400 \times 0.0996 = 538 \text{ seconds.} \quad (21)$$

4.3 Outage calculation—selectivity only

It is apparent from eq. (20) that most of the outage for the system under study is caused by selectivity, fades characterized by A and B values in Region 1. From eqs. (14) and (17), we may express P_o , the probability of outage due to selectivity, as

$$P_{os} = \int_{-\pi}^{\pi} \int_{B_c}^{\infty} p_o(\phi) p_B(X) dX d\phi. \quad (22)$$

For the system studied for a BER of 10^{-3} , a finite B_c is obtained only for $|\phi_i| < 90$ degrees. Hence, we may use eq. (7) to simplify (22)*

$$P_{os} = \frac{2\Delta\phi}{216} \sum_{i=1}^{10} e^{-B_c(\phi_i)/3.8}. \quad (23)$$

From eq. (23) we see that the outage due only to selectivity depends on the relationship between B_c , the asymptote of critical B values, and the notch angle or notch frequency. Figure 13 shows the relationship between B_c and the notch frequency for four values of BER. It is apparent from eq. (22) that the outage probability is the probability of finding B and f_o values in the region above this curve. Such curves, therefore, provide a useful basis for evaluating the selectivity outage of a digital radio system.

4.4 Outage calculation—approximate method

For a radio system sensitive to both thermal noise and selectivity, the calculation of Section 4.3 is inadequate and that of Section 4.2 is unduly cumbersome.

To illustrate a simpler, but generally applicable, method and at the same time to provide a useful incidental result, let us evaluate the effect of reducing the transmitted power by 10 dB. For the reduced power system, the carrier-to-noise ratio would be 52 dB for the unfaded channel, and the critical curves of A and B would be shifted by 10 dB. Figure 14 shows the critical curve of A and B for a 10^{-3} BER and $f_o = -19.8$ MHz with an overplot of the conditional mean of the distribution of A . The dotted curves on Fig. 14 represent 2-sigma intervals on either side of the mean. From the properties of the Gaussian distribution, one may determine that more than 95 percent of the values of A and B will lie between these two dotted curves. We designate as A_m and B_m the coordinates of the intersection of two curves: the critical $A - B$ curve and the conditional mean curve. Then approximating the critical curve of A and B with a straight line segment tangent at (A_m, B_m) , with slope s , we may approximate the probability of outage by integrating the probabilities over the region to the right of the tangent line. Using eqs. (15) and (16), we obtain

$$P_o = \Delta\phi \sum_{\text{all } \phi_i} p_o(\phi_i) \int_0^{\infty} \int_{A_m + s(B - B_m)}^{\infty} p_A(Y) p_B(X) dY dX. \quad (24)$$

* The factor of two is required in eq. (23) because the indicated summation corresponds to an integration only over negative notch frequencies ($\phi_i < 0$).

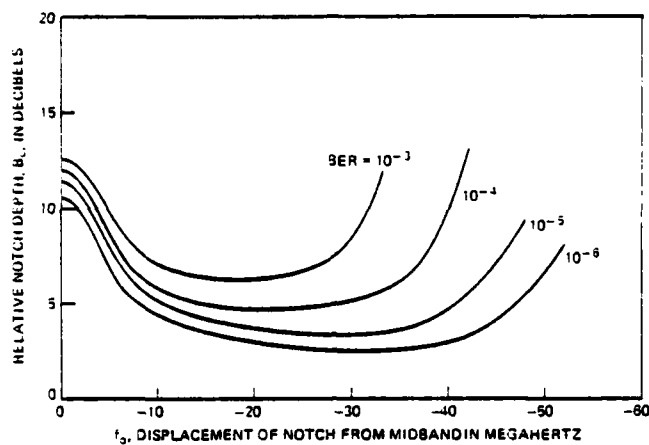


Fig. 13—Asymptotic performance curves. Locus of values of f_n and B that produce a fixed BER at high carrier-to-noise ratio.

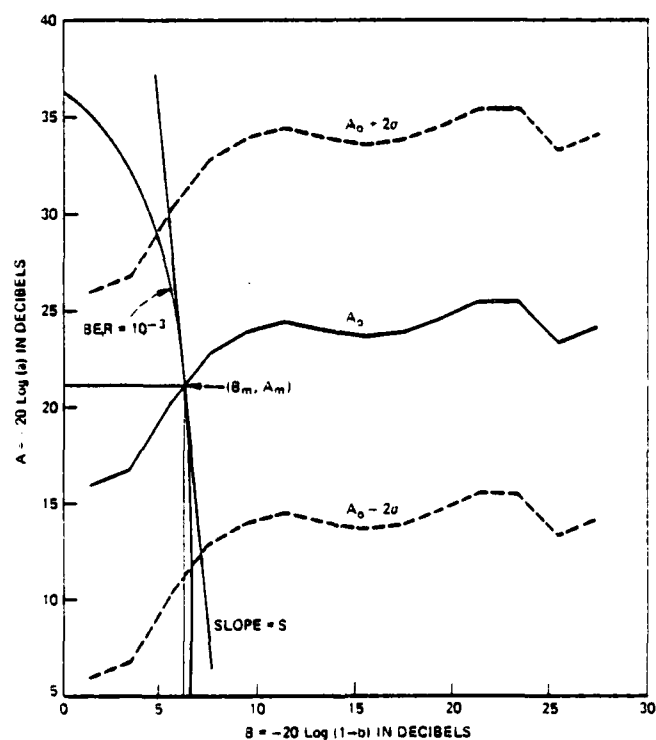


Fig. 14—Approximate outage calculation for 10 dB less transmitted signal.

Interchanging the order of integration and ignoring* the B dependence of $A_0(B)$, this becomes

$$P_o = \Delta\phi \sum_{\text{all } \phi_i} p_o(\phi_i) e^{-B_m/3.8} e^{0.886/\sigma^2} \quad (25)$$

Evaluating eq. (25) for a 10^{-3} BER and multiplying the result by 5400 gives an outage estimate for the data base period of 602 seconds. Recalculating the total outage time at a 10^{-3} BER using the method of Section 4.2 [eqs. (16) and (18)] gives 636 seconds, which verifies the accuracy of the approximate method. The estimate of 636 seconds was calculated as an upper bound; the 602 seconds calculated using (25) tend to be a lower bound. We conclude that backing off transmitted power by 10 dB would increase the outage by about 12 percent (538 to 602).

4.5 A further simplification

In this section, we show that the outage due to selectivity can be estimated approximately for a given BER from a determination of the in-band selectivity required (with the notch out-of-band) to produce that BER. Such a measurement may provide a useful approximation for any digital system using quadrature modulation components;⁹ however, we provide a justification based on the performance of the system at hand. In-band selectivity is defined as the difference between the maximum and minimum attenuation present in the (25.3-MHz) channel bandwidth.

Since the in-band selectivity is a constant for any of the curves shown in Fig. 9, one can use Fig. 9 to plot the asymptotic BER against in-band selectivity for $f_o = -19.8$ MHz. Such a plot was generated for each notch position measured to produce the family of curves shown in Fig. 15. Note that, except for notch positions near the band center, the BER is uniquely related to the in-band selectivity. Neglecting the in-band notches, we find that a 10^{-3} BER corresponds to an in-band selectivity of 5.5 dB.

If we use the original model of eq. (2) to determine the values of B that will produce an in-band selectivity of 5.5 dB for a number of different notch positions, we would generate Fig. 16. It is apparent that for this system there is a good correspondence between the curves of asymptotic performance (Fig. 13) and the curves of constant in-band selectivity (Fig. 16).

To reinforce this conclusion, we provide Figs. 17, 18, and 19. Figure 17 shows the locus of in-band selectivity in a 25.3-MHz band corre-

* Including the effect of the slope of $A_0(B)$ at $B = B_m$ gives the same symbolic result with s interpreted as the algebraic sum of the slope of the tangent and dA_0/dB evaluated at $B = B_m$.

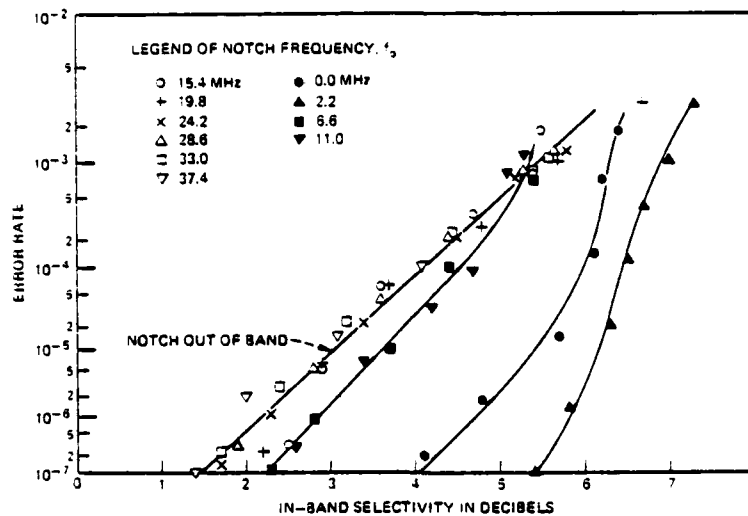


Fig. 15—Measured asymptotic bit error rate vs peak-to-peak amplitude difference in a 25.3-MHz band.

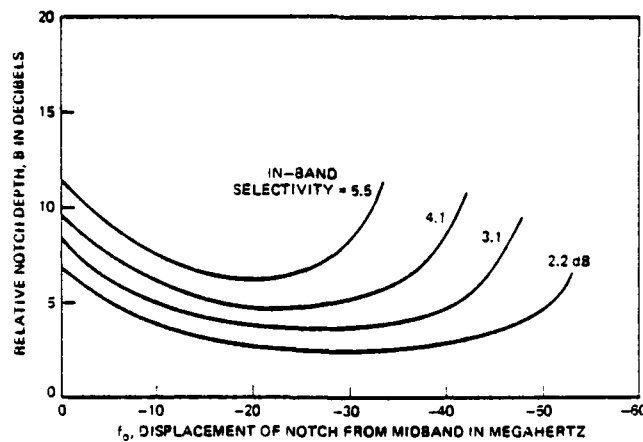


Fig. 16—Locus of B and f_n for modeled fades that have fixed peak-to-peak amplitude in a 25.3-MHz band.

sponding to each of the curves of constant BER in Fig. 13. That is, for each BER and each value of notch position, f_n , we have plotted the peak-to-peak amplitude difference in the band for the corresponding value of B_c , the asymptotic critical value of B . Figure 18 shows a similar set of curves with the peak-to-peak delay distortion in a 25.3-

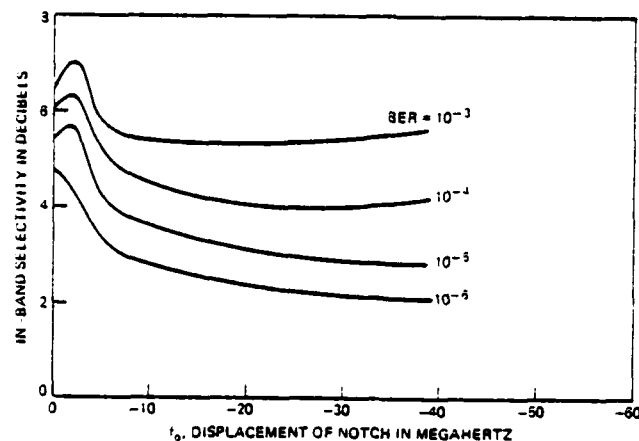


Fig. 17—In-band selectivity (in 25.3-MHz bandwidth) corresponding to asymptotic critical values of notch depth (B_c) for several values of BER.

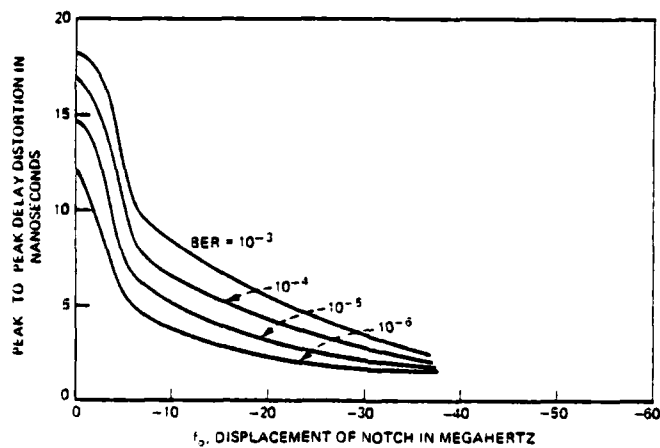


Fig. 18—Peak-to-peak envelope delay distortion in 25.3-MHz bandwidth corresponding to asymptotic critical values of notch depth (B_c) for several values of BER.

MHz band as the ordinate. Similarly, Fig. 19 has as the ordinate the "slope," or amplitude difference at a separation of 25.3 MHz. It is again clear from these three figures that the in-band selectivity is the relevant channel impairment giving rise to errors. We see from Fig. 18 that, for out-of-band notches, high BERs are obtained with very small values of peak-to-peak delay distortion, and from Fig. 19 that for in-band notches high BERs are obtained for very small values (zero at mid-band) of slope.

DIGITAL RADIO OUTAGE DUE TO FADING

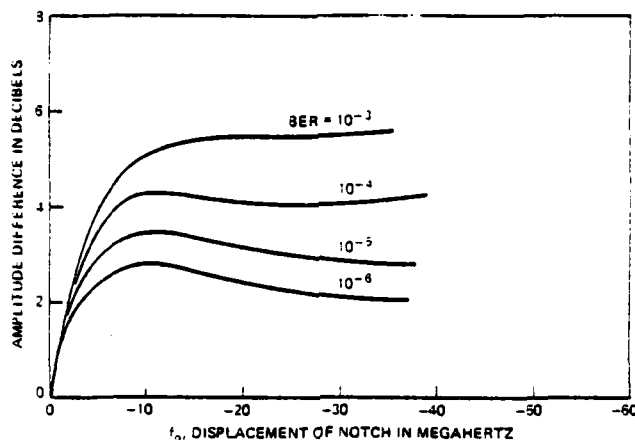


Fig. 19—Amplitude difference at a 25.3-MHz frequency separation corresponding to asymptotic critical values of notch depth (B_c) for several values of BER.

The model data base was analyzed to determine the time during which the in-band selectivity in a band of 25.3 MHz exceeded a given value. Figure 20 presents this distribution for in-band selectivity as calculated from the modeled fits. Figure 20 can be used directly in conjunction with Fig. 15 to calculate the outage times for the model data base.* For instance, from Fig. 15 we note that 5.5 dB of selectivity corresponds to a 10^{-3} BER. We use Fig. 20 to determine that 5.5 dB was exceeded for 520 seconds.

V. COMPARISONS OF CALCULATED AND OBSERVED OUTAGES

Using the methods of Sections 4.2 to 4.5, outage times were calculated for bit error rates of 10^{-3} to 10^{-6} for both the model data base period and for a heavy fading month, by multiplying the outage probabilities by 5400 and 8100, respectively.

5.1 Model data base period

Calculated and observed† outages for the model data base period are shown in Table I. In general, comparing the calculated results with observed results, we see that the outage is underestimated at high BERs and overestimated at low BERs. Any estimation procedure based on the current modeled state of the channel will tend to underestimate

* In practice, one would use a single measurement of in-band selectivity. For instance, in Fig. 9 one would take the 5.7-dB value corresponding to the curve asymptotic at a 10^{-3} BER.

† Because of quantization, the outage times observed from the field experiment correspond to bit error rates of 1.26×10^{-3} , 1.57×10^{-4} , 0.981×10^{-5} , and 1.19×10^{-6} .

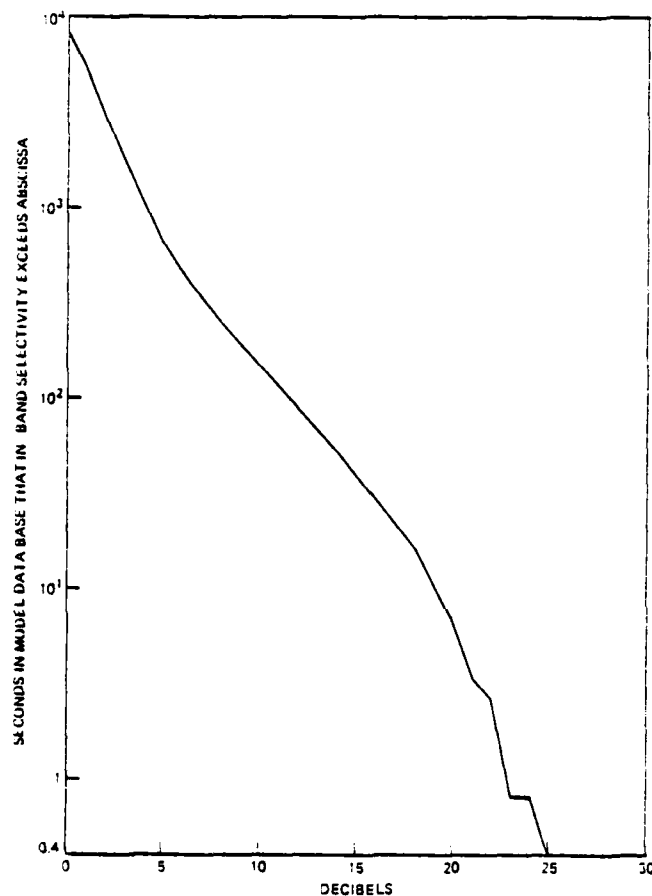


Fig. 20—Distribution of in-band selectivity (25.3-MHz bandwidth) for model data base.

Table I—Outage in modeling data base period (seconds)

	BER =			
	10^{-1}	10^{-2}	10^{-3}	10^{-4}
Observed	636	903	1191	1487
Detailed calculation (Section 4.2)	538	960	1430	1860
Approximate calculation (Section 4.4)	527	950	1420	1830
Asymptotic calculation (Section 4.3)	527	950	1420	1830
Selectivity calculation (Section 4.5)	510	900	1570	2730

outage at high BERs because of hysteresis effects in the radio receiving equipment. That is, when the channel condition becomes sufficiently severe, the bit error rate becomes high enough (on the order of 10^{-3}) that the timing and/or phase of the radio system breaks lock. If the

DIGITAL RADIO OUTAGE DUE TO FADING

channel impairment becomes less severe, the BER will not improve until the system resynchronizes. The hysteresis is important at the 10^{-3} BER, since a significant fraction of the events that cause 10^{-3} BER will cause the system to break lock.

One would expect to overestimate the outage at low BERs because of the method of taking data. Recall that, in measuring the curves in Fig. 9, it was found that the BER depended on the phase to which the system had locked. The recorded performance represented the worst-phase condition. At a 10^{-6} BER, the best phase produces a BER that is about $\frac{1}{3}$ that produced by the worst phase; the difference in BER from worst to best phase at a 10^{-3} BER is negligible. Hence, one would expect outage to be overestimated significantly at low bit error rates.

In comparing the outage calculated from in-band selectivity (Section 4.5) to the outage observed, we find that the overestimation of outage at low BERs is more severe than with the other methods. This is due to the greater sensitivity of the differential selectivity method to the bias induced by choosing the worst-case phase. For instance, comparing calculations at a 10^{-6} BER, we find that Fig. 20 is steeper for amplitude differences near 2 dB than is Fig. 3 near B values of 3.5 dB. (Figure 9 verifies the appropriateness of this comparison). More generally, one expects the method based on in-band selectivity to overestimate the outage because the method is based on notches out of band. From Fig. 15, it is apparent that, for a given ΔA , some scans will not have the BER specified.

We conclude that, although calculation of outage from sensitivity to in-band selectivity provides quick estimates, they are less accurate. The calculation requires knowledge of the distribution of in-band selectivity over a specified bandwidth. These statistics are neither simple nor generally available. It has been shown,¹⁰ for instance, that slope statistics have a nontrivial dependence upon the measurement bandwidth.

It is clear that the calculations based on selectivity (Sections 4.3 and 4.5) agree for the system studied here because that system has very little outage due to thermal noise limitations, and because it is sensitive primarily to in-band amplitude excursions. The extent to which these statements are true for other systems is currently unknown.

5.2 Outage on a monthly basis

The results in Table I may be put on the basis of a heavy fading month by increasing them by a factor of 1.5, as discussed in Section 2.2. The resulting outages (including the scaled observed outage) are compared with the outage observed in a one-month period⁸ in Table II. We see that the outage times observed in the total one-month period agree well with the values obtained by scaling the observed

Table II—Outage in a heavy fading month (seconds)

	BER =	10^{-4}	10^{-5}	10^{-6}	10^{-7}
Observed (Ref. 8)		1000	1320	2100	2900
Scaled observation from Table I		955	1350	1790	2230
Calculation (Section 4.2-4.4)		800	1430	2140	2760
Selectivity calculation (Section 4.5)		770	1350	2350	4100

outage for the data base period used in modeling, except for the slight divergence appearing at low BERs. This divergence should not be unexpected for this equipment. As may be seen in Fig. 15, a 10^{-6} BER may be caused by differential amplitude selectivity in band of 2 dB. Such modest amounts of selectivity may be expected to occur sometimes in the presence of very moderate selective fading. The modeling data base was constructed by selecting only periods of significant selective fading. This reinforces the comments made in conjunction with Fig. 3, namely, that the model distribution of B represents a lower bound for small values of B which can contribute to outage at the 10^{-6} BER level.

VI. CONCLUSIONS

We have demonstrated the validity of a technique for estimating the unprotected outage of a digital radio system due to selective fading on a particular hop in the 6-GHz common carrier band. The technique required field measurements to statistically characterize the parameters of a model of propagation on the hop. It also requires performance data obtained in the laboratory for the radio system by stressing it with a two-path fade simulator with a differential path delay of 6.3 ns, corresponding to the fixed delay channel model. Since the radio path on which these measurements were made has a length close to the average for the Bell System long haul radio network and has an average incidence of fading activity, the channel model is representative of a typical path. At the very least, the technique provides a basis for determining the relative merits of various digital radio systems operating without benefit of space diversity.

For the system under test, outage was calculated by four different methods. Because this system was selectivity-limited rather than noise-limited, all four methods predicted approximately the same outage as that summarized in Table I; however, the method based on in-band selectivity is more severely biased at low BERs. The method based on asymptotic performance and that based on in-band selectivity can only be used to estimate outage due to selectivity. If the transmitted power of the system under test were reduced by 10 dB, both of the other two methods, the detailed and the approximate method, would predict an increase in outage time of about 12 percent.

VII. ACKNOWLEDGMENTS

The conclusions of this effort depend upon data collected on a 6-GHz digital radio hop installed by R. A. Hohmann and L. J. Morris, using instrumentation designed by G. A. Zimmerman. M. V. Pursley's assistance in processing the data was invaluable. Consistent laboratory data used to close the loop reflect contributions by T. J. West and G. B. Thomas to the methodology of selective fade simulation at IF, and A. E. Resch who performed the measurements.

REFERENCES

1. E. Takeuchi and P. Tobey, "A 6 GHz Radio for Telephony Applications," Conference Record ICC 1976, Vol. II, June 1976, p. 18-27.
2. P. R. Hartman and J. A. Crossett, "A 90 MBS Digital Transmission System at 11 GHz using 8 psk Modulation," Conference Record ICC 1976, Vol. II, June 1976, p. 18-8.
3. A. J. Giger and T. L. Osborne, "3A-RDS 11 GHz Digital Radio System," Conference Record ICC 1976, Vol. II, June 1976, p. 18-1.
4. I. Godier, "DRS-8 Digital Radio for Long-Haul Transmission," Convention Record ICC 1977, Vol. I, June 1977, p. 102.
5. W. A. H. Wood, "Modulation and Filtering Techniques for 3 Bits/Hertz Operation in the 6 GHz Frequency Band," Convention Record ICC 1977, Vol. I, June 1977, p. 97.
6. W. D. Rummier, "A New Selective Fading Model: Application to Propagation Data," B.S.T.J., this issue, pp. 1037-1071.
7. W. T. Barnett, "Multipath Propagation at 4, 6, and 11 GHz," B.S.T.J., 51, No. 2 (February 1972), pp. 321-361.
8. W. T. Barnett, "Measured Performance of a High Capacity 6 GHz Digital Radio System," Conference Record ICC 1978, Vol. III, June 1978, pp. 47.4.1-47.4.6.
9. J. R. Gray and T. J. West, private communication.
10. G. M. Babler, "A Study of Frequency Selective Fading for a Microwave Line-of-Sight Narrowband Radio Channel," B.S.T.J., 51, No. 3 (March 1972), pp. 731-757.

7. EFFECTS OF FREQUENCY SELECTIVE FADING ON DIGITAL RADIO

A. Vigants
Bell Telephone Laboratories
Holmdel, NJ

NOTE: The materials presented in this section are copies of a Bell System Technical Journal article and a preprint of an article given at the 1979 National Telecommunications Conference used as the basis for the extemporaneous remarks given by Mr. Vigants.

Transmission Unavailability of Frequency-Diversity Protected Microwave FM Radio Systems Caused by Multipath Fading

By A. VIGANTS and M. V. PURSLEY

(Manuscript received April 2, 1979)

Estimates of transmission unavailability caused by multipath fading are needed to determine the adequacy of diversity protection arrangements. A computer program producing such estimates was made available for general Bell System use in 1977. In this paper, we summarize the underlying mathematical model of frequency diversity operation and atmospheric multipath fading and use it to study frequency diversity behavior.

1. INTRODUCTION

Microwave FM radio systems utilized in the Bell System provide protected broadband communications channels that generally have a capacity, depending on the frequency band and on the type of equipment, of 1200 to 2400 message circuits per channel. The protected channels, with protection provided by radio switching systems, are referred to as "working" channels, to distinguish these from the actual radio channels, which are assigned as either "regular" or "protection" channels. The number of regular channels in a radio system equals the number of working channels. Equipment failures, atmospheric fading, or other impairments in a regular channel cause temporary transfers of the communications traffic to a protection channel at a different radio frequency, if an unoccupied and unimpaired protection channel is available. In the case of fading, such frequency-diversity protection switching capitalizes on the frequency selectivity of the multipath fading process, where, at an instant in time, the strength of the received signal is a function of frequency. The Bell System long-haul microwave FM radio network contains approximately 1600 one-way frequency-diversity switching sections (800 route segments) with an average of three radio hops per switching section.

The communications traffic in a working channel can be temporarily subjected to high noise when, in a switching section, the number of impaired radio channels exceeds the number of protection channels. Bell System practice is to describe this in terms of the amount of time during which the noise in a working channel exceeds 55 dBm in a message circuit at the top frequency assignment in the baseband.¹ In this paper, this time is referred to as "service failure time" in accordance with designations on protection switching equipment and terminology used in the operation of the plant. The terms "service failure" and "outage" are frequently synonymous,¹ but use of the latter term can sometimes result in semantic difficulties, since some service failures may not result in outages as perceived or defined by some communications users.

In modern microwave radio systems, protection requirements are frequently governed by the presence of multipath fading,²⁻¹³ as opposed to causes associated with equipment or human intervention.¹ Estimates of service failure time due to multipath fading are therefore needed to determine the adequacy of diversity protection arrangements when new routes are planned, when transmission parameters of existing routes are changed, or when alternate protection strategies are considered for future use. In 1977, a computer program producing such estimates was made available for general Bell System application. It is extensively used to treat everyday design and planning tasks on an individualized basis for microwave FM radio routes equipped with frequency-diversity and space-diversity³ protection.

A mathematical model of frequency-diversity operation and multipath fading is central to the computer program. In this paper, the model is summarized and utilized to study representative radio systems on fully and partially developed routes. The effect of radio channels with reduced fade margins, the service failure time of individual channels, and parameters that can be used to characterize frequency-diversity systems are treated. A discussion is included of the addition of space-diversity protection to frequency-diversity protection, often necessary to reduce service failure time.

The numerical results presented in this paper should be considered in the context of transmission performance objectives. A proposed design or modification of a frequency-diversity protection switching section containing S radio hops is satisfactory when

$$\sum_{h=1}^S T_h \leq T_{obj}, \quad (1)$$

where T_h is the estimated service failure time of an average radio channel due to multipath fading on a particular radio hop. The service failure time due to simultaneous deep fading on different hops is much

smaller and is therefore neglected in the above expression. The design-objective time T_{obj} is obtained from the reliability objectives for microwave FM radio, which specify an annual outage of 0.02 percent or less due to all causes for a two-way circuit on a 4000-mile long-haul or a 250-mile short-haul route.¹ In practice, this objective is prorated to the actual distance and applied to the service failure time. One-half the objective is allocated to multipath fading, and the other half to equipment, maintenance, and other causes.⁹ For multipath fading, one-half the 0.01-percent two-way allocation is applied to each direction of transmission. This accommodates customers that may transmit in only one direction and conforms to the structure of the plant, where independent protection switching systems and different radio frequencies are used in the two directions of transmission. Furthermore, the service failure time associated with a single protection switching system can be expected to be substantially larger than the service failure time occurring simultaneously in the two directions, since the latter kind of failure requires simultaneous deep fading on a larger number of radio channels. Consequently, the one-way multipath-fading service failure time objective for a section of a route containing S hops is, in seconds per year,

$$T_{obj} = (1600/D_{ref}) \sum_{h=1}^S D_h, \quad (2)$$

where D_{ref} is 4000 miles for long-haul and 250 miles for short-haul radio, and D_h is the hop length in miles. In the case of a frequency-diversity switching section containing a single 25-mile hop, the values of T_{obj} are 10 seconds per year for long-haul and 160 seconds per year for short-haul radio. In the past, it was often assumed that only half the hops on a long route would experience significant fading.^{1,9} This assumption is no longer necessary, since fading estimates can now be made for every hop on a route.^{3,9}

II. THE MATHEMATICAL MODEL

The service failure time of an average working channel, caused by multipath fading on a particular radio hop, can be expressed as

$$T_h = N^{-1} Z_h, \quad (3)$$

where N is the number of working channels and Z_h , referred to as the facility service failure time, is the sum of the service failure times of the working channels. The facility service failure time can be expressed as

$$Z_h = \sum_{i=1}^N i T''(i), \quad (4)$$

TRANSMISSION UNAVAILABILITY

where $T''(i)$ is the accumulated time during which exactly i of the N working channels experience service failure. The terms in this sum are associated with simultaneous fading of radio channels. For a frequency-diversity protection switching section with M radio channels of which u are protection channels,

$$M = u + N, \quad (5)$$

eq. (4) becomes

$$Z_h = \sum_{i=1}^N i T''(u + i), \quad (6)$$

where $T''(u + i)$ is the accumulated time during which exactly $u + i$ of the M radio channels have failed simultaneously. A failure in this context is an exceedance of the 55-dBrnc0 noise value.

The simultaneous fading of radio channels is normally described in terms of the amount of time during which particular sets of $u + i$ channels have failed, with the status of the other $M - u - i$ channels not specified. With such a time denoted by $T_k(u + i)$, the expression for Z_h becomes an alternating series

$$Z_h = \sum_{i=1}^N \sum_{k=1}^{J(u+i)} (-1)^{k-1} C_{u+i}^{u+i-k} T_k(u + i), \quad (7)$$

where $J(u + i)$ is the binomial coefficient C_{u+i}^M , and where the subscript k enumerates the sets of $u + i$ channels obtainable from the M channels. This expression has been used by other authors,¹ but its general mathematical equivalence to the definition in eq. (6) has not been demonstrated; a proof of this equivalence is supplied in Appendix A.

The expressions for the simultaneous failure time of a number of radio channels, denoted by $T_k(u + i)$, are based on a generalized model of simultaneous multipath fading in an arbitrary number of radio channels obtained empirically from experimental data. The estimation of the amount of fading and the calculation of $T_k(u + i)$ are summarized in Appendix B. A simplified form of $T_k(u + i)$, without path length dependence and without accommodation of fade margin differences between radio channels, has been utilized previously to demonstrate the feasibility of joint frequency-diversity protection for radio systems in the 4-GHz and 6-GHz bands.¹

Numerical evaluation of Z_h from the alternating series requires a computer program that efficiently selects and classifies radio channel combinations from a particular frequency plan and calculates the corresponding values of $T_k(u + i)$, since the number of terms can be large. For example, there are 184,756 ten-channel combinations when all radio channels in the 4-GHz and 6-GHz bands are used (400A

protection system with 2 protection and 18 regular channels). The computation of the combinations is discussed in Appendix C.

III. REPRESENTATIVE RESULTS FOR FULLY DEVELOPED ROUTES

A fully developed 4-GHz route contains a total of 12 radio channels consisting of one protection channel and 11 regular channels. The notation 1×11 is used to describe this. On fully developed 6-GHz routes, the total number of radio channels is 8 and the protection scheme is 1×7 . When both bands are utilized, the two protection channels can be placed in the 6-GHz band, which results in 2×18 protection.

Representative estimated values of service failure times for these protection schemes can be obtained from calculations for a switching section containing one 25-mile hop with average terrain and climate. Without diversity protection, the service failure time of an average channel in the 4-GHz band is 269 seconds per year for a fade margin of 37 dB. In the 6-GHz band, the corresponding service failure time is 208 seconds per year for a fade margin of 40 dB.

When 2×18 protection is applied, the calculated service failure time is 6 seconds per year, which meets the long-haul objective of 10 seconds per year. Use of one of the protection channels for temporary service in the fading season increases the service failure time to 15 seconds per year as a result of the 1×19 configuration. The fade margin affects the service failure time. With diversity protection applied, a 5-dB fade margin decrease in all channels increases the service failure time by a factor of ten (Fig. 1).

For 1×11 and 1×7 protection, the calculated service failure times are about 15 seconds per year (Fig. 1). Prior to a conversion to one protection channel per band, required by spectrum conservation measures, the service failure times for 2×10 and 2×6 protection would have been about 6 seconds per year, meeting the long-haul objective.

The relative positions of the curves in Fig. 1 are significant. For example, the service failure time of an average channel in the 2×18 scheme is between those for average channels in the 2×10 and 2×6 schemes. This suggests that, because of decorrelation of fading between the 4-GHz and 6-GHz bands, the 2×18 functions part of the time as a 2×12 and part of the time as a 2×6 .

The frequency-diversity parameters that can be used to scale the results to other path lengths and climatic conditions are discussed in Appendix D.

IV. PARTIALLY DEVELOPED ROUTES

On partially developed routes where only a part of all available frequency assignments is utilized, the service failure time is a function

TRANSMISSION UNAVAILABILITY

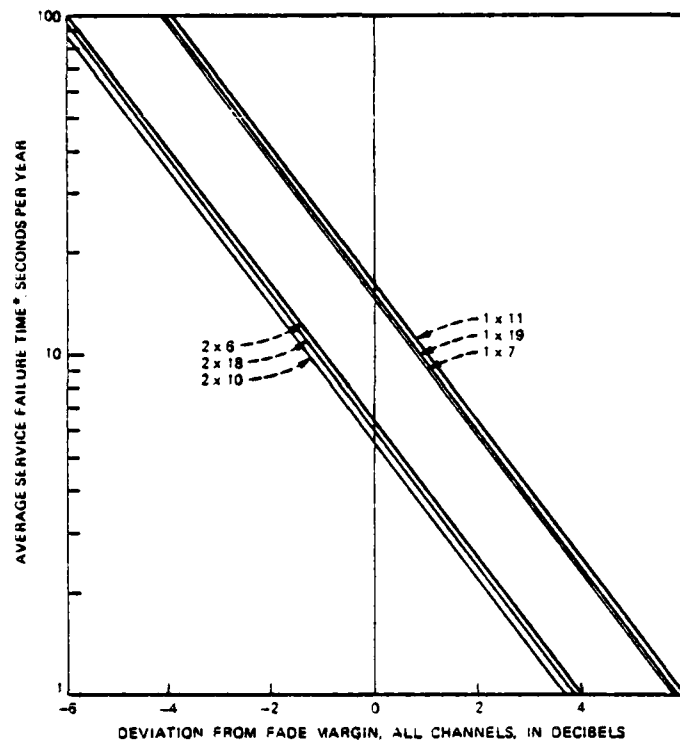


Fig. 1—Service failure time of average working channel due to multipath fading on a 25-mile hop with average climate and terrain. Fade margin = 37 dB, 4-GHz band; fade margin = 40 dB, 6-GHz band; average annual temperature = 55°F; terrain roughness = 50 ft.

* Average service failure time and service failure time of average working channel are synonymous in the context of this work.

of the frequency arrangement of the radio channels. A "best-case" arrangement is one where the frequency separation of adjacent channels is maximized. In a "worst-case" arrangement, the channels are crowded into the high end of the frequency band. Such arrangements do not necessarily correspond to actual or permitted growth strategies, but they do provide bounds for the variation of service failure time on partially developed routes.

In continuation of the example in Fig. 1, calculated results for the best and worst cases are shown in Fig. 2 as a function of the number of working channels. The best-case results for the 4-GHz band show that the 10 seconds-per-year long-haul objective cannot be met by

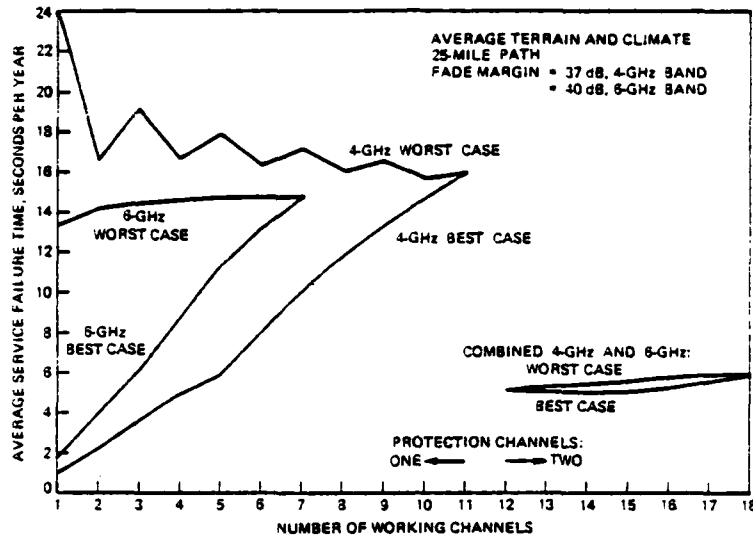


Fig. 2—Bounding cases for service failure time of average working channels. Frequency assignments are listed in Appendix E.

frequency diversity alone when the number of working channels is larger than seven. The ripple in the worst case is caused by the alternating 20-MHz and 60-MHz increments as channels are added.

In the 6-GHz band, the long-haul objective cannot be met by frequency diversity alone when the number of working channels is larger than four. The 6-GHz worst case is better than the 4-GHz worst case because the 6-GHz fade margin is larger than the 4-GHz fade margin in this example.

In a combined protection system for the two frequency bands, introduced after the 4-GHz band is fully developed, the arrangement of the channels in the 6-GHz band has only a small effect on the service failure time of an average channel, which varies between 5 and 6 seconds per year.

V. EFFECT OF CHANNELS WITH REDUCED FADE MARGINS

A radio channel with a substandard fade margin experiences a failure time that is larger than normal. The presence of such a channel increases protection unavailability, which results in increased service failure times for all working channels. The increase in the service failure time of an average working channel, caused by the presence of one or two substandard radio channels on a fully developed route, is shown in Fig. 3 as a function of the reduction of the fade margin from

TRANSMISSION UNAVAILABILITY

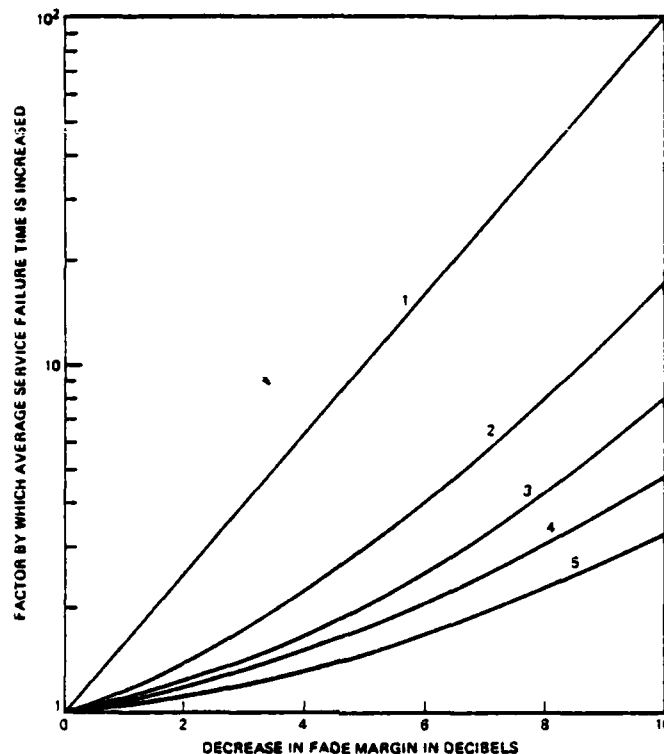


Fig. 3—Increase in service failure time of average working channel when fade margins are reduced for: (1) all radio channels; (2) two midband channels in 1×7 system, 6 GHz; (3) two midband channels in 1×11 system, 4 GHz; (4) one midband channel in 1×7 system, 6 GHz; (5) one midband channel in 1×11 system, 4 GHz.

its normal value. As an example, the service failure time of an average working channel in a 1×11 system is doubled when the fade margin of one midband radio channel is degraded by 7 dB; this is equivalent to a 1.5-dB degradation of the fade margins of all channels.

The service failure time indicated by a protection switching monitor actuated by the protection switching equipment can be larger than the actual service failure time if adjustments in the protection switching system are incorrect so that, for a particular channel, a transfer to protection occurs early, at a noise value smaller than 55 dBmco. The actual service failure time, while smaller than that indicated (Fig. 4), is larger than normal because occupancy of the protection channel has been increased.

Transfers to protection are normally permitted only when the amount of noise after the transfer is at least a few decibels smaller

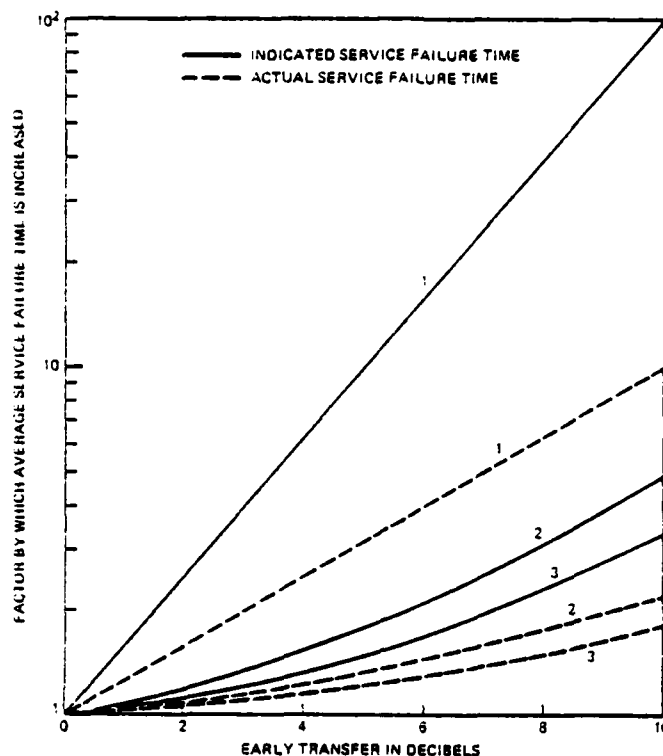


Fig. 4—Increase in service failure time of average working channel when transfer to protection occurs early for: (1) all channels; (2) one midband channel in 1×7 system, 6 GHz; (3) one midband channel in 1×11 system, 4 GHz.

than 55 dBm. The increase in service failure time due to a 3-dB difference of this kind is very roughly the same as that due to transfers to protection that occur 3 dB early. From Fig. 4, this is equivalent to a fraction of a decibel decrease in the fade margins of all channels. Consequently, such differences associated with the protection channels are not included in the mathematical model presented in this paper, since their relatively small effects do not justify the added analytical and computational complexity.

VI. SERVICE FAILURE TIME OF INDIVIDUAL CHANNELS

In addition to the service failure time of an average channel utilized in engineering applications, the mathematical model developed in this work can provide other information about the operation of frequency-diversity protection. In particular, the service failure times of individ-

TRANSMISSION UNAVAILABILITY

ual working channels can be obtained from a decomposition of the facility service failure time.

As an example, consider a 1×3 protection system in the 4-GHz band with parameters as in Fig. 2, utilizing channels 2, 4, 6 and 8 (80-MHz separation of adjacent channels). The simultaneous failure times for particular sets of exactly $u + i$ channels are needed in the decomposition. These times, denoted by $T'_k(u + i)$ and listed in Table I, are summations [as specified in eq. (14)] of the failure times $T_k(u + i)$ calculated as outlined in Appendix B. The numerical values illustrate the frequency selectivity and frequency dependence of multipath fading. For example, the failure time of channels 2 and 4, but not 6 and 8, which can be caused by a slope in the frequency response, is 2.58 seconds. The failure time of channels 6 and 8, but not 2 and 4, is 3.07 seconds. This is larger than the 2.58 seconds because the amount of fading increases with frequency. The failure time of channels 4 and 6, but not 2 and 8, is 2.22 seconds. This is smaller than either the 2.58 seconds or the 3.07 seconds because this failure results from a minimum in the frequency response. The facility service failure time for this example is, from eq. (6),

$$\begin{aligned} Z_A &= \sum_{k=1}^6 T'_k(2) + 2 \sum_{k=1}^4 T'_k(3) + 3 T'_1(4) \\ &= 8.81 + 2 \times 2.12 + 3 \times 1.00 \\ &= 16.05 \text{ channel-seconds per year.} \end{aligned} \quad (8)$$

The corresponding service failure time of an average channel is, from eq. (3), one-third of this

$$T_A = 5.35 \text{ seconds per year.} \quad (9)$$

About 45 percent of this time occurs when 3 or all 4 of the radio channels have failed simultaneously.

The expressions for the service failure time of individual channels are obtained by inspection from Table I. In the case where channel 2 is used for protection, the service failure time of the working channel assigned to channel 4 is

$$\begin{aligned} T_{A,4} &= T'_1(2) + (\frac{1}{2}) T'_4(2) + (\frac{1}{2}) T'_5(2) \\ &\quad + T'_1(3) + T'_2(3) + (\frac{2}{3}) T'_4(3) + T'_1(4) \\ &= 6.484 \text{ seconds per year,} \end{aligned} \quad (10)$$

where the fractions are based on statistically equal protection occupancy in cases of simultaneous failures.

The results of such calculations (summarized in Table II) show that the location of the protection channel affects the spread of the individ-

Table I—Simultaneous failures of exactly $u + i$ radio channels. Channel numbers: 2, 4, 6, 8; frequencies, GHz: 3.73, 3.81, 3.89, 3.97.

$u + i$	k	Channels	$T_k(u + i)$, sec/year
2	1	2, 4	2.58
2	2	2, 6	0.37
2	3	2, 8	0.17
2	4	4, 6	2.22
2	5	4, 8	0.40
2	6	6, 8	3.07
3	1	2, 4, 6	0.77
3	2	2, 4, 8	0.23
3	3	2, 6, 8	0.23
3	4	4, 6, 8	0.89
4	1	2, 4, 6, 8	1.00

Table II—Service failure time of individual working channels for a 1×3 system in the 4-GHz band. Channel numbers: 2, 4, 6, 8; frequencies, GHz: 3.73, 3.81, 3.89, 3.97.

Working Channel*	Service Failure Time, Seconds/Year (percent of average in parentheses)			
	Protection channel assignment			
	2	4	6	8
2	—	5.003 (94)	3.898 (73)	3.618 (68)
4	6.484 (121)	—	6.524 (122)	5.434 (101)
6	5.608 (105)	6.753 (126)	—	6.998 (131)
8	3.968 (74)	4.294 (80)	5.628 (105)	—
Total seconds	16.05	16.05	16.05	16.05
Range of percent:				
Minimum	74	80	73	68
Maximum	121	126	122	131

* Working channels in this table are identified by the number of the corresponding regular radio channel.

ual service failure times. The facility service failure time and, therefore, the service failure time of an average channel are not affected by the location of the protection channel. The largest spread of the individual service failure times (68 to 131 percent of average) occurs when the channel at the highest frequency (channel 8) is used for protection.

Protection channel assignments could be optimized based on results such as those presented in Table II. However, a general treatment of this is beyond the current scope of this study.

TRANSMISSION UNAVAILABILITY

VII. ADDITION OF SPACE DIVERSITY TO FREQUENCY DIVERSITY

Space-diversity protective switching capitalizes on the spatial selectivity of the multipath fading process, where, at an instant in time and at a given radio frequency, the strength of the received signal is a random function of location along the height of the receiving tower.^{6,7,9} For FM radio carrying analog message traffic, space-diversity in most cases in the Bell System consists of two vertically separated receiving antennas and, for each radio channel, a waveguide switch that connects a receiver to either of the two antennas. The switch is activated when the receiver input decreases below a threshold.

The presence of digital traffic in the FM radio network affects the choice of timing in the switch. The number of antenna-to-antenna transfers should be as small as possible, since these can cause errors in digital transmission. For thresholds corresponding to fades deeper than about 35 dB, this is accomplished when, in the case of simultaneous fading on the two antennas, the interval between repeated transfers is 10 seconds. Intervals longer than this cause significant increases in the service failure time of analog message circuits.

When added to frequency-diversity to reduce service failure time, space-diversity is activated before frequency-diversity to avoid undesirable interactions of the two protection systems. Currently, frequency-diversity is activated at a noise threshold of 55 dBm, and 52 dBm is the desired threshold value for space-diversity activation when it is added to frequency-diversity. Such an arrangement has assured orderly evolution and uniform maintenance procedures of protection switching systems. In the future, because of increased use of space-diversity, changed threshold values may be desirable, ideally 58 dBm for frequency-diversity and 55 dBm for space-diversity, to further reduce service impairments.

The reduced service failure time resulting from an addition of space diversity in the manner described above can be calculated from eq. (7) with the values of $T_k(u + i)$ divided by the appropriate improvement value for threshold-switched space-diversity.⁹ Such calculations, which can be readily incorporated in a computer program, will not be pursued in this paper where the emphasis is on an exploration of frequency-diversity behavior.

VIII. ACKNOWLEDGMENTS

We wish to express our appreciation to W. T. Barnett, whose model of simultaneous fading we utilize, and to H. Adams, who helped to develop the computer program.

THE BELL SYSTEM TECHNICAL JOURNAL, OCTOBER 1979

APPENDIX A

Derivation of the Alternating Series

Generally, we prefer to describe fading in terms of time rather than in terms of probability, since the latter description can lead to inadvertent confusion because of the nonstationarity of the fading process. However, for the purposes of combinatorial manipulation, T_h can be converted to a fraction designating a probability

$$P_h = T_h/T_b, \quad (11)$$

where T_b is an observation period (time base) such as a year. From eqs. (3) and (6),

$$P_h = N^{-1} \sum_{i=1}^N i P'(u+i), \quad (12)$$

where

$$P'(u+i) = T'(u+i)/T_b. \quad (13)$$

To derive the alternating series from eq. (12), we apply a theorem from probability theory (page 77 in Ref. 14). According to it, the probability that exactly $u+i$ out of M channels fail simultaneously is

$$P'(u+i) = \sum_{r=u+i}^M (-1)^{r-u-i} C_{u+i}^r S(r), \quad (14)$$

where

$$S(r) = \sum_{k=1}^{J(r)} P_k(r) \quad (15)$$

in which $J(r)$ is the binomial coefficient C_r^M , and where, in the context of this work,

$$P_k(r) = T_k(r)/T_b. \quad (16)$$

After substitution into eq. (12), and collection of like terms,

$$P_h = N^{-1} \sum_{i=1}^N \sum_{p=1}^i (-1)^{i+p} p C_{u+p}^{u+i} S(u+i). \quad (17)$$

Application of the recursion relationship

$$C_n^m = C_{n-2}^{m-2} + 2C_{n-1}^{m-2} + C_n^{m-2} \quad (18)$$

reveals that, because of cancellation of terms,

$$\sum_{p=1}^i (-1)^{p+1} p C_{u+p}^{u+i} = C_{u-1}^{u+i-2}. \quad (19)$$

TRANSMISSION UNAVAILABILITY

Therefore

$$P_A = N^{-1} \sum_{i=1}^N (-1)^{i-1} C_{u+i}^{-2} S(u+i). \quad (20)$$

After multiplication by NT_b , this becomes the alternating series expression for Z_A in eq (7).

APPENDIX B

Simultaneous Failure of Radio Channels

In the case of a single radio channel, the annual amount of time during which the received signal is below a level, as a result of multipath fading, is^{5,9}

$$T = rT_0L^2, \quad L < 0.1, \quad (21)$$

where L describes a normalized voltage such that the level in decibels relative to a nonfaded received signal is $20 \log L$. For a fade margin of F dB, where F is a positive number, the corresponding voltage level is

$$L_0 = 10^{-(F/20)}. \quad (22)$$

When L_0 is used as value of L in eq. (21), T becomes the time during which the channel has failed, where failure is defined as noise in excess of 55 dBm. The quantity T_0 is a time interval related to the length of the fading season [eq. (20) in Ref. 9]. The fade occurrence factor is^{5,9}

$$r = c(f/4)D^3 10^{-5}, \quad (23)$$

where D is the path length in miles, f is the carrier frequency in gigahertz, and c describes the climate and terrain (eqs. (4) and (5) in Ref. 9). The value of c is unity when the climate and terrain are average.

Empirical expressions for simultaneous fading of radio channels have been obtained by W. T. Barnett from experimental data. From these, expressed in a form similar to that for a single channel, the time during which $u+i$ radio channels have failed simultaneously is

$$T_k(u+i) = r_k(u+i)T_0L_0^2, \quad (24)$$

where the subscript k is used to identify various sets of $u+i$ channels. This expression is valid when $T_k(u+i)$ is smaller than the values of T for the channels in question. The simultaneous failure time varies with fade margin more than the single channel failure time (L_0^2 versus L_0^2 variation). The quantity L_0 describes the actual fade margin when it is the same for all channels. In the case of channels with differing fade margins, L_0 describes a nominal fade margin, and the description of differences from it is contained in $r_k(u+i)$. The occurrence factor is

$$r_k(u+i) = (cD^3 10^{-5}/400)f_k(u+i), \quad (25)$$

where

$$f_h(u+i) = (u+i) / \sum_{p=1}^{I(u+i)} (L_0/L_{1p})^2 (L_0/L_{2p})^2 (\delta_p/f_p^2). \quad (26)$$

The quantities in this expression are associated with pairs of channels formed from the $u+i$ channels. The number of such pairs is

$$I(u+i) = C_2^{u+i}. \quad (27)$$

The subscript p identifies the pairs. The fade margins of the channels in a pair are described by L_{1p} and L_{2p} . The corresponding carrier frequencies f_{1p} and f_{2p} are expressed in gigahertz ($f_{1p} < f_{2p}$). The average frequency for a pair is

$$f_p = (f_{1p} + f_{2p})/2 \quad (28)$$

and the fractional frequency difference is

$$\delta_p = (f_{2p} - f_{1p})/f_p. \quad (29)$$

A value of 0.05 is used for δ_p when one of the channels is in the 4-GHz band and the other in the 6-GHz band.

APPENDIX C

Computation of Combinations of Channels

The evaluation of Z_h in eq. (7) requires identification of the combinations of r frequencies that can be formed from the M carrier frequencies of the radio channels. If the frequencies are tagged using the integers 1 through M , then the combinations required are subsets of the set $\{1, 2, \dots, M\}$. The integers appearing in the subsets serve as pointers (used pairwise) to precalculated values of δ_p/f_p^2 for frequency pairs in a subset [eqs. (28) and (29)].

Given M and r , the computation is initialized by defining (for $i = 1, 2, \dots, r$)

$$\alpha_i = i, \quad i \neq r \quad (30)$$

$$\alpha_i = (r-1), \quad i = r \quad (31)$$

$$\beta_i = M - r + i. \quad (32)$$

The subsets are then generated as follows:

- (i) Starting with $j = r$, find the first j such that $\alpha_j < \beta_j$.
- (ii) Replace α_j with $\alpha_j + 1$.
- (iii) For $k = (j+1), (j+2), \dots, r$ replace α_k with $\alpha_{k-1} + 1$.

In this procedure, elements of subsets are incremented to form new subsets, and the elements of each subset are ordered within the vector α such that $\alpha_j < \alpha_{j+1}$. Repeated generation of the same combination of

TRANSMISSION UNAVAILABILITY

frequencies is thereby avoided. The first iteration after initialization produces the subset $\{1, 2, \dots, r\}$. The iteration is continued until execution of step (i) fails, when all the required C^M combinations have been produced. The potentially large number of combinations necessitates double precision computation in summations over the subsets.

APPENDIX D

Frequency-Diversity Parameters

The service failure time of an average channel can be expressed as

$$T_h = T_{uh}/I_h, \quad (33)$$

where T_{uh} is the unprotected service failure time for the hop in question obtained from eq. (21) after substitution of L_0 from eq. (22). The improvement resulting from the use of frequency-diversity protection is

$$I_h = qL_0^{-2}, \quad (34)$$

where

$$q = 100 f_0/DG, \quad (35)$$

in which D is the path length in miles and f_0 is the frequency in gigahertz at which T_{uh} is calculated. An average of the carrier frequencies of the radio channels is a suitable value for the reference frequency f_0 . Alternatively, f_0 can be the center frequency of a band, which facilitates band identification when the calculations are performed for frequency plans formulated by the International Radio Consultative Committee (CCIR). The parameter G is determined by the carrier frequencies of the radio channels and by the channel-to-channel variations of fade margins

$$G = N^{-1} \sum_{i=1}^N \sum_{k=1}^{J(u+i)} (-1)^{i-1} C_{u-1}^{u+i-2} f_h(u+i), \quad (36)$$

where $f_h(u+i)$ and the summation are defined in Appendix B. In the simple case of 1×1 frequency diversity with the same fade margin for both channels,

$$G = 2f_p^2/\Delta f, \quad (37)$$

where f_p is the average and Δf is the difference of the two carrier frequencies, expressed in GHz. The corresponding value of q in this 1×1 case,

$$q = (f_0/f_p)(50/f_p D)(\Delta f/f_p) \quad (38)$$

has been used previously with the factor f_0/f_p approximated by unity.⁹

When the fade margins of all radio channels are identical, the

Table III—Values of G for fully developed routes. Fade margins are identical for all radio channels in a given protection scheme.

Frequency Band, GHz	Protection Scheme	Value of G
4	2×10	1597
4	1×11	4682
6	2×6	7380
6	1×7	17059

Frequencies in the 4-GHz band:
 $3.670 + 0.040 i$, $i = 1, 3, 5, \dots, 11$
 $3.650 + 0.040 i$, $i = 2, 4, 6, \dots, 12$
Frequencies in the 6-GHz band:
5.9452, 5.9748, 6.0045, 6.0342,
6.0638, 6.0935, 6.1231, 6.1528

parameter G depends only on the frequency arrangement of the channels. Tabulated values of G , such as shown in Table III for fully developed routes, can therefore be used in eq. (33) to calculate the service failure time for common frequency arrangements.

In the 2×18 case in Fig. 1, the choice of reference fade margin ($-20 \log L_0$) becomes arbitrary because there are two fade margins (37 and 40 dB, in the 4- and 6-GHz bands, respectively). The choice has no effect on T_h , but it does affect the various factors in T_h such as G . When T_{wh} and f_0 are the averages for the 20 radio channels, the reference fade margin is 38.27 dB [obtained from eq. (21)]. The value of G is 3129 for this choice of reference values.

APPENDIX E

Frequency Assignments in Figure 2

To simplify presentation, the radio channels in this work are numbered 1 to 20 in order of increasing frequency. The frequencies range from 3.71 to 6.1528 GHz as listed in Table III.

In the 4-GHz worst case, channels 12 and 11 are utilized in the 1×1 protection scheme, and the sequence in which additional working channels are assigned is 10, 9, 8, \dots , 1. In the best case, channels 2 and 12 (same polarization) are used for the 1×1 scheme, and then channel 6 is added to form a 1×2 scheme. Channels 2, 4, 8, and 12 are utilized in the 1×3 scheme, and the sequence in which additional working channels are assigned is 6, 10, 1, 3, 5, 7, 9, and 11.

In the 6-GHz worst case, channels 20 and 19 are utilized in the 1×1 scheme, and the sequence in which additional working channels are assigned is 18, 17, \dots , 13. In the best case, the channel utilization is

TRANSMISSION UNAVAILABILITY

$1 \times 1 - 13, 20$
 $1 \times 2 - 13, 16, 20$
 $1 \times 3 - 13, 15, 17, 20$
 $1 \times 4 - 13, 14, 16, 18, 20$
 $1 \times 5 - 13, 14, 15, 17, 19, 20$
 $1 \times 6 - 13, 14, 15, 16, 18, 19, 20$
 $1 \times 7 - 13, 14, 15, 16, 17, 18, 19, 20$

In the combined protection system for the 4-GHz and 6-GHz bands, all 4-GHz channels and channels 20 and 19 are used in the worst-case 2×12 scheme. The sequence in which additional working channels are assigned is 18, 17, 16, ..., 13. In the best-case 2×12 scheme, all 4-GHz channels are also used, but the 6-GHz channels are 13 and 20. The pattern for the utilization of additional channels is the same as that in the 6-GHz best case.

REFERENCES

1. W. Y. S. Chen, "Estimated Outage in Long-Haul Radio Relay Systems with Protection Switching," B.S.T.J., 50, No. 4 (April 1971), pp. 1455-1485.
2. A. B. Crawford and W. C. Jakes, Jr., "Selective Fading of Microwaves," B.S.T.J., 31, No. 1 (January 1952), pp. 68-90.
3. R. L. Kaylor, "A Statistical Study of Selective Fading of Super-High Frequency Radio Signals," B.S.T.J., 32, No. 5 (September 1953), pp. 1187-1202.
4. W. T. Barnett, "Microwave Line-of-Sight Propagation With and Without Frequency Diversity," B.S.T.J., 49, No. 8 (October 1970), pp. 1827-1871.
5. W. T. Barnett, "Multipath Propagation at 4, 6, and 11 GHz," B.S.T.J., 51, No. 2 (February 1972), pp. 321-361.
6. A. Vigants, "Space-Diversity Performance as a Function of Antenna Separation," IEEE Trans. Commun. Tech., COM-16, No. 6 (December 1968), pp. 831-836.
7. A. Vigants, "The Number of Fades in Space-Diversity Reception," B.S.T.J., 49, No. 7 (September 1970), pp. 1513-1530.
8. A. Vigants, "Number and Duration of Fades at 6 and 4 GHz," B.S.T.J., 50, No. 3 (March 1971), pp. 815-841.
9. A. Vigants, "Space-Diversity Engineering," B.S.T.J., 54, No. 1 (January 1975), pp. 103-142.
10. S. H. Lin, "Statistical Behavior of a Fading Signal," B.S.T.J., 50, No. 10 (December 1971), pp. 3211-3270.
11. S. H. Lin, "Statistical Behavior of Deep Fades of Diversity Signals," IEEE Trans. Commun., COM-20, No. 6 (December 1972), pp. 1100-1107.
12. G. M. Babler, "A Study of Frequency Selective Fading for a Microwave Line-of-Sight Narrowband Radio Channel," B.S.T.J., 51, No. 3 (March 1972), pp. 731-757.
13. G. M. Babler, "Selectively Faded Nondiversity and Space Diversity Narrowband Microwave Radio Channels," B.S.T.J., 52, No. 2 (February 1973), pp. 239-261.
14. E. Parzen, *Modern Probability Theory and Its Applications*, New York: John Wiley and Sons, 1960, Chapter 2, Section 6.

FREQUENCY DIVERSITY PERFORMANCE DURING MULTIPATH FADING

by

A. Vigants and M. V. Pursley
Bell Telephone Laboratories, Inc.
Holmdel, New Jersey 07733

NTC '79
PREPRINT

ABSTRACT

Noise performance of average as well as individual working channels in microwave line-of-sight FM radio systems can be estimated from a model of multipath fading and frequency-diversity operation utilized in the Bell System. The performance degradation imposed by radio channels with substandard fade margins can also be estimated from the model.

INTRODUCTION

Microwave FM radio systems utilized in the Bell System provide protected broadband communications channels that generally have a capacity, depending on the frequency band and on the type of equipment, of 1200 to 2400 message circuits per channel. The protected channels, with protection provided by radio switching systems, are referred to as "working" channels, to distinguish these from the actual radio channels, which are assigned as either "regular" or "protection" channels.

The communications traffic in a working channel can be temporarily subjected to high noise when the number of impaired radio channels exceeds the number of protection channels. Bell System practice is to describe this effect in terms of the amount of time during which the noise in a working channel exceeds 55 dBmCO in a message circuit at the top frequency assignment in the baseband¹. In this paper, this time is referred to as "service failure time".

In modern microwave radio systems, protection requirements are frequently governed by the presence of multipath fading²⁻¹³, as opposed to causes associated with equipment or human intervention¹. Estimates of service failure time due to multipath fading are therefore needed to determine the adequacy of diversity protection arrangements when new routes are planned, when transmission parameters of existing routes are changed, or when alternate protection strategies are considered for future use.

A mathematical model¹⁴ utilized in the Bell System to obtain such estimates for frequency-diversity protected FM radio systems is summarized and illustrated in this paper. The

improvement resulting from additions of space-diversity protection⁹ to frequency-diversity protection can be incorporated in this model.

PERFORMANCE OF AVERAGE CHANNELS

In FM radio systems, the dominant form of noise during deep multipath fading is thermal noise, which is proportional to fade depth. The annual amount of time during which a particular value of noise is exceeded can therefore be described in terms of the amount of time during which, as a result of multipath fading, the received signals on a radio hop are below particular levels. The performance of a frequency-diversity switching section containing a number of hops is obtained by addition of the time-below-level values for the various hops, since the probability of simultaneous deep fading on different hops is much smaller than the probability of simultaneous fading in radio channels on the same hop.

In the case of a single unprotected radio channel, the estimated annual time-below-level on a particular radio hop is^{5,9}:

$$T_u = rT_0L^2, \quad L < 0.1 \quad (1)$$

where L describes a normalized voltage, such that the level in dB relative to a nonfaded received signal is $20 \log L$. The time T_0 is related to the length of the fading season. Its value is 3×10^5 seconds for an average geographic location in the United States.⁹ The fade occurrence fact is^{5,9}:

$$r = c(f/4)D^3 10^{-5} \quad (2)$$

where D is the path length in miles and f is the carrier frequency in GHz. The value of c is unity when the climate and terrain are average.^{5,9} For a fade margin of F dB (defined by noise of 55 dBmCO) where F is a positive number, the corresponding voltage level is:

$$L_0 = 10^{-(F/20)} \quad (3)$$

When L_0 is used as a value of L in equation (1), T_u becomes the time during which the channel has failed, where failure is defined as noise in excess of 55 dBm/Hz at the top frequency assignment in baseband.

The equivalent time-below-level of an average working channel in a frequency-diversity protection system (Figure 1) can be expressed as:

$$T = (DG/100f_0) r T_0 L_0^4, \quad T < T_u \quad (4)$$

where f_0 is the frequency, expressed in GHz, at which r is calculated. An average of the carrier frequencies of the radio channels is a suitable value for the reference frequency f_0 . The parameter G is determined by the carrier frequencies of the radio channels and by the channel-to-channel departures of fade margins from the reference value L_0 . The mathematical model from which equation (4) is obtained, and from which G can be calculated, is described in Appendix A. The expression for T describes the service failure time occurring in switched frequency-diversity systems in which the values of noise defining the fade margins and the initiation of switching are identical.

Representative estimated values of service failure time can be obtained from calculations for a switching section containing one 25-mile hop with average terrain and climate. In this case, for a fully developed 4-GHz route (one protection channel, 11 working channels), the calculated service failure time of an average working channel is approximately 15 seconds/year when all channels have a fade margin of 37 dB (Figure 2). The service failure time changes by a factor of ten when the fade margins of all channels change 5 dB. Similarly, a one-dB decrease in the fade margins increases the service failure time by approximately 60 percent.

Transmission performance objectives, as currently applied to the engineering of microwave FM radio routes¹⁴ allocate one-quarter of a 0.02 percent annual objective to service failures caused by multipath fading in a one-way circuit on a 4000-mile long-haul or 250-mile short-haul route. This allocation is prorated to the actual length of the switching section. In the case of a 25-mile switching section in long-haul service, the

service failure time should be less than 10 seconds/year. In the example in the previous paragraph, where the estimated service failure time was 15 seconds/year, larger fade margins or addition of space-diversity protection are needed to meet design objectives.

When the fade margins of all radio channels are identical, the parameter G depends only on the frequency arrangement of the channels. Tabulated values of G , such as shown in Table 1 for fully developed 4-GHz and 6-GHz routes, can be used in such cases to simplify calculations for standard frequency arrangements. The value of G is 4682 in the 1 x 111 example discussed above.

On partially developed routes where only a part of all available frequency assignments is utilized, the service failure time is a function of the frequency arrangement of the radio channels. A "best case" arrangement is one where the frequency separation of adjacent channels is maximized. In a "worst case" arrangement, the channels are crowded into the high end of the frequency band. Such arrangements do not necessarily correspond to actual or permitted growth strategies, but they do provide bounds for the variation of service failure time on partially developed routes.

In continuation of the example in Figure 2, calculated results for the best and worst cases are shown in Figure 3 as a function of the number of working channels. The best case results for the 4-GHz band show that the 10 sec/year long-haul objective cannot be met by frequency diversity alone when the number of working channels is larger than seven. The ripple in the worst case is caused by the alternating 20 MHz and 60 MHz increments as channels are added¹⁴.

In the 6-GHz band, the long-haul objective cannot be met by frequency diversity alone when the number of working channels is larger than four. The 6-GHz worst case is better than the 4-GHz worst case because the 6-GHz fade margin (40 dB) is larger than the 4-GHz fade margin (37 dB) in this example.

In a combined protection system for the two frequency bands, introduced after the 4-GHz band is fully developed, the arrangement of the channels in the 6-GHz band has only a small effect on the service failure time of an average working channel, which varies between 5 and 6 sec/year.

PERFORMANCE OF INDIVIDUAL CHANNELS

In addition to the service failure time of an average working channel utilized in route design, the mathematical model presented in the work can provide other information about the operation of frequency-diversity protection. In particular, the service failure times of individual working channels can be obtained from a summation of the times during which particular

sets of radio channels have failed.

As an example, consider a 1 x 3 protection system in the 4-GHz band with parameters as in Figure 3, utilizing channels 2, 4, 6 and 8 (80 MHz separation of adjacent channels). The simultaneous failure times for particular sets of exactly $u + 1$ channels, denoted by $T'_k(u+1)$ and listed in Table 2, have been calculated as outlined in Appendix A. The numerical values illustrate the frequency selectivity and frequency dependence of multipath fading. For example, the failure time of channels 2 and 4, but not 6 and 8, which can be caused by a slope in the frequency response, is 2.58 seconds. The failure time of channels 6 and 8, but not 2 and 4, is 3.07 seconds. This is larger than the 2.58 seconds because the amount of fading increases with frequency. The failure time of channels 4 and 6, but not 2 and 8, is 2.22 seconds. This is smaller than either the 2.58 seconds or the 3.07 seconds because this failure results from a minimum in the frequency response, which has a smaller probability of occurrence than a slope in the frequency response.

The service failure time of an average working channel in this example is, from the definition in equation (7) in Appendix A,

$$T = (1/3) \left(\sum_{k=1}^5 T'_k(2) + 2 \sum_{k=1}^4 T'_k(3) + 3 T'_1(4) \right) \quad (5)$$

$$= (1/3) (8.91 + 2 \times 2.12 + 3 \times 1.00)$$

$$= 5.35 \text{ seconds/year}$$

About 45 percent of this time occurs when 3 or all 4 of the radio channels have failed simultaneously. This example demonstrates that the contribution of higher order simultaneities to the service failure time cannot be neglected.

The expressions for the service failure time of individual channels are obtained by inspection from Table 2. In the case where channel 2 is used for protection, the service failure time

of the working channel assigned to channel 4 is:

$$T_{ch4} = T_1'(2) + (1/2) T_4'(2) + (1/2) T_5'(2) \quad (5)$$

$$+ T_1'(3) + T_2'(3) + (2/3) T_4'(3) + T_1'(4)$$

$$= 5.484 \text{ seconds/year}$$

where the fractions are based on statistically equal protection occupancy in cases of simultaneous failures.

The results of such calculations (summarized in Table 3) show that the location of the protection channel affects the spread of the individual service failure times. The service failure time of an average channel is not affected by the location of the protection channel. The largest spread of the individual service failure times (68 to 131 percent of average) occurs when the channel at the highest frequency (channel 9) is used for protection (Figure 4).

Protection channel assignments could be optimized based on results such as presented in Table 3. However, a general treatment of this is beyond the current scope of this study.

THE EFFECT OF SUBSTANDARD CHANNELS

A radio channel with a substandard fade margin experiences a failure time that is larger than normal. The presence of such a channel increases protection unavailability, which results in increased service failure times for all working channels. The increase in service failure time of an average working channel, caused by the presence of one or two substandard radio channels on a fully developed route, is shown in Figure 5 as a function of the reduction of the fade margin from its normal value. As an example, the service failure time of an average working channel in a 1 x 11 system is doubled when the fade margin of one midband radio channel is degraded by 7 dB; this is equivalent to a 1.5 dB degradation of the fade margins of all channels.

ACKNOWLEDGEMENTS

We wish to express our appreciation to W. T. Barnett, whose model of simultaneous fading we utilize, and to H. Adams who helped develop the computer program.

REFERENCES

1. W. Y. S. Chen, "Estimated Outage in Long-Haul Radio Relay Systems with Protection Switching", BSTJ, 50, No. 4, April 1971, pp. 1455-1485.
2. A. B. Crawford and W. C. Jakes, Jr., "Selective Fading of Microwaves", BSTJ, 31, No. 1, January 1952, pp. 68-90.
3. R. L. Kaylor, "A Statistical Study of Selective Fading of Super-High Frequency Radio Signals", BSTJ, 32, No. 5, September 1953, pp. 1187-1202.
4. W. T. Barnett, "Microwave Line-of-Sight Propagation With and Without Frequency-Diversity", BSTJ, 49, No. 8, October 1970, pp. 1827-1871.
5. W. T. Barnett, "Multipath Propagation at 4, 6, and 11 GHz", BSTJ, 51, No. 2, February 1972, pp. 321-361.
6. A. Vigants, "Space-Diversity Performance as a Function of Antenna Separation", IEEE Transaction on Communications, COM-16, No. 6, December 1968, pp. 831-836.
7. A. Vigants, "The Number of Fades in Space-Diversity Reception", BSTJ, 49, No. 7, September 1970, pp. 1513-1530.
8. A. Vigants, "Number and Duration of Fades at 6 and 4 GHz", BSTJ, 50, No. 3, March 1971, pp. 815-841.
9. A. Vigants, "Space-Diversity Engineering", BSTJ, 54, No. 1, January 1975, pp. 103-142.
10. S. H. Lin, "Statistical Behavior of a Fading Signal", BSTJ, 50, No. 10, December 1971, pp. 3211-3270.
11. S. H. Lin, "Statistical Behavior of Deep Fades of Diversity Signals", IEEE Transaction on Communications, COM-20, No. 6, December 1972, pp. 1100-1107.

REFERENCES (cont'd.)

12. G. M. Babler, "A Study of Frequency Selective Fading for a Microwave Line-of-Sight Narrowband Radio Channel", BSTJ, 51, No.3, March 1972, pp. 731-757.
13. G. M. Babler, "Selectively Faded Nondiversity and Space Diversity Narrowband Microwave Radio Channels", BSTJ, 52, No. 2, February 1973, pp. 239-261.
14. A. Vigants and M. V. Pursley, "Transmission Unavailability of Frequency-Diversity Protected Microwave FM Radio Systems Caused by Multipath Fading", BSTJ, 58, October 1979.
15. E. Parzen, Modern Probability Theory and Its Applications, New York: John Wiley and Sons, 1960, Chapter 2, Section 6.

APPENDIX A
THE MATHEMATICAL MODEL

The service failure time of an average working channel is defined as

$$T = N^{-1} \sum_{i=1}^N iT'(u+i) \quad (7)$$

where N is the number of working channels and u is the number of protection channels. The total number of radio channels is

$$M = u + N \quad (8)$$

The quantity $T'(u+i)$ is the accumulated time during which exactly $u+i$ of the M radio channels have failed simultaneously.

The simultaneous fading of radio channels is normally described in terms of the amount of time during which particular sets of $u+i$ channels have failed, with the status of the other $M-u-i$ channels not specified. With such a time denoted by $T_k(u+i)$, the expression for T becomes an alternating series^{1, 14}

$$T = N^{-1} \sum_{i=1}^N \sum_{k=1}^{J(u+i)} (-1)^{i-1} C_{u-1}^{u+i-2} T_k(u+i) \quad (9)$$

Where $J(u+i)$ is the binomial coefficient C_{u+i}^M , and where the subscript k enumerates the sets of $u+i$ channels obtainable from the M channels.

Empirical expressions for simultaneous fading of radio channels have been obtained by W. T. Barnett from experimental data:

$$T_k(u+i) = (C D^4 10^{-5} / 400) f_k(u+i) T_0 L^4 \quad (10)$$

where

$$f_k(u+i) = (u+i) / \sum_{p=1}^{I(u+i)} (L_0/L_{1p})^2 (L_0/L_{2p})^2 (\delta_p/f_p^2) \quad (11)$$

The quantities in this expression are associated with pairs of channels formed from the $u+i$ channels. The number of such pairs is

$$I(u+i) = C_2^{u+i} \quad (12)$$

The subscript p identifies the pairs. The fade margins of the channels in a pair are described by L_{1p} and L_{2p} . The corresponding carrier frequencies f_{1p} and f_{2p} are expressed in GHz ($f_{1p} < f_{2p}$). The average frequency for a pair is

$$f_p = (f_{1p} + f_{2p})/2 \quad (13)$$

and the fractional frequency difference is

$$\delta_p = (f_{2p} - f_{1p})/f_p \quad (14)$$

A value of 0.05 is used for δ_p when one of the channels is in the 4-GHz band and the other in the 6 GHz band.

The sum

$$G = N^{-1} \sum_{i=1}^N \sum_{k=1}^{J(u+i)} (-1)^{i-1} C_{u-i}^{u+i-2} f_k(u+i) \quad (15)$$

contains the effects of the frequency arrangement of the radio channels and the deviations of the fade margins from a reference value. A simplified form of $T_k(u+i)$ has been used previously to demonstrate the feasibility of joint frequency-diversity protection for radio systems in the 4 GHz and 6 GHz bands.¹

The alternating series in equation (9) can be derived formally from the definition in equation (7) when a theorem from probability theory¹⁵ is used to relate the primed and unprimed quantities¹⁴

$$T'(u+i) = \sum_{r=u+i}^M (-1)^{r-u-i} C_{u+i}^r S(r) \quad (16)$$

where

$$S(r) = \sum_{k=1}^{J(r)} T_k(r) \quad (17)$$

in which $J(r)$ is the binomial coefficient C_r^M .

AD-A087 793

DEFENSE COMMUNICATIONS ENGINEERING CENTER RESTON VA
PROCEEDINGS OF SEMINAR ON FREQUENCY SELECTIVE FADING AND ITS EF--ETC(U)
JAN 80 D R SMITH

F/G 17/2.1

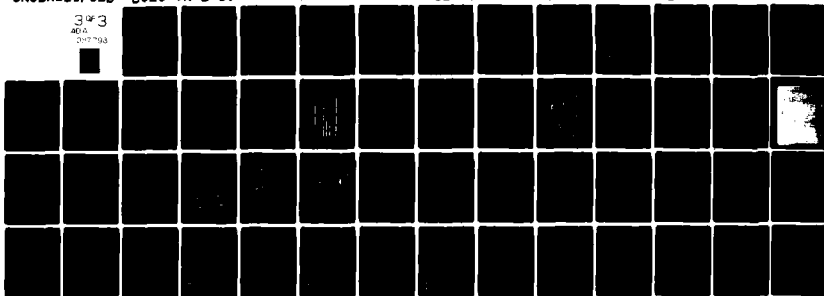
UNCLASSIFIED

DCEC-TN-2-80

SBIE-AD-E100 375

NL

3 OF 3
AD-A
312703



END

DATE

FILED

8-80

DTIC

The quantity $T'(u+i)$ can be decomposed into a sum of terms, denoted by $T'_k(u+i)$, describing the failure of particular sets of exactly $u+i$ radio channels. This and equation (16) provide sets of equations from which values of $T'_k(u+i)$ can be calculated.

VALUES OF G FOR FULLY DEVELOPED ROUTES

FADE MARGINS ARE IDENTICAL FOR ALL RADIO CHANNELS IN A GIVEN PROTECTION SCHEME

FREQUENCY BAND, GHz	PROTECTION SCHEME	VALUE OF G
4	2X10	1597
4	1X11	4682
6	2X 6	7380
6	1X 7	17059

FREQUENCIES IN THE 4-GHz BAND:

$3.670 \pm 0.040i$, $i = 1, 3, 5, \dots, 11$

$3.650 \pm 0.040i$, $i = 2, 4, 6, \dots, 12$

FREQUENCIES IN THE 6 GHz BAND:

5.9452, 5.9748, 6.0045, 6.0342,
6.0638, 6.0935, 6.1231, 6.1528

TABLE 1

SIMULTANEOUS FAILURES OF EXACTLY $u+i$ RADIO CHANNELS.
 CHANNEL NUMBERS: 2, 4, 6, 8.
 FREQUENCIES, GHz: 3.73, 3.81, 3.89, 3.97

$u+i$	k	CHANNELS	$T_k(u+i)$, SEC/YEAR
2	1	2, 4	2.58
2	2	2, 6	0.37
2	3	2, 8	0.17
2	4	4, 6	2.22
2	5	4, 8	0.40
2	6	6, 8	3.07
3	1	2, 4, 6	0.77
3	2	2, 4, 8	0.23
3	3	2, 6, 8	0.23
3	4	4, 6, 8	0.89
4	1	2, 4, 6, 8	1.00

TABLE 2

**SERVICE FAILURE TIME OF INDIVIDUAL WORKING CHANNELS
FOR A 1x3 SYSTEM IN THE 4-GHz BAND**

CHANNEL NUMBERS: 2, 4, 6, 8

FREQUENCIES, GHz: 3.73, 3.81, 3.89, 3.97

WORKING CHANNEL *	SERVICE FAILURE TIME, SECONDS/YEAR PERCENT OF AVERAGE IN BRACKETS			
	PROTECTION CHANNEL ASSIGNMENT			
	2	4	6	8
2	—	5.003 (94)	3.898 (73)	3.618 (68)
4	6.484 (121)	—	6.524 (122)	5.434 (101)
6	5.608 (105)	6.753 (126)	—	6.998 (131)
8	3.958 (74)	4.294 (80)	5.628 (105)	—
TOTAL SECONDS	16.05	16.05	16.05	16.05
RANGE OF PERCENT: MINIMUM MAXIMUM	74 121	80 126	73 122	68 131

* WORKING CHANNELS IN THIS TABLE ARE IDENTIFIED BY THE
NUMBER OF THE CORRESPONDING REGULAR RADIO CHANNEL.

TABLE 3

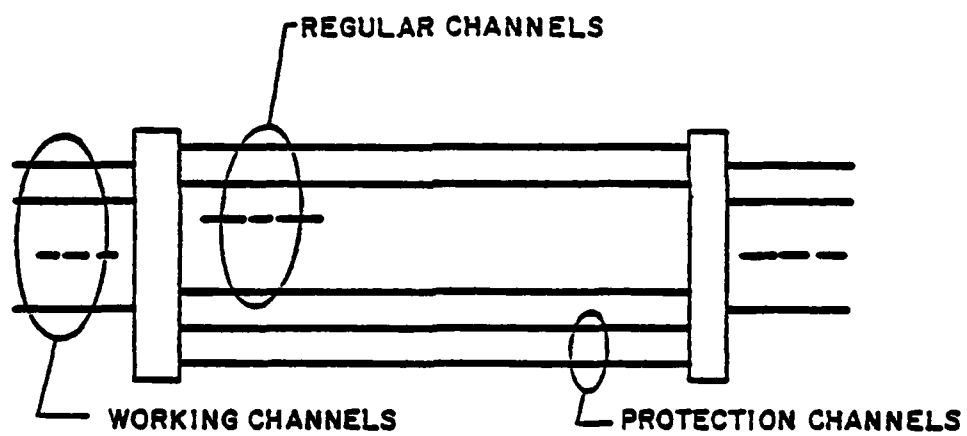


FIGURE 1 FREQUENCY DIVERSITY PROTECTION

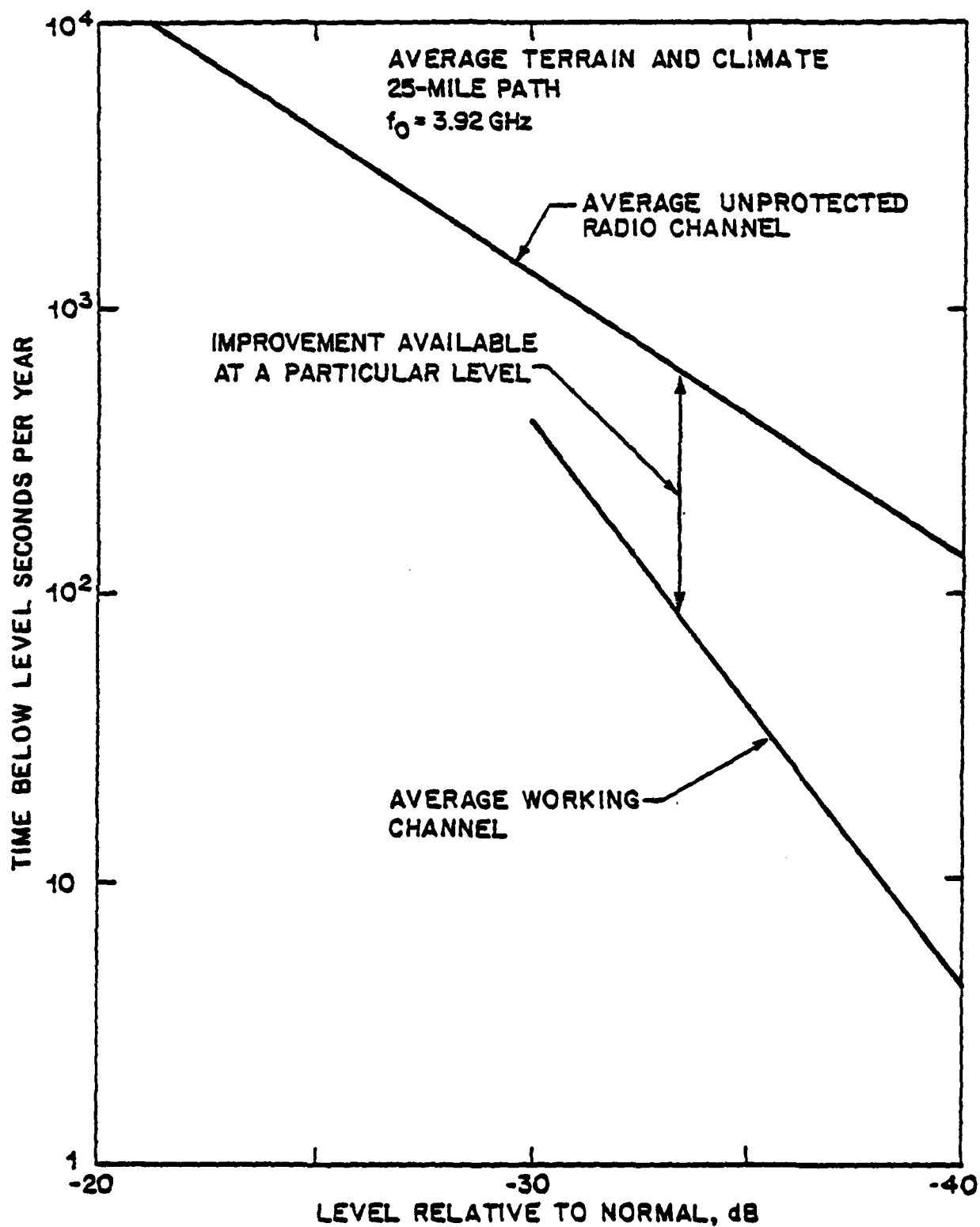


FIGURE 2 TIME BELOW LEVEL FOR A FULLY DEVELOPED (1x11) 4-GHz ROUTE

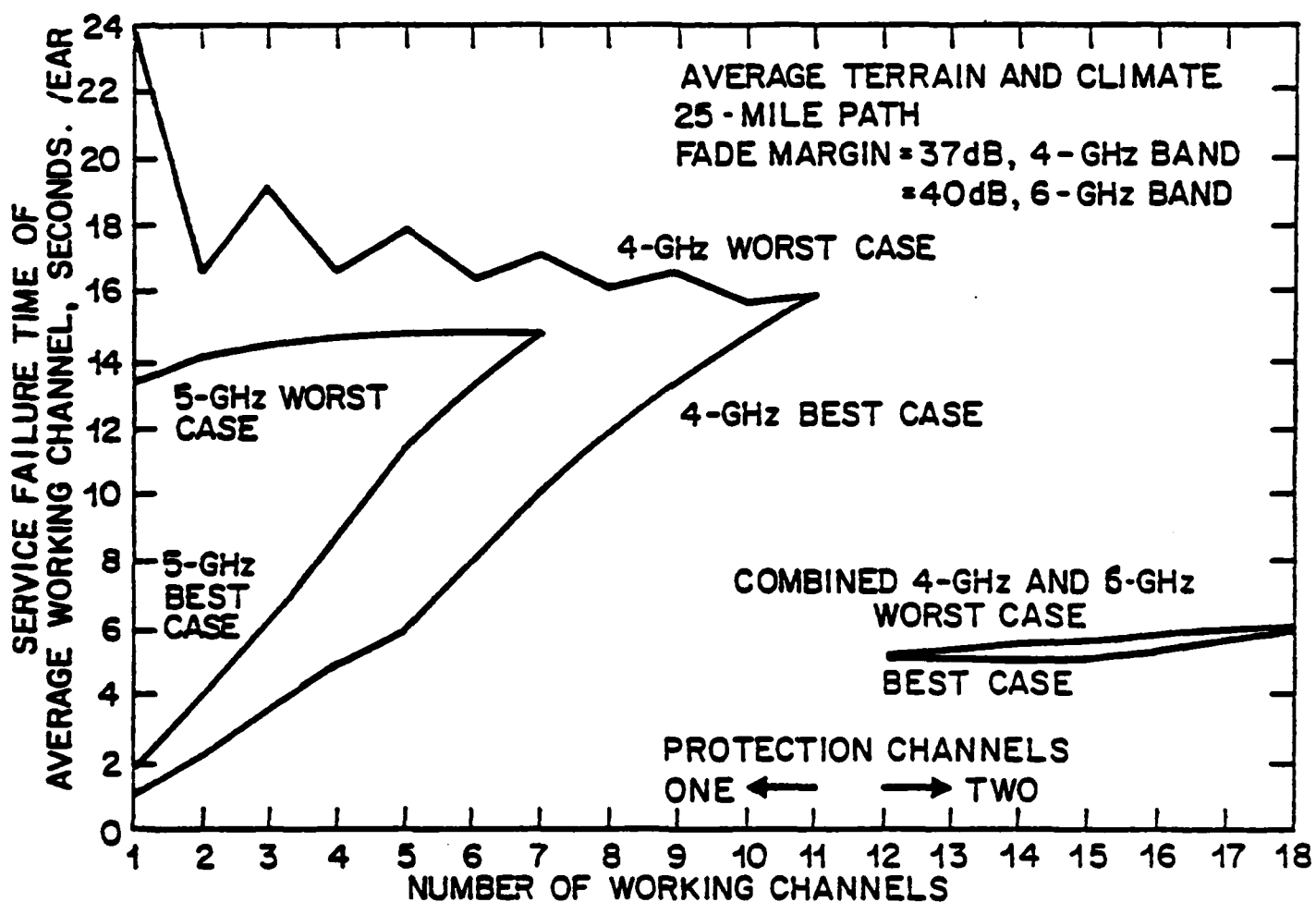


FIGURE 3 BOUNDING CASES FOR SERVICE FAILURE TIME OF AVERAGE WORKING CHANNELS

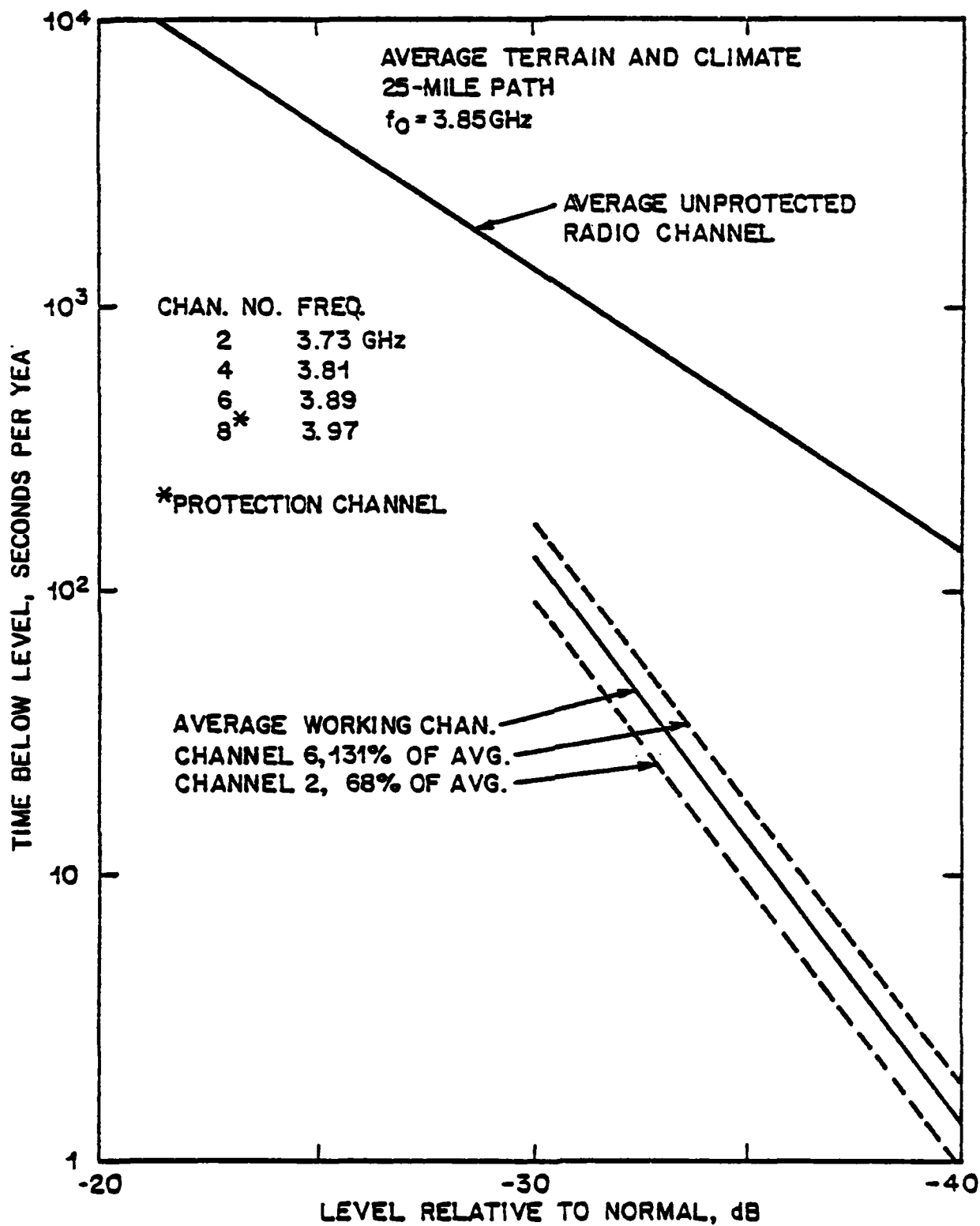


FIGURE 4 EXAMPLE OF TIME BELOW LEVEL FOR INDIVIDUAL WORKING CHANNELS

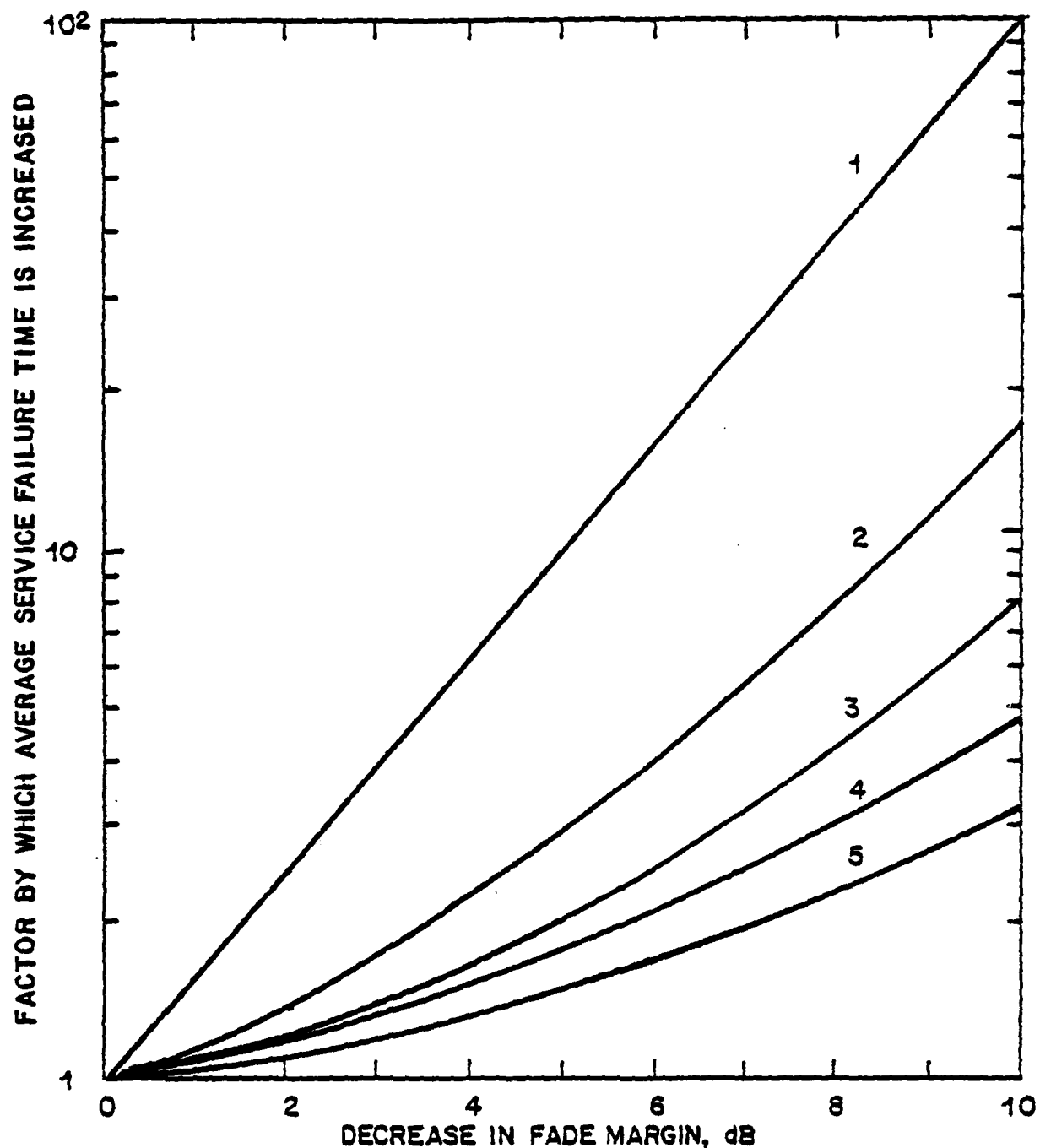


FIGURE 5 INCREASE IN SERVICE FAILURE TIME OF AVERAGE WORKING CHANNEL WHEN FADE MARGINS ARE REDUCED FOR:

- 1) ALL RADIO CHANNELS
- 2) TWO MIDBAND CHANNELS IN 1x7 SYSTEM, 6GHz
- 3) TWO MIDBAND CHANNELS IN 1x11 SYSTEM, 4GHz
- 4) ONE MIDBAND CHANNEL IN 1x7 SYSTEM, 6GHz
- 5) ONE MIDBAND CHANNEL IN 1x11 SYSTEM, 4GHz

8. THE EFFECT OF SELECTIVE FADING ON DIGITAL RADIO

Steve Barber
Bell-Northern Research
Ottawa, Ontario, Canada

NOTE: The materials provided in this section are copies of an article from the 1978 International Conference on Communications used as the basis for the extemporaneous remarks given by Mr. Barber.

THE EFFECT OF SELECTIVE FADING ON DIGITAL RADIO

C.W. Anderson

S. Barber

R. Patel

Bell-Northern Research, Ottawa, Canada

Abstract

In the course of development of the DRS-8 Digital Radio System a series of digital propagation trials were conducted over a 51 km path at 8 GHz to determine the effect of multipath propagation on a 40 MHz bandwidth digital radio system. It was found that the effects of frequency selective fading result in unacceptably high system unavailability unless adaptive equalization and space diversity are employed. Specifically the results are:

1. Multipath induced outage is much higher than would be predicted from the measured flat fade margin of the equipment. For a non diversity system, the probability of outage for a single hop in the worst fading month is approximately 1×10^{-3} . This is 700 times the objective for a long haul system and corresponds to an effective fade margin of only 27 dB.
2. The primary cause of outage is inband distortion caused by the frequency selectivity of the multipath fading process.
3. Phase adaptive space diversity combining is very effective in reducing the amount of fading. In addition it affords some increase in the effective fade margin of the radio, i.e., it reduces the severity of inband distortion for a given fade depth. Outage for the system with space diversity combining was 2.6×10^{-4} which is about 18 times the long haul objective.
4. A simple adaptive linear amplitude equalizer in conjunction with the phase adaptive space diversity combining provides an additional improvement of approximately a factor of 20, reducing the multipath outage to levels compatible with long haul availability objectives.
5. This same equalizer when applied to a non diversity channel provides an improvement of about 2. Thus the preconditioning effect of phase adaptive space diversity combining is necessary to reduce distortions sufficiently that they can be dealt with by a relatively simple adaptive equalizer.

Introduction

Spurred by the cost advantages of digital multiplex and switching there is an accelerating move towards all digital networks. Development of digital modulation techniques with bandwidth efficiency greater than 2 bits/hertz has made digital radio transmission a practical way of implementing the trunks in such a network. In Canada, the 8 GHz band has been rechannelized for 40 MHz channels to facilitate digital transmission.

The Northern Telecom DRS-8 Digital Radio System was developed for long haul transmission in this band. The DRS-8 System consists of the MR-3A MULDEM which synchronizes and conditions two DS3 signals into a single 91.04 Mb/s digital stream (1344 PCM voice channels), the CE-4 1 x N Automatic Protection Switching which provides equipment protection and the RD-3 Digital Radio which transmits 91.04 Mb/s in a 40 MHz RF bandwidth using Quadrature Partial Response Signalling (QPRS). To achieve the maximum economic advantage, the system is designed to be overbuilt on existing 4 GHz routes using existing sites, buildings, towers and antennas. This fixes the hop lengths at approximately 45-55 km. The availability objective is 99.98% for a 6560 km connection. Of the allowable .02% outage, .01% was allocated for equipment failure, .005% for rain and .005% for multipath fading. This requires a per hop outage probability of 1.43×10^{-6} in the worst fading month. To design a system to these stringent requirements more information was required on the effect of multipath propagation on wideband digital transmission over long hops. Although information has been published⁴ on the frequency selective nature of fading, little or no quantitative information was available on the effects of frequency selective fading on digital radio system availability. A series of digital propagation trials have been conducted over a 51 km path at 8 GHz to provide more information on space diversity, inband distortion, and cross polarization discrimination during multipath fading.

Space Diversity

Space diversity is required to meet the long haul availability objective at 8 GHz. Frequency diversity which is normally used to combat fading in the 4 GHz band would be a more economical solution but it does not provide adequate improvement for a fully built-out system because of the increased fading activity and smaller fractional channel separation at 8 GHz.⁽¹⁾ Space diversity switching, either at RF or IF, is unsuitable for a digital radio system because of the excessive number of interruptions that such an arrangement would produce during fading. Although post regenerative switching can be made hitless, it is very expensive since two complete receiver-demodulators are required.

Adaptive inphase IF combining (Fig. 1) was selected because it is hitless and requires duplication of only the mixer-preamplifier and channel dropping filter. The combiner consists of a summing junction, an electronic phase shifter, and an electronic control system to maintain the two IF input signals in phase. Because the wanted signals are added coherently and the noise from the two receivers adds incoherently, the combiner yields a better signal to noise ratio than switched space diversity whenever the difference in signal levels is less than 7.7 dB.

Reprinted from 1978 International Conference on Communications Record, pp. 33.5.1 - 33.5.6.

A consequence of adjusting the phase rather than the delay of the input signals is that the bandwidth of the system is inversely proportional to the absolute time delay between signals. If the dynamic delay difference between antennas during multipath fading is large, significant signal distortion results. To check this and to confirm that the response of the combiner was fast enough to follow fading activity, it was desirable to verify the performance of the combiner under actual multipath fading conditions.

Inband Distortion

If the only effect of multipath fading were a reduction in the receive signal level during fading, it would be possible to calculate, using Barnett's empirical fading formulas⁽²⁾, that the fade margin required to achieve the outage objective over an average 50 km path with a nondiversity system would be 56 dB. Similarly, applying Vigant's expression⁽³⁾ for space diversity improvement, the fade margin required for a switched space diversity system with a 9 m separation between antennas and a diversity antenna system gain of 2 dB less than the main, would be 37 dB. However, it is known that multipath fading is accompanied by severe amplitude and delay distortion. Babler⁽⁴⁾ presented detailed statistics of amplitude distortion on a 20 MHz channel at 6 GHz for non diversity and switched space diversity systems from which it is apparent that amplitude slope could be a serious problem for both types of systems. A limited amount of information was available for delay distortion on a nondiversity system^(5, 6). The published information was not sufficient to predict the availability of the DRS-8 system because of the unknown effect of inphase combining, the wider bandwidth of the RD-3 system and the limited information available on delay distortion.

Cross-Polarization Discrimination

Barnett⁽⁷⁾ reported severe deterioration of cross-polarization discrimination (XPD) during multipath fading. This effect combined with differential up fading of adjacent channels could be a problem in a system which relies on cross-polarization discrimination to provide some protection from adjacent channel interference. Since this effect will also be modified by the space diversity combiner, field measurements were desirable to confirm that the RD-3 objective for tolerance to adjacent channel interference (1 dB degradation in thermal fade margin for two adjacent channels at 0 dB C/I) was adequate.

To determine the impact of multipath propagation on system availability and provide data to guide remedial action, an extensive experimental program was undertaken during the summers of 1975 to 1977. The remainder of this paper reports the results of these experiments.

Experiment Description

Experiments have been conducted at 8 GHz over the past 3 years on the 51 km path from Kempville to Avonmore, Ontario, which is part of the Bell Canada 4 GHz analog radio system. The path profile and the 8 GHz first fresnel zone for this hop (Fig. 2), show average terrain and adequate clearance. An early prototype of the RD-3 Digital Radio was installed using the existing antennas and waveguide. Block diagrams of the experiment are shown in Figures 3 and 4.

In the transmit site (Fig. 3), digital transmitters transmitted pseudo random bit streams on channel 4

(8173.15 MHz) horizontally polarized as well as on the two adjacent channels, 3 (8132.41 MHz) and 5 (8213.89 MHz), vertically polarized. In addition, FM transmitters, modulated by distinct single frequency tones, transmitted on the horizontal and vertical polarizations on channel 2 (8091.67 MHz) for measurement of cross-polarization interference.

In the receive site the signals were received by the standard KS horn antenna and a space diversity dish 3 m in diameter located 9 m below the horn antenna. On channel 4, three digital receivers were used to demodulate and regenerate signals from the main antenna, space diversity antenna, and the output of the space diversity combiner. Error rates on the three digital channels were measured by bit-by-bit comparison with locally synchronized replicas of the transmitted pseudo random sequences. The level on these channels was monitored by the linearized AGC control voltage of the IF amplifiers. In addition, narrowband detectors at ± 13 MHz from the center of the channel were included to give an indication of inband amplitude distortion. The adjacent channels were monitored for level only. To provide indications of equipment malfunction, alarms were brought out for carrier recovery lock, clock recovery lock, and the primary power supply. The data was recorded by a PDP/11-E10 data acquisition system, which sampled all of the measured parameters every 100 ms and wrote a record on disk when errors or significant changes in a parameter occurred. The contents of the disk were periodically transferred by a high speed data line to the IBM 370 computer at the Bell-Northern Research Laboratories in Ottawa, where the data was stored on tape for later analysis.

For the cross-polarization experiment, relative levels of the tones at the output of the FM demodulators provided a measure of the carrier-to-interference ratio for both horizontal into vertical and vertical into horizontal interference on channel 2. Carrier-to-interference ratio is the combined effect of differential fading between horizontal and vertical polarization and deterioration of cross-polarization discrimination.

In a supplementary experiment to provide detailed in-band distortion characterization during multipath fading, a swept microwave link analyzer with sample and hold circuit at the output of the receiver was used to sample the amplitude and delay distortion at 5 frequencies across a ± 15 MHz band.

Propagation Experiment Results - Space Diversity

Figure 5 shows the probability distribution of fading for the main, diversity and combined channels. Comparison of the fading distribution of the main channel to that predicted for an average hop using Barnett's formula⁽²⁾ shows the fading to be typical. The joint fading distribution for main and space diversity antennas, which represents the performance of an ideal comparative space diversity switch, shows that the combiner has slightly better performance than the comparative switch. A more exact evaluation of the IF combiner performance was obtained by comparing its output level distribution with that of the ideal in-phase combiner computed from the main and space diversity levels, sample by sample. The measured fade distribution was found to accurately coincide with that of the ideal combiner. To confirm that it was accurately tracking dynamic variations in the input signals, internal voltages which give a measure of a phase error, were monitored over a period of several weeks. This test confirmed that the dynamic response of the space diversity combiner was satisfactory.

Digital Performance

The performance of the digital transmission system can be described by two complementary criteria: the outage probability, defined as the probability of bit error rate greater than 10^{-4} and the effective fade margin, defined as that fade depth which has the same probability as the observed probability of outage. The effective fade margin is a convenient way of normalizing the outage to the amount of fading observed, thereby providing a meaningful reference and facilitating extrapolation to other situations. The difference between the effective fade margin and the flat fade margin of the equipment measured with an attenuator is a measure of the severity of selective fading effects. These quantities are shown for the three digital channels in Table I.

TABLE I
RADIO PERFORMANCE WITHOUT ADAPTIVE EQUALIZATION

	Outage Probability	Effective Fade Margin
Main	1.2×10^{-3}	26.5 dB
Space Diversity	7.5×10^{-4}	23.5 dB
Combined	2.6×10^{-5}	30.0 dB
Joint	1.9×10^{-5}	-

Non-Diversity Channel

The outage on the non-diversity channels exceed the objective by a factor of about 700 which corresponds to an effective fade margin of only 27 dB. The measured flat fade margin of the radio was 48 dB. This clearly indicates that a design method using the flat fade margin in conjunction with empirical formulas for fading will not provide a good estimate of the availability of a digital radio system over paths of this length. The narrowband detectors at ± 13 MHz give an indication of linear and quadratic amplitude distortion during fading. In Figure 7, the unconditional probability distribution of amplitude slope is compared with the distribution conditioned on outage of the digital receiver for a non-diversity system. This illustrates the high degree of correlation of outage and amplitude slope. Although quadratic distortion does not show a similar correlation, the initial uniform slope of the conditional distribution suggests that other factors such as group delay distortion may be contributing causes of outage. Because of an equipment malfunction a similar comparison is not possible for the combined channel.

Initially there was concern that the modulation scheme, QPRS, was more susceptible to inband distortion than other methods; however this proved not to be the case. Since the dominant multipath effects are odd order distortions which cause crosstalk between in-phase and quadrature channel, all two dimensional modulation systems such as Quadrature Amplitude Modulation or Multiphase PSK which have comparable noise resistance are similarly affected. This was confirmed by computer simulation⁽⁸⁾ for 8 PSK which was the other major contending modulation system for this application. Another question of interest is why the severe inband distortion experienced in these experiments was never a problem for analogue radio transmission systems. Four factors are significant, first the raw fading is only half as severe at 4 GHz compared to 8 GHz. Second, the larger frequency diversity improvement (8 times higher than at 8 GHz)

reduces the 4 GHz fading activity even further. Thirdly, Frequency Modulation, and modulation method commonly used for analogue transmission, is inherently more resistant to odd order inband distortion than the digital modulation systems which are suitable for bandwidth efficient transmission. Last of all the susceptibility of FM systems to inband distortion increases with the loading, that is the number of voice channels carried. Since most frequency selective multipath fading occurs during the night when the network is lightly loaded, the effect is reduced. Digital modulation systems on the other hand employ scrambling devices which ensure that the system is fully loaded all the time.

Combined Channel

The outage on the combined channel exceeded the per hop objective by a factor of 18. Note that in addition to providing an improvement in the time below level for the combined channel, the combiner improves the effective fade margin from 27 to 30 dB. That is, it provides some measure of relief from selective fading effects. Frequency diversity would provide some improvement for an initial 1×1 system but the improvement for a fully built out system is very small. The evaluate methods of further improving the availability the detailed distortion characteristics of the combined channel was obtained by means of a supplementary experiment in which the sampled amplitude and delay outputs of a swept link analyzer were recorded. Figure 8 and 9 show the probability distributions of the coefficients of a 3rd-order least-squares Chebyshev polynomial fit to the amplitude and delay measured at 5 points over a ± 15 MHz band on the combined channel. Note that the linear amplitude component dominates the amplitude distortion and that delay distortions are very small. These results suggest that a simple amplitude slope equalize would provide a substantial improvement in availability. To confirm this, a linear analysis program⁽⁸⁾ was employed to compute the eye opening with and without a linear amplitude equalizer for each data record which showed a significant distortion on the combined channel. The probability distributions. Figure 10, show that the improvement in the 0-10% range of eye opening is approximately 20, which indicates that a linear amplitude equalizer in conjunction with the space diversity combiner would provide sufficient improvement to meet the long haul availability objective.

Adaptive Equalizer Field Trial

An adaptive linear amplitude equalizer was developed and during the summer of 1976, the performance of a prototype was evaluated on the test hop. In this period there were several periods of anomalous fading. This fading was characterized by prolonged simultaneous signal depressions on both antennas on the main digital channel and on both polarizations of the cross-polarization experiment, 80 MHz away. In one instance, both main and space diversity antennas were continuously faded below 20 dB for 84 minutes, 221 times the mean fade duration reported by Vigants⁽³⁾. Such periods are, of course, characterized by poor space diversity improvement and excessive fading on the combined channel. Since the fading behaviour during these periods is different from anything encountered during the rest of the two years of experiments and is different from that reported in the extensive literature on multipath fading, it is concluded that a mechanism other than multipath fading was responsible. Rain can be excluded since the fading exhibits frequency selectivity. The results of an experiment conducted concurrently on an

antenna 15 dB below grazing show that these events are not caused by atmospheric subrefractivity. In view of these facts, the data were analyzed separately, with and without these anomalous events.

With the anomalous fading included, the overall performance of the RD-3 radio bay with adaptive equalizer is satisfactory. The effective fade margin of the equalized combined channel for the data set was 40 dB which exceeds the objective of 37 dB. In spite of this, the outage exceeds the objective by 5.5 because of extreme fading on the combined channel (28 times higher than in the 1975 experiment). The cause of the excessive fading was low space diversity improvement caused by high correlation of the fading experienced on the main and space diversity antennas. These observations reflect the presence in this data set of a disproportionate amount of deep flat fading. Both the combiner and adaptive equalizer fail to show the expected improvement during such fading and the effective fade margin appears better than it would be for more typical fading. The 4 GHz system also suffered abnormally long outages on these evenings. Since anomalous fading does not create a problem on the 4 GHz network we conclude that it is a sufficiently rare occurrence on a network wide basis to not have a major impact on system availability.

With the anomalous fading activity excluded the fading on main and space diversity antennas was only slightly less than for the hypothetical reference hop down to approximately 40 dB. The combined channel exhibited fairly typical fading down to approximately 30 dB after which the probability falls off rapidly. No fades greater than 33 dB were experienced. This is typical of the original experimental results of Vigants. The effective fade margin of the unequaled channel is 30 dB which is equal to the value for the 1975 experiment. In the selected data set 134 seconds of fading induced outage were recorded on the unequaled combined channel compared to 0.8 seconds on the equalized channel. The calculated improvement of 167 is probably not an accurate estimate of the average improvement because of the small amount of equalized channel outage on which it is based. However, since it is an order of magnitude better than required we may safely conclude that the improvement is satisfactory. A separate experiment to evaluate the performance of the linear amplitude equalizer on a non-diversity channel yielded an effective fade margin of only 30 dB. This indicates that the combiner plays an essential part in dealing with inband distortion and that a simple amplitude slope equalizer is not satisfactory for a non-diversity system.

Cross-Polarization Discrimination

Results from the cross-polarization discrimination (XPD) portion of the experiment confirmed the severe deterioration of XPD on a non-diversity system reported by Barnett(2). However the XPD performance on a combined channel obtained numerically by processing the simultaneous measurements on the two antennas showed that the XPD was considerably improved by combining. The performance was good enough to suggest that, with some further work, co-frequency cross-polarized operation would be possible permitting increasing the capacity of the 8 GHz band from 6 to 12 channels.

Conclusions

An experimental investigation into the effects of multipath propagation on a wideband digital radio system over a 51 km hop has been carried out at 8 GHz. It was found that the effects of frequency selective fading result in unacceptably high system unavailability unless adaptive equalization and space diversity are employed.

operates over long hops using a two dimensional modulation system such as QAM or multiphase PSK.

Specifically it is concluded that:

1. Multipath induced outage is much higher than predicted from the measured flat fade margin of the equipment. For a non-diversity system, the probability of outage for a single hop in the worst fading month is approximately 1×10^{-3} . This is 700 times the objective for a long haul system and corresponds to an effective fade margin of only 27 dB.
2. The primary cause of outage is inband distortion caused by the frequency selectivity of the multipath fading process.
3. Phase adaptive space diversity combining is very effective in reducing the amount of fading. In addition it affords some increase in the effective fade margin of the radio i.e., it reduces the severity inband distortion for a given fade depth. Probability of outage for the system with space diversity combining was 2.6×10^{-5} which is about 18 times the long haul objective.
4. A simple adaptive linear amplitude equalizer in conjunction with phase adaptive space diversity combining provides an additional improvement of approximately 20, reducing the multipath outage to levels compatible with long haul availability objectives.
5. This same equalizer when applied to a non-diversity channel provides an improvement of about 2. The preconditioning effect of the phase adaptive space diversity combiner is necessary to reduce distortion sufficiently that they can be dealt with by a relatively simple adaptive equalizer.

References

1. I. Godier, "System Planning for Digital Radio", IEEE International Conference on Communications, ICC 77, Chicago, June 1977
2. W.T. Barnett, "Multipath Propagation at 4, 6 and 11 GHz", BSTJ, February 1972, pp. 321 to 361.
3. A. Vigants, "The Number of Fades in Space Diversity Reception", BSTJ, September 1970, pp. 1513-1530.
4. G.M. Babler, "Selectivity Faded Non-Diversity Space Diversity Narrowband Microwave Channels", BS February 1973, pp. 230-261.
5. G.M. Babler, "Measurements of Delay Distortion During Selective Fading", IEEE International Conference on Communications, ICC 74, Minneapolis, Minn., June 17-19, 1974, pp. 12A-1.
6. Subramanian, K.C., O'Brien, P.J. Plugis, "Phase Dispersion Characteristics During Fade in a Microwave Line of Sight Radio Channel", BSTJ, December 1973, pp. 1877-1900.
7. W.T. Barnett, "Deterioration of Cross-Polarization Discrimination During Rain and Multipath Fading at 4 GHz", IEEE International Conference on Communications, Minneapolis, Minn., June 17-19, 1974, pp. 12D-1, 4.
8. S. Barber, C.W. Anderson, "Modulation Considerations for the RD-3 91 MB/s Digital Radio", IEEE International Conference on Communications, ICC 77, Chicago, Ill., June 1977. Expanded version submitted for publication in IEEE Trans. on Communications.

9. B.W. Gostrey, Q.S. Chew, F.T. Halevy,
 "Practical Considerations in the Design of the RD-3 Digital Radio", IEEE
 International Conference on Communications,
 ICC 77, Chicago, 111., June 1977.

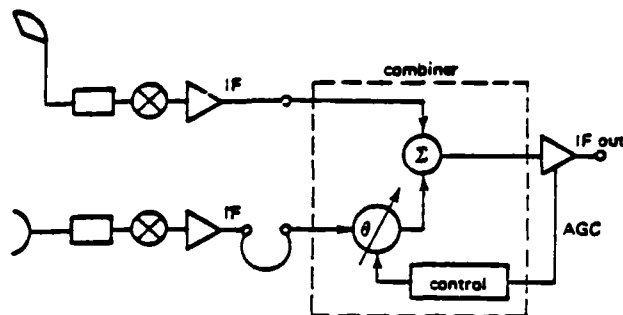


FIG. 1 SPACE DIVERSITY COMBINER

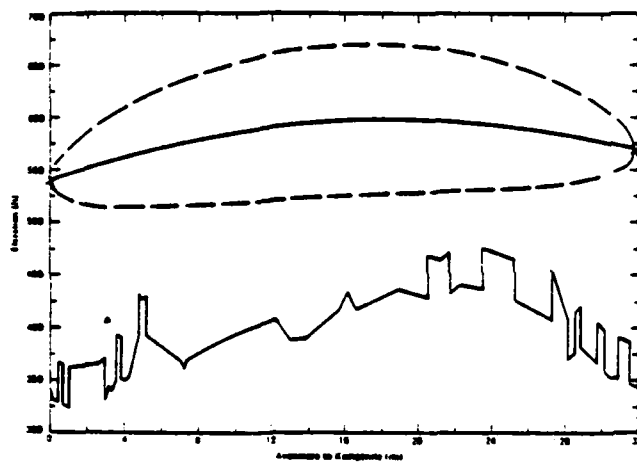


Figure 2 Path Profile Including Terrain - Normal Atmosphere

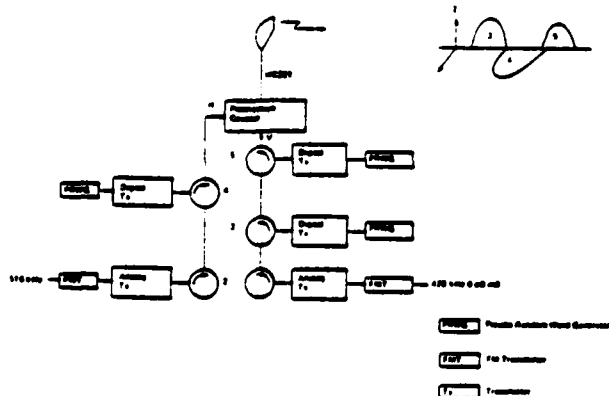


Figure 3 Space Diversity Receiver Block Diagram

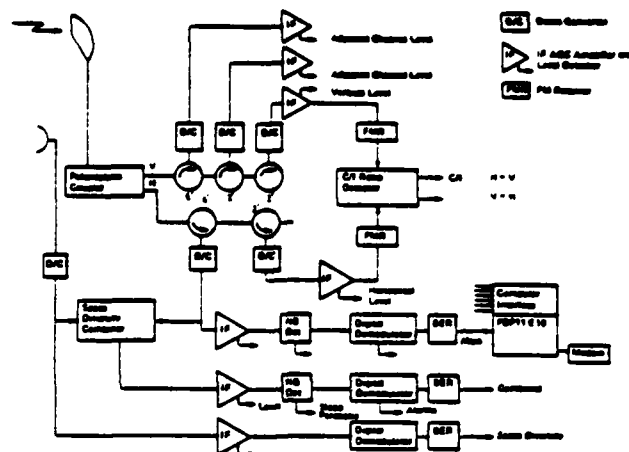


Figure 4 Space Diversity Receiver Block Diagram

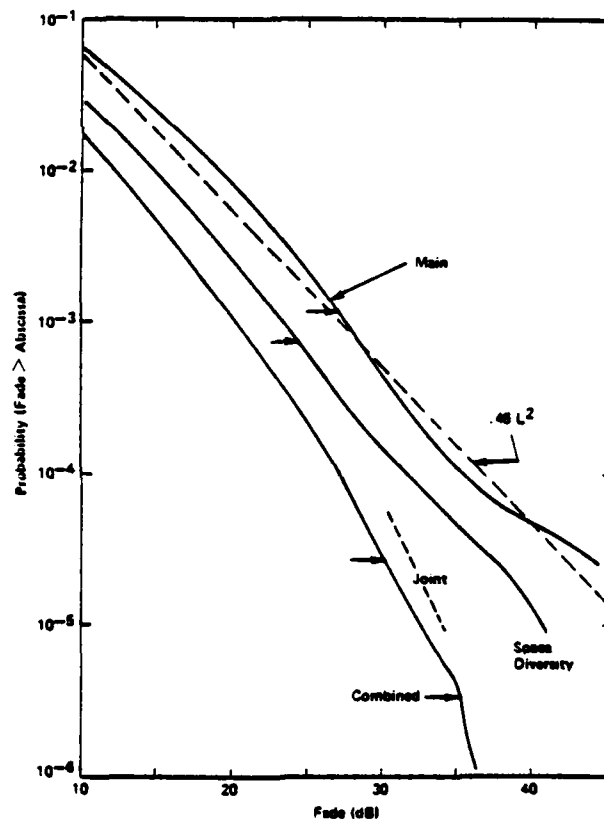


Figure 5 Fade Distributions for Main, Space Diversity and Combined Channels

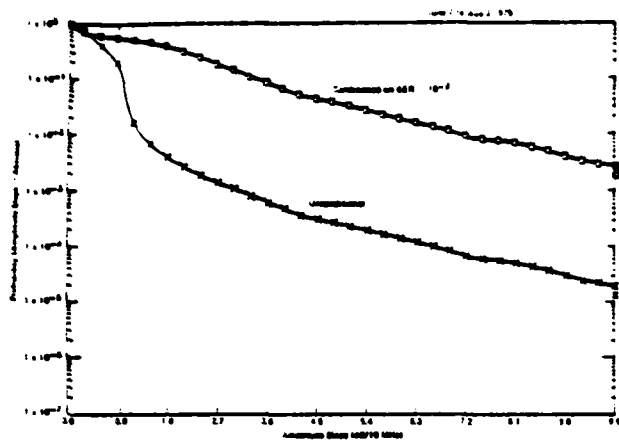


Figure 7 Probability Distribution of Amplitude Slope Computed on Output Performance

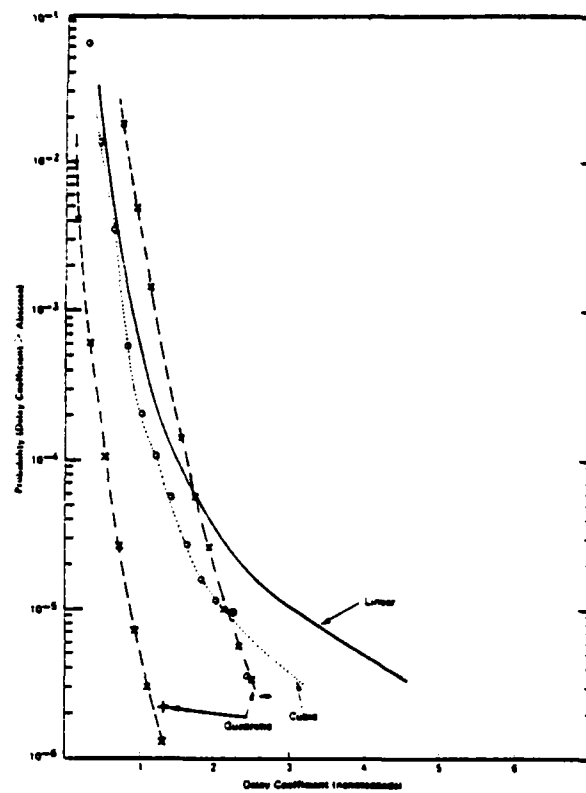


Figure 8 Probability Distribution of Chebyshev Delay Coefficients on Combined Channels

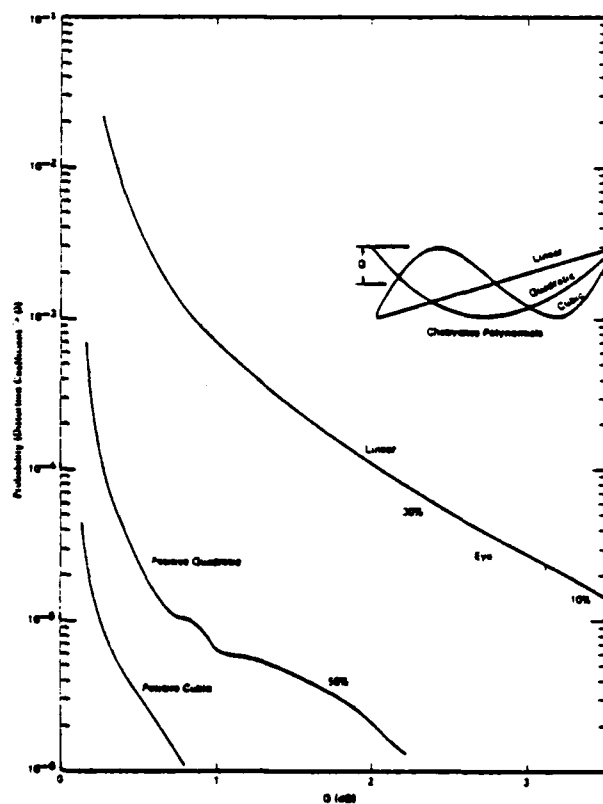


Figure 9 Probability Distribution of Chebyshev Coefficients of Third Order Fit to Measured Amplitude Response

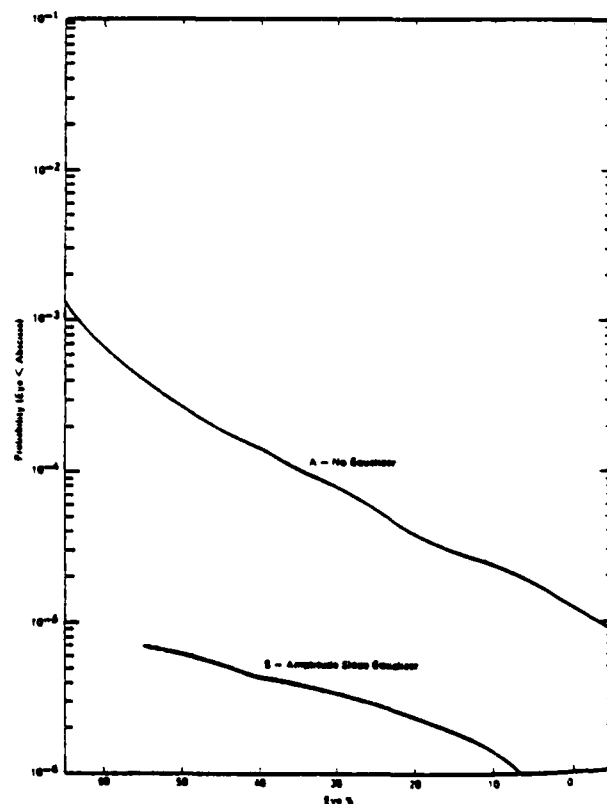


Figure 10 Probability Distribution of Computed Eye Opening for Inband Distortion Experiment at No Equalizer or with Linear Amplitude Slope Equalizer

9. ATMOSPHERIC STRUCTURE AND MULTIPATH EFFECTS

Owen Cote'
Staff Meteorology Office
Electronic System Division
Hanscom AFB, MA

NOTE: The materials provided in this section are copies
of the visuals used with the extemporaneous remarks
given by Mr. Cote'.

MEASUREMENT POSSIBILITIES

RADIOSONDE RELEASE AT POINT OR POINTS ALONG PATH

AIRCRAFT REFRACTOMETER

TETHERED BALLOON

DIRECT TURBULENCE MEASUREMENTS AT MICROWAVE SITE LOCATIONS

MULTI-FREQUENCY ELECTROMAGNETIC RADIATION TRANSMISSION

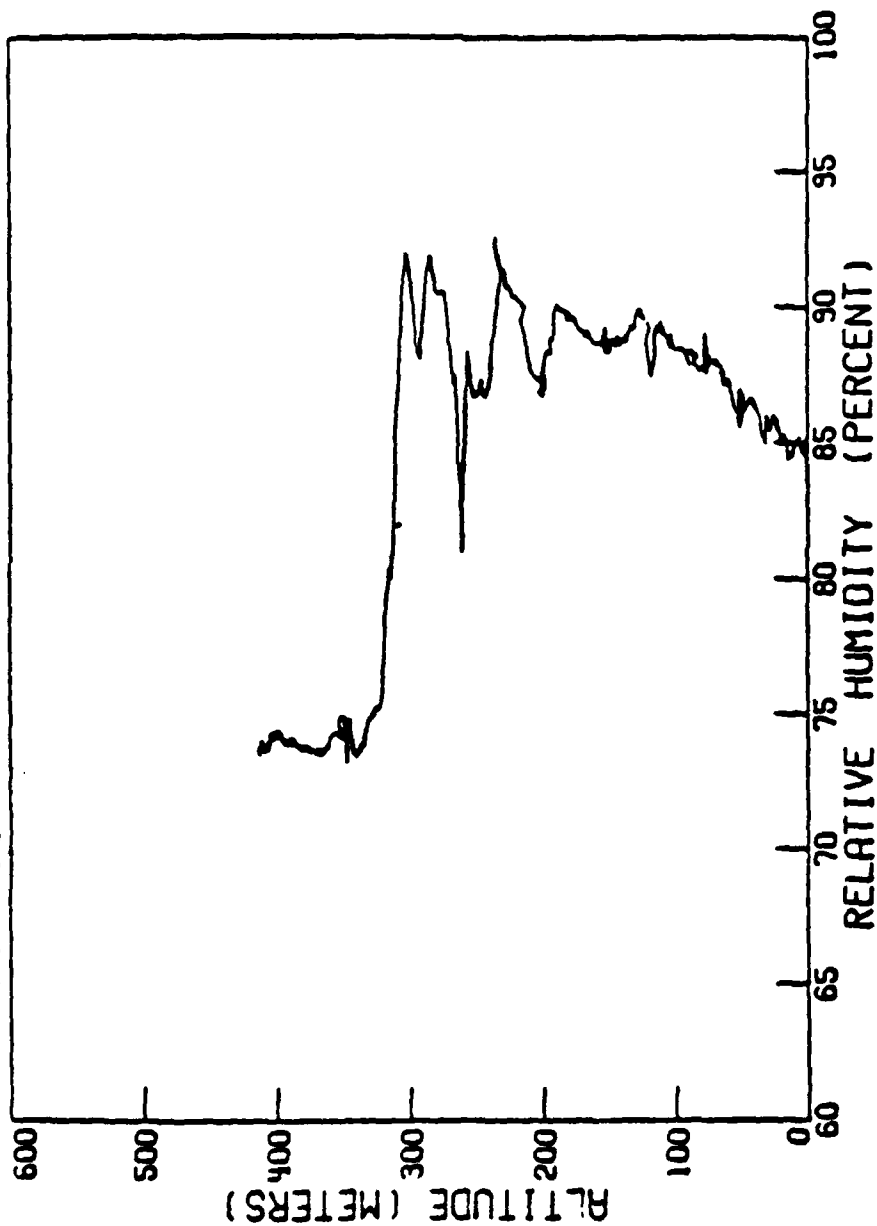
EFFECT OF HIGH ALTITUDE MULTIPATH ON

KAUAI - OAHU TEST OF RDS MODEL 6200

January 1978

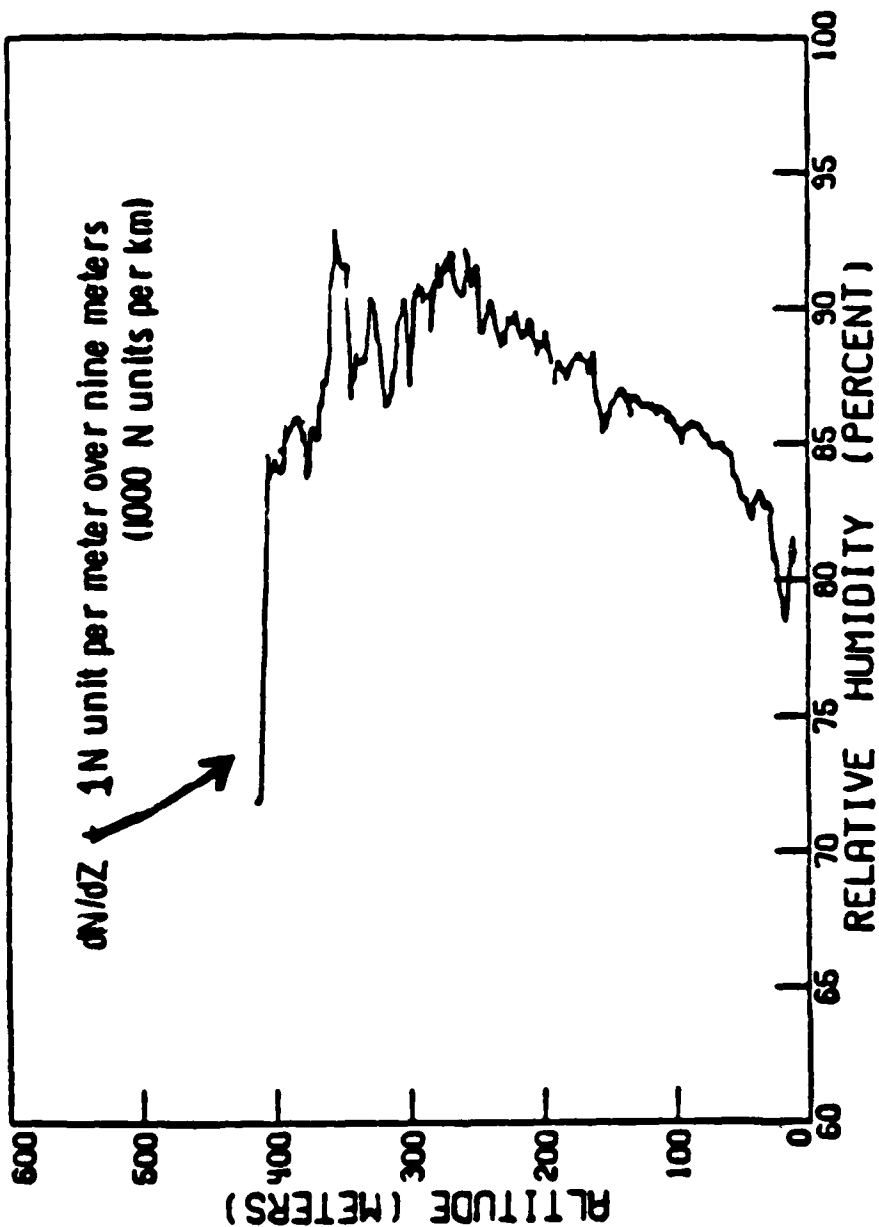
<u>DAY</u>	<u>ERROR</u> (seconds)	<u>AVAILABILITY</u>	<u>COMMENTS</u>	<u>WINDS</u>
1/11 to 1/12	907.8	98.95%	HEAVY FADES w/ few errors change to errors w/o fades	KONA/south
1/12 to 1/13	8,382.6	90.31%	no fades/errors in cluster	"
1/13 to 1/14	10,871.5	87.43%	11 fades/ hvy errors 1400 to 1900 hrs	"
1/14 to 1/15	111.1	99.87%	No fades	"
1/15 to 1/16	3.0	99.996%	11 fades	Trade (northeast)
1/16 to 1/17	0.8	99.999%	no fades	"

ASCENDING 0629081415 0629082629

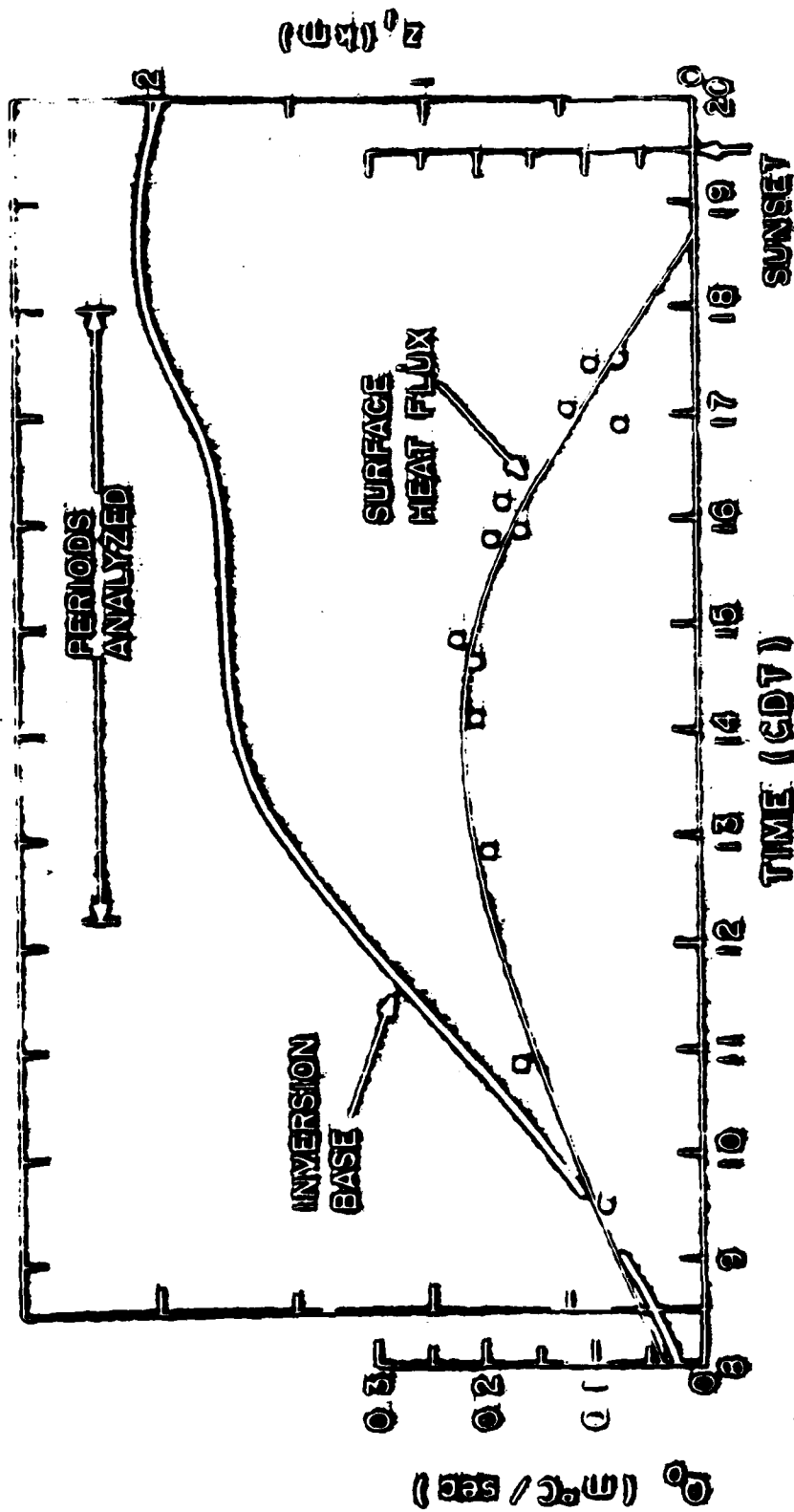


Tethered Balloon Profile 8:20 AM June 29 1976

DESCENDING 0629085518 0629090519

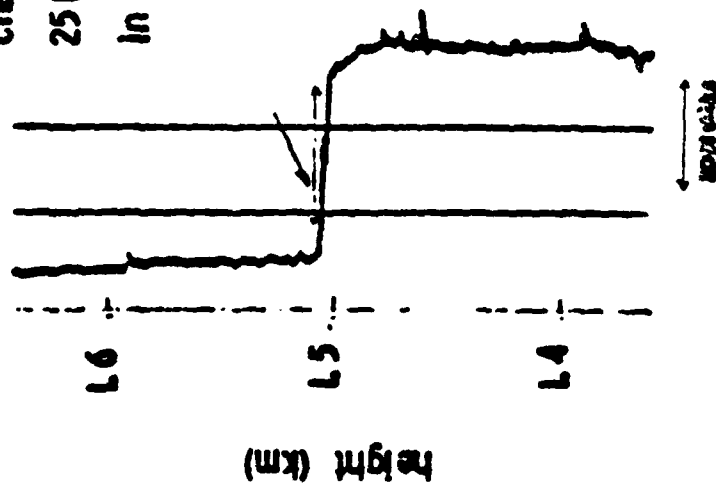


TETHERED BALLOON PROFILE - 9 AM JUNE 26 1976



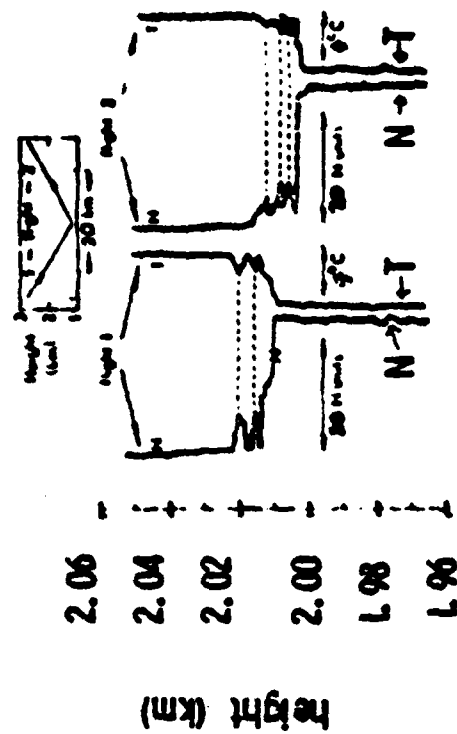
REFRACTOMETER MEASUREMENTS - AIRCRAFT

change of
25 N units
in 2 meters



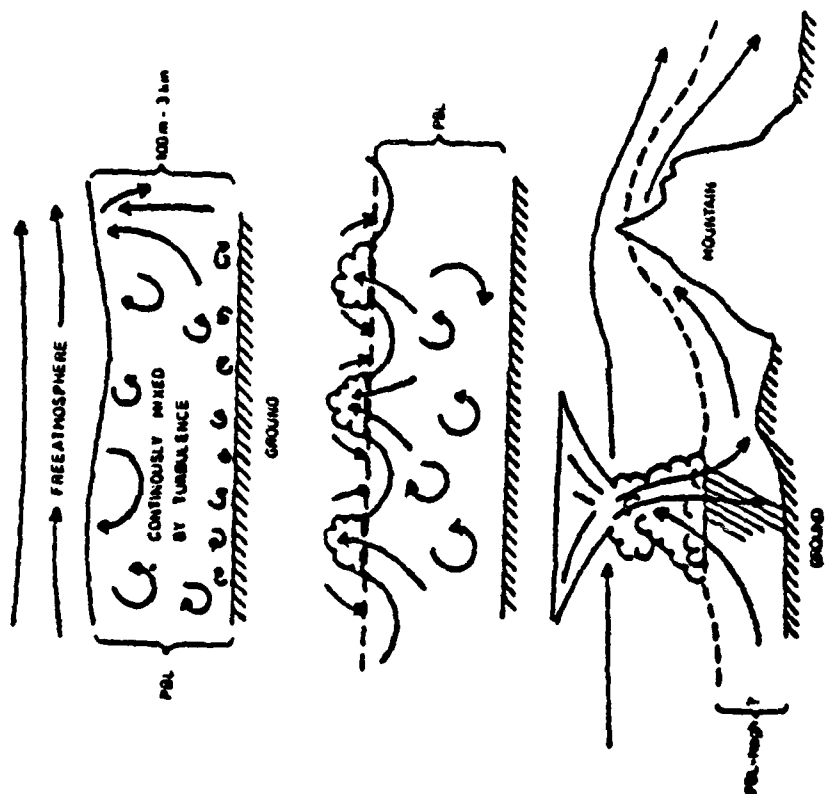
1400 GMT 9/26/60

refractometer in
subsidence inversion



Inversion Farnborough

16 July 1962



REFRACTIVITY REVIEW

index of refraction $n = \frac{c}{v} = 1.000350$

refractivity, $N = (n - 1) \times 10^6 = 350$

$$N = \frac{A\rho}{T} + \frac{Be}{T^2}$$

ρ = pressure, e = water vapor pressure, T = temperature

$N = \bar{N} + N'$ = mean and fluctuation

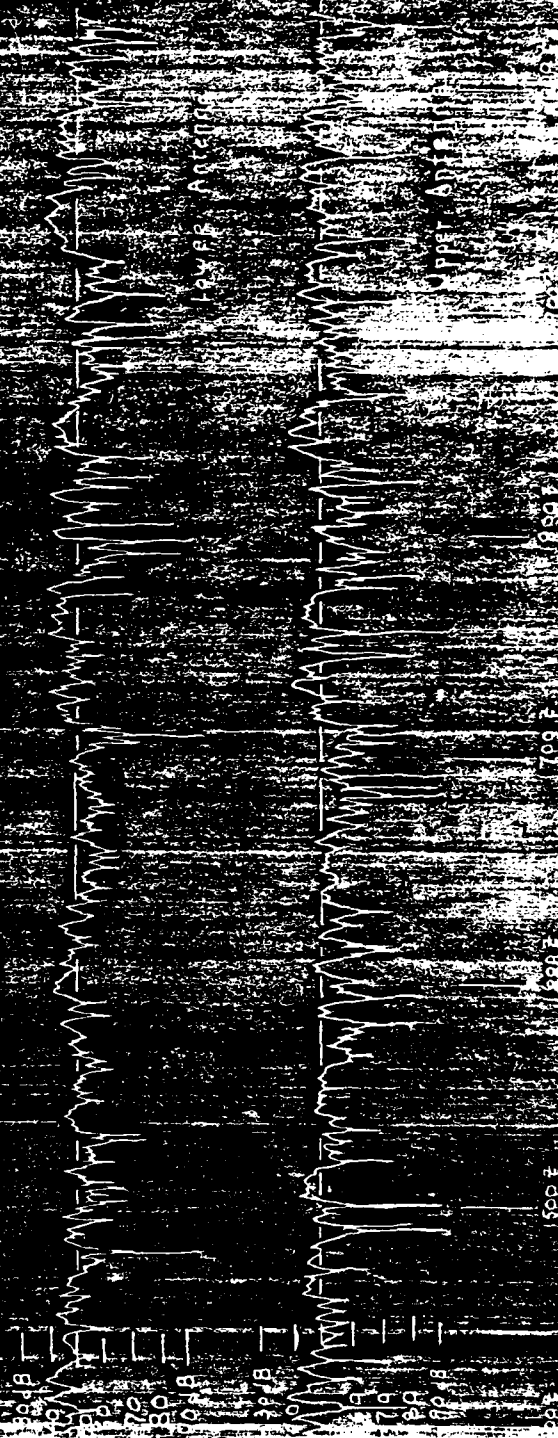
$\overline{N'^2}$ = mean square fluctuation

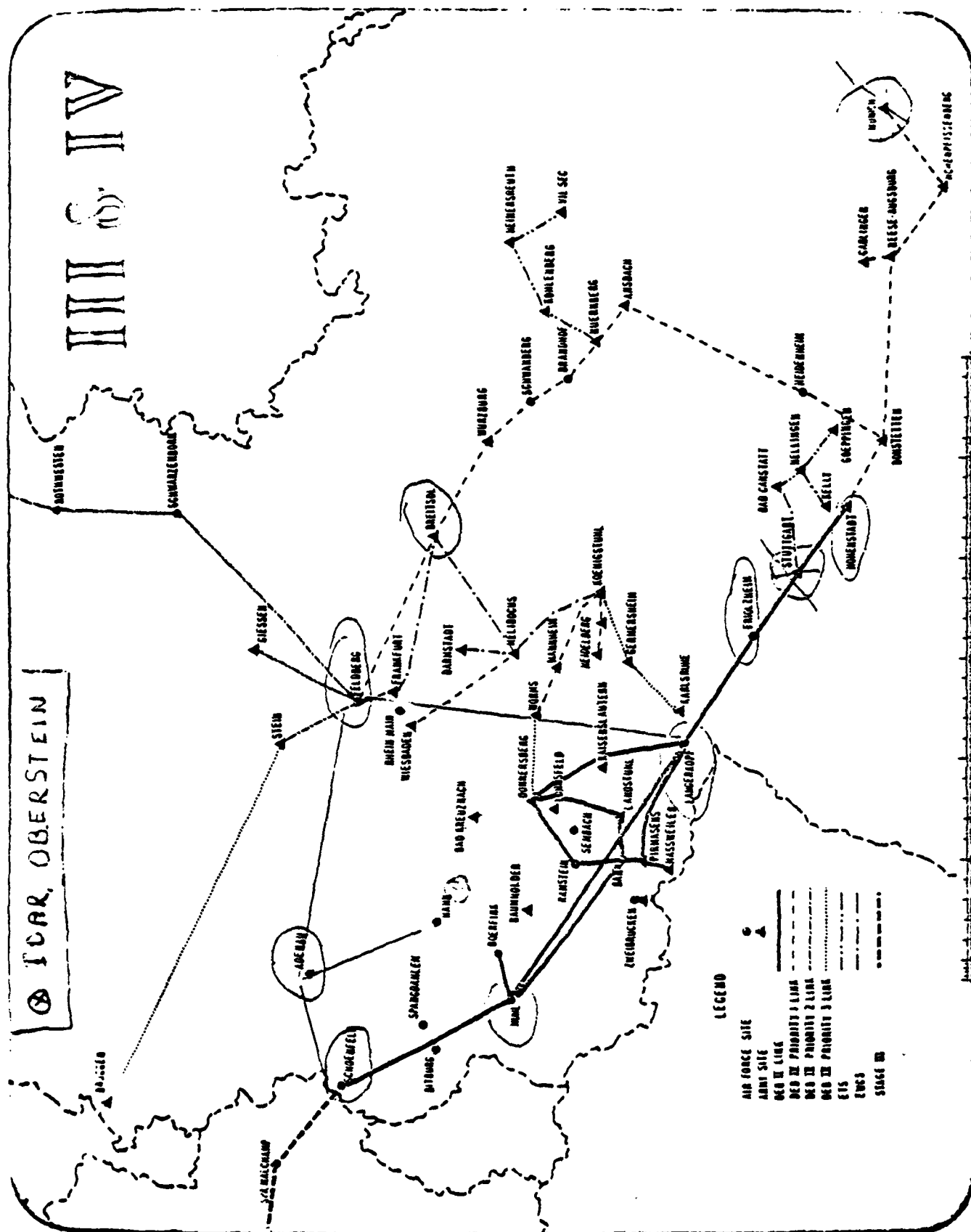
$$\overline{N'^2} = \overline{(N' - \bar{N})^2} = \overline{N'^2} - 2\bar{N}\bar{N}' + \bar{N}^2$$

RECEIVED SIGNAL LEVEL

Zugspitze to Hohenstadt

19 October 1977





10. ADAPTIVE EQUALIZATION FOR CORRECTION OF MULTIPATH DISTORTION
IN A 8 PSK DIGITAL RADIO

Paul Hartmann
Collins Transmission Systems Division
Rockwell International
Dallas, TX

NOTE: The materials provided in this section are copies
of a 1979 International Conference on Communications
article used as the basis for the extemporaneous
remarks given by Mr. Hartmann.

AN ADAPTIVE EQUALIZER FOR CORRECTION OF MULTIPATH DISTORTION IN A 90 MB/S 8 PSK SYSTEM

Paul R. Hartmann
Eddie W. Allen

Collins Transmission Systems Division
Rockwell International

ABSTRACT

Digital transmission over LOS microwave is now a well established technique. As the number of digital microwave systems has grown, there has been an increasing need for an adaptive equalizer to correct for the amplitude distortion that arises during multipath propagation conditions.

This paper describes a series of lab experiments designed to verify the nature and extent of degradation to the 8 PSK signal arising from a two-ray multipath geometry. It also describes the performance improvement that can be obtained with an adaptive equalizer.

INTRODUCTION

The use of digital microwave for transmission of PCM voice signals is expanding at a rapid rate. As the data rate and bandwidth efficiency of digital microwave systems has increased, the distortion effects of multipath have become an increasingly serious problem. Adaptive equalizer circuits have been developed that correct the more serious distortion effects.

This paper describes an adaptive equalizer, a multipath model, effects of multipath on a digital radio system, and the system performance improvements that can be effected through the use of an adaptive equalizer.

MULTIPATH MODEL

Multipath propagation studies in the past have, in general, concentrated on the received carrier level for analog transmission. In analog transmission systems, the distortion effects of multipath were not so important because the degradation from the distortion effects were graceful and the loading conditions on the analog system were often light during multipath propagation.

In digital systems, however, the distortion mechanisms are more critical because the system has data scrambling, which means that the loading is constant at all times. With scrambling, the transmit spectrum is well defined and, therefore, multipath distortion conditions can be much

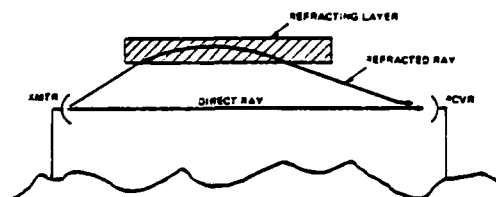


Figure 1. Basic Refraction Geometry that Results in Multipath Propagation.

more readily measured and corrected than in analog systems.

Over the years many multipath propagation models have been proposed. These models vary from simple two- and three-ray models to elaborate multi-ray models. The two-ray model is the most understood model for multipath propagation and it accounts for most of the distortion effects that are seen in multipath propagation. Therefore, the two-ray model was used for this investigation. This model is shown in Figure 1. It consists of a direct ray, and a single reflected or refracted secondary ray. These two rays add at some frequencies and cancel at others. The amplitude and group delay effects that are caused by the two-ray multipath are shown in Figure 2.

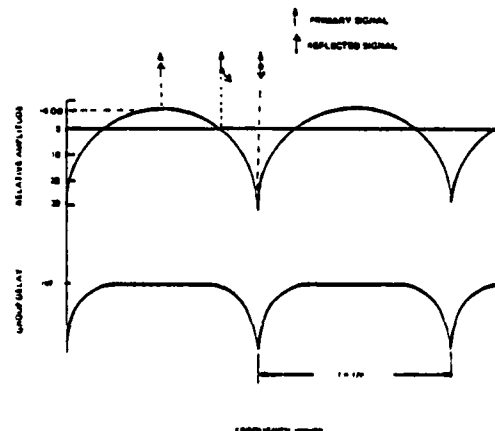


Figure 2. Amplitude and Delay Characteristics in Multipath.

Reprinted from the 1979 International Conference on Communications Record,
pp. 5.6.1 - 5.6.4.

CH1435-7/79/0000-0029\$00.75 © 1979 IEEE

The spacing between amplitude nulls is inversely proportional to the absolute delay difference (τ) between the direct and reflected ray. The null depth is determined by the relative amplitudes of the direct and reflected rays.

EFFECTS OF MULTIPATH ON DIGITAL SYSTEMS

In digital radio systems, the bit error rate (BER) during multipath is controlled by intersymbol interference resulting from frequency dependent amplitude and group delay effects. To evaluate these effects on digital transmission, a series of experiments was conducted which measured the threshold degradation resulting from linear amplitude slopes, linear group delay slopes and symmetrical parabolic group delay. These measurements were conducted on a 6 GHz 90 MBS radio system operating at 3 bits/Hz. Figure 3 shows the threshold degradation resulting from linear amplitude effects (gain slope). Figure 4 shows the effects of linear group delay slope and Figure 5 shows the effects of parabolic group delay.

To evaluate the importance of each of these effects, it is necessary to understand the degree to which each of these effects is present in multipath. Figures 6 and 7 show the calculated amplitude and group delay slopes in a 30 MHz bandwidth resulting from two-ray 10 dB fades at various absolute delays. It can be seen from Figures 3-7 that for a given delay and fade depth, the effect of amplitude slope on threshold degradation is more drastic than that due to delay slope or parabolic delay. This implies that amplitude slope is the primary source of perfor-

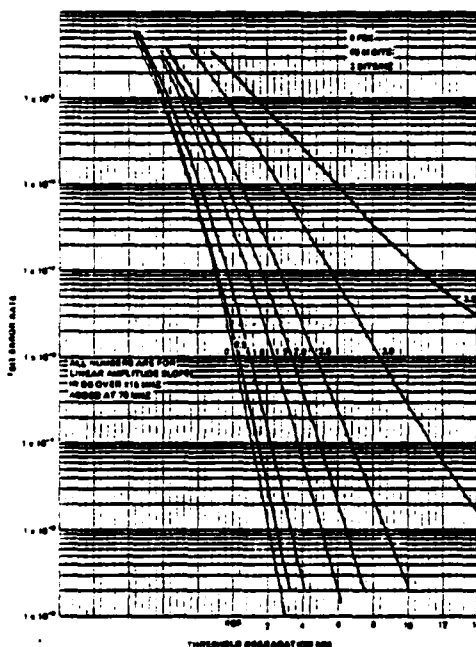


Figure 3. BER Threshold Degradation for Linear Amplitude Slope on MDR-6.

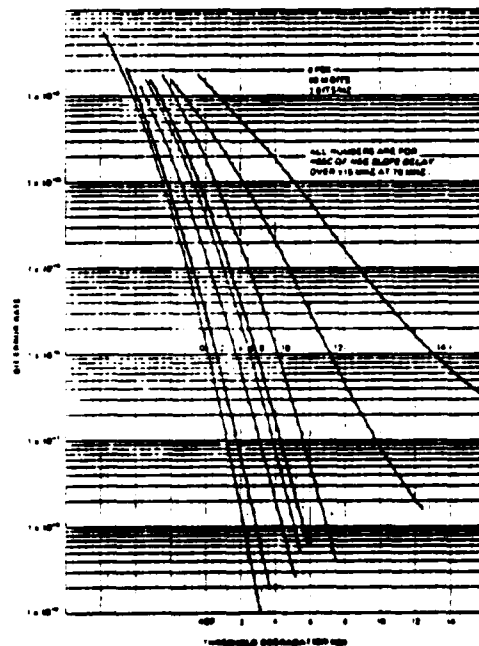


Figure 4. BER Threshold Degradation for Linear Group Delay on MDR-6.

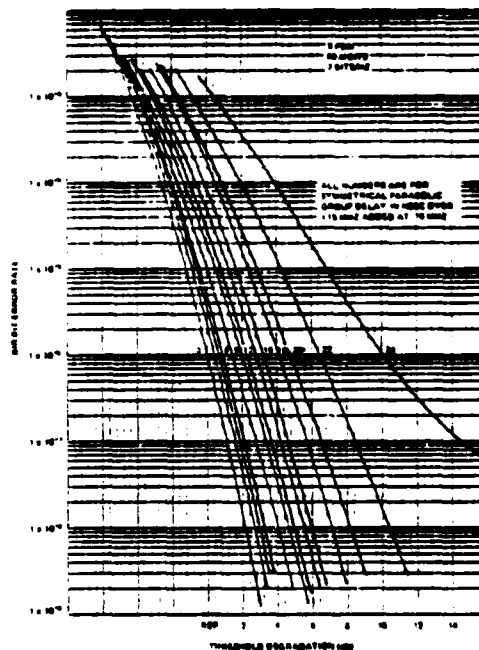


Figure 5. BER Threshold Degradation for Symmetrical Parabolic Group Delay on MDR-6.

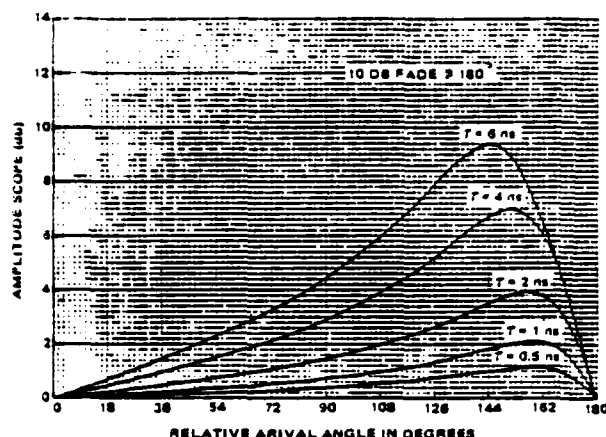


Figure 6. Amplitude Slope vs. Phase Angle of Reflected Signal for 10-dB Fade.

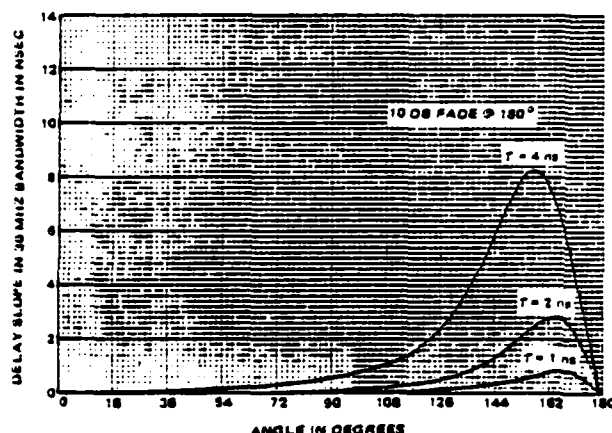


Figure 7. Delay Slope vs. Phase Angle of Reflected Signal for 10-dB Fade.

mance degradation during multipath. Also, it can be shown that when the amplitude slope is removed, the next most serious problem is a symmetrical null at the center of the passband.

ADAPTIVE EQUALIZER

The adaptive equalizer circuit is incorporated in the receiver 70 MHz IF amplifier. It consists of an amplitude slope detector which controls an amplitude slope correction circuit and a symmetrical null detector which controls the null correction circuit. The slope detector operates by comparing the amplitude near the high end of the passband with the amplitude near the low end of the passband. The linear amplitude slope correction circuit maintains the desired passband slope. The null detection circuit operates by comparing the energy at the center of the passband with the total energy in the passband.

The amplitude slope correction circuit can correct for positive or negative values of amplitude slope of up to 12 dB over a 30 MHz bandwidth. The null or bow correction circuit can correct for up to 12 dB of amplitude null.

The amplitude slope correction circuit has essentially no group delay effects. The null correction circuit provides the required group delay characteristics necessary to compensate for the group delay associated with the amplitude null.

SYSTEM PERFORMANCE

To evaluate the performance of an adaptive equalizer under multipath conditions, a series of experiments were performed that simulated the passband distortion arising from two-ray multipath. The results of these experiments verified that amplitude slope is the most serious distortion that arises in multipath. Thus, the most important part of the adaptive equalizer is an amplitude slope correction circuit. The effectiveness of this circuit is shown in Figures 8 and 9. Figure 8 shows the BER threshold improvement using an adaptive equalizer in the presence of amplitude slope. The upper curve is the result of a severe multipath condition which resulted in errored performance at all signal levels. When the adaptive equalizer is turned on, the threshold performance returns to within 0.5 dB of its normal value.

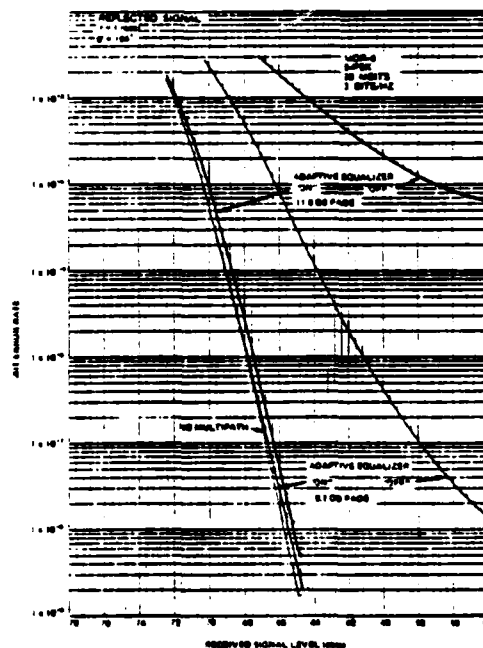


Figure 8. BER Threshold Improvements Using An Adaptive Equalizer in the Presence of Amplitude Slope.

Figure 9 shows the BER threshold improvement with an adaptive equalizer in the presence of a symmetrical null. Errored performance at all signal levels is again present in the upper curve and normal threshold performance is obtained when the adaptive equalizer is turned on.

The cumulative effects of amplitude slope and nulls are shown in Figure 10. The two outer lobes show the performance without adaptive equalizers. The peak of these two lobes correspond to the arrival angles that result in maximum amplitude slope. When the slope correction circuit is applied, error free performance is obtained at all arrival angles. As the fade depth is increased, the next region of degradation that is encountered is the point where the amplitude null is exactly at the center of the passband.

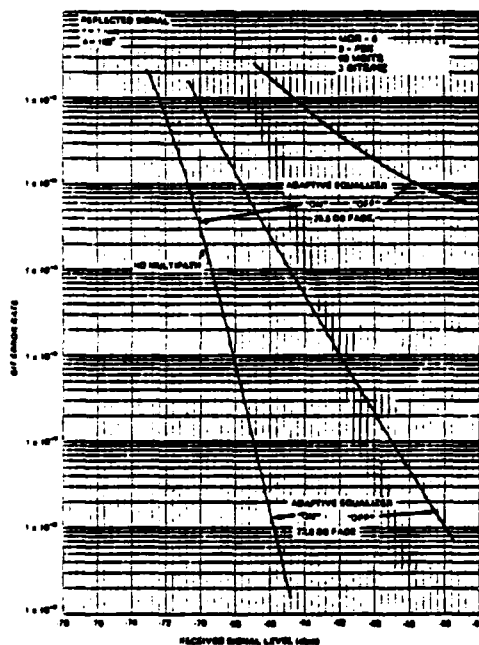


Figure 9. BER Threshold Improvements Using An Adaptive Equalizer in the Presence of a Symmetrical Null.

This point is shown in Figure 10 as the center lobe centered on 180°. Note that the fade depth needed to produce this effect is 5 dB deeper than that originally needed to produce the amplitude slope problem. When the null correction circuit is turned on, error-free performance is again restored at all phase angles. Now the depth of fade is again increased until errors are present. This region is shown by the two narrow spikes in Figure 10 and correspond to an in-band amplitude null halfway between the center and edge of the passband.

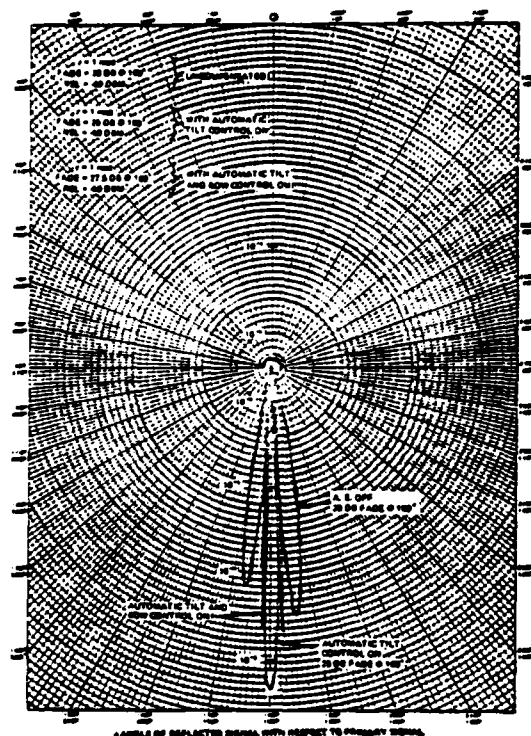


Figure 10. Polar Plot of BER Improvements Using An Adaptive Equalizer.

The importance of this data is twofold. First, the usable fade margin in multipath has been increased significantly. Second, the relative phase angles of the multipath at which transmission errors result are greatly reduced. Both of these factors help to reduce the outage time on digital systems. It is anticipated that adaptive equalizers used in conjunction with space diversity will allow digital systems to meet long-haul multipath outage objectives. This particular adaptive equalizer is now being evaluated under actual field conditions.

11. ADAPTIVE EQUALIZATION

Robert Wallace
Ratheon, Inc.
Sudbury, MA

NOTE: The materials provided in this section are copies of the visuals used with the extemporaneous remarks given by Mr. Wallace.



RAYTHEON DATA SYSTEMS MULTIPATH EXPERIENCE HISTORY

RAYTHEON
DATA
SYSTEMS

Equipment - RDS-6200, 6 Ghz-8PSK Digital radio 90.148 MB/S in 30 Mhz allotted bandwidth

1. Over water

A. Hawaii test bed (9/77 :- 1/78) Oahu to Kauai Islands path length 98 miles

- 1~2 CGA daily for unprotected receiver
- CGA's reduced in excess of a factor of 10 with space diversity (hit less baseband switching)
- 96.1% typical weekly availability with diversity falls short of the 99.9965% objective for voice
- Greatest cause of errors believed to be high altitude multipath caused by temperature inversion layer movement.

B. Lake Pontchartrain, Louisiana test bed (1/79 - 3/79) path length 26 miles

- Simultaneous measurement of unprotected receiver with and without adaptive equalization.
- Adaptive equalization, amplitude slope capability range ± 7.5 dB over 30 Mhz channel.
- Occurrences exceeding 1×10^{-5} BER
 - 2~5 factor reduction with adaptive equalization
- Occurrences exceeding 1×10^{-3} BER
 - 3~7 factor reduction with adaptive equalization
- Multipath fading in excess of 7.5 dB amplitude dispersion noted as well as upfades of > 7 dB indication multiple rays.



RAYTHEON DATA SYSTEMS MULTIPATH EXPERIENCE HISTORY

RAYTHEON
DATA
SYSTEMS

2. Over land

A. El Dorado to Hampton, Arkansas (8/78 - 11/78) path length 25 miles

- Space diversity protection only

Equivalent Fade margin 10^{-3} BER	Time Faded Below 30 dB Primary Antenna	Time faded Below 30 dB Diversity Channel	Time faded Below 30 dB Improvement	Outage \div Time	Time Faded \div below 30 dB primary antenna
30 dB	1904 Sec.	210 Sec.	9.1	0.104	

* Outage time - defined when $BER > 10^{-3}$

B. El Dorado to Hampton, Arkansas (7/79 - 8/79) path length 25 miles

- With the addition of adaptive equalization, amplitude capability range ± 12.5 dB over 30 Mhz channel.

Better than an order of magnitude improvement in

$$\left(\text{Outage Time} \div \begin{array}{l} \text{Time Faded} \\ \text{Below 30 dB} \\ \text{Primary Antenna} \end{array} \right)$$

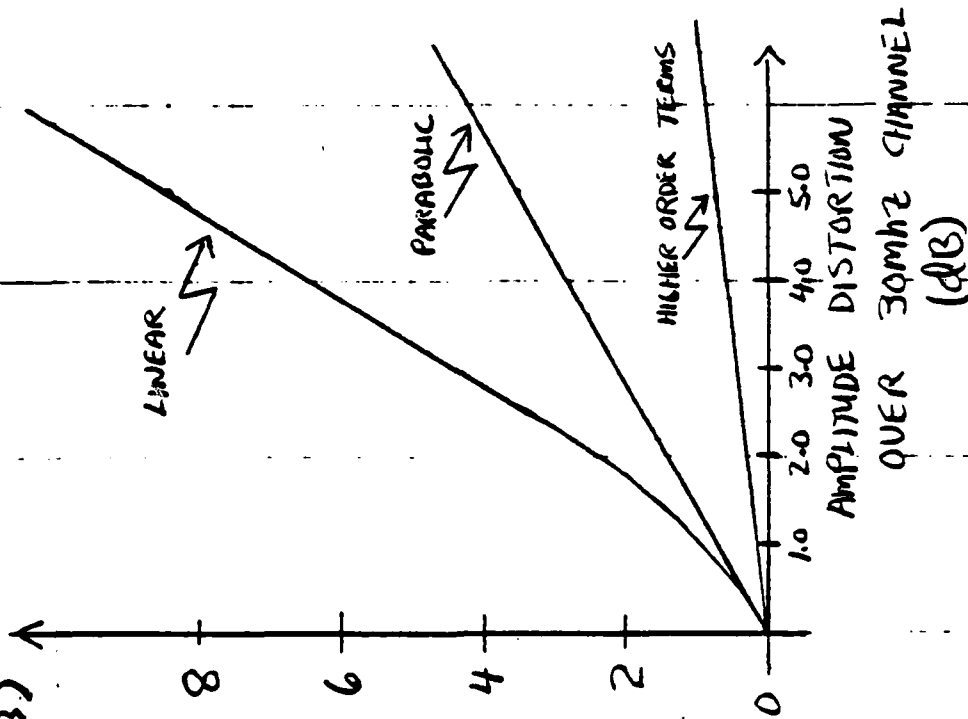
- Amplitude dispersion is the predominant distortion caused by multipath.
- The dispersion experienced at 6 Ghz correlates well as being linear amplitude slope in dB Vs. frequency.
- Amplitude dispersion has no frequency preference.
- Envelope delay distortions comparable to the symbol rate of a digital signal will cause outage.
- Large envelope delay distortions become evident only for more severely faded channels.
- Amplitude dispersion detection and correction is feasible while carrying traffic, group delay dispersion detection is not.
- Little correlation between received average power and BER performance.



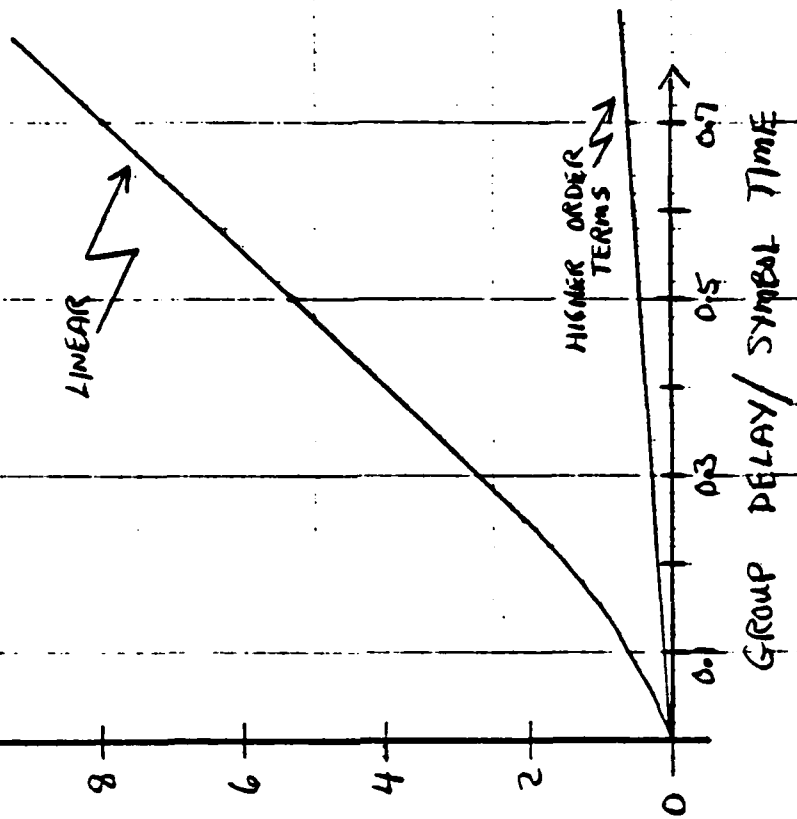
RDS-6200 TRANSMISSION SENSITIVITIES AT 3 BITS/HZ

RAYTHEON
DATA
SYSTEMS

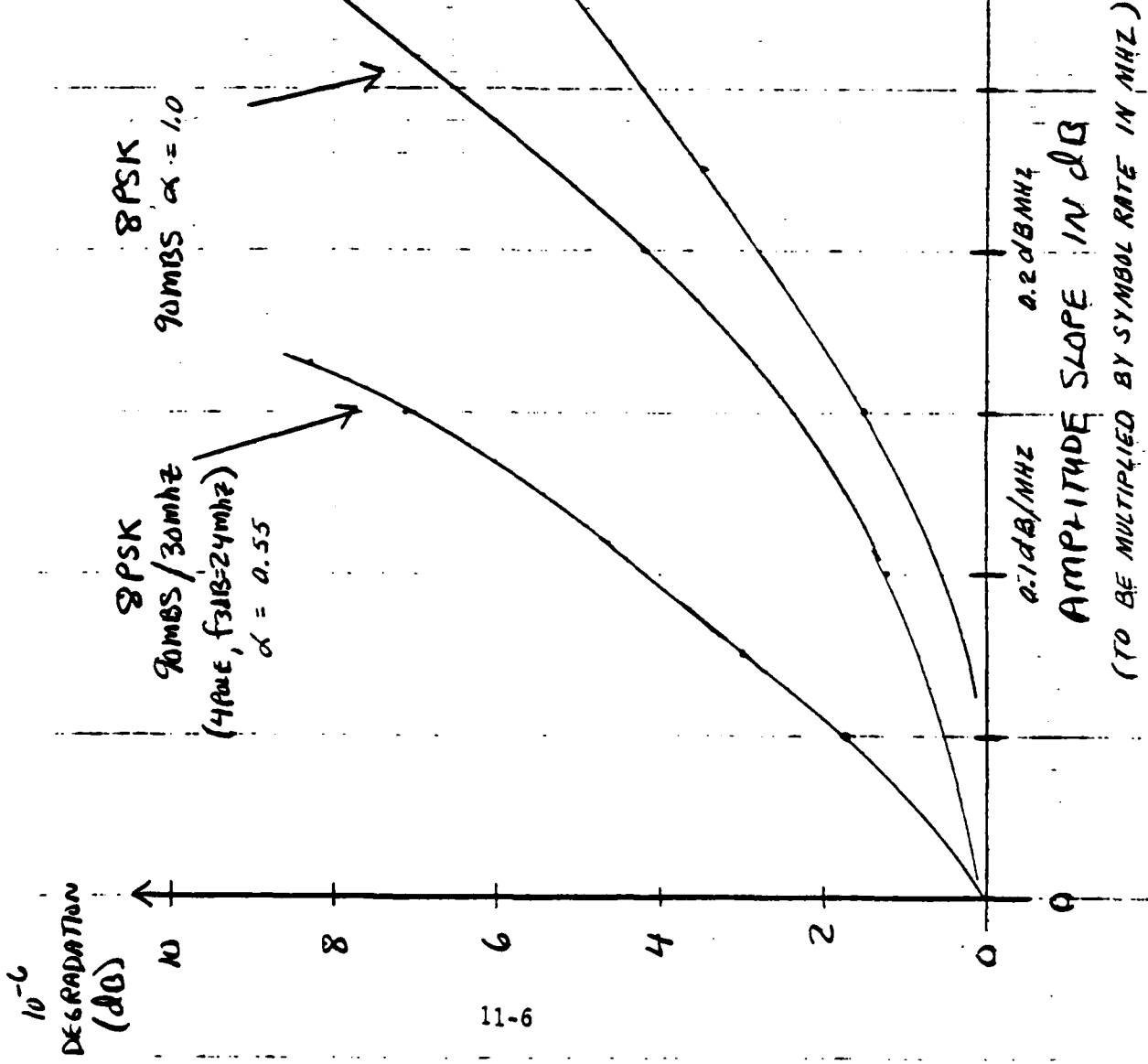
10^{-6}
DETERMINATION
(dB) \uparrow



10^{-6}
DEGRADATION
(dB) \uparrow



- Fixed modulation type & symbol rate alpha determines amplitude slope susceptibility (i.e. \uparrow alpha factor $\Rightarrow \uparrow$ slope susceptibility for same degradation)
Bandwidth only effects mismatch loss
- Spectral efficiency $\uparrow \Rightarrow \uparrow$ alpha factor for practical systems
- Number of modulation states $\uparrow \Rightarrow \downarrow$ slope susceptibility for same degradation





90 MBS, 3 BITS/HZ DESIGN CONSIDERATIONS

RAYTHEON
DATA
SYSTEMS

1. Diversity Baseband Hitless Switching Versus IF Combining
 - A. Baseband switching is applicable for both space and frequency diversities. Combining requires space diversity.
 - B. For a 1 for 1 radio protection scheme both methods have comparable equipment costs.
 - C. For a 1 for N radio protection scheme the combiner offers lower equipment costs.
 - D. Multipath considerations
- When the combined channel amplitude dispersion is greater than either input signal the baseband hitless switch is advantageous.
- When the combined channel amplitude dispersion is smaller than either input signal the combiner is advantageous.
2. Adaptive Equalizer Design Requirements
 - A. Correction based upon a 2-ray multipath model with field optimization.
 - B. Design shall not impact system performance under non-fading conditions.
 - C. Include capability to dynamically track multipath fade rates.
 - D. Maximize the effective fade margin of systems.



DIVERSITY HITLESS BASEBAND SWITCHING FOR 8 PSK

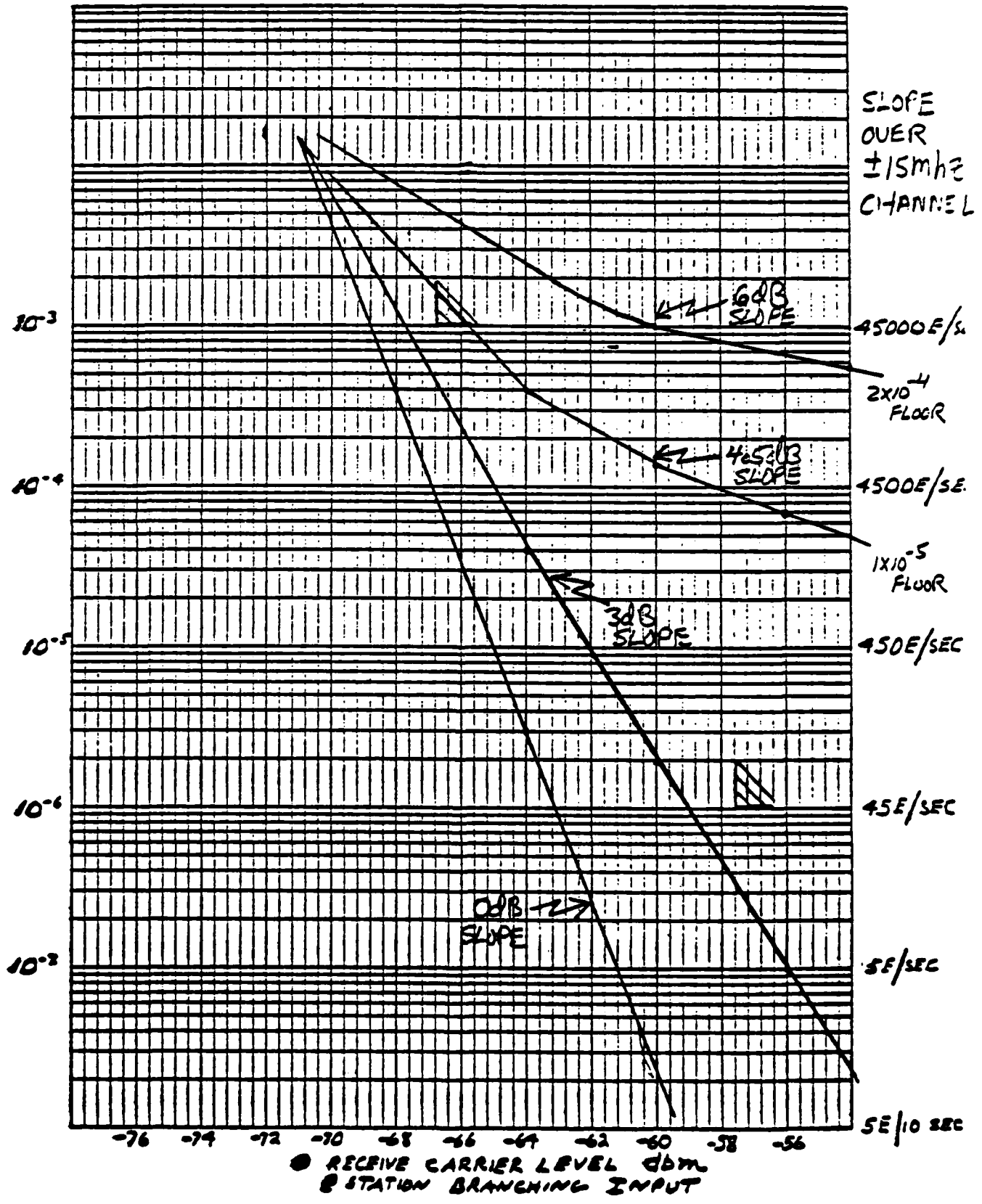
RAYTHEON
DATA
SYSTEMS

1. Switching algorithm based upon faults, BER performance, and RSL
2. BER performance details:
 - A. Modified gray encoding/decoding scheme producing 2 errors/50% time & 3 errors 50% time for each channel error
 - B. Continuous performance assessment of the parity bit stream frame bit (one in 4080 at 90 MBS, 22 KHz aggregate)
 - C. Randomization/derandomization multiply error rate by factor of 3.
 - D. 1 parity error implies 15 errors at 90 MBS
 - E. Performance switching is field adjustable between 10^{-3} and 10^{-8} BER at 90 MBS. (latter takes 200 seconds to resolve)

- Adaptive Equalizer is a control loop design which focuses on the comparison and regulation of the signal energy in a narrow bandwidth, symmetrically offset above and below the channel center.
- ± 12.5 dB amplitude slope dynamic range over 30 Mhz IF Passband
- Design implementation of the most probable group delay polarity and magnitude which can be expected to accompany a given amount of linear amplitude slope.
 - This represents minimum group delay shape change up to ± 8.0 dB amplitude slope correction.
 - Exponentially increasing to $12 \sim 15$ nano-sec of slope at ± 12.5 dB amplitude slope correction.
 - Dynamic tracking high-speed multipath fades at rates up to 100 dB/second.
- A BER of better than 1×10^{-4} over ± 16 dB input slope measured in a 2-ray model set up with path delays of 2.2, 5.0 & 7.2 nano-sec and center frequency fade depths up to 30 dB.

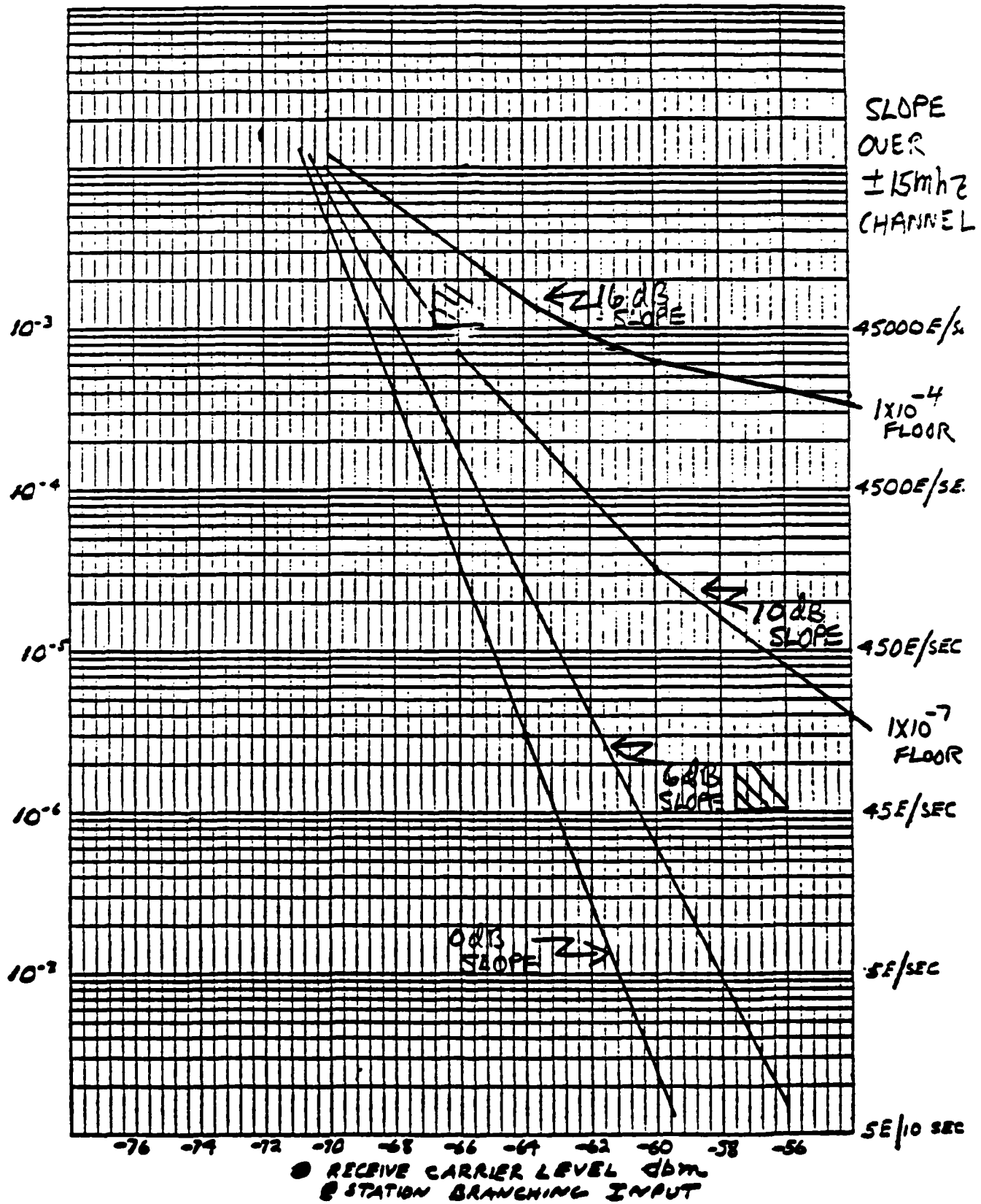


RS-6200 3BIT/HZ
BER SENSITIVITY TO 2-RAY SIMULATIONS ($\tau=2.2NS$)
(NO ADAPTIVE EQUALIZATION)





RS-6200 3BIT/HZ
BER SENSITIVITY TO Z-RAY SIMULATIONS ($\tau=2.2\text{NS}$)
(WITH 961086 G1 ADAPTIVE EQUALIZER)





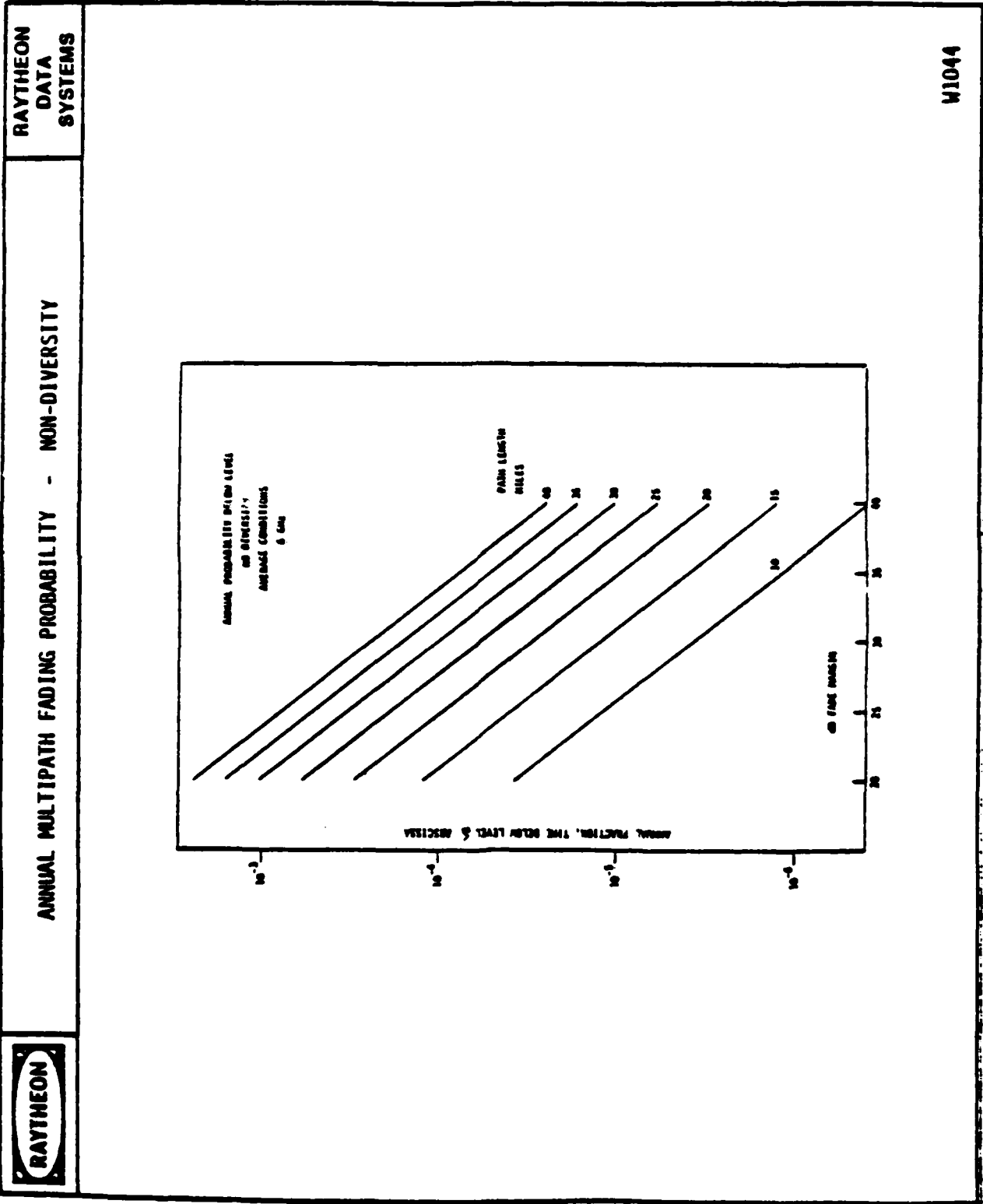
ESTIMATING PERFORMANCE OF ADAPTIVE EQUALIZATION

RAYTHEON
DATA
SYSTEMS

- Digital Microwave LOS Radio BER performance in the presence of multipath can best be specified by calculating an in band linear amplitude dispersion path fade margin.
- The in band linear amplitude dispersion path fade margin specifies a bandpass amplitude slope correction factor and an equivalent flat fade margin.
- DURING NORMAL PROPAGATION AND NO MULTIPATH FADING, THERE WILL BE NO AMPLITUDE DISPERSION.
- DETERMINE THE PROBABILITY THAT FADES OF VARIOUS DEPTHS WILL OCCUR.
- ESTIMATE THE CONDITIONAL PROBABILITY THAT SLOPE IN EXCESS OF A SPECIFIED AMOUNT WILL ACCOMPANY THESE FADES.
- FOR EACH INCREMENT OF FADE DEPTH, DETERMINE THE PROBABILITY THAT THE SPECIFIED SLOPE WILL BE EXCEEDED.
- SUM THESE INCREMENTAL PROBABILITIES OVER THE FLAT FADE MARGIN TO DETERMINE THE ADVERSE EFFECT ON TRANSMISSION.
- RELATE THIS DEGRADATION TO THE CORRECTING RANGE OF THE ADAPTIVE EQUALIZER TO ESTIMATE THE EQUIVALENT FADE MARGIN TO BE REALIZED.

RAYTHEON DATA SYSTEMS	PROBABILITY OF MULTIPATH FADES
	<p>● FROM VIGANTS BSTJ JANUARY, 1975</p> <p>FOR NON-DIVERSITY OCCURANCE OF MULTIPATH FADES.</p> <p>● $T = 20 K(W/50)^{-1.3} (t/50) f D^3 L^2$ (1)</p> <p>WHERE T = ANNUAL TIME BELOW LEVEL, SECONDS</p> <p>K = CLIMATE FACTOR = 2 COASTAL CLIMATE 1 AVERAGE CLIMATE 0.5 DRY CLIMATE</p> <p>W = ROUGHNESS FACTOR, RMS DEVIATION FROM HORIZONTAL, FEET $2 \leq W \leq 140$</p> <p>t = ANNUAL MEAN TEMPERATURE, DEGREES F, $35 \leq t \leq 75$</p> <p>D = PATH LENGTH, MILES</p> <p>L = LEVEL PARAMETER, DB RELATIVE TO NORMAL IS 20 LOG L</p> <p>f = FREQUENCY, GHZ</p> <p>● $F = T/\text{SECONDS PER YEAR} = T/31.536 \times 10^6$</p> <p>F = FRACTION OF YEAR BELOW LEVEL</p>

H 1065

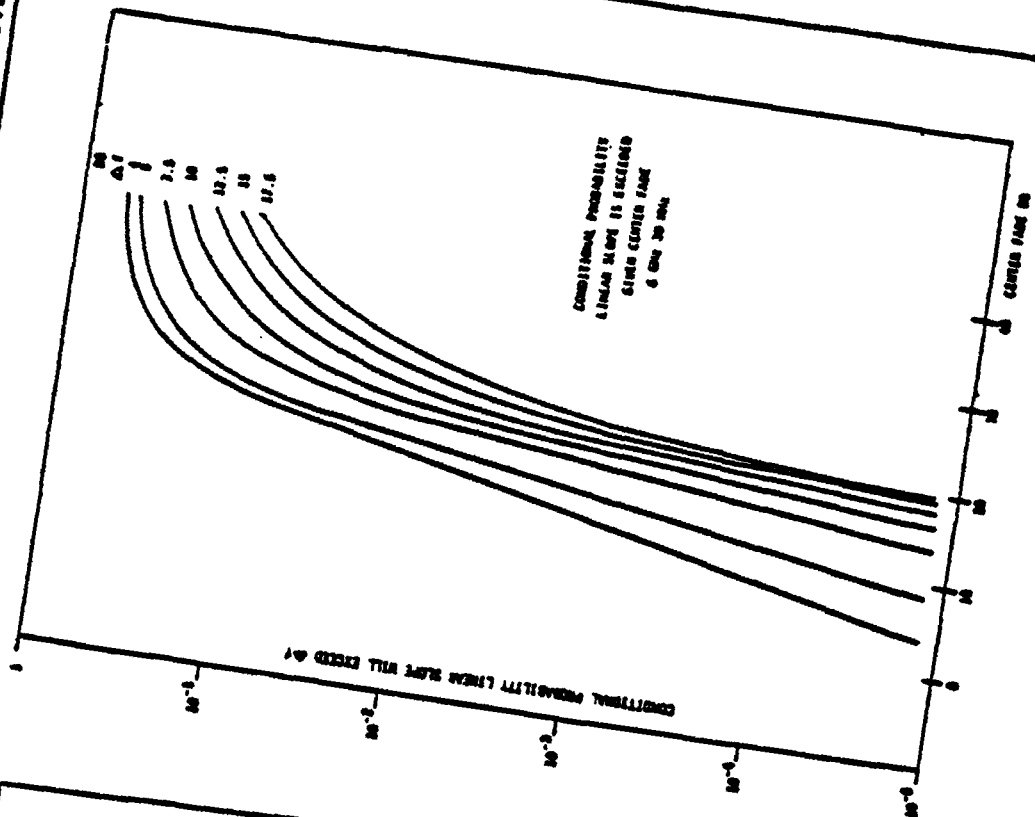
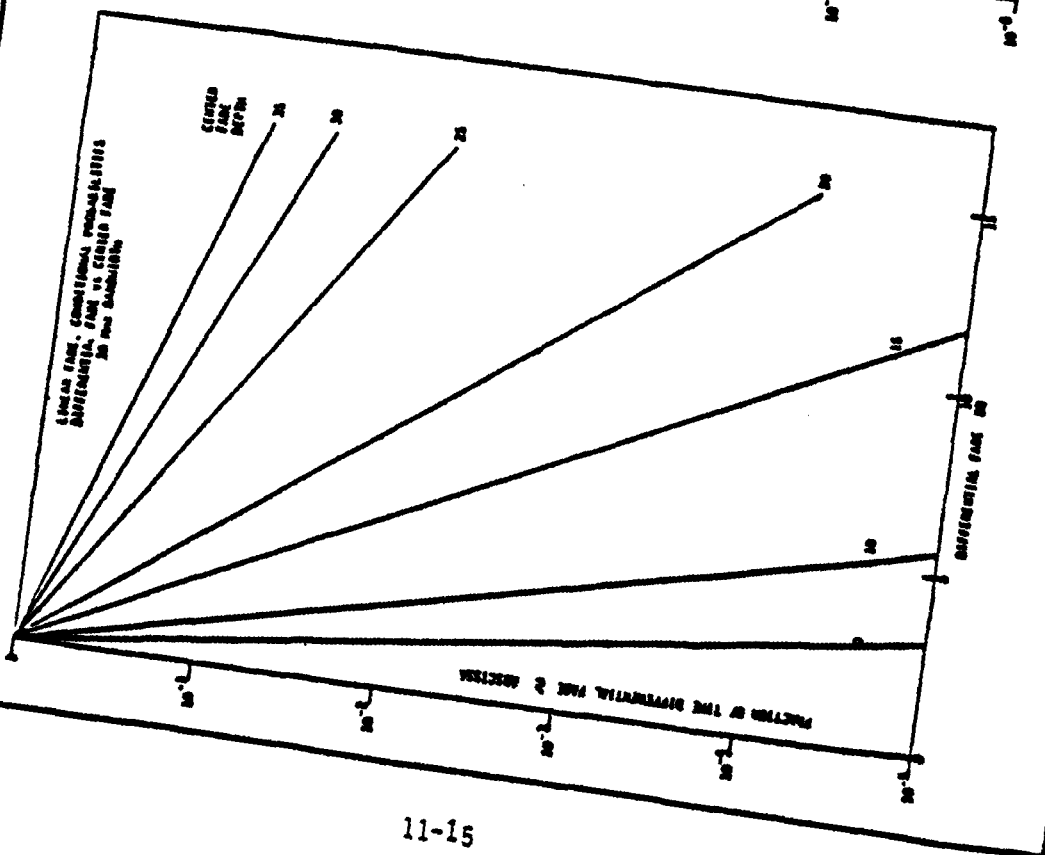


W1044

RAYTHEON

LINEAR DISTORTION, CONDITIONAL PROBABILITIES 30 MHZ SPACING

RAYTHEON
DATA
SYSTEMS



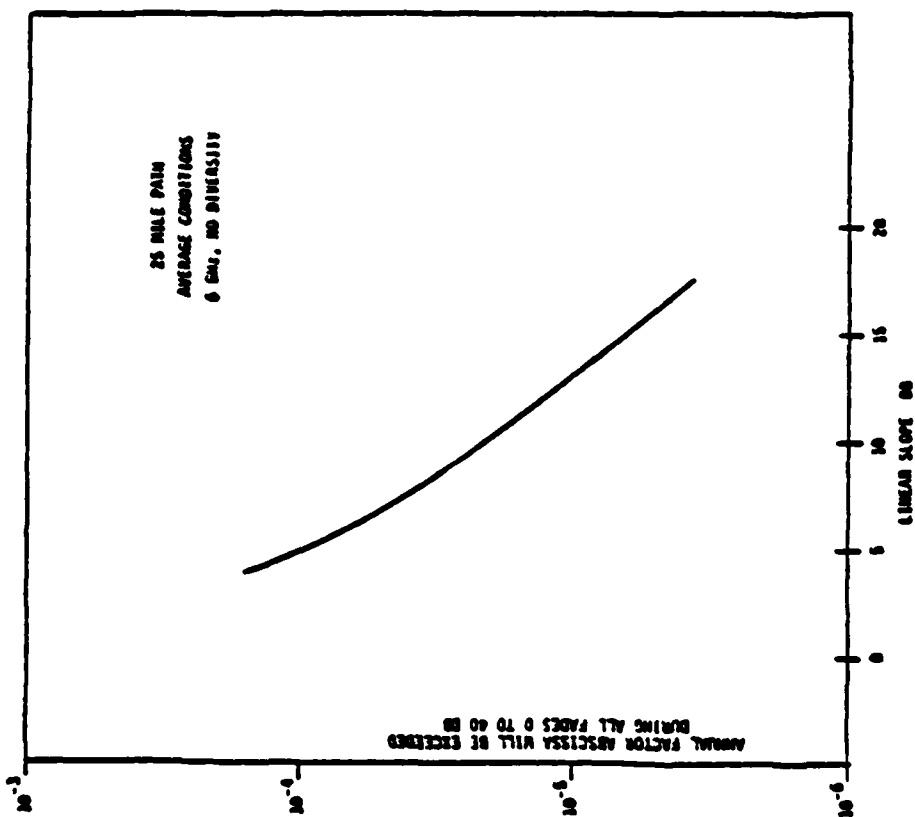
W1047

RAYTHEON		SAMPLE WORK SHEET			RAYTHEON DATA SYSTEMS	
SLOPE $\Delta f = \text{dB}$		6 GHz 25 MILE AVERAGE PATH NON-DIVERSITY				
CENTER FREQ f_c	ANNUAL PROB OF > f_c	PROB $f_c < f < f_c + 1$ f	COND PROB Δf EXCEEDED	ANNUAL PROB Δf EXCEEDS CORRECTION		
.		
.		
.		
8	9.4231×10^{-3}	1.9381×10^{-3}	9×10^{-6}	1.7442×10^{-8}		
9	7.4850×10^{-3}	1.5394×10^{-3}	1.8×10^{-5}	2.77×10^{-8}		
10	5.9456×10^{-3}	1.2229×10^{-3}	3.7×10^{-5}	4.5247×10^{-8}		
11	4.7227×10^{-3}	9.717×10^{-4}	7.5×10^{-5}	7.287×10^{-8}		
12	3.7514×10^{-3}	7.712×10^{-4}	1.5×10^{-4}	1.1568×10^{-7}		
13	2.9798×10^{-3}	6.129×10^{-4}	3×10^{-4}	1.8387×10^{-7}		
14	2.3669×10^{-3}	4.868×10^{-4}	6×10^{-4}	2.9208×10^{-7}		
15	1.8801×10^{-3}	3.867×10^{-4}	1.2×10^{-3}	4.64×10^{-7}		
16	1.4934×10^{-3}	3.071×10^{-4}	2.5×10^{-3}	7.6775×10^{-7}		
17	1.1863×10^{-3}	2.439×10^{-4}	5×10^{-3}	1.2195×10^{-6}		
18	9.4231×10^{-4}	1.9381×10^{-4}	1.1×10^{-2}	2.1319×10^{-6}		
19	7.4850×10^{-4}	1.5394×10^{-4}	2.2×10^{-2}	3.3866×10^{-6}		
20	5.9456×10^{-4}	1.2229×10^{-4}	4.3×10^{-2}	5.2584×10^{-6}		
.		
.		
.		
TOTAL FOR f_c FROM 0 TO 40 dB				Σ	9.78×10^{-5}	

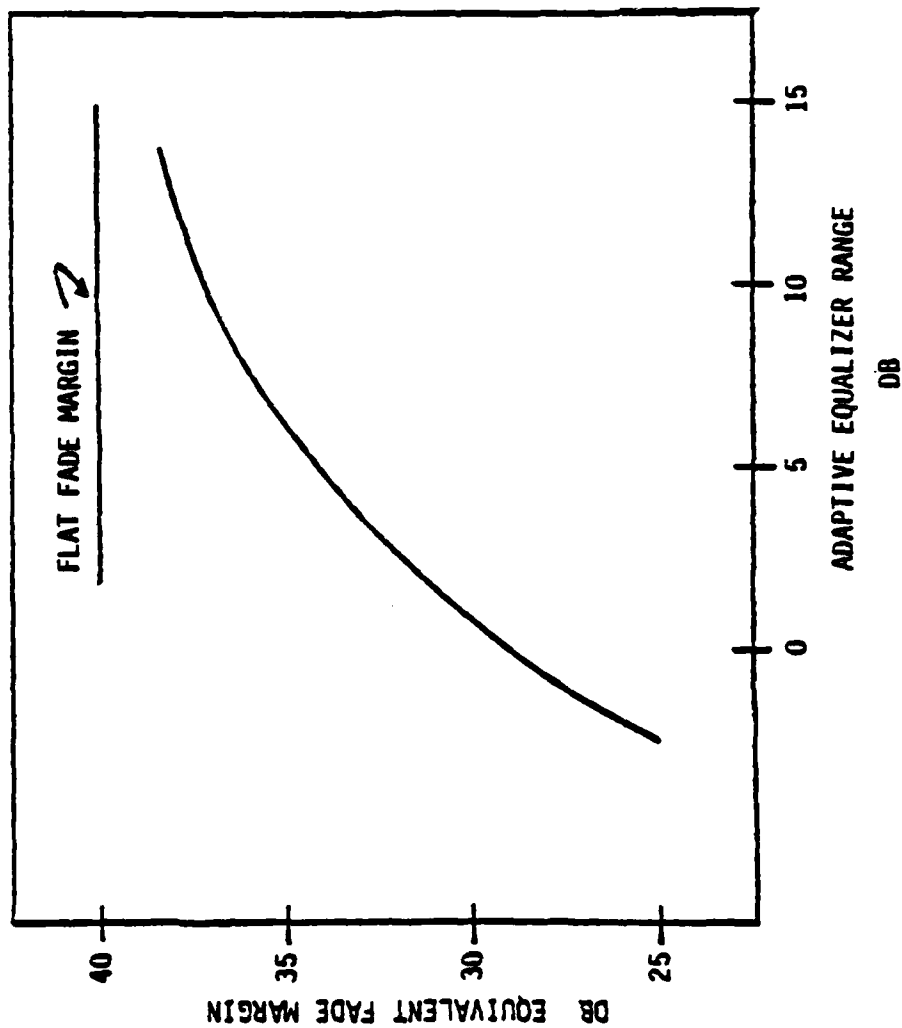


ANNUAL FACTOR - SLOPE WILL BE EXCEEDED

RAYTHEON
DATA
SYSTEMS

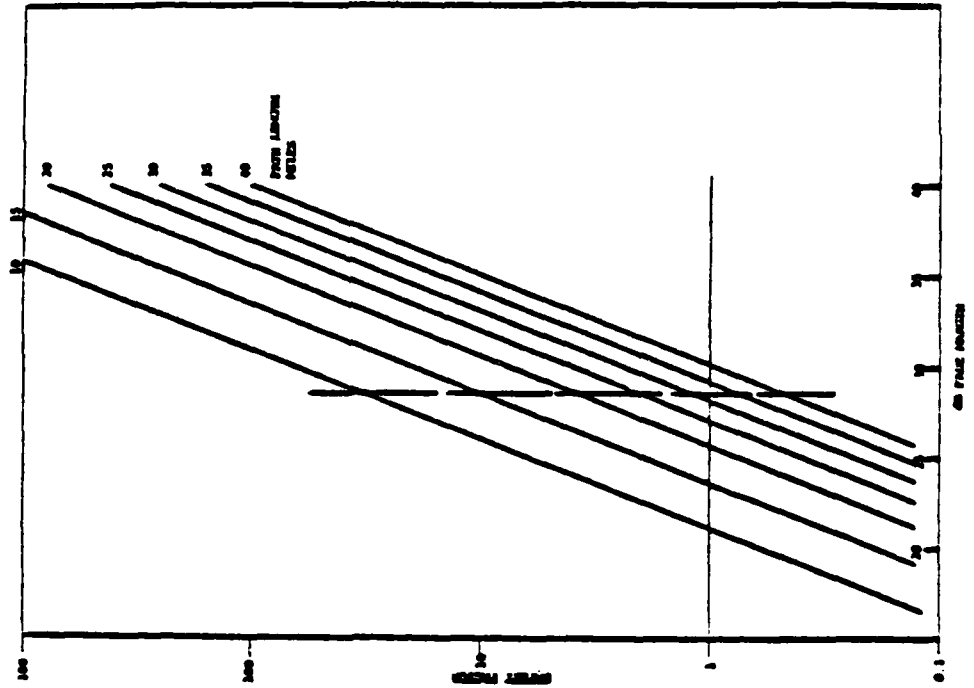


W1038



RAYTHEON
DATA
SYSTEMS

PERFORMANCE SAFETY FACTOR, SPACE DIVERSITY



40 FT. SPACE DIVERSITY
AVERAGE CONDITIONS

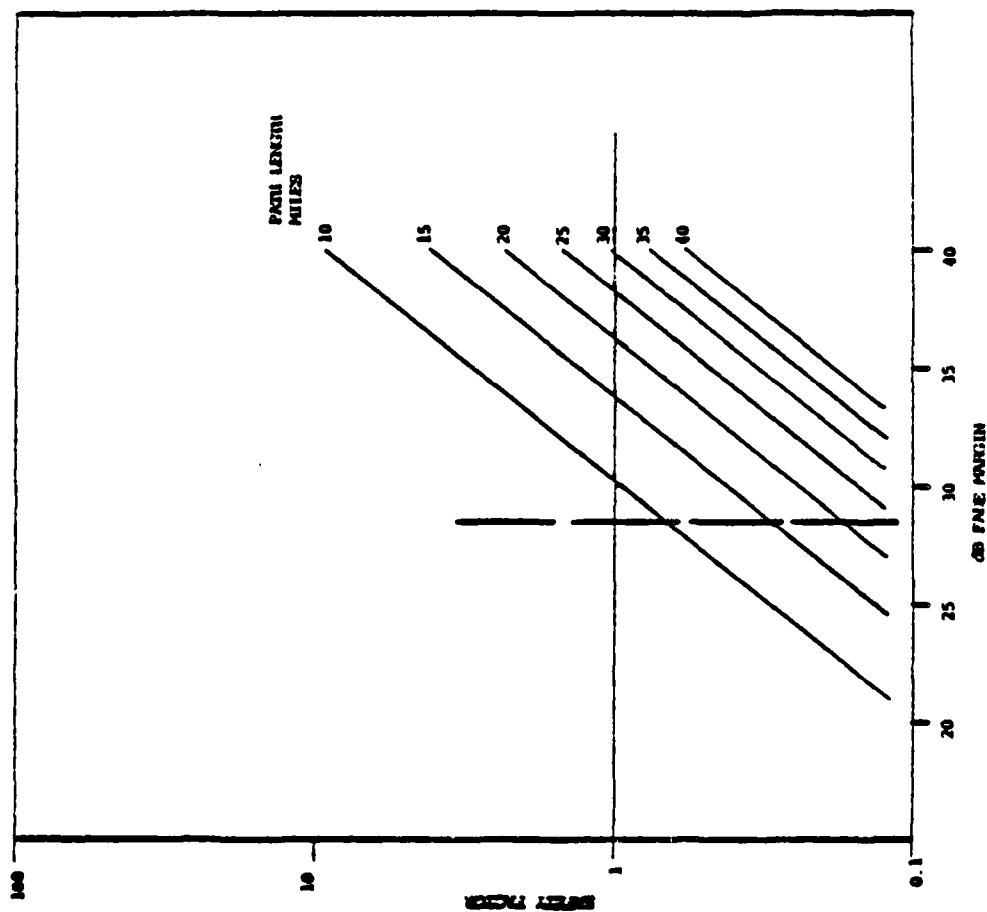
SAFETY FACTOR = $\frac{\text{SHORT HAUL OBJ.}}{\text{UNAVAILABILITY}}$

W1062



PERFORMANCE SAFETY FACTOR, NON-DIVERSITY

RAYTHEON
DATA
SYSTEMS



6 G12 NON-DIVERSITY
AVERAGE CONDITIONS

$$\text{SAFETY FACTOR} = \frac{\text{SHORT HAUL OBJ.}}{\text{UNAVAILABILITY}}$$

APPENDIX A
LIST OF SEMINAR ATTENDEES

<u>NAME</u>	<u>ORGANIZATION</u>	<u>PHONE</u>
Paul Hartmann	Rockwell International	(214) 996-6359
Tom Giuffrida	Bell Labs	(201) 229-6850 x2485
Stephen Matsuura	USACEEIA	VON 879-2187
Andrew E. Hooper	NUWES	(805) 982-8971 VON 744-4963
Henry C. Merhoff	PACMISTESTCEN	VON 351-7881
Adrian Eley	Ft. Meade	(301) 796-6835
Steve Barber	Bell-Northern Research	(613) 596-5036
Arvids Vigants	Bell Labs	(201) 229-6850 x2450
Larry Hause	DOC/NTIA/ITS	(303) 449-1000 x3945
Robert W. Hubbard	DOC/NTIA/ITS	(303) 449-1000 x3414
James L. Weblemoe	PACMISTESTCEN	(805) 982-8971 VON 351-8971
John Osterholz	DCEC/R410	(703) 437-2453
Matthew Blanding	DCEC/R210	(703) 437-2266
Jyoti S. Sharma	Western Union	(201) 825-5148
John M. Reardon	Western Union	(703) 790-2248
Ralph Morris	Western Union	(703) 790-2350
Ed Lyons	Ft. Meade	(301) 796-6835
John J. Knab	Digital Comm. Corp.	(301) 840-3468
Pete Plotkin	DCEC/R310	(703) 437-2261
Dennis Buck	1842EEG Scott AFB, IL	VON 638-4185
C. H. Blackerby	DCEC/R710	(703) 437-2237
J. A. Rose	DCEC/R710	(703) 2236

<u>NAME</u>	<u>ORGANIZATION</u>	<u>PHONE</u>
Walter Cybrowski	DCEC/R220	(703) 437-2316
Victor Weill	DCEC/R230	(703) 437-2416
Harris A. Stover	DCEC/R220	(703) 437-2316
John J. Cormack	DCEC/R220	(703) 437-2316
M. W. Horowitz	DCEC/R220	(703) 437-2316
Jim Vest	DCEC/R540	(703) 437-2441
Joe Mensch	DCEC/R220	(703) 437-2316
H. L. McKinley	DCEC/R200	(703) 437-2466
D. O. Schultz	DCEC/R201	(703) 437-2466
Allen E. Post	MITRE	(617) 271-4885
John K. Webb	MITRE	(617) 271-2596
Owen Cote'	MITRE	VON 478-3237
Tom Shimabukuro	DCEC/R710	(703) 437-2348
Robert Wallace	Raytheon	(617) 762-6700
J. A. O'Brien	DCEC/R210	(703) 437-2266
Gayton Yancey	Raytheon	(617) 762-6700
George H. Hagn	SRI International	(703) 524-2053
David R. Smith	DCEC/R220	(703) 437-2316